Sonochemical Production of Hollow Polymer Microspheres for Responsive Delivery

Skinner, Emily

Award date:
2013

Awarding institution:
University of Bath

Sonochemical Production of Hollow Polymer Microspheres for Responsive Delivery

Emily K Skinner

A thesis submitted for the degree of Doctor of Philosophy

University of Bath

Department of Chemistry

January 2013

Abstract

Ultrasound irradiation of a protein or polymer solution at the air:water interface can be used to form hollow microspheres containing an air bubble. By introducing a layer of oil and sonicating the oil:water interface, microspheres containing an oil droplet are formed. The microspheres are stabilised by disulfide crosslinking, have diameters of between 1-20 μm and have a number of applications; gas filled protein microspheres are used as ultrasound contrast agents and oil filled microspheres are being developed for delivery of lipophilic drugs.

This project extends the scope of sonochemically produced microspheres to include water-in-oil emulsion filled microspheres, which facilitate encapsulation of hydrophilic species, and polymer microspheres that release their contents in response to an external stimulus. Successful encapsulation of a water in oil emulsion phase is demonstrated using confocal microscopy. Release studies are reported for a number of hydrophilic species (*in vitro*) including 5,6-carboxyfluorescein, 5-fluorouracil and sodium chloride. Release can be triggered by sonochemical disruption of the microsphere shells or cleavage of the disulfide cross links.

Thiol-ene coupling reactions initiated by ultrasound irradiation are reported. In water, ultrasound initiation of thiol-ene reactions with electron rich alkenes results in rates of reaction which compare favourably with conventional thermal initiation. Thiol-ene crosslinking is proposed as an alternative to disulfide crosslinking to stabilise sonochemically produced microspheres.

Temperature responsive microspheres are produced via the sonochemical method using a block copolymer of N-isopropylacrylamide and thiolated methacrylic acid, P(MA_{SH}-b-NIPAm). The block co-polymer is synthesised using reversible addition-fragmentation transfer (RAFT) polymerisation and has a lower critical solution temperature (LCST) of 37 ºC. The microspheres formed from this block copolymer can be seen to rupture, releasing their internal oil phase, when heated above 37 ºC. These findings provide a basis from which to develop sonochemically produced polymer microspheres for responsive delivery of both hydrophilic and lipophilic species.

Acknowledgments

I would like to thank the University of Bath for funding this PhD project and the following people for their help and support over the last 3 years' adventures:

Gareth Price, thank you for making this PhD project possible, for your help and support along the way and for introducing me to the Southern hemisphere, not to mention a certain patch of Malaysian rainforest. Matthew Jones, thank you for your supervisory support, encouragement and advice in progressing my thiolene experiments.

Ashok, Meifang and Boon, thank you for your kindness, friendship and hospitality during my visit to Melbourne and for getting my investigation into microspheres off to such a good start. John Lowe, thank you for your ever patient help and support in NMR experiments, for keeping me company in my enthusiasm for DOSY NMR and for cheering me up on grey days. Adrian Rogers, thank you for enabling me to include some illuminating confocal microscopy in this thesis. Wing, thank you for your advice, all the time you spent over our HPLC analysis and for being great company in the tricky latter stages of this project.

Joyce, thank you for being a lovely lab mate, a kind friend throughout the highs and lows of the last 3 years and for all the giggles that we have shared. Saskia, thank you for your friendship, encouragment, advice and for the many hours of discussion that we have shared. Karen, Ilaria, Duygu, Matt, Jim, Rob, Daniel, Lynne, Hannah and Katy, thank you all for your lovely company and for sharing fun times in and around the chemistry department and the Raven.

Claire, Steve, Jonathan, Hazel, Aled, Katie and Alice, thank you for your kindness and friendship over the happy 7 years I've spent in Bath and for always cheering me up or making me laugh when it was most needed.

Thank you Jon for your love, care and unending patience in the many PhD based discussions we have shared whilst looking at Bath's skyline. Finally, thank you Mum, Dad and Sal, for all your love, patient care and for inspiring me to keep going and enjoying my studies over the last 22 years.

Contents

1 Introduction

The sonochemical method for protein microsphere production was first introduced by Suslick and co-workers in 1990[1]. Since then sonochemically produced microspheres and microbubbles (Figure 1.1) have been the subject of active research both as contrast agents for medical imaging and as therapeutic delivery devices. Although recent advances have broadened the scope of shell materials to include DNA and RNA[2;3], graphene oxide[4] and Chitosan[5], the most common shell material for sonochemically produced microspheres and microbubbles is still protein. Sonochemical production of microspheres and microbubbles is dependent upon emulsification or foaming caused by ultrasound irradiation at the interface of the protein solution, hence microspheres reported to date have encapsulated either a hydrophobic (oil) droplet or a gas bubble[6].

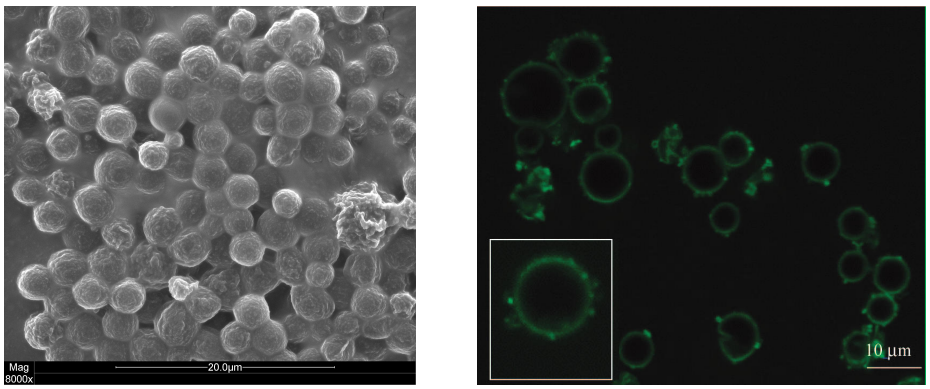

Figure 1.1: (left) Scanning electron microscopy (SEM) image of air filled lysozyme microspheres formed sonochemically, (right) "Confocal laser scanning microscopy (CLSM) image of lysozyme microbubbles." (*sic*) Reprinted with permission[7]. Copyright (2012) American Chemical Society.

This project aims to extend the scope of sonochemically produced microspheres from that reported in the literature to date. There are four fundamental factors in the sonochemical method which

can be altered or developed to improve performance: the shell material, the crosslinking mechanism, the encapsulated core and surface functionalisation. These factors have been addressed within the objectives of this project, the results of which are discussed in later chapters.

Firstly the encapsulated core was considered. Literature reports describe the encapsulation of hydrophobic species within the oil core[8;9] or entrapment of more hydrophilic species in the shell region[10–12] of microspheres. Simultaneous encapsulation of both hydrophobic and hydrophilic species within the core of microspheres would facilitate controlled tandem delivery of two species or co-transport of an imaging agent alongside a therapeutic agent. It was proposed that simultaneous encapsulation could be achieved by using a pre-formed water in oil (w/o) emulsion as the 'hydrophobic' phase in the sonochemical method. Chapter four reports the novel production of water in oil in water (w/o/w) protein microspheres for encapsulation and subsequent delivery of hydrophilic species.

Of equal importance when developing microspheres for delivery applications is the choice of shell material. Proteins and naturally occurring polymers have been extensively studied and characterised as suitable shell materials[6]. However the extent to which microspheres can be 'designed' for a delivery purpose is limited unless the scope of microspheres is extended to include synthetic polymers. This is particularly of interest with respect to designing responsive delivery systems which can be triggered to release their pay load by an external stimulus, for example, heating, light or mechanical stress. At present protein microspheres release their cargo as a result of mechanical stress from ultrasound irradiation[13] or enzymatic degradation[14]. Chapter five reports the synthesis of block copolymers designed for use in the production of temperature responsive microspheres and the initial characterisation of the responsive microspheres produced.

Further to considering the core and shell materials used in sonochemical microsphere synthesis, an alternative method of stabilising and functionalising the microsphere shell has been investigated. Protein microspheres are stabilised either by covalent (disulfide) cross linking[1;15] or by favourable intermolecular forces, most notably the hydrophobic effect[16]. The use of polymers as shell materials opens

up the opportunity to explore alternative methods of stabilising and subsequently functionalising the microsphere shells. Chapter three reports the novel use of ultrasound to initiate thiol-ene coupling of small organic molecules. It is anticipated that this coupling method would have useful application as an alternative sonochemical cross linking mechanism with the potential to include 'one-pot' functionalisation of polymer microspheres with alkene or thiol containing ligands.

The developments described above and detailed in later chapters have their basis in the model lysozyme and poly(methacrylic acid) (PMA) systems developed by our collaborators[8;17] and transferred to the research laboratories in Bath by the author. Initial studies carried out at the Universities of Melbourne and Bath, together with additional release studies conducted in Bath are described in chapter three.

In summary the project objectives are:

- To encapsulate an aqueous phase within protein or polymer microspheres in order to facilitate transport of hydrophilic species in addition to lipophilic species. Then to characterise release of these hydrophilic species upon destruction of the microspheres.

- To demonstrate ultrasound initiation of radical mediated thiol-ene coupling and establish its practicality as an alternative to conventional thermal initiation. Apply this sonochemical methodology as an alternative to disulfide cross linking in the microsphere protocol. Investigate the potential for using thiol-ene chemistry as a means of functionalising the microsphere shells.

- To synthesize a thiolated triblock copolymer of methacrylic acid and N-isopropylacrylamide and use it to form microspheres with the sonochemical method. Characterise the temperature responsive behaviour of the microspheres formed and release of hydrophilic or lipophilic species on heating.

The following literature review gives a background to sonochemistry, describes the sonochemical method and places this project in the context of the 'state of the art' with respect to sonochemical production of microspheres and their use in delivery applications as well as comparing the sonochemical method to other commonly used methods of hollow/liquid core microsphere production.

1.1 Ultrasound and Sonochemistry

Sonochemistry is a term that refers to the chemistry which occurs when a system is irradiated with sound[18] and it is frequencies in the ultrasound range which are used to induce these chemical reactions. Ultrasound can be defined as having a frequency higher than the limit of human hearing i.e. greater than 20 kHz[19].

Low frequency ultrasound (20-100 kHz) is termed power ultrasound, it is in this frequency range that the majority of sonochemistry occurs[18]. However it is possible to observe some sonochemical effects at frequencies as high as 2 MHz[18]. High frequency ultrasound (0.5 MHz – 10 MHz)[20] is typically used in medical applications for diagnosis and therapy.

The chemical effects of ultrasound were first observed in 1927 and reported by Loomis *et al.*[21]. Since then many applications of ultrasound and sonochemistry have been found. High frequency ultrasound is well known for its diagnostic uses in medicine, for sonography imaging[22]. However ultrasound at frequencies around 1 MHz is also used to aid drug delivery[23;24], discussed later in this chapter, and High Intensity Focussed Ultrasound (HIFU) is used in surgery to breakdown blood clots and destroy tumours[25–29]. Both of these applications utilise the micro jets created as a result of cavitational collapse of bubbles caused by ultrasound. Cavitation, described in more detail below, results in radical production and is the source of the chemistry caused by ultrasound[30].

Sonochemistry has been utilised in synthetic chemistry[31], and has been widely researched as a means to purify water by degrading contaminants, for example textile dyes[32]. Ultrasound irradiation is used in polymer chemistry both as a means to initiate radical mediated polymerisations[33] and to cleave polymer chains[34]. Further to these uses the strong mixing effect created by ultrasound can be used as a means of emulsifiying oil and water phases[35]. This makes ultrasound irradiation a useful means by which to carry out emulsion polymerisations[36]. These mixing and cavitation effects also mean that ultrasound is a very efficient method of cleaning debris from surfaces which has lead to wide use in industry and research. Many chemistry laboratories are equipped with an ultrasonic cleaning bath[18].

Ultrasound is generated from electrical energy using a transducer. Two of the most commonly used transducer types are piezoelectric and magnetostrictive transducers[20]. Magnetostrictive materials are ferromagnetic and change their dimensions in response to changes in the applied magnetic field, examples include nickel, nickel-iron and iron-cobalt alloys[22]. A magnetostrictive transducer is comprised of an electrical coil wrapped around the magnetostrictive core. The oscillating magnetic field generated by the coil causes the core to deform, these vibrations are converted to ultrasound[22]. The frequency of ultrasound produced is dependent on the size of the magnetic core which, for practical reasons, restricts these transducers to 20-100 kHz. Magnetostrictive transducers also generate a large amount of heat which must be removed by a cooling system[22].

Piezoelectric crystals are so called because when pressure is applied along a crystallographic axis, electrical charges are produced on the perpendicular crystal faces. This is as a result of electric dipoles in the crystallographic planes aligned in parallel to one another and perpendicular to the surfaces. Application of pressure or tension to the surfaces results in movement of the charges in the dipoles[22]. The inverse is also true, so if a voltage is applied to the crystal surface stress is generated along the crystallographic axis and the crystal will expand or contract according to the potential. Hence, the piezoelectric element in an ultrasonic transducer subjected to an oscillating voltage generates ultrasound at the corresponding frequency[22]. Lead zirconate is a commonly used piezoelectric material in ultrasonic transducers, including those used in this project. Piezoelectric materials can be used to generate ultrasound across the whole frequency range and the transducers require less cooling than magnetostrictive transducers. However the piezoelectric element is fragile and is destroyed if over heated[22].

The most common use of ultrasound in a general chemistry laboratory is for cleaning and in such cases an ultrasound bath can be used. However in order to carry out sonochemistry a more powerful ultrasound source is normally required. In this project horn transducers are used to supply high intensity power ultrasound to small volumes of liquid. The horn assembly utilises a piezoelectric transducer to convert the supplied electrical energy into 20 kHz ultrasound which is transmitted

to the sonicated liquid via a titanium horn. A photograph of the horn used is shown in Figure 2.1.

Sonochemistry

A sound wave is a longitudinal pressure wave. As the wave moves through a medium the medium experiences phases of compression and rarefaction. Particles in the medium respond to these pressure cycles, resulting in propagation of the sound wave. Figure 1.2 shows a representation of this effect in a schematic of beads on a thread corresponding to an acoustic pressure plot. At low ultrasonic frequencies and high intensities the negative pressure experienced during the rarefaction phase is sufficient to overcome intermolecular interactions and form voids. This is the start of cavitation.

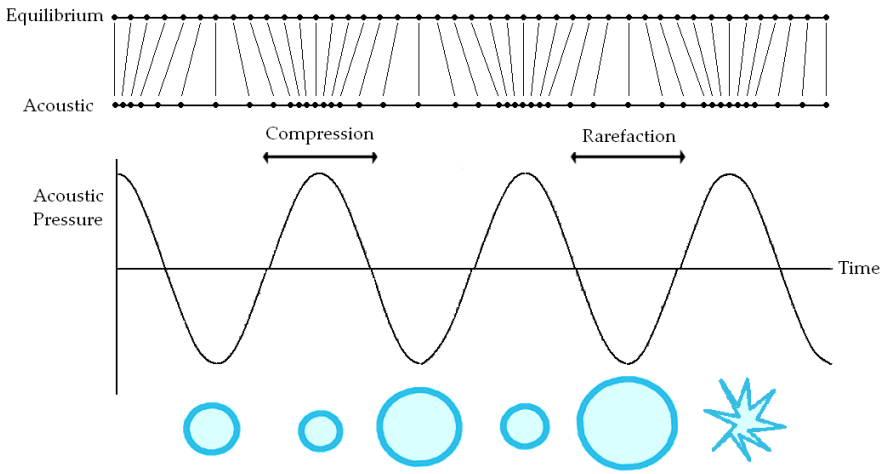

Figure 1.2: Schematic of the interaction of a cavitation bubble with a propagating sound wave, including particle movements under ultrasound irradiation and an acoustic wave form.

Cavitation is the process whereby a bubble is formed in a liquid as a result of the propagation of a sound wave, and then collapses[19]. Cavitation bubbles are usually nucleated by microscopic particles in the liquid which cause weak spots[37]. Once the bubble has formed it can remain trapped in the acoustic pressure field and will expand and contract accordingly whilst growing in volume as solvent vapour and dissolved gases diffuse into the cavity, a process known as rectified diffusion (Figure 1.2). After a period of time the bubble will have

grown to a size that is no longer stable, at this point the bubble will undergo implosive collapse[18]. Adiabatic collapse of the cavitation bubble results in the formation of a micro-scale 'hotspot' which experiences high temperature (4000-6000 K) and pressure (1000-2000 bar)[19]. The associated heating and cooling rates, 10^{10} Ks^{-1}, are far more rapid than thermal diffusion meaning that the hotspots only exist for a matter of microseconds creating a unique environment in which to carry out chemistry[30]. These transient hotspots provide conditions which facilitate solvent lysis and degradation of molecules in solution, resulting in the formation of radicals which are responsible for many chemical reactions, whilst mild conditions are maintained in the bulk solution. In an aqueous system, $H^{\bullet}$ and $OH^{\bullet}$ are formed from the lysis of water upon cavitational collapse. These radicals are capable of diffusing out of the hotspot to undergo further radical reactions (Figure 1.3). Of particular interest in microsphere production is the formation of superoxide ($HO_2^{\bullet}$) which is needed for disulfide cross linking of microspheres.

$$H_2O \rightleftharpoons H^{\bullet} + {}^{\bullet}OH$$

$$H^{\bullet} + H^{\bullet} \rightarrow H_2$$

$${}^{\bullet}OH + {}^{\bullet}OH \rightarrow H_2O_2$$

$$H^{\bullet} + O_2 \rightarrow HO_2^{\bullet}$$

$$H^{\bullet} + HO_2^{\bullet} \rightarrow H_2O_2$$

$$HO_2^{\bullet} + HO_2^{\bullet} \rightarrow H_2O_2 + O_2$$

$$H_2O + {}^{\bullet}OH \rightarrow H_2O_2 + H^{\bullet}$$

Figure 1.3: Sonochemical reaction scheme in water.

There are three main environments in the sonochemical system: The bulk liquid where there are no direct sonochemical events but sonochemically formed radicals may diffuse into the bulk before reacting further. In the centre of the bubble itself, the hotspot, the conditions are very harsh causing reactions to occur in the gases present in the bubble. Between the bubble centre and the bulk liquid is the interfacial region where large gradients of temperature, pressure and shear are experienced[19]. Based on 'comparative rate thermometry' experiments carried out with volatile metal carbonyl

complexes Suslick *et al.*[30] propose a two site model for regions of sonochemical reactivity (Figure 1.4). The most important site is the bubbles interior vapour phase where the majority of radical production is thought to occur, the second site is the layer of liquid immediately surrounding the cavitation bubble which is injected into the bubble upon cavitational collapse[30].

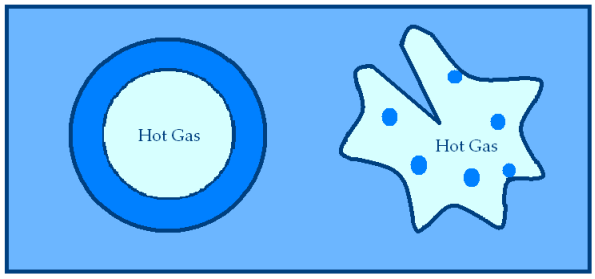

Figure 1.4: Two proposed sonochemical sites[30].

The lifetime of a cavitation bubble before collapse varies. Transient cavitation bubbles collapse after one acoustic cycle having grown quickly to a large size. These bubbles are the ones thought to be responsible for the majority of chemical activity in the system. Stable cavitation bubbles persist for a greater number of acoustic cycles and create large shear gradients when they collapse[19]. These shear forces perform an important role in sonochemical systems and allow emulsions to be formed very efficiently in a two phase liquid system.

Superoxide formation and the emulsification caused as a result of cavitation are important in contributing to the formation of protein microspheres[1]. A horn assembly is used to generate ultrasound in the microsphere system. The cavitation bubbles can be seen to form in a cloud at the end of the horn tip.

Cavitation also causes sonoluminescence, emitted as a result of reactions between sonochemically produced radicals in the vicinity of cavitational hot spots. Multibubble sonoluminescence provides a useful tool for mapping cavitation clouds and sonochemical activity. The intensity of the light given out can be enhanced by using a solution of 5-amino-2,3-dihydro-1,4-phthalazinedione (luminol) to generate sonochemiluminescence. The luminol molecules react with $HO^{\bullet}$ and emit intense blue light in the vicinity of the cavitation bubbles[38], this blue light can be captured photographically. The

sonochemiluminescence produced by the probe used for microsphere production is shown in Figure 1.5.

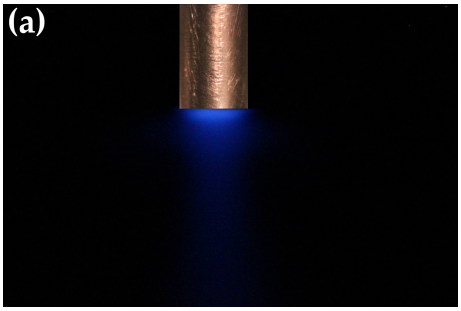

Figure 1.5: (a) Sonochemiluminescence observed in a luminol solution when irradiated with ultrasound from the 3 mm micro-tip attached to generator B (section 2.1.11).

1.2 Sonochemical Microsphere Production

There are a number of benefits associated with using the sonochemical method to produce microspheres for delivery applications: The experimental method facilitates rapid production of microspheres, sonication times range from 30 seconds to 10 minutes. The equipment required is cost effective and simple to use compared to microfluidics and Coaxial Electro Hydrodynamic Atomisation (CEHDA). The method is versatile allowing a range of proteins and other materials to be used in the production of stable microspheres[6]. In addition the sonochemical method can be used to carry out simultaneous surface functionalisation of microspheres produced[39;40]. Development of innovative shell materials and surface functionalisation chemistries for drug delivery applications are active areas of research and are addressed in this thesis. The sonochemical method has not, historically, provided such effective size control as the methods detailed below but new technological developments are being made which have been shown to significantly narrow the size distribution of microspheres produced[41].

Disulfide stabilised microspheres

In 1990 Suslick and co-workers reported an investigation into the formation of protein microspheres under sonochemical conditions[1]. The microspheres consisted of a disulfide crosslinked protein shell encapsulating an oil core. The proteins chosen in that initial study were bovine serum albumin (BSA), human serum albumin (HSA) and haemoglobin (Hb) all of which contain cysteine residues (Figure 1.6) that are capable of forming disulfide bonds.

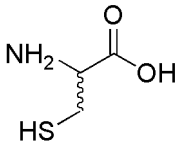

Figure 1.6: Cysteine

In this first study Suslick's group focussed on the synthesis of microspheres encapsulating the hydrophobic liquids; n-dodecane, n-decane, n-hexane, cyclohexane and toluene. Successful encapsulation of the hydrophobic liquids was demonstrated using a solution of the lipophilic molecule 10,15,20-tetraphenylporphyrin (H2TPP) in toluene as a model. Microspheres which had encapsulated H2TPP showed a strong absorbance in the blue region of the visible spectrum.

In later papers the group also demonstrated the formation of air filled microspheres using BSA, HSA[42] and Hb[15]. The Hb microspheres formed were shown to be approximately 2.5 μm in diameter, smaller than red blood cells, with shells that were 6 protein molecules thick[15].

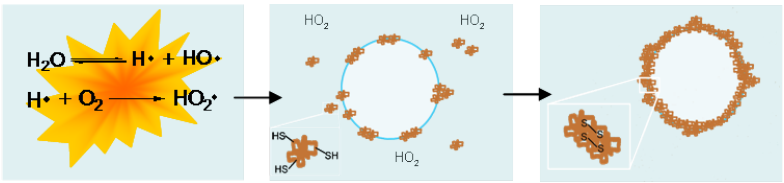

Figure 1.7: Sequence of events leading to the formation of disulfide cross-linked microspheres.

From their investigations Suslick's group were able to propose a mechanism for the formation of such microspheres based upon the emulsification and cavitation effects observed in the sonochemical system[1;42]. Amphiphilic protein molecules aggregate at the interface

of bubbles (or droplets) formed in the foam (or emulsion) in order to reduce the surface energy[7]. However emulsification alone is not sufficient to generate stable protein microspheres. When the proteins were emulsified using a high shear stirring system no stable microspheres were formed[1].

Chemical cross-linking of the aggregated proteins to form a network of intermolecular disulfide bonds between the thiol groups present in the cysteine residues facilitated the production of stable microspheres. By studying the effect of introducing a number of different radical traps into the system, Suslick's group showed that superoxide ($HO_2^{\bullet}$) acts as the oxidising agent in the sonochemical formation of intermolecular disulfide bonds[1] illustrated in Figure 1.7. Superoxide is formed in an oxygen rich system as a result of the reaction of hydrogen radicals (generated during cavitational collapse) with oxygen molecules (Figure 1.3).

As a proof of principle Suslick's group compared Hb and Myglobin (Mb) systems. Hb and Mb are very similar in structure with the exception that Mb does not contain any cysteine residues. When both solutions were sonicated under the same conditions many fewer microspheres were formed from Mb than were formed from Hb. This demonstrates the key importance of cysteine residues in the stabilisation of microspheres. The presence of disulfide bonds in the shells of BSA/toluene and Hb/toluene microspheres was confirmed by adding a disulfide cleavage agent, DL-dithiothreitol (DTT), to suspensions of the microspheres. In both cases the protein shells of the microspheres were destroyed[1].

Lysozyme microspheres

More recent work conducted in the area of protein microspheres has been presented by Cavalieri *et al*. and focuses on the synthesis of lysozyme microspheres[7;8]. It is this work that will form the basis for the initial stages of the investigation reported below.

Lysozyme (Figure 1.8)[a] is an enzyme that has antibacterial properties due to its ability to catalyse hydrolysis of 1,4-beta-linkages in the

[a]Image on right generated using the protein workshop software run by the RCSB Protein Data Bank.

peptidoglycans that make up bacterial cell walls[43]. It is made up of 129 amino acids (approximately 14.7 kDa). The variant used in this investigation is isolated from chicken egg white. The structure contains four intra-molecular disulfide bonds attached to cystine residues which must be reduced leaving eight free thiol groups which can take part in the intermolecular covalent bonding at the interface as described by Suslick[1].

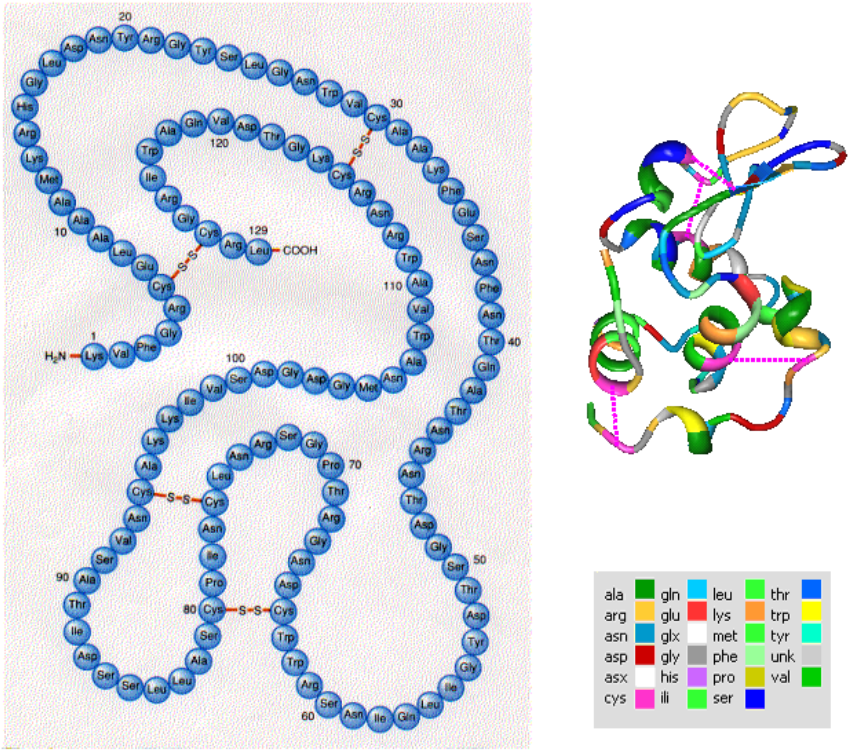

Figure 1.8: Lysozyme molecule (left) Primary amino acid sequence showing 4 disulfide bonds between cysteine residues[44], (right) image shows the secondary structural elements together with the amino acid sequence. The pink dotted lines represent disulfide bonds.

In the existing papers on sonochemically produced air filled lysozyme microspheres it is demonstrated that microspheres are only formed after the disulfide bonds within lysozyme have been reduced, lending evidence to the suggestion that thiol cross-linking is the stabilisation mechanism at work[7]. It is also shown that the extent of cross-linking can be controlled by either the denaturation time or the sonication time

(http://users.rcn.com/jkimball.ma.ultranet/biologypages/L/lysozyme.html) Accessed on 11/08/2010.

resulting, in turn, in different size distributions[7]. These microspheres are interesting because, not only are they stable for several months, but it has also been shown that the surface can be modified by carrying out layer by layer deposition of polyelectrolytes. This suggests that surface functionalisation with drug molecules may be possible in the future[7]. Lysozyme microspheres can also be formed by encapsulating hydrophobic liquids including sunflower oil, tetradecane, dodecane and perfluorohexane[8]. The encapsulation of oil containing the fluorescent dye nile red is also demonstrated[8]. This supports the hypothesis that lipophilic drug molecules could be encapsulated using this methodology without damage from the high intensity ultrasound, a promising indication for future research in this area. A recent study on the behaviour of lysozyme microspheres *in vivo* has shown them to be biodegradable in the presence of proteolytic enzymes with no residual, potentially toxic, insoluble protein fragments[14], an important criterion for a drug delivery system.

PMA_{SH} microspheres

In 2011 Cavalieri *et al.*[17] reported the first sonochemical synthesis of microspheres from a synthetic polymer. The microspheres are formed from thiol functionalised poly(methacrylic acid) (PMA_{SH}) (Figure 1.9). Functionalisation of PMA with cysteamine not only provides thiol groups for cross-linking purposes, but also increases the hydrophobicity of the polymer giving it the foaming properties required for successful microsphere formation. The authors report co-formation of perfluorohexane (PFH) filled microspheres and gas filled microspheres. Interestingly they were unable to form gas filled microspheres in the absence of PFH. The authors suggest that the co-formation of gas filled microspheres is due to the presence of PFH gas which provides osmotic stabilisation to the gas core[17].

The mean diameter of the PFH filled microspheres decreased as the thiol content of the PMA_{SH} increased (from 1.8 μm for 5% functionalised PMA_{SH} to 0.7 μm for 30% functionalised PMA_{SH}), it was suggested that this was due to a higher likelihood of cross-linking prior to coalescence of the droplets. The converse was true in the case of the gas filled microspheres (4.3 μm for 10% functionalised

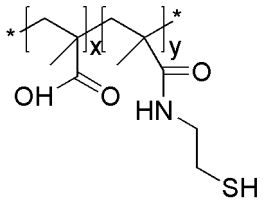

Figure 1.9: PMA_{SH}

PMA_{SH} compared to 8.0 μm for 30% PMA_{SH}, 5% PMA_{SH} microspheres were not stable) and it was suggested that this was due to loss of the gas bubbles to dissolution before cross-linking could occur due to the slower diffusion rate of the more highly functionalised, and therefore more hydrophobic, PMA_{SH} nano-aggregates. Changes in shell thickness were also observed, via SEM, with changing thiol content. The shells containing a higher thiol content undergo more cross-linking and hence are thicker and more textured in appearance, it was suggested that this would enhance the mechanical stability of the microspheres[17]. The microspheres were loaded with Doxorubicin, a positively charged anti-cancer drug, in order to demonstrate the potential for encapsulation of drug molecules. Breakdown of the microspheres using 1 MHz ultrasound was reported although no release curves for Doxorubicin were published[17].

Size distribution

In order to be used safely as ultrasound contrast agents or drug delivery agents microspheres must be small enough to pass easily through the circulatory system without causing a blockage i.e. less than 10 μm diameter[45]. The production method used must form microspheres within the chosen size range consistently in order to allow safe administration and in this respect a narrow size distribution is preferential. A narrow size distribution of microspheres is less easily achieved in sonochemical systems than in the case of some of the synthetic methods discussed below. There is, however, precedent for gaining some control over the size distribution of microspheres produced sonochemically by understanding and controlling some of the variables in the system.

Han *et al.*[46] synthesised silicone oil filled HSA microspheres and demonstrated that for their system the mean size decreased with increasing sonication time up until an equilibrium point. In addition it was demonstrated that the mean size decreased with increasing acoustic intensity. Absolute values for the mean sizes varied between 35 μm and 2 μm for sonication times between 30 seconds and 5 minutes, and intensities between 125 W and 500 W[46]. However due to the fact that the acoustic effects created by ultrasound pressure waves are not only volume dependent but are also affected by the shape of the vessel, comparison of absolute sizes is of limited value. It is more useful to discuss the general trends observed. Zhou *et al*. published a report describing how lysozyme microsphere size distributions and morphologies can be affected and controlled by altering the sonication time and sonication intensity[47]. Contrary to Han's report, Zhou *et al*. found that microsphere size increased with sonication time and/or power. It was suggested that this was due to the increased coalescence that would occur as a result of the high shear forces experienced at high intensities and that a similar argument could be used at long sonication times which would allow more time for coalescence processes to occur. Successful microsphere formation is a balance between microsphere production and degradation. This was demonstrated at longer sonication times and higher intensities where fragments of broken shell were observed in the SEM images of microspheres produced and reduced yields were obtained[47].

It was noted by Han *et al*. that in a system which has poor circulation the distribution of power is inhomogeneous across the volume of the vessel[46]. As a result a broad distribution of microsphere sizes will be observed. This is a problem that can be overcome by ensuring that there is sufficient circulation in the system to create a homogeneous distribution of power.

Makino *et al*. observed that for BSA microspheres formed with a number of different hydrophobic liquids the size distribution narrowed at higher ultrasonic frequency (45 kHz compared to 28 kHz)[48]. This suggests that the emulsion formed at higher frequency is more monodisperse. They also found that the nature of the encapsulating liquid affects the size distribution of the microspheres produced[48]. Toluene filled HSA microspheres were not only smaller than their

chloroform analogues but they also had a narrower size distribution. It is suggested by the authors that this was a result toluene being less miscible in water than chloroform and hence the interface at the surface of the toluene emulsion droplet is finer than for a chloroform droplet. Hence the region in which the protein can aggregate around a toluene droplet is much more narrowly defined giving a smaller range of sizes. In the case of vegetable oils (soy bean oil and peanut oil) the microspheres formed were much smaller than those formed from either toluene or chloroform[48]. It is thought that this is due to the higher viscosity of the vegetable oils in comparison to the organic solvents, resulting in a smaller emulsion droplet size.

In addition to adapting experimental parameters during production of microspheres and microbubbles, techniques such as filtration or further sonication can be employed 'post production' to reduce the size distribution of a sample. Zhou *et al*. report the use of a 'post sonication' technique to adjust the size distribution of lysozyme microbubbles produced according to their standard procedure[7;45]. It was shown that sonication of an aqueous dispersion of microbubbles at 212 kHz could reduce the size distribution from an initial distribution of diameters between 0.5-4.0 μm (mean: 2 μm) to a final distribution of 0.5-2.0 μm (mean: 1 μm), albeit with a sacrifice of yield that results from destruction of the larger microbubbles.

In developing the sonochemical method as a microsphere/bubble production technique it is of more interest to obtain a controlled size distribution without the inevitable sacrifice in yield made by post production processes. In a recent paper Zhou *et al*. report the first example of a sonication technique capable of producing near monodisperse populations of nano and microbubbles[41]. The technique uses a flow through horn (20 kHz) to confine the active cavitation zone in which microspheres are produced, this results in a more homogeneous distribution of power than is achieved by the standard probe horns and therefore a narrower distribution of diameters (Figure 1.10). The technique can also be run in a continuous manner, facilitating scale-out of the sonochemical method.

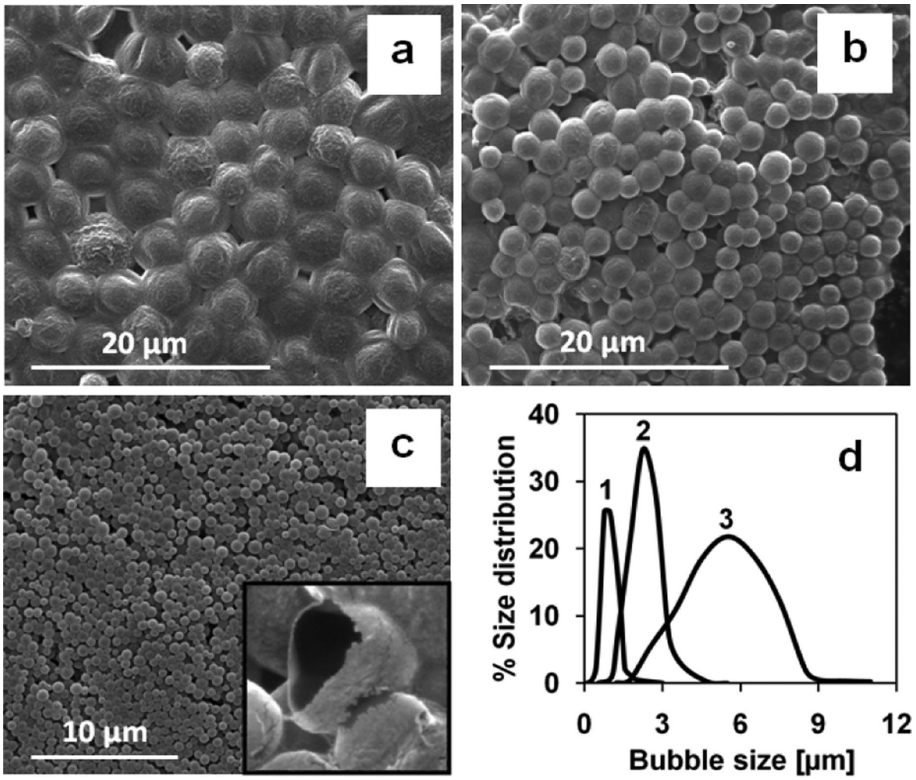

Figure 1.10: "SEM images of lysozyme microbubbles synthesized using (a) a 1 cm standard horn (160 W), (b) a 3 mm standard horn (120 W), and (c) a flow-through horn (240 W). Inset (c): Broken nanobubbles. Size distribution of lysozyme bubbles (d): (1) a flow-through horn, (2) a 3 mm standard horn, and (3) a 1 cm standard horn" (*sic*). Reprinted with permission[41]. Copyright (2012) American Chemical Society.

Non-covalently stabilised microspheres

Since the initial investigations of Suslick *et al*. Gedanken's group have broadened the field of sonochemical microsphere production to proteins which do not contain sulfur residues[49]. Streptavidin was used as a model protein because it has a similar structure to avidin, which has been shown to form disulfide cross linked microspheres[50], but does not itself contain any sulfur residues. At acidic pH, decalin filled streptavidin microspheres were formed sonochemically and were stable for several hours at 25°C or 1 month at 4°C[16]. The fact that an acidic pH was required to facilitate microsphere formation was believed to give some indication as to the mechanism of microsphere stabilisation. It was shown that streptavidin microspheres can

be formed both in an air saturated solution and argon saturated solution[16]. This suggests that the mechanism for formation is not dependent on superoxide. Instead it is thought that the main factor in the formation and stabilisation of streptavidin microspheres is the hydrophobic effect.

The hydrophobic effect occurs when proteins are placed in a polar solvent such as water. In order to reduce unfavourable interactions between the hydrophobic parts of the protein and the polar solvent the protein will fold and converge into a smaller volume, reducing its surface area[51]. It is proposed by Gedanken *et al*. that this hydrophobic effect leads the proteins to aggregate in a stable manner around oil droplets formed in the sonochemical emulsion[16]. Aggregating at the interface allows the proteins to stabilise one another by creating a more hydrophobic environment for their neighbour. Microsphere formation is promoted in an acidic medium because the carboxylic acid groups on the protein are neutralised thus increasing the hydrophobicity of the protein surface and reducing electrostatic repulsions[16].

Its is important to emphasise that although this hydrophobic mechanism does increase the scope for hollow microsphere formation in terms of the number of proteins or polymers that can be used, it is limited by the lack of long term stability in the microspheres formed. Microspheres formed as a result of thiol cross-linking are stable for several months at room temperature as compared to hours for streptavidin microspheres[16].

In an effort to further prove the action of the hydrophobic mechanism Gedanken *et al*. demonstrated the formation of decalin filled poly(glutamic acid) microspheres[49]. Poly(glutamic acid) is an amide linked backbone with only carboxylate side chains (Figure 1.11). Poly(glutamic acid) was chosen as a simplified model of streptavidin and it was hoped that it would confirm the effect of the carboxylic acid groups on microsphere formation. The study showed that these microspheres could only be formed below pH 4.5. The pK_as of aspartic and glutamic acid are between 4.0-4.8[49]. Hence it was concluded that microspheres could only form when the carboxylic acid groups were in the protonated form and the hydrophobic interactions were dominant. The microspheres formed were reported to be stable for one

month, a significant improvement on the stability of the streptavidin microspheres[49].

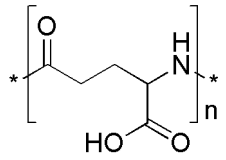

Figure 1.11: Poly(glutamic acid)

Suslick *et al*. also conducted an investigation into the synthesis of poly(glutamic acid) microspheres this time encapsulating vegetable oil[52]. They used the sodium salt, polyglutamate. The microspheres formed were only 1 μm in diameter, small enough to allow extrvasation (escape from the blood pool) especially in tumours where the vasculature is known to be more permeable[52]. The microspheres were very stable, with a half life of over a month at 2 °C, they were also demonstrated to be thermally stable for over an hour at 60 °C.

Contrary to Gedanken's hypothesis, Suslick suggested that the dominant intermolecular interaction was in fact hydrogen bonding between carboxylates. Suslick *et al*.[52] found that it was not possible to form microspheres in the low pH range quoted by Gedanken. They hypothesised that this was due to the fact that at low pH the protonated carboxylic acid groups would not be able to hydrogen bond. Suslick demonstrated that hollow microspheres had been formed at higher pH using Transmission electron microscopy (TEM) pictures that clearly show the core shell nature of the microspheres[52]. It was suggested that the microspheres formed in Gedanken's investigation were in fact solid particles due to the fact that poly(glutamic acid) (MW > 6000 Da) is insoluble at low pH. Hydrogen bonding between carboxylates is the strongest form of hydrogen bonding[52] which may account for the extended shelf life of the poly(glutamic acid) microspheres synthesised by Suslick *et al*. as compared to other non-covalently cross linked systems.

The observations found in the literature suggest that the mechanism by which non chemically cross-linked microspheres are stabilised can be as a result of one or a number of intermolecular forces including hydrogen bonding, van der Waals, hydrophobic and electrostatic interactions[49]. It is likely that the mode of stabilisation will vary

with the system used. A very recent study conducted by Silva *et al.* into the mechanism of sonochemical microsphere formation provides further insight into the stabilisation of microspheres with and without disulfide bonds[53]. Computer simulations were used to demonstrate that BSA was able to adapt its tertiary structure to fit the oil-water interface so as to expose hydrophobic regions of the protein to the internal oil phase and hydrophilic regions of the protein to the external aqueous phase. In addition greater colloidal stability could be achieved by increasing the surface charge of the microspheres, a function of the number of BSA molecules in the shell. Building on these observations Silva *et al.* were able to demonstrate the importance of clearly defined hydrophobic and hydrophilic regions in the protein for shell stability by trialling a range of synthetic polypeptides[53]. It was found that polypeptides which mimicked a fatty acid model; a short hydrophilic section coupled with a longer hydrophobic tail were most effective in forming a high yield of stable microspheres. Based on this study, it appears that it is these structural factors that are most important in the initial formation of microspheres and that disulfide bonding is not crucial to the initial formation, provided that the protein fragments have strong intermolecular interactions at the oil:water interface[53].

Further to polypeptide and protein based microspheres Gedanken *et al.* have reported microspheres formed using the sonochemical method from the polysaccharides starch[12] and chitosan[5] as well as graphene oxide[4]. None of these systems accommodate disulfide crosslinking and the mechanisms of stabilisation in each case, whilst proposed as being sonochemical in basis, are yet to be fully understood.

1.3 Methods for producing polymer and protein microspheres

Aside from the sonochemical method there are a number of other methods commonly used to synthesise hollow protein or polymeric microspheres. These methods fall broadly into four categories; emul-

sion techniques, layer-by-layer assembly, inkjet printing and coaxial electro hydrodynamic atomisation, and microfluidic techniques.

Emulsion techniques and Interfacial polymerisation

All of these techniques create similar emulsion systems from which hollow microspheres can be formed. The differences are in the means of producing the emulsion which in turn affect the breadth of utility of the system.

One of the simplest techniques is high shear emulsification. As the name implies an emulsion is formed under high shear stirring. This emulsion is then stabilised by an amphiphilic polymer or protein. The amphiphilic molecules are attracted to the oil:water interface where they will either chemically crosslink or aggregate due to the hydrophobic effect[16;54]. Often a volatile oil phase is used, the oil will evaporate causing the polymer surrounding the emulsion droplets to precipitate over the internal surface of the droplet forming a hollow or partially liquid filled shell[55]. The size of the microspheres formed in this system can vary from the nano scale to the micro scale[55]. In addition, stabilisers such as poly(vinyl alcohol) (PVA) can be used to change the interfacial energy of the system and thus change the size distribution of the spheres formed[55].

High shear emulsification is commonly applied synergistically with interfacial polymerisation to stabilise emulsion droplets and form capsules[56–58]. Interfacial polymerisation describes polymerisation reactions which occur either at an air:water interface or the interface between a hydrophilic region and a hydrophobic region and is therefore ideal suited to capsule formation. An example of this approach is provided by Jiang *et al.* who use interfacial polymerisation to crosslink oligomers of poly(methacrylic acid) (PMA) and polylactide (PLAM) in an oil/water emulsion with a water soluble free radical initiation system[55]. The hydrophobic PLAM crosslinks with hydrophilic PMA across the oil/water interface of the emulsion droplets forming a mesh of copolymer which surrounds the oil droplet. Again a volatile solvent is used, chloroform, which evaporates after a period of continued stirring to leave hollow capsules. It was observed that once a thin shell of copolymer had formed around the emulsion droplet diffusion of the

initiator across the interface and interaction between the two types of oligomer was hindered preventing further polymerisation. As a result unreacted PLAM oligomers precipitated onto the internal surface of the microspheres as the chloroform evaporated increasing the shell thickness but perhaps not its strength[55].

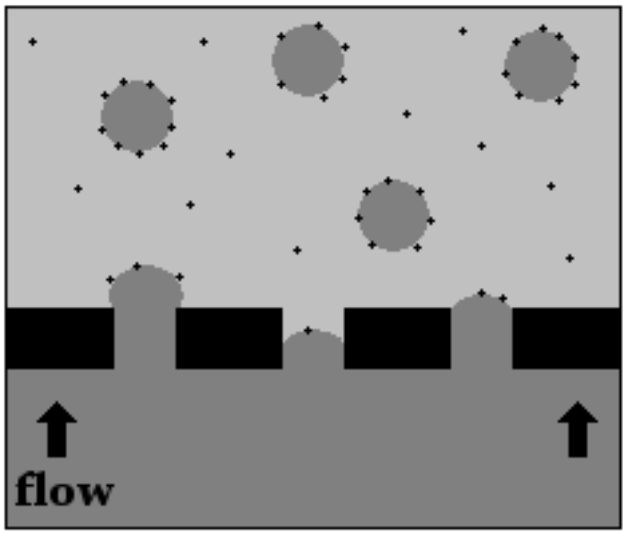

Figure 1.12: Schematic of the membrane emulsification process; dark grey: oil phase, pale grey: aqueous phase, black: membrane, black dot: surfactant molecule.

Membrane emulsification provides an alternative method of forming an emulsion system without the need for high shear forces. This has advantages for more fragile systems where high shear forces might damage the proteins used[59]. In membrane emulsification the oil is forced through a porous membrane into a bulk aqueous phase generating an emulsion with a narrow distribution of droplet sizes[60](Figure1.12). As a result this system gives better control over the microsphere size distribution than in the high shear case[60]. After the emulsion has been generated a methodology similar to that described above (utilising amphiphilic molecules or interfacial polymerisation) can be used to stabilise the emulsion and form microspheres. A recent example from Akamatsu et al.[61] demonstrates the use of a porous glass membrane to form Chitosan microspheres and shows that is possible to form a monodisperse emulsion with a droplet size controlled by the pore size of the glass membrane. Although the microspheres formed

were solid the method could be used to form oil/water emulsions which could be further modified to form hollow microspheres[61].

Layer-by-layer assembly

Layer-by-layer (l-b-l) assembly of capsules provides a means of forming capsules with a controlled wall thickness by using a sacrificial template, usually monodisperse silica particles[62]. Originally l-b-l capsules were formed from polyelectrolytes in a step wise manner: The template particles used had a surface charge and were incubated with oppositely charged polyelectrolytes which coated the template. The excess polyelectrolyte was removed by centrifugation and rinsing, the coated particles were then incubated with the oppositely charged polyelectrolyte to form a second layer of polymer on the particles. This process of incubation with polymers of opposite charges could be repeated as many times as desired to form capsules with the required wall thickness (Figure 1.13). After deposition of the layers the template particle was removed to leave a hollow capsule[62].

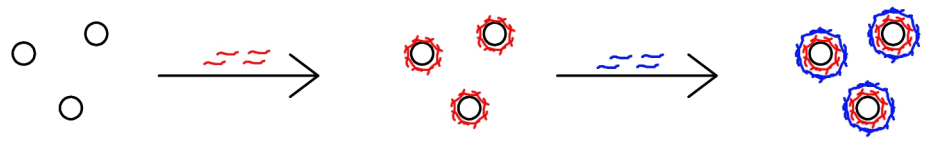

Figure 1.13: Schematic of layer by layer capsule assembly. Red and blue strands denote oppositely charged polymers.

More recent investigations have explored hydrogen bonding and covalent bonding strategies, including disulfide bonding[63] and click chemistry[64], as alternative means of stabilising l-b-l capsules. Utilising hydrogen bonding as a means of building microspheres has extended the scope of l-b-l capsules to include neutral responsive polymers, for example PNIPAm[65], providing potential for use of l-b-l capsules as responsive delivery systems. A recent paper from Caruso *et al.*[66] reported the synthesis of polymer capsules stabilised by thiol-ene cross-linking. The group used l-b-l deposition at pH 4 to alternately deposit PMA_{SH} and PMA_{ene} interspersed with layers of poly(vinylpyrrolidone) onto a silica particle forming a coating which was stabilised by hydrogen bonding. The coated particles were

exposed to UV light (256 nm) for two hours and thiol-ene cross-linking occurred between the deposited layers of PMA. The particles were exposed to pH 7 to disrupt the hydrogen bonding and wash away the poly(vinylpyrrolidone) leaving a thiol-ene stabilised shell. Finally the silica particle was etched away to leave a stable thiol-ene cross-linked capsule.

Loading of l-b-l films and capsules with therapeutic species such as drug molecules or DNA for delivery can be achieved via three different methods[67]. The stepwise approach to shell formation allows incorporation of drug species into the capsule shell during production[68–70]. For small drug molecules this can be achieved by first encapsulating the drug species within polymeric micelles, these micelles can then be introduced into the shell as one of the layers[69;70]. Alternatively in order to form capsules that have an oil core containing the lipophilic species, dehydrated l-b-l capsules can be soaked in an oil phase containing the drug, for example a solution of the anti-cancer drug doxorubicin in oleic acid[71]. When the capsules are then transferred to a buffer and rehydrated they retain their oil core. This method is effective in forming very similar structures to those formed via the sonochemical method but wastes a large percentage of the oil phase used in loading the capsules[67;71]. More efficient loading can be achieved if the molecules are loaded onto the sacrificial particle prior to layer assembly, this technique has been demonstrated in the case of loading PMA_{SH} capsules with DNA[72]. Loading and subsequent release of DNA was achieved whilst maintaining the structural integrity of the DNA strands.

Layer-by-layer deposition provides a means of forming capsules with well controlled size distributions from a variety of polymers and has great potential for future development of drug delivery agents. Unfortunately the process of formation is relatively labour intensive and loading of lipophilic species into the core is inefficient compared to the sonochemical method and emulsion techniques available.

Ink jet printing and Coaxial Electro Hydrodynamic Atomisation (CEHDA)

Ink jet printing provides an efficient method of generating a monodisperse population of microspheres. A 'drop on demand' ink jet printing system can be used to dispense uniform droplets of a hydrophobic liquid into a bulk aqueous phase at a very fast drop rate (4000 drops per second)[73]. Drop on demand systems provide a high level of control as droplets will only be produced when triggered, for example by a voltage pulse passing through a piezoelectric actuator. The voltage pulse is controlled by a computer data stream which allows great flexibility and precision in the size of the droplets produced. Once the emulsion has been formed chemical cross-linking of polymers or proteins in the aqueous phase can be used to stabilise the emulsion and form monodisperse microspheres[73]. Gas filled microspheres can be generated by using a jet in jet technique consisting of an inner jet of nitrogen and an outer jet of polymer solution[73]. Alternatively the jet in jet technique can be used for drug encapsulation by replacing the inner gas jet with a stream of drug solution[73].

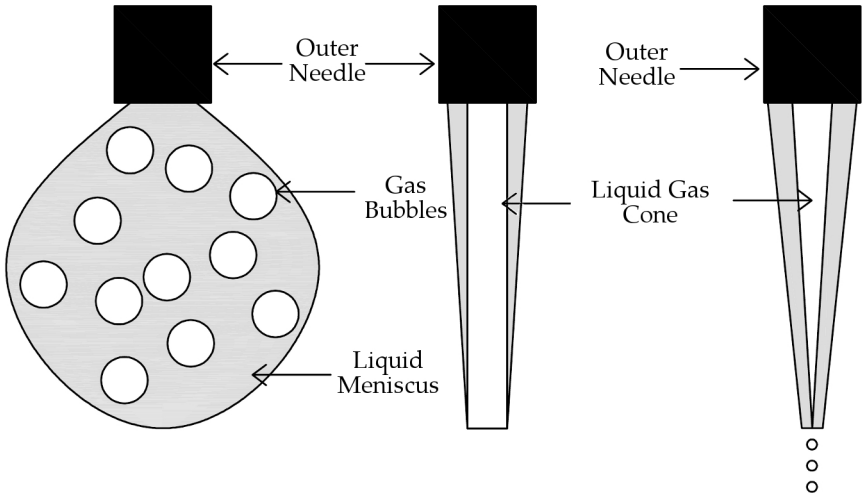

Figure 1.14: Microbubble production by coaxial electro hydrodynamic atomisation. Left to right: bubble dripping mode, coning mode, continuous microbubbling mode[60]. Image adapted from reference.

CEHDA is similar to ink jet printing and can be used to generate well controlled distributions of hollow or liquid filled microspheres. Two streams of liquid are focussed into a coaxial jet under the influence of an electric field. The jet then breaks into droplets and if the two liquids are immiscible then the outer liquid will encapsulate the inner liquid to form core shell microspheres[60]. Alternatively in order to form gas filled microspheres the inner liquid stream can be replaced with a stream of gas (Figure 1.14). The size and dispersity of the microspheres produced can be controlled by adjusting the respective flow rates of the two liquid streams and the applied voltage of the electric field. For example the diameter of the microspheres can be reduced by reducing the flow rate of the inner stream[60]. Phospholipid microspheres have been formed by this method with a mean diameter of 6.6 μm ± 2.5 μm and are stable for over 2.5 hours at room temperature[60]. The major advantage of this method is that several coaxial jets can be set up together to generate microspheres with multilayer shells in one step[74]. This gives the opportunity for highly controlled drug release profiles to be designed, however the applicability of this method to drug delivery is currently limited by the stability of the microspheres formed. No chemical methods of stabilisation have yet been applied to the CEHDA system, although more stable microspheres have been formed from polymethylsilsesquioxane (a biocompatible silicone polymer)[75].

Microfluidics

Microfluidic systems offer a very high degree of control over the size and dispersity of the microspheres formed achieving near monodisperse size distributions. Two types of system are currently in use; flow focussing units and T-junction units, both form microspheres via a 'pinch off' process.

The flow focussing unit forms microspheres which are small enough for intravenous injection (nitrogen filled microspheres with a mean diameter of 1.5 μm ± 0.1 μm have been reported which are stable for at least 9 hours at room temperature[76]) however it should be noted that this system is expensive to run as experiments must be conducted under clean room conditions in order to prevent blockage

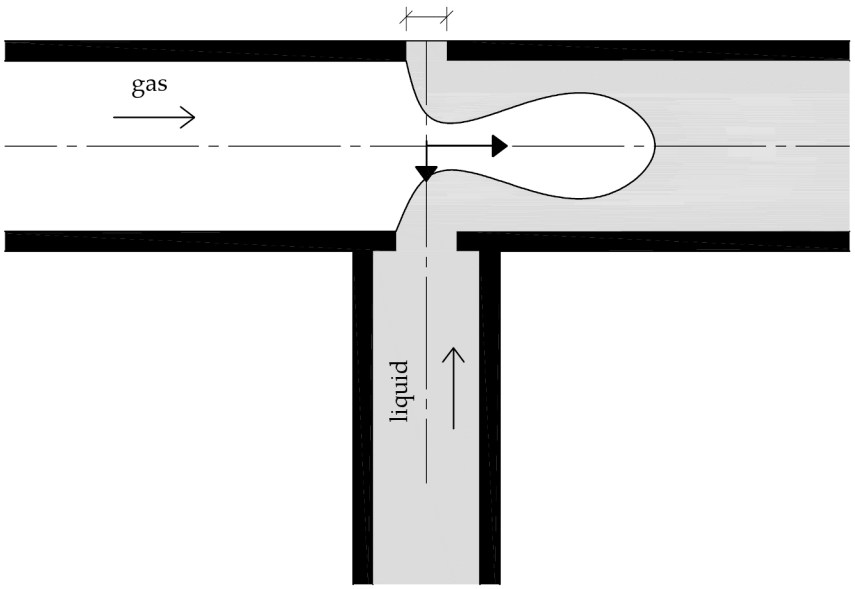

Figure 1.15: Schematic to show microbubble production using a microfluidic T-junction[60]. Image adapted from reference.

of the fine channels used[60]. The T-junction system (depicted in Figure 1.15) is based on capillaries and does not require clean room conditions making it more convenient. Unfortunately the microspheres produced are not yet small enough for intravenous injection (mean diameters in the range of 30-100 μm)[77] limiting its utility in drug delivery applications. However there is future potential is this area as the formation of hollow microspheres from silk worm cocoon silk (a biocompatible, biodegradable polymer) has been demonstrated and may be useful for drug delivery if the mean diameter can be reduced[78].

1.4 Biological Activity and Applications of Sonochemically produced Microspheres

Conventional administration of drugs in therapy has a number of pitfalls and drawbacks; side effects can result from systemic delivery of drug molecules throughout the body, rather than specifically to the site of action[79]. This is especially relevant in the case of anti-cancer drugs which have strong systemic toxicity[80]. Encapsulation of such drugs within a biocompatible protein shell is advantageous in terms of reducing systemic toxicity and increasing the half life of the drug[79 81 81]. Loading drug molecules into or onto carriers has the additional benefit of protecting the drug from degradation *in vivo*, therefore reducing the dose required to achieve the desired therapeutic effect[81]. The sonochemical approach provides a facile method for forming biocompatible[6;14] microspheres encapsulating hydrophobic liquids and associated lipophilic solutes[1], and additionally provides a platform for surface coating facilitating the carriage of more hydrophilic species[82] or targeting ligands[83].

Biological activity of microspheres

Irradiation of proteins with high intensity ultrasound in the presence of an organic solvent, as is necessary for microsphere formation, is known to result in significant levels of inactivation and also precipitation of the protein[84]. It is proposed by Krishnamurthy *et al.*[84] that this inactivation is caused by protein denaturation as a result of exposure to the aqueous:organic interface, pyrolysis in the vicinity of cavitation events and degradation of the protein's active sites by sonochemically produced free radicals. This is not unexpected, it is perhaps more surprising to find that some enzymatic activity can be retained in the microspheres subsequent to formation.

Gedanken *et al*. have used a sonochemical approach to synthesise decalin filled microspheres from an enzyme α-amylase which hydrolyses polysaccharides[85]; α-chymotrypsin which is less thermally stable and breaks peptide bonds[85]; and avidin which is known to bind biotin very strongly ($K_a \sim 10^{15}$ M^{-1})[50]. Gedanken *et al*. observed that although the activity of the proteins was reduced in all three

cases it was not destroyed totally. This suggests that the sonochemical treatment does not denature all of the active sites responsible for the activity of the proteins. From these results it can be inferred that the secondary structure of the proteins is left partially or wholly intact despite the large shear forces acting in the solution and the formation of intermolecular disulfide bonds. Further information could be gathered on this aspect of microsphere formation through using circular dichromism spectroscopy to study changes in the protein's secondary structure more closely[7]. A report from Suslick *et al*. also indicates the retention of secondary structure; microspheres formed from Hb retain the secondary structure surrounding the Heme site and Hb molecules in the microsphere shell are still able to bind oxygen in a reversible manner and display cooperative behaviour[15]. In fact the microspheres had better oxygen binding efficiencies than red blood cells. Residual enzymatic activity may have implications for drug delivery applications, if enzymatic activity is retained it may cause harmful side effects if microspheres are administered in vivo. Alternatively, as with the case of Hb microspheres, the retained activity may offer useful applications, for example as a blood substitute.

Beyond simply using the cross-linked protein shell as a carrier for the encapsulated payload, it is interesting to consider forming the shell itself from a therapeutic agent to create a very simple carrier. DNA is a large negatively charged molecule which cannot readily pass through cell walls and into the cell nucleus, it is also subject to attack and breakdown by nucleases present in cells. Therefore in order to carry out effective gene therapy an efficient and safe means of facilitating entry of DNA into cells needs to be developed[86]. Shimanovich *et al.*[2;3] have demonstrated that stable nanospheres could be formed by sonicating DNA or RNA with dodecane. The nanospheres can be taken up by mammalian cancer cells and these nanospheres could provide a potential method of delivery for DNA and RNA in gene therapeutics. Its is suggested that forming nanospheres can protect the strands from *in vitro* and *in vivo* degradation, enhancing the efficacy of delivery to the cell without the need for additional mediators[2;3]. Preliminary experiments show that plasmid DNA can be released from the nanosphere shells and can replicate[2] (within E-coli) and,

under denaturing conditions, RNA molecules can be released and are able to refold into their native form[87].

Drug encapsulation/entrapment

There have been a number of reports in the literature of successful drug[9–12;79;88] and dye[8;89] encapsulation within sonochemically produced microspheres. Encapsulation can be carried out in a one step process during microsphere production, the drug molecule is either dissolved in the oil core material or the aqueous buffer resulting in encapsulation within the core of the microspheres or entrapment under/in the protein shell. Gedanken *et al.* demonstrated encapsulation of a mesitylene phase containing Taxol within BSA spheres[9], loadings of over 90% were achieved (as a function of the total amount of taxol initially added to the system). The taxol microspheres were tested for their anticancer activity against cells taken from a mouse myeloma cell line and it was found that the deaths of cancer cells increased with increased taxol loading but that in addition the mesitylene solvent was responsible for further cell death. Aside from protein microspheres Zhou *et al*. demonstrated, qualitatively, encapsulation of the fluorescent anti-cancer drug Doxorubicin within PMA_{SH} microspheres[17].

Similar studies were carried out with Gemcitabine[79], another anti-cancer drug, and Tetracyline[10], an antibiotic, in these cases the drug was loaded from the aqueous protein solution into microspheres containing a dodecane core. The action of sonication resulted in partial solubilisation of the drug molecules in the oil core in both cases and the microspheres produced contained drug encapsulated in the core and drug entrapped in the shell, 30% and 65% loadings were achieved respectively[10;79]. Again the drugs' activities were maintained on incorporation into the microspheres, indeed in this case the Gemcitabine was seen to exhibit greater activity than standard Gemcitabine; only a fifth of the dose of microspheres was required compared to standard Gemcitabine to achieve the same extent of cell death[79]. The Gemcitabine microspheres are stable to release in buffer at 37 ºC over a period of 100 hours so it was thought that release in the cell environment was triggered by protease degradation of the

shells[79]. The mechanism for release and observed activity is still under investigation.

An interesting alternative method of loading a therapeutic agent within the microspheres is to incorporate it structurally into the shell wall as was demonstrated with starch-insulin microspheres[12]. Insulin contains disulfide bridges in its protein structure and hence is a potential candidate for microsphere formation, however starch being a polysaccharide does not have any such functionality. Despite this it was shown by Gedanken *et al.*[12] that starch microspheres can be formed, the authors suggest that the mechanism of stabilisation of the microspheres results from sonochemical reduction of glycosidic bonds and thermodynamically driven assembly of starch fragments. If insulin is added to the starch solution prior to sonication 'double walled' microspheres can be formed containing an inner structural component of insulin and an external shell of starch. The microspheres formed incorporate up to 93% of the insulin present in the starting solution and are stable to release making them potential future candidates for insulin delivery[12].

More recently interest has focussed on characterising the release of drug molecules from microsphere carriers with a view to further developing their potential as drug delivery agents. Prolonged release of a hydrophobic dye, sudan III, from BSA microspheres into chloroform or sodium dodecyl sulfate solution has been studied[89]. It was shown in this study that release could be sustained over several days and that the rate of release could be enhanced by heating the microspheres from ambient to physiological temperature[89]. Silva *et al.* report encapsulation of the hydrophilic drug Piroxicam within BSA or HSA microspheres using polyvinyl alcohol (PVA) as a stabiliser[11]. PVA was found not only to reduce the z-average diameter of the microspheres produced, perhaps due to steric stabilisation of smaller droplets/microspheres during formation, but also a greater proportion of the available drug was incorporated when PVA was present. The PVA-BSA microspheres were stable over several months but when incubated with protease 100% release was achieved within a two hour period. The release profile initially followed that typical of a 'burst' release followed by slower continuous release, suggesting release from the surface followed by release of those molecules bound

on the inside of the shell. It is likely that introduction of the additional PVA layer provided greater protection to the drug trapped within in the shell, preventing it from leeching away on storage.

An example of functionalising the surface of microspheres in order to achieve a therapeutic effect can be seen in the case of BSA microspheres which have recognition peptides for Amyloid-β covalently attached[39]. Amyloid-β is the main pathogen in Alzheimer's disease, its toxicity is derived from its tendency to form neurotoxic aggregates. The surface functionalised microspheres were able to bind Amyloid-β and, in fact, were more effective in binding and reducing the toxicity of Amyloid-β than the free recognition peptide chains. It was proposed that this was due to the multivalency effect created by the relatively large microsphere structures, as also observed in the case of Hb microspheres[15;39;90].

The formation of microspheres from DNA or RNA was discussed above, however it is also possible to protect DNA for delivery by coating it on the surface of protein microspheres. The surface of protein microspheres is often highly charged due to the number of ionisable groups in the protein molecules. For example at pH 7 the net charge on a BSA molecule is -17, a typical microsphere (with a diameter of 2 μm) has approximately 106 BSA molecules in the shell, hence the microsphere shell is highly negatively charged[83]. This makes protein microspheres ideal substrates for electrostatic layer by layer deposition. Lentacker *et al.* report the synthesis of perfluorocarbon filled BSA microspheres which are coated with a layer of poly(allylamine hydrochloride) (PAH). The coating of PAH gives the microspheres a cationic surface which can bind the negatively charged DNA molecules[86]. Firstly this protects the DNA from attack by nucleases at the point of delivery, secondly it facilitates the transfer of the DNA molecules into the cell under ultrasound irradiation[86;91], see below. A similar study has been carried out by Melino *et al.* and used the cationic surface of lysozyme microspheres to bind DNA without the need for additional polymer coatings[14]. They too were able to show protection of the loaded DNA with respect to enzymatic breakdown. Further studies are now required to fully investigate the potential for DNA delivery via sonochemically produced microspheres.

Biodistribution and targeting

In the context of considering microspheres for drug delivery applications it is important to address the way in which microspheres are distributed in the body and the measures which can be undertaken to influence that distribution. Sonochemical microspheres can be formed in a size range of 1-15 μm[47], it is widely accepted that particles greater than 7 μm in diameter are cleared from the circulation by mechanical filtration in the lungs whereas those with a diameter smaller than 5 μm are taken up in the vasculature of the liver[92]. Thus controlling the size distribution of microspheres administered can facilitate passive targeting of the pulmonary vasculature for the delivery of drugs specific to the respiratory system[92]. Alternatively, Albunex[93] microspheres with a smaller number average diameter (4 μm) are subject to hepatic uptake as a result of macrophages present in the liver. In a study of the biodistribution of polystyrene spheres labelled with intercellular adhesion molecule 1 (ICAM-1) antibodies (ICAM-1 is upregulated in endothelial cells as a result of a number of disease states) it was found that spheres in the size range 1-10 μm were cleared from the blood circulation more quickly than sub-micron diameter spheres but that once inside the cell sub-micron spheres were transported much more rapidly into lysozomes[90]. These factors are important considerations in designing microsphere based drug delivery systems, however there is also significant interest in decorating the surface of microspheres in order to achieve site specific targeting of microspheres further reducing the occurrence of unwanted side effects.

Suslick *et al.* have used layer by layer deposition to functionalise the surface of BSA microspheres with peptides which contain sequences that are specific for intergrin receptors[83]. Intergrin receptors are known to be over-expressed in tumour cells so the peptides on the microsphere surface will cause the microspheres to accumulate in areas which have a high density of cancer cells and this has been demonstrated *in vitro* using colon tumour cells[83]. At the current time the localisation of microbubbles by targeting moieties is yet to be fully optimised, the quantity of microspheres that retain their ligands and reside at the target site is small[94], so there is significant scope for future

development. In an alternative approach to the classical layer by layer functionalisation of microspheres, Skirtenko *et al.*[40] report a one pot method to functionalise tetracyline loaded BSA microspheres with a thiol functionalised mannosyl derivative which can be bound by *E-coli*. Targeting the microspheres to *E-coli* facilitates maximum antibacterial activity of the loaded tetracyline and gives the synergistic effect of disabling the bacteria through agglutination[40].

As an adjunct to chemical and biological targeting the use of magnetic microbubbles is emerging as a method of increasing the dwell time of drug carriers in the vicinity of a desired administration site[95]. Magnetic nanoparticles alone are imperfect transport mediators, the diminutive magnetic strength which results from their small size means that a strong magnetic field must be applied in order to achieve effective localisation[95]. However systems incorporating magnetic nanoparticles within the shell of sonochemically produced protein microspheres, either via post production layer-by-layer deposition[96] or in one step using protein coated nanoparticles[97], are showing promise as effective targeted drug delivery agents.

Ultrasound Contrast Agents and Bimodal Imaging

Ultrasound is widely used in clinical applications for imaging parts of the body. The area under examination is irradiated with high frequency ultrasound (2-10 MHz[98]). When the sound waves reach boundaries between different tissue types some will be reflected as echoes due to the change in tissue density at the boundary. It is these echoes which are detected and processed to generate an image of the internal organs[99]. The intensity of the echoes reflected depends on the difference in density between the two tissue types. A large difference will result in more echoes and hence a greater signal intensity. Soft body tissues often have very similar densities and as a result it can be difficult to generate strong echo signals and achieve good contrast in the images generated[99]. Ultrasound contrast agents offer a solution to this problem and can be defined as follows:

> "An ultrasound contrast agent is an exogenous substance, consisting of gas or air microbubbles encapsulated by a shell of different

composition, that can be administered intravenously or into a body cavity to enhance ultrasonic signals."[99]

The difference in density between the gas encapsulated in the microsphere and the surrounding body tissues is large. This creates greater contrast in the image generated and allows tissues containing microspheres to be clearly distinguished. The microspheres commonly used in imaging have a diameter of between 2-6 μm and as such are confined to the blood pool[99]. As a result organs which are highly perfused will show strong contrast to other tissues.

Microbubbles have soft shells and are able to resonate with a sound wave and so have harmonic frequencies. The resonant frequency of a microsphere is dependent on its diameter[98]. Normal body tissue does not resonate and therefore does not have harmonics. Hence the tissue under investigation can be irradiated at the resonant frequency of the microspheres and the detector can be set to only detect a signal at twice the applied frequency (second harmonic). Any signal detected will be as a result of the microspheres, not the surrounding tissue, giving a clear indication of the distribution of blood in a tissue[98]. This can be particularly useful when screening for tumours which are known to be more highly perfused than normal tissue.

Ultrasound contrast agents need to be biocompatible, in particular the breakdown products must be readily processed and disposed of by the body so that side effects are minimised. It is also important that the microspheres used have a narrow size distribution. A broad size distribution would mean that the tissue would need to be irradiated with a wide range of ultrasound frequencies in order to generate a strong resonance field[98]. This would reduce the quality of the image produced. The *in vivo* half life of the microspheres must also be considered. At present the commercial microspheres used persist in the blood for a matter of minutes, for example, Levovist^{TM} (galactose based microspheres) is stable in the blood for 1-4 minutes[98]. It would be useful to develop microspheres which persist in the blood stream for longer to allow more detailed diagnosis to be carried out.

It is also possible to use microspheres for Magnetic Resonance Imaging (MRI). MRI imaging traditionally uses the signals from ^{1}H nuclei in water to image regions of tissue, ^{19}F can be used as an alternative

nucleus for MRI imaging[100]. The ^{19}F isotope is 100% abundant but is only present in the body as a solid (in teeth and bones) and is therefore not detectable by MRI. Hence small quantities of injected ^{19}F nuclei introduced into the body can be imaged without competition from naturally occurring nuclei[100]. Perfluorocarbons provide a sufficiently high local concentration of ^{19}F nuclei that an adequate signal to noise ratio can be achieved and the transit or localisation of small volumes of perfluorocarbons can be imaged in the body[101]. Webb *et al.* encapsulated perfluorocarbons within BSA microspheres to produce robust MRI agents which increased the observed signal to noise ratio by up to 300% compared to similar emulsions of the time[102]. Microbubbles that contain magnetic nanoparticles in their shells[95;96;103] can also be used as contrast agents for MRI. The nanoparticles provide contrast in ^{1}H-MRI by increasing the relaxation rate of protons adjacent to the microspheres and therefore reducing the signal observed in regions where microspheres are present[104]. These microbubbles provide the additional benefit of also being able to act as ultrasound contrast agents, bimodal imaging facilitates improved accuracy and greater flexibility in clinical diagnosis[95;96;103] .

Image aided delivery and triggered release

In surgical procedures using high intensity focussed ultrasound (HIFU) (1 MHz, typical peak negative acoustic pressure: 4.6 MPa)[29] it has been demonstrated that the presence of microbubbles can increase cavitation in the chosen location[25]. It has also been reported that low intensity diagnostic ultrasound irradiation (typical peak negative pressure 0.4 MPa)[105] *in vivo*, in the presence of microbubbles, can result in localised heating and some cavitation[106]. Ultrasound irradiation in the presence of microbubbles is known to improve drug and gene uptake[86;107;108]. This effect is given the umbrella term 'sonoporation'[107]. Although sonoporation has been shown empirically to aid uptake[86;107] the mechanisms involved are not fully understood. It is proposed that irradiation of a tissue with medical ultrasound (0.5-2 MHz[91]) in the presence of microspheres results in temporary perforation of cell walls facilitating delivery of molecules that would otherwise struggle to traverse the cell membrane readily, for example

DNA[86]. The upper pore size limit is estimated to be approximately 75 nm and the larger pores can be viewed by SEM[107]. The pores exist in a transient manner so delivery across the cell membrane is limited by the proximity of drug molecules to the pore sites, in this sense it is an asset to deliver the drug on the surface of the microbubbles. In this way it is more likely that the drug molecule can be propelled across the cell membrane by a micro-jet[107]. A more recent study has shed some further light on the mechanism, establishing that the shear stress induced by microstreaming in the vicinity of cavitating microbubbles causes increased F-actin production and cytoskeleton rearrangement, indicative of transient changes to the cell's structure[108]. Additionally it was found that sonochemically produced hydrogen peroxide resulted in increased membrane permeability to calcium ions, indicating that local effects of ultrasound irradiation have a notable effect on cell signalling and transport mechanisms. Finally there is evidence to show that cell viability is not changed by ultrasound irradiation and that the cell membrane integrity is restored within 30 minutes[108].

The sonoporation effect can be utilised to convey large molecules , e.g. DNA, into cells and to aid uptake of drugs either from the surface of microbubbles or co-administered with microbubbles. Ultrasound triggered delivery is appealing because it can be focussed accurately and precisely into a specific region of tissue to maximise therapeutic uptake and minimise unwanted side effects whilst being minimally invasive[13]. Sonochemically produced liquid filled microspheres have their primary application in drug delivery whereas traditionally sonochemically produced microbubbles have their application in imaging as ultrasound contrast agents.

Surface functionalisation of microbubbles, opens the opportunity for combined imaging and therapy[106]. Administration of microbubbles that have been surface-loaded with drug molecules can be guided by ultrasound imaging. Fokong *et al.*[23] report an example of polymer microbubbles which have been surface functionalised with antibodies to target tumour vasculature. The microbubbles could be clearly imaged in the tumour and subsequently burst open to release their pay load of 2 'model drug' fluorescent dyes (Rhodamine B and Coumarin 6)[23]. Hence sonochemically produced microspheres provide a straight forward method by which to form drug carriers which can act

simultaneously as imaging agents, opening up the potential for accurate, monitored delivery of a drug payload to a specific disease site.

Further to this Moehwald *et al.* demonstrate the use of protein microspheres containing a gel core to carry out temperature responsive release of a lipophilic drug, Indomethacin[109]. By incorporating a gelator, 12-hydroxystearic acid, into the vegetable oil core BSA microspheres could be formed which had a gel core at 25 °C but underwent a phase transition to an oil phase at 40 °C. The phase transition occurs as a result of breakdown of the hydrogen bonding network between the gelator molecules which removes the porous gel structure, causing the microspheres to shrink around the more compact liquid oil phase[109]. As a result drug release can be observed over a 20 hour period, culminating in 100% release, compared to 16% release observed at 25 °C. In control experiments it was demonstrated that similar behaviour was observed at 25 °C with simple gel particles (without the protein shell), this indicates that the protein shell adds little benefit to the stabilisation of the system on storage. This work opens up new potential for controlling drug release from protein microspheres in response to external stimuli by adapting the core substituents, it was suggested by the authors that these microspheres could be further adapted for temperature responsive release by incorporating light sensitive nanoparticles, e.g. gold aggregates into the shells of the protein containers to allow remotely controlled release by infra-red laser irradiation[109].

Topical Delivery

Beyond systemic delivery, sonochemically produced microspheres lend themselves well to topological delivery. There is evidence to show that protein microspheres can be attached to the fibre strands in cotton and polyester fabrics[110–112]. This is achieved by carrying out the standard sonochemical preparation procedure with a piece of fabric present in the protein solution. After extensive washing the microspheres can be seen to have been retained on the fabric fibres[112], although more so in the case of cotton than polyester. The significant question of how the microspheres attach to the fabric fibres

still remains unanswered but this methodology provides potential for future development, particularly in the production of antimicrobial fabrics for wound dressings.

An alternative approach is to trap microspheres containing the desired therapeutic molecules in a thin film, as demonstrated by Borodina *et al.*[88], with calcium alginate films. They were able to show that by entrapping Vitamin E in gum acacia microspheres release could be controlled and sustained over a much longer period than if vitamin E was entrapped in the film in its free state (100% release was observed after 96 hours as compared to 5 hours). Such biodegradable films have potential for use in topical delivery applications.

Other delivery applications

The ability to encapsulate molecules within a protein or polymeric shell has the potential for applications which extend beyond drug delivery and therapeutics. Flavour encapsulation is one area where the biocompatibility of microspheres could be utilised. By encapsulating flavour compounds and incorporating the microspheres formed into manufactured foods, for example biscuits, flavours could be locked away and protected from degradation processes increasing the shelf life of the food. The flavour would be released upon chewing as the microspheres were mechanically broken open. This would extend work already reported in the literature where flavour compounds are encapsulated in the matrix of an edible film[113].

Beyond flavour enhancement the same approach could also be used to encapsulate nutrients allowing foods to be fortified with a wider range or higher concentration of nutrients than would naturally be present, possibly an important application in an ever more health conscious society. Nutrient encapsulation has previously been demonstrated using emulsion technology to fortify processed cheese with an emulsion of fish oil in order to provide the consumer with an alternative source of omega 3 oils[114] and there have been other examples of proteins used for nutrient delivery[115]. Microspheres would provide an alternative approach to delivering these so-called nutraceuticals by stabilising the emulsion over a longer time period, improving the product shelf life.

Protein microspheres have been investigated as potential carriers for fragrant molecules; Gedanken *et al*. have demonstrated that fragrance can be released over a 24 hour period if amyl acetate, a fragrant oil, is encapsulated within BSA microspheres[116]. Considered alongside the recent developments in modification of fabrics with microspheres (discussed above) this system has potential for slow release fragrances built into fabric products

A further potential application for biodegradable microspheres is in fertiliser and pesticide release. Over application of fertilisers and pesticides is a well known environmental problem. Slow release of chemicals could be achieved by applying a solution of microspheres which degraded over a period of days or weeks gradually releasing a known quantity of chemical which had been tuned to meet the needs of the crop. Hence the problems of run off and pollution could be reduced without the need for multiple applications. There does not appear to be a precedent yet for encapsulation of agricultural chemicals in microspheres, although some similar work has been reported based on polyelectrolyte complexes[117].

2 Experimental methods

2.1 Chapter 3: Lysozyme and poly(methacrylic acid) microspheres

All reagents were purchased from Sigma Aldrich and used without further purification.

A Bruker Avance 300 MHz NMR was used to collect the ^{1}H NMR spectra used during this study. DOSY NMR experiments were performed using the 400 MHz Bruker Avance NMR spectrometer. The DOSY spectra were acquired using the ledbpgp2s pulse program provided with the Bruker topspin software The gradient strength was incremented in 8 steps from 5 to 95% of the total gradient strength. The gradient pulse length was set at 4 ms to ensure full signal attenuation and the relaxation delay was 5 s (5 x T_1 relaxation). The probe head temperature was kept at 298 K during the experiments. The data set was processed using the dosy2d program provided with the Bruker topspin software.

Fluorescence images were captured using an Olympus IX71 microscope fitted with a mercury lamp. Optical microscopy images were captured using a GX optical L3001 microscope fitted with an Infinity 2 camera. Laser scanning confocal microscopy experiments were carried out using a Zeiss LSM 510 META microscope at the University of Bath Microscopy and Analysis Suite.

The microsphere diameters were measured from the optical micrographs taken. A calibration slide was used to define the length scale in terms of μm/pixel. Measurements were made using the freely available graphics software ImageJ 1.42q. A sample size of 75-100 microspheres was typically used to estimate size distributions.

UV/VIS spectra were collected using an Agilent 8453 spectrophotometer and quartz cuvette (path length: 1 cm). Fluorescence spectra were collected using a Perkin Elmer LS 55 luminescence spectrometer (excitation slit: 10.0 nm, emmission slit: 4.0 nm, scan speed: 300 nm/min).

Fourier Transform Infra-Red (FTIR) spectra were collected using a Perkin Elmer FT-IR Spectrometer fitted with an ATIR (Diamond PIKE MIRacle) attachment. Raman spectra were collected using a Renishaw inVia Raman microscope. In both cases the samples were oven dried as amorphous powders prior to measurement.

Two ultrasonic generators were used during the course of this study; generator A: a Branson digital sonifier (20 kHz/400 W) connected to a horn with a microtip (diameter: 3 mm) at the University of Melbourne and generator B: a Sonics and Materials VC600 generator (23 kHz/600W) also connected to a horn with a microtip (diameter 3 mm) at the University of Bath.

2.1.1 Calibration of ultrasound generator B and horn

100 g of de-ionised water, equilibrated to the ambient room temperature, was accurately measured into a 150 mL beaker. The micro-tip was positioned in the mid-depth of the water and the water was sonicated at a chosen arbitrary power level. The temperature was monitored with a thermocouple over a known time period in order to establish the heat energy dissipated into the water. The power output of the horn was then calculated as a function of the surface area of end of the micro-tip using equation 2.1 where P: power, m: mass, c: specific heat capacity of water, T: temperature, t: time and SA: tip surface area. The surface area was calculated from the tip diameter which was measured with callipers. The measured intensities are reported in Table 2.1 and are used in this and forthcoming chapters.

$$P = \left(\frac{mc\Delta T}{\Delta t} \right) / SA \tag{2.1}$$

Power level	Power dissipated / W	Intensity / Wcm^{-2}
1	2.0	7
2	4.0	14
3	8.1	29
4	13	45

Table 2.1: Ultrasonic intensities calculated from thermal calorimetry data for generator B.

2.1.2 Air filled lysozyme microspheres

Figure 2.1 shows the experimental set up for microsphere production used with generator B in the laboratories at Bath (which was identical to the set up used with generator A in the laboratories at Melbourne). The tip of the horn was placed at the solution-air interface in order to maximise foaming, promoting microsphere formation. If the protocol is carried out with the tip submerged in the protein solution then microsphere production is negligible. The large scale photograph in figure 2.1 was taken during sonication and shows the foaming achieved with the tip positioned at the interface.

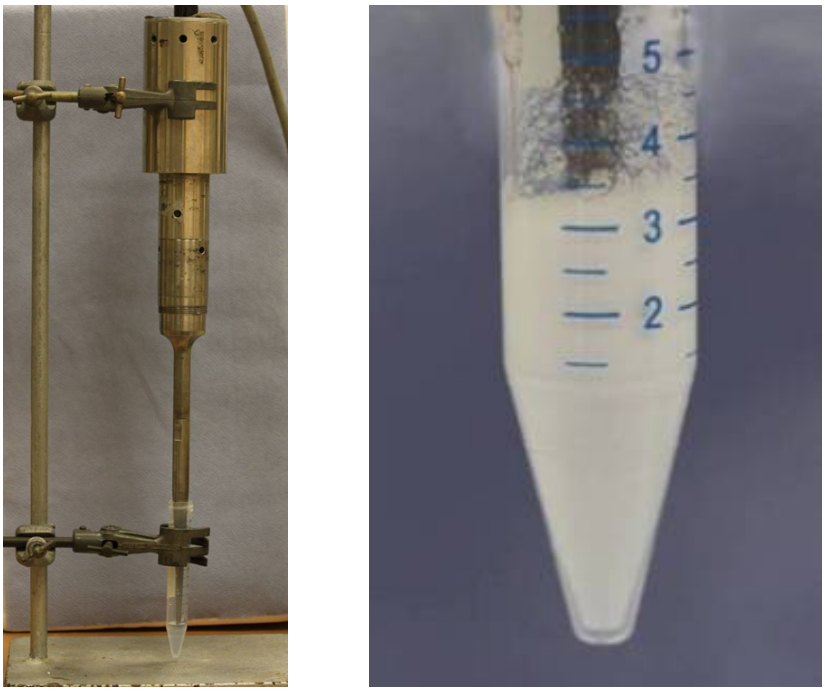

Figure 2.1: Experimental apparatus for microsphere production, horn transducer attached to generator B and the microsphere suspension during sonication.

In a 15 mL plastic centrifuge tube, 50 mg of lysozyme was dissolved in 1 mL of 50 mM pH 8 tris(hydroxymethyl)aminomethane (tris) buffer and left to stand for 1 hour. 30 mg of DL-dithiothreitol (DTT) was added to the lysozyme solution and left to stand at 22 °C for 2 minutes. The horn tip was placed at the air:water interface and the solution was sonicated at 7, 14, 29 or 45 Wcm^{-2} for the required time (15-60 s). After sonication the solution was diluted up to 14 mL with deionised water and left to stand overnight. The microspheres formed were washed by replacing the deionised water 5 times at 6 – 24 hour intervals.

2.1.3 Tetradecane filled lysozyme microspheres

In a 15 mL plastic centrifuge tube, 50 mg of lysozyme was dissolved in 1 mL of 50 mM pH 8 Tris buffer and left to stand for 1 hour. 30 mg of DTT was added to the lysozyme solution and left to stand at 22 °C for 2 minutes. 100 μL of tetradecane was layered on top of the lysozyme solution. The horn tip was then placed at the oil:water interface and the solution was sonicated at 7, 14, 29 or 45 Wcm^{-2} for the required time (15-60 s). After sonication the solution was diluted up to 14 mL with deionised water and left to stand overnight. The microspheres formed were washed by replacing the deionised water 5 times at 6 – 24 hour intervals. For the encapsulation studies tetradecane saturated with nile red was used.

The yield of tetradecane filled microspheres was estimated by imaging an accurately measured volume of microsphere suspension by optical microscopy. The number of microspheres in the micrographs taken was scaled to represent the contents of the coverslip and in turn the total population of microspheres produced. The extent of encapsulation was estimated from the mean diameter of the microspheres measured and the estimated microsphere population.

2.1.4 High speed video imaging

The video footage was collected according to the method reported by T.J. Tiong[118]. "A high-intensity white light connected to a fibre-optic tube was used to shine through a 3.5 mL cuvette without giving out much heat as compared to a xenon light source. The light source used

for our experiment was a Solarc®-powered metal-halide light (Everest VIT, ELSV-60 light source operating at 90-240 VAC 50-400 Hz, 1 A (@ 120 VAC). The experiments were performed by using a high speed video camera (Photron FASTCAM Digital Video Recorder (DVR)), mounted onto a Navitar 18-108 mm zoom lens with an aperture value of f2.8. The videos were captured at 1000 frames per second, so as to obtain a good resolution per frame rate ratio for all the files taken. Videos were exported out on two different formats: Bitmap (.bmp) and Audio Video Interleave (.avi) for both image frames and videos respectively"[118]. Microsphere preparation was carried out as per the standard protocol but in a 3.5 mL cuvette to facilitate filming of the microspheres.

2.1.5 Fluorescent staining of air filled lysozyme microspheres

500 μL of air filled microspheres in aqueous suspension were added to a concentrated aqueous solution of Fluorescein isothiocyanate isomer 1 and left to stand for 10 minutes.

2.1.6 SEM sample preparation

Scanning electron microscopy (SEM) micrographs were taken at the SEM facility (FEI Quanta) in the Bio 21 Institute, University of Melbourne. Samples were prepared for SEM by first drying in air on a SEM stub covered with carbon tape and then sputter coating with a thin film of gold.

2.1.7 Incubation of air filled lysozyme microspheres with DTT

A sample of air filled microspheres was made according to the procedure in section 2.1.2. A 1 mL aliquot of concentrated microsphere suspension was collected from the surface of the washed solution and placed in a plastic vial. 60 mg of DTT was added to the suspension; the

suspension was shaken gently and left to stand at room temperature for 24 hours.

2.1.8 Homogenisation of aqueous lysozyme solution

A 50 mg/mL solution of lysozyme solution in 50 mM tris buffer was treated with 30 mg/mL DTT at 22 °C for 2 minutes and then homogenised at 24000 rpm for 1 minute at the air:water interface with a IKA T18 basic Ultra-turrax homogeniser.

2.1.9 *tert*-butanol radical trapping

Air filled lysozyme microspheres were synthesised according to the procedure in section 2.1.2. Directly prior to sonication (after treatment with DTT) 10 μL of tert-butanol was charged to the lysozyme solution. The solution was sonicated for 1 min at 14 Wcm^{-2}.

2.1.10 Superoxide radical trapping

Air filled lysozyme microspheres were synthesised according to the procedure in section 2.1.2. Directly prior to sonication (after treatment with DTT) a prescribed portion of 0.1599 mg/mL superoxide dismutase (SOD) in 0.1 M phosphate buffer at pH 7.5 was added to the lysozyme solution. The solution was sonicated for 1 min at 14 Wcm^{-2}.

2.1.11 Sonochemiluminescence imaging with luminol

The distribution of the cavitation cloud produced by the horn and microtip attached generator B was mapped by photographing (in a dark box) the sonochemiluminescence generated in a luminol solution when sonicated. Luminol solution: 1 mM luminol and 0.1 mM Ethylenediaminetetracetic acid (EDTA) in aqueous solution buffered to pH 12 with sodium hydroxide. 0.1 mM of hydrogen peroxide was added to the solution immediately prior to sonication. A Canon EOS 500D camera was used with a 60 mm EF-S macro lens. Camera settings: F2.8, ISO 3200, focal length: 20 cm, exposure: 30 s.

2.1.12 Measurement of Sonoluminescence

The experimental setup used for this experiment was that used by Lee *et al.*[119] 200 mL of MilliQ water (18.2 MΩ·cm) was placed in a cylindrical Pyrex cell which was mounted over a 35 mm 236 kHz flat plate unfocused transducer. The transducer was connected to a 236 kHz generator (Undatim Ultrasonics D-reactor). The power was adjustable between 0 and 100 W. The generator had been modified in-house to allow pulsed energy delivery so that both the pulse on and off time could be varied. For this investigation the acoustic pulse was fixed at 4 ms on and 12 ms off. The power amplitude used was 40 %. An end on photomultiplier tube (Hamamatsu model No. R647-04) was used to record the sonoluminescence intensity. The output from the photomultiplier was fed to a digital oscilloscope (Tektronix, model no. TDS 320). The oscilloscope was triggered by the ultrasound generator and recorded the signals at set time intervals. The equipment was set up within a light proof box. For the first experiment air saturated water was used. For the second the water was degassed under a vacuum for 20 minutes before sonication. In the final experiment 2 mL of a concentrated suspension of air filled microspheres was added to the degassed water before sonication.

2.1.13 Synthesis of PMA_{SH}

10 g of 30 wt% PMA sodium salt solution (4 kDa) (0.83 mmol of PMA) was diluted into 200 mL of 0.1 M pH 7.2 phosphate buffer in a 500 mL round bottomed flask. 2.8 g (18 mmol) of N-ethyl-N´-(3-dimethylaminopropyl)carbodiimide (EDC) and 2.0 g (18 mmol) of N-hydroxysuccinimide (NHS) were charged to the solution and the solution was allowed to stir for 15 minutes. 2.1 g (18 mmol) of cysteamine HCl was charged to the solution. The solution was left to stir overnight at room temperature. The reaction solution was dialysed for 5 days in deionised water. The polymer was then isolated using a rotary evaporator, re-dissolved in a small volume of deionised water and precipitated in a 10x excess of 1:1 methanol:diethyl ether. The precipitated polymer was collected by vacum filtration and dried under a vacuum at 40 °C. Yield: 2.43 g (20%). ^{1}H-NMR (250 MHz, D_2O)

δ: 0.84 (3H, br m), 1.12 (br t), 1.56 (1H, br m), 1.96 (1H, br m), 2.90 (2H, br m), 3.06 (br m), 3.20 (br d), 3.28 (br t), 3.46 (br t), 3.55 (2H, br m), 3.86 (br t) ppm.

2.1.14 PMA_{SH} tetradecane or perfluorohexane filled microspheres

A 50 mg/mL solution of PMA_{SH} (prepared according to the procedure in section 2.1.13) was made up in 1 mL of 50 mM pH 8 Tris buffer. 50 μL of tetradecane or perfluorohexane was placed in a layer on top of the PMA_{SH} solution. The horn tip was then placed at the oil:water interface and the solution was sonicated for 60 s at 14 Wcm^{-2}. After sonication the solution was diluted up to 14 mL with deionised water and left to stand overnight. The microspheres formed were washed by replacing the deionised water 5 times at 6 – 24 hour intervals.

2.1.15 Homogenisation of PMA_{SH}

A 50 mg/mL solution of PMA_{SH} in 50 mM Tris buffer was acidified to form a small amount of fine white precipitate and then homogenised at 24000 rpm at the air:water interface with a IKA T18 basic ultra-turrax for 1 minute.

2.1.16 Surface tension measurements

The surface tension of lysozyme and PMA_{SH} solutions were measured using an Attension Sigma701 tensiometer (KSV Instruments) fitted with a Du Noüy ring. All solutions were prepared in deionised water (Milli Q, 18.2 MΩ·cm). The surface tension was measured continuously in a cyclical manner until a constant value was reached. In the case of denatured lysozyme the solution was treated with 30 mg/mL DTT for two minutes directly prior to measurement.

2.1.17 Effect of external pH

PMA_{SH} microspheres were produced from a 40 mg/mL solution of PMA_{SH} in tris buffer according to the method described in section

2.1.14 and left to stand overnight. 100 μL of microsphere suspension was mixed with 200 μL of 100 mM phosphate buffer at pH 4,5,6,7,8 or 9, left to stand for 2 hours and observed under the optical microscope.

2.1.18 Release of nile red from lysozyme microspheres

Lysozyme microspheres were formed from 50 μL of nile red saturated tetradecane using the method described in section 2.1.2, sonicating at 14 Wcm^{-2} for 1 minute. The batches of microspheres were dialysed into 10 mL of deionised (MilliQ, 18.2 MΩ·cm) water or DMSO for 24 hours. The microspheres were then broken by sonication at 40 Wcm^{-2} for 2 minutes and returned to the dialysis system for a further 24 hours. Samples were taken from the dialysis receptor before and after sonication. In the aqueous dialysis the samples were freeze dried and the residues re-dissolved in DMSO. The samples were analysed for nile red concentration by fluorescence intensity, ex: 550 nm, em: 630 nm. The fluorescence intensities measured were within the linear range established upon calibration with standard DMSO solutions of nile red, Figure 2.2.

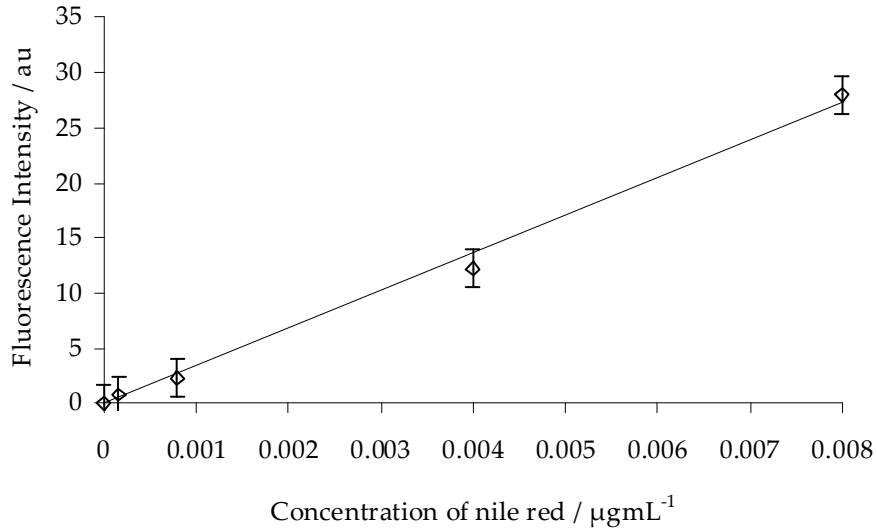

Figure 2.2: Fluorescence calibration plot for nile red in DMSO

2.1.19 Release of sudan III from PMA_{SH} microspheres

PMA_{SH} microspheres were formed from a 50 mg/mL solution of PMA_{SH} with 50 μL of tetradecane saturated with sudan III according to the method described in section 2.1.14, sonicating at 14 Wcm^{-2} for 1 minute. The microsphere suspensions were treated either with 60 mg/mL DTT, or sonication at 40 Wcm^{-2} for 2 minutes, or acidification to pH 1 with HCl or pH 14 with NaOH. The released oil phase was extracted into 2 mL of isopropyl mysristate (IPM) by gentle shaking of the two phases together for two minutes, the IPM phase was then immediately removed. The concentration of sudan III was quantified by UV/VIS spectroscopy, the linear range of absorbance was established from standard solutions of sudan III in IPM, ε: 0.0267 μmol^{-1} dm^3 cm^{-1}, Figure 2.3.

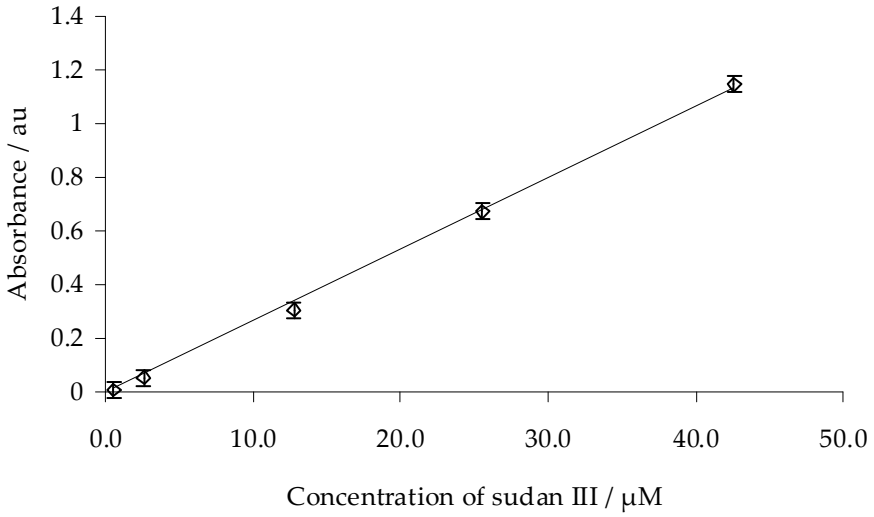

Figure 2.3: UV/VIS calibration plot for sudan III in IPM

2.2 Chapter 3: Thiol-ene chemistry

All chemicals used were purchased from Sigma Aldrich and used as received (with the exception of 2,2-diphenyl-1-picryhydrazyl which was purchased from Fluka).

Samples for absorbance were measured using an Agilent 8453 UV-Visible Spectrophotometer with a quartz cuvette, path length: 1 cm. Samples for fluorescence were measured using a Gilden Photonics FluoroSENS fluorimeter with a polystyrene cuvette.

The ultrasound generators used were a Sonics and Materials VC600 generator (20 kHz / 600W) (generator B) connected to an ultrasound horn fitted with a micro-tip (3 mm diameter) and a Sonic Systems Sonic Processor L500-20 generator fitted with a 20 kHz Horn attachment (generator C). The generator was calibrated for ultrasonic intensity at each arbitrary power level according to the method described in section 2.1.1, see Table 2.2.

Power level	Power dissipated / W	Intensity / Wcm^{-2}
2	4.5	3.8
4	9.1	7.6
6	14	11
8	20	17
10	25	21

Table 2.2: Ultrasonic intensities calculated from thermal calorimetry data for generator C.

Bruker Avance 250 and 400 MHz NMR spectrometers were used to collect the ^{1}H-NMR spectra.

Samples for GC and GCMS analysis were prepared by taking a 300 μL sample from the reaction which was made up to 1500 μL with methanol diluent.

GC method: Samples were analysed for % conversion on an Agilent 6890N Network GC System using the following method: Injection volume: 1.0 μL, N2 carrier gas, Split Ratio: 50.0, Flow rate: 2 mL/min, FID detector temperature: 300 °C, Column: Agilent 19091J-413 HP-5 5% Phenyl Methyl Siloxane 300 m x 320 μm x 0.25 μm, Temperature program: starting temperature; 50 °C, ramp: 40 °C/min to 70 °C (hold

for 0.25 min), ramp: 60 °C/min to 85 °C, ramp 15 °C/min to 100 °C, ramp 100 °C/min to 300 °C (hold for 4 min).

Alkene	Alkene RT / min	Thioether RT / min
Norbornene	2.17	5.32
Butyl vinyl ether	2.07	5.12
N-isopropylacrylamide	3.34	5.89
1-heptene	2.05	5.21
1-pentene	1.78	4.42
Allyl amine	1.82	n/a
Allyl butyl ether	2.38	5.45

Table 2.3: GC retention times (RT)

GC-MS method: Thioether products were identified by GCMS analysis using an EI-MS Agilent 5975C inert MSD Triple Axis Detector coupled to an Agilent 7890A GC System with a HP 5MS 30 m x 25 mm x 0.25 μm column: carrier gas: He, flow rate: 2 mL/min, split ratio: 10:1, inlet temperature: 300 °C, oven temperature ramp: 20 °C/min from 70 °C to 230 °C, FID: 300 °C, MS Source 230 °C, MS Quad 150 °C.

Alkene	Alkene RT / min	Thioether RT / min
Norbornene	2.7	9.8
Butyl vinyl ether	2.4	9.4
N-isopropylacrylamide	6.3-6.7	11.1
1-heptene	2.3	9.58
1-pentene	n/a	8.1
Allyl amine	1.65	n/a
Allyl butyl ether	3.7	10.0

Table 2.4: GCMS retention times (RT)

2.2.1 DPPH dosimetry

Radical production was quantified using a 0.08 mM solution of 2,2-diphenyl-1-picryhydrazyl (DPPH) in toluene. In the sonochemical case a 4 necked pear shaped flask was assembled with the ultrasound horn connected to generator C. 90 mL of DPPH solution and the prescribed amount of 2,2'-Azobis(2-methylpropionitrile) (AIBN) were then charged to the flask. The solution was purged with nitrogen for 45 minutes at a moderate flow. The solution was cooled to 24 °C

with a constant water flow. The nitrogen flow was then reduced to a slow flow in order to maintain a positive pressure of nitrogen in the flask. The solution was sonicated for 20-60 minutes at an intensity of 17 W/cm^{-2}. Samples were taken at periodic time intervals and the absorption was measured at a wavelength of 520 nm, all samples taken were within a linear concentration range for absorbance, ε: 1.135 mol^{-1} dm^3 cm^{-1}, Figure 2.4.

In the thermal case the glassware was assembled as in the protocol detailed below. 25 mL of DPPH solution was charged to the flask and the solution was purged with nitrogen for 15 minutes. The solution was then heated to 50 °C. When at 50 °C, the prescribed amount of AIBN was charged as a solution in 5 mL of toluene. Samples were taken periodically over a 10 minute period and the absorbance measured as in the sonochemical case.

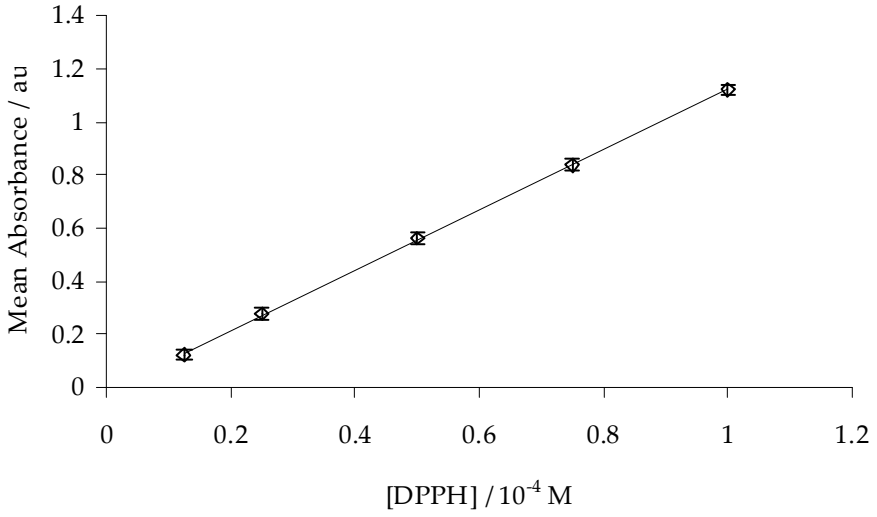

Figure 2.4: UV/VIS DPPH calibration in toluene at 520 nm.

2.2.2 Terephthalic acid dosimetry

Radical mediated production of fluorescent 2-hydroxyterephthalic acid (HTA) from an aqueous solution of terephthalic acid (TA) can be used to gain a measure of relative rates of radical production in thermal and sonochemical systems. HTA production, and therefore,

the change in solution fluorescence is directly proportional to radical production in a given system. Comparison of the rate of change of fluorescence in different systems can be used as a means to compare the radical production in those systems.

In order to conduct the sonochemical dosimetry 85 mL of a 0.0002 M solution of TA in pH 8 phosphate buffer and 0.04 g (0.15 mmol, 1.75 mM) of potassium persulfate were charged to the 4 necked pear shaped flask (assembled with the ultrasound horn connected to generator C). The solution was cooled to 24 °C with a constant water flow. The solution was sonicated for 60 minutes at an intensity of 17 W/cm^{-2}. Samples were taken at periodic time intervals and fluorescence was measured using an excitation frequency of 310 nm and an emission frequency of 410 nm.

The thermal dosimetry was conducted in a similar manner using the apparatus described below. 20 mL of 0.0002 M TA solution in pH 8 phosphate buffer was heated to 45 °C and 0.012 g (0.04 mmol, 1.75 mM) of potassium persulfate in 5 mL of TA solution was then charged to the flask. Samples were taken periodically over a 60 minute time period and the fluorescence of each sample was measured as above. All samples measured were within the linear range shown in Figure 2.5.

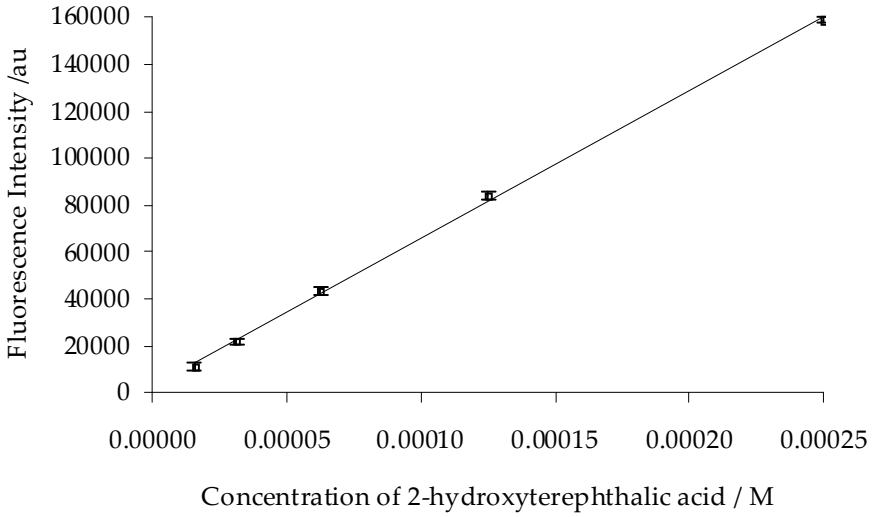

Figure 2.5: Calibration of the fluorescence 2-hydroxyterephthalic acid in aqueous solution.

2.2.3 Sonochemical protocol in toluene with AIBN

85 mL of toluene and 0.3 g (18 mmol., 0.03 molar eq.) of AIBN were charged to a 3 necked pear shaped jacketed flask which fitted the ultrasound horn assembly for generator C. The flask was fitted with a thermocouple and the jacket was cooled to 24 °C with a constant water flow. The flask was covered to protect it from ambient UV light. The flask was sealed and purged with nitrogen for 45 minutes on a moderate flow rate. After purging a slow flow of nitrogen was maintained. 55 mmol (limiting reagent) of alkene and 9 mL (83 mmol, 1.5 molar eq.) of 1-butanethiol were charged to the reaction flask by injection. The reaction was then sonicated at an intensity of 17 Wcm^{-2} for 4 hours. Regular samples were taken during the reaction time and analysed by GC and GC-MS (see details above). Control reactions were carried out according to this procedure but omitting the AIBN charge.

2.2.4 Optimised sonochemical reaction conditions for butyl-vinyl-ether in toluene with AIBN:

The reaction was conducted according to the protocol described in section 2.2.3, but with a higher ultrasound intensity (21 Wcm^{-2}) and the following reagent charges: 7.2 mL (55 mmol, limiting reagent) of butyl vinyl ether, 30 mL (278 mmol, 5 molar eq.) of 1-butanethiol, 0.9 g (54 mmol, 0.09 molar eq.) of AIBN and 50 mL of toluene.

2.2.5 Thermal protocol in toluene with AIBN

25 mL of toluene was charged to a 2 necked 50 mL round bottomed flask fitted with a thermometer and a magnetic stirrer hot plate assembly. The flask was covered to protect it from ambient UV light. The flask was then sealed and purged with nitrogen for 15 minutes on a moderate flow rate. After purging, a slow flow of nitrogen was maintained and the flask was heated to 50 °C. Once the solvent was at 50 °C, 6.6 mmol (limiting reagent) of alkene and 9.9 mmol (1.5 molar eq.) of 1-butanethiol were charged to the flask. The reaction was started by charging 0.025 g (0.15 mmol, 0.02 molar eq.) of AIBN in 5

mL of toluene to the reaction. The reaction was allowed to proceed for 2 hours. Regular samples were taken during the reaction time and analysed by GC and GC-MS. Control reactions were carried out according to this procedure but omitting the AIBN charge.

2.2.6 Sonochemical protocol in water with potassium persulfate

85 mL of de-ionised water, 6.6 mmol (limiting reagent) of alkene, 0.04 g (0.15 mmol., 0.02 molar eq.) of potassium persulfate ($K_2S_2O_8$) and 3.75 g (33 mmol., 5 molar eq.) of cysteamine HCl were charged to a 3 necked pear shaped jacketed flask which fitted the ultrasound horn assembly for generator C. The flask was fitted with a thermocouple and the jacket was cooled to 24 °C with a constant water flow. The flask was covered to protect it from ambient UV light. The reaction was then sonicated at an intensity of 17 Wcm^{-2} for 2 hours. Regular samples were taken during the reaction time, quenched into 2 wt% hydroquinone solution in D_2O to prevent any further reaction and analysed for conversion by ^{1}H-NMR. Control reactions were carried out according to this procedure but omitting the potassium persulfate charge.

2.2.7 Thermal protocol in water with potassium persulfate

25 mL of deionised water, 1.95 mmol. (limiting reagent) of alkene, 1.12 g (9.86 mmol., 5 molar eq.) of cysteamine HCl and 0.012 g (0.04 mmol 0.02 molar eq.) of $K_2S_2O_8$ was charged to a 2 necked 50 mL round bottomed flask fitted with a thermometer and a magnetic stirrer hot plate assembly. The flask was covered to protect it from ambient UV light. The flask was heated to 45 °C. The reaction was allowed to proceed for 2 hours. Regular samples were taken during the reaction time, quenched into 2 wt% hydroquinone solution in D_2O to prevent any further reaction and analysed for conversion by ^{1}H-NMR. Control reactions were carried out according to this procedure but omitting the $K_2S_2O_8$ charge.

Alkene	Alkene CH_2(ppm)	Thioether CH_2(ppm)
4-pentenoic acid	5.8 (2H, m)	1.5 (2H, m)
3-allyloxy-2-hydroxy-1-propanesulfonic acid	5.9 (1H, dd)	1.8 (2H, m)
N-isopropylacrylamide	5.6 (1H, dd)	2.4 (2H, t)
Allyl alcohol	5.9 (1H, dd)	1.8 (2H, m)
Acrylamide	6.2 (2H, d)	2.5 (2H, t)
Allyl amine	5.8 (2H, m)	3.2 (2H, t)

Table 2.5: ^{1}H-NMR Marker peaks.

2.2.8 PMA_{ene} synthesis

10 g of 30 wt% PMA sodium salt solution (4 kDa) (0.83 mmol of PMA) was diluted into 200 mL of 0.1 M pH 7.2 phosphate buffer in a 500 mL round bottomed flask. 2.8 g (18 mmol) of N-ethyl-N´-(3-dimethylaminopropyl)carbodiimide (EDC) and 2.0 g (18 mmol) of N-hydroxysuccinimide (NHS) were charged to the solution and the solution was allowed to stir for 15 minutes. 1.4 mL (18 mmol) of allyl amine was charged to the solution. The solution was left to stir overnight at room temperature. The reaction solution was dialysed for 5 days in deionised water. The polymer was then isolated using a rotary evaporator, re-dissolved in a small volume of deionised water and precipitated in a 10x excess of 1:1 methanol:diethyl ether. The precipitated polymer was collected by vacuum filtration and dried under a vacuum at 40 °C. Yield: 0.3 g (3%). ^{1}H-NMR (400 MHz, D_2O) δ: 0.88 (3H, br m), 1.09 (t), 1.60 (1H, br m), 1.85 (1H, br m), 2.56 (s), 2.785 (s), 3.26 (q), 3.48 (d), 3.69 (2H, br m), 5.09 (2H, br m), 5.36 ppm (1H, br m).

2.2.9 PMA_{ene}/DTT microsphere production

50 mg of PMA_{ene} was made up in 1 mL of pH 8 50 mM tris buffer, 35 mg (0.23 mmol, 2 mol. eq.) of DTT was charged to the solution and the solution was then sonicated at 14 Wcm^{-2} for 30 s with 100 μL of tetradecane (using generator B). After sonication the solution was diluted up to 14 mL with deionised water and left to stand overnight. The microspheres formed were washed by replacing the deionised water 5 times at 6 – 24 hour intervals.

2.3 Chapter 4: Water in oil emulsion filled microspheres

All chemicals were purchased from Sigma Aldrich and were used as received. Generator B was used in the microsphere synthesis and release studies.

Dynamic light scattering (DLS) studies were carried out using a Malvern Nano-S instrument.

Optical micrographs were captured using a GX optical L3001 microscope fitted with an Infinity 2 camera. Laser scanning confocal microscopy experiments were carried out using a Zeiss LSM 510 META microscope.

Fluorescence experiments were carried out using a Spectrostar Omega plate reader (BMG Labtech) with NUNC 12 plates, the cycle time was 299s, 20 flashes per cycle with double orbital shaking at a frequency of 300 rpm for 289 s after each cycle, excitation filter; 485 nm, emission filter; 520 nm.

A Mettler Toledo Seven Easy conductivity meter was used to carry out the conductivity measurements together with a Techne Tempette Junior TE-8J water bath.

HPLC method for 5FU: Dionex machine (Sunnyvale, CA, USA). Column: HiQ Sil C_{18}HS 250×4.6 mm, Flow rate: 0.7 mL/min, Mobile phase: 40:60 methanol:water, Temperature 25 ºC, UV detection wavelength: 265 nm, Injection volume: 20 μL, Run time: 15 minutes, 5-fluorouracil retention time: 4.7 - 4.9 min.

2.3.1 w/o emulsion preparation

An oil phase of tetradecane containing Span 80® and an aqueous phase of pure water or sodium chloride solution were sonicated at the oil : water interface at a power of 45 Wcm^{-2}. The initial experiments covered a variety of different conditions, the following optimised conditions were chosen for later experiments: oil phase: 4 wt% Span 80® in tetradecane, aqueous phase: 1 M $NaCl_{(aq)}$, emulsion: 40% aqueous phase, sonication time: 5 minutes.

2.3.2 Dynamic Light Scattering (DLS)

Water in oil emulsions were prepared as detailed in section 2.3.1 then diluted to achieve a 4 wt% water fraction. The Span 80® concentration in the diluent tetradecane was matched to the Span 80® concentration in the w/o continuous phase. Samples were measured in a 4 mL polystyrene disposable cuvette.

2.3.3 w/o emulsion filled lysozyme microspheres

In a 15 mL plastic centrifuge tube, 50 mg of lysozyme was dissolved in 1 mL of 50 mM pH 8 Tris buffer and left to stand for 1 hour. 30 mg of DTT was charged to the lysozyme solution and left to stand for 2 minutes. 100 μL of freshly prepared w/o emulsion was layered on the surface of the lysozyme solution. The horn tip was placed at the emulsion:water interface and the system was sonicated for 30 s at 14 Wcm^{-2}. After sonication the suspension was diluted to 15 mL with deionised water and left to stand overnight. If required, the suspension of microspheres was washed, by sequential re-dilution of the creamed suspension in clean deionised water.

2.3.4 w/o emulsion filled PMA_{SH} microspheres

In a 15 mL plastic centrifuge tube, 50 mg of PMA_{SH} was dissolved in 1 mL of 50 mM pH 8 Tris buffer, the solution was slightly acidified. 100 μL of freshly prepared w/o emulsion was layered on the surface of the lysozyme solution. The horn tip was placed at the oil:water interface and the system was sonicated for 30 s at 14 Wcm^{-2}. After sonication the suspension was diluted to 15 mL with deionised water and left to stand overnight. If required, the suspension of microspheres was washed by sequential re-dilution of the creamed suspension in clean deionised water. Samples for confocal microscopy were prepared using a w/o emulsion in which the tetradecane phase was saturated with nile red and/or the aqueous phase contained 1 mM 5(6)-carboxyfluorescein.

2.3.5 Laser Scanning Confocal Microscopy

The LSCM experiments were carried out using a Zeiss LSM 510 META microscope. The samples were prepared as per the protocols in section 2.3.3 and 2.3.4 with 1 mM carboxyfluorescein solution in 10 mM HEPEs buffer as the internal aqueous phase and 4 wt% Span 80® tetradecane saturated with nile red as the oil phase. In analysis of the micrographs gathered co-localised pixels with an intensity greater than 100 grays were removed, leaving an image that showed only those pixels which were not colocalised.

2.3.6 Release of 5(6)-carboxyfluorescein

These experiments were carried out using a Spectrostar Omega Plate reader (BMG Labtech). NUNC 12 plates were used and the machine settings were as follows: cycle time; 299 s, 20 flashes per well and cycle, double orbital shaking with a frequency of 300 rpm for 289 s after each cycle, excitation filter; 485 nm, emission filter; 520 nm. The fluorescence intensity was calibrated to carboxyfluorescein concentration using carboxyfluorescein solutions made up in 10 mM HEPEs buffer. Experiments were conducted within this concentration range that had a linear relationship with fluorescence intensity. Microsphere samples were prepared according to the protocol detailed in sections 2.3.3 and 2.3.4 using a w/o emulsion containing 50 mM 5(6)-carboxyfluorescein in 10 mM HEPEs buffer. The microsphere suspension was washed once before the release experiment was carried out. Release was monitored using the fluorescence plate reader, each well contained 50 μL of microsphere suspension in 2 mL of HEPES buffer with the prescribed amount of DTT. Fluorescence was measured at 5 minute intervals over a 12 hour time period, during which time the plate was incubated at 37 °C. Each DTT concentration was run in triplicate.

In the case of mechanical breakdown by ultrasound (45 Wcm^{-2}), triplicate 50 μL samples were taken from the microsphere suspension at chosen time points and diluted for measurement on the plate reader as described above. For both experiments the fluorescence measured was within the linear range shown in Figure 2.6.

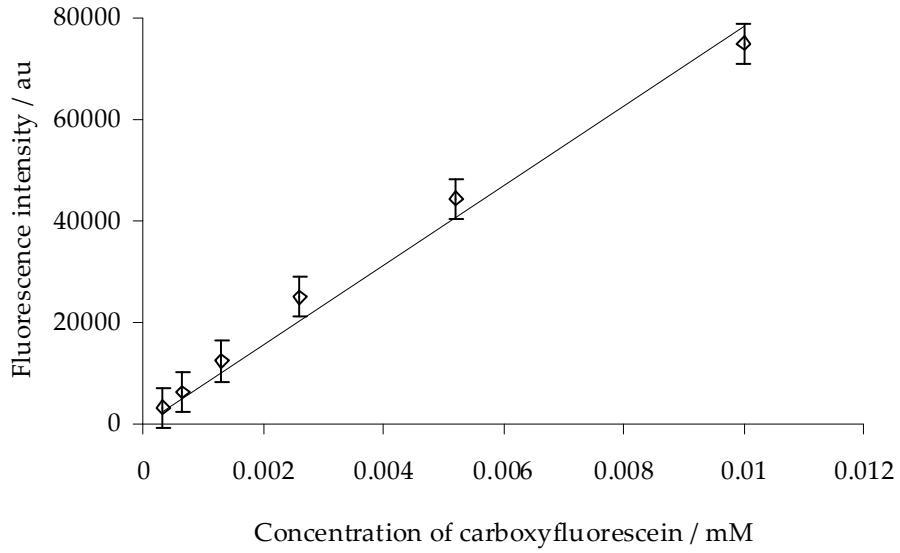

Figure 2.6: Fluorescence calibration plot for 5(6)-carboxyfluorescein in HEPEs buffer

2.3.7 Release of sodium chloride

Microsphere samples were prepared according to the protocol detailed in section 2.3.3 using a w/o emulsion containing a 6.1 M solution of NaCl. For each experiment the microsphere suspension was diluted to exactly 10 mL using deionised water (MilliQ 18.2 MΩ·cm). The suspension temperature was equilibrated to 25 ± 0.5 °C using a water bath prior to each conductivity measurement. The conductivity of the freshly prepared suspension was measured, the microspheres were then sonicated for 2 minutes at 45 Wcm^{-2} to cause rupture. The conductivity of the degraded suspension was measured. Control samples were treated in an identical manner. The first control was carried out using oil filled microspheres formed according to the protocol above but with 100 μL of tetradecane in place of the primary emulsion phase. The second control was carried out using identical oil filled microspheres but the suspension was doped with 40 μL of 6.1 M NaCl solution prior to the first conductivity measurement. Experiments were carried out on each sample type in triplicate and used NaCl concentrations within the linear range shown in Figure 2.7.

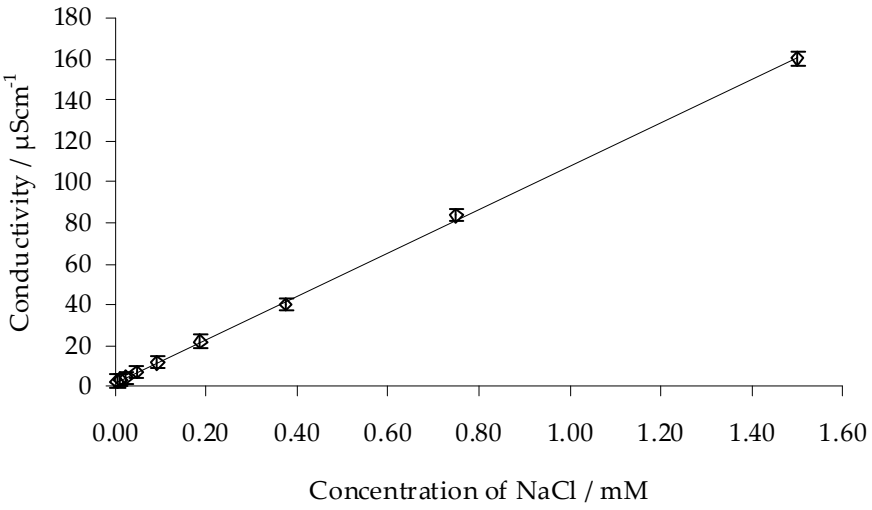

Figure 2.7: Calibration plot for NaCl in MilliQ water

2.3.8 Release of 5FU

Microsphere samples were prepared according to the protocol detailed in section 2.3.3/4 using a w/o emulsion containing a 0.1 M solution of 5-Fluorouracil in 1 M sodium chloride solution. Release was measured directly after formation via dialysis into 10 mL of MilliQ water (18.2 MΩ·cm), samples were taken directly from the receptor. A schematic diagram of the experimental set up is shown in Figure 2.8. Release by incubation with DTT was achieved by adding the required amount of DTT to the receptor. In order to measure release upon sonochemical breakdown the microsphere sample was sonicated for a chosen time period before returning it to the dialysis for 30 minutes, after which time a sample was taken from the receptor. The procedure was repeated to achieve the cumulative sonication time reported. The 5FU concentrations in the samples collected were measured by HPLC, method detailed at the start of this section. A linear range was established with standard solutions of 5FU, Figure 2.9. Limit of detection: 0.34 μg/mL, limit of quantification: 1.04 μg/mL.

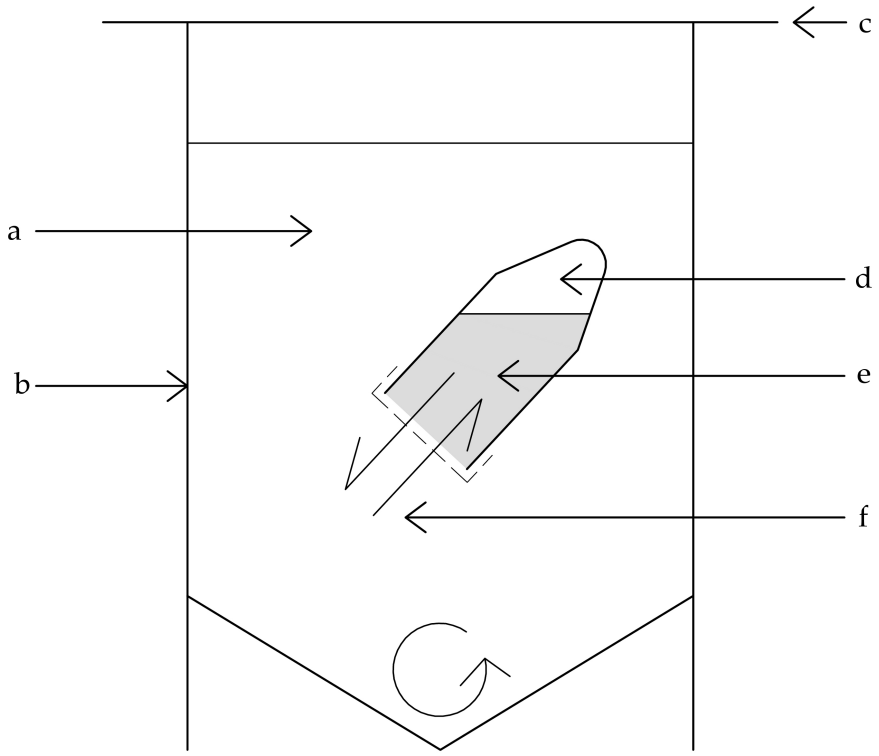

Figure 2.8: Schematic of the experimental set up used to carry out the dialysis described in section 2.3.8; (a) receptor medium, (b) skirted 100 mL centrifuge tube sealed with film or a lid (c), (d) 2 mL capped centrifuge tube with its lid hollowed out so that it acts only to hold the dialysis membrane in place, (e) microsphere suspension (where the initial release of 5FU occurs due to rupture of the microspheres), (f) transfer of the released 5FU across the dialysis membrane.

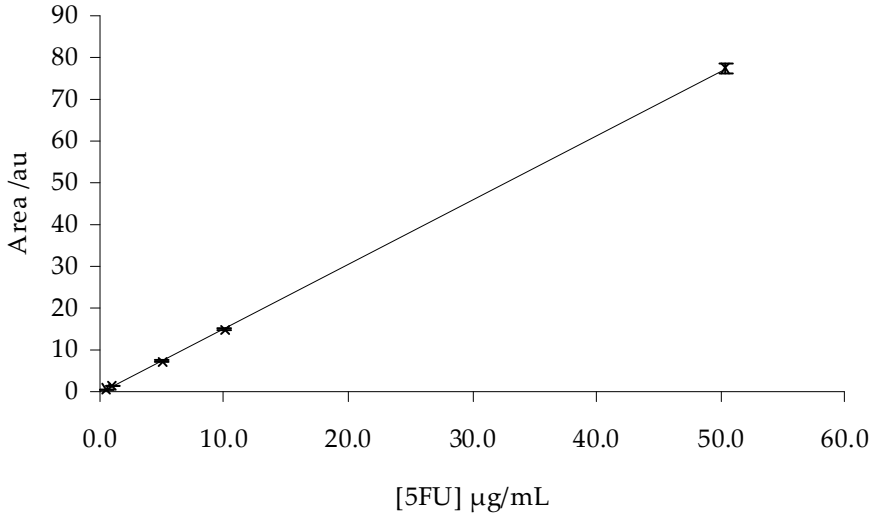

Figure 2.9: HPLC calibration Plot for 5FU in MilliQ water

2.4 Chapter 5: Responsive polymers and microspheres

All reagents were purchased from Sigma Aldrich. N-isopropylacrylamide (NIPAm) was recrystallised from toluene/hexane (6:4). *tert*-butyl methacrylate (*t*BMA) was purified from its inhibitor using an inhibitor removal column supplied by Sigma Aldrich and used immediately and methacrylic acid (MA) was vacuum distilled to purify it from its inhibitor and used immediately. All other reagents were used as received. All glassware was oven dried at 80 °C prior to use.

^{1}H-NMR spectra of the polymers were obtained using Bruker Avance 250, 300 and 400 MHz NMR spectrometers. DOSY NMR spectrometer experiments were performed using the 400 MHz Bruker Avance NMR. The DOSY spectra were acquired using the ledbpgp2s pulse program provided with the Bruker topspin software The gradient strength was incremented in 8 steps from 5 to 95% of the total gradient strength. The gradient pulse length was set at 4 ms to ensure full signal attenuation and the relaxation delay was 5 s (5 x T_1 relaxation). The probe head temperature was kept at 298 K during the experiments. The data set was processed using the dosy2d program provided with the Bruker topspin software.

Polymer molecular weights and weight distributions were obtained using a Varian PL-GPC 50 Plus system using THF solvent, calibrated with 12 polystyrene standards with M_ns ranging from 1060 - 2650000.

Optical micrographs were captured using a GX optical L3001 microscope fitted with an Infinity 2 camera. Laser scanning confocal microscopy (LSCM) was carried out using a Zeiss LSM 510 META microscope at the University of Bath Microscopy and Analysis Suite. Dynamic light scattering experiments were carried out using a Malvern Zetasizer Nano ZS machine. Sonication protocols used a Sonics and Materials VC600 generator (20 kHz / 600W) (generator B) connected to an ultrasound horn fitted with a micro-tip (3 mm diameter).

CTA1: 4-cyano-4-(phenylcarbonothioylthio) pentanoic acid, CTA2: S-(Thiobenzoyl) thio glycolic acid, CTA3: 2-cyano-2-propyl dodecyl trithiocarbonate.

2.4.1 Synthesis of P(*t*BMA) with CTA1

12.5 mg (0.045 mmol, 0.25 mol. eq.) of 4,4-Azobis(4-cyanovaleric acid) (ABCV) and 50 mg (0.179 mmol, limiting reagent (LR)) of CTA1 were charged to the reaction flask and deoxygenated by five vacuum-nitrogen purge cycles. In a separate flask 6.36 g (44.74 mmol, 250 mol. eq.) of *t*BMA and 2.5 mL of 1,4 dioxane were purged for 15 minutes with nitrogen. The monomer solution was charged to the reaction flask using a nitrogen flushed syringe and the reaction was heated to 85 ºC with stirring for 17 hours. The polymer was isolated by precipitation into a 10 fold excess of cold methanol/water (1:1 ratio) and characterised by GPC and ^{1}H-NMR: M_n: 33.1 kDa, M_w: 42.2 kDa, $Đ_M$: 1.28. ^{1}H-NMR (250 MHz, $CDCl_3$) δ: 0.97 (3H, br m), 1.35 (9H, br s), 1.83 ppm (2H, br m). Protocol carried out as part of an attempted one-pot diblock synthesis so no yield reported.

2.4.2 Synthesis of PNIPAm with CTA1

12.5 mg (0.045 mmol, 0.25 mol. eq.) of ABCV, 50 mg (0.179 mmol, LR) of CTA1 and 5 g (44.74 mmol, 250 mol. eq.) were charged to the reaction flask and deoxygenated by five vacuum-nitrogen cycles. In a separate flask 2.5 mL of 1,4-dioxane was purged with nitrogen for 15 minutes. The solvent was charged to the reaction flask with a nitrogen flushed syringe and heated to 85 ºC for 17 hours. A sample of the polymer was isolated by precipitation into a 10 fold excess of cold diethyl ether and characterised by GPC and ^{1}H-NMR: M_n: 3.2 kDa, M_w: 5.4 kDa, $Đ_M$: 1.67. ^{1}H-NMR (250 MHz, $CDCl_3$) δ: 1.07 (6H, br s), 1.58 (br m), 1.75 (br m), 2.08 (br m), 2.50 (2H, br m) 3.94 ppm (1H, br m). Protocol carried out as part of an attempted one-pot diblock synthesis so no yield reported

2.4.3 Synthesis of PMA with CTA1

The methacrylic acid was purified by vacuum distillation at 50 ºC. 3.85 g (44.74 mmol, 250 mol. eq.) of methacrylic acid, 50 mg (0.179 mmol, LR) of CTA1, 12.5 mg (0.045 mmol, 0.25 mol. eq.) of ABCV and 15 mL of dry methanol were charged to the reaction flask. The flask was deoxygenated with four freeze-pump-thaw cycles under argon before heating to 65 ºC for 19 hours. The polymer formed was precipitated into a 10 fold volume excess of cold diethyl ether. The precipitate was collected by filtration and dried under vacuum at 50 ºC. Yield: 120 mg (3.1%). The product was characterised by ^{1}H-NMR (250 MHz, D_2O) δ: 0.91 (3H, br m), 1.85 (2H, br m).

2.4.4 Synthesis of PMA with CTA2

The methacrylic acid was purified by vacuum distillation at 50 ºC. 4.24 g (29.8 mmol, 100 mol. eq.) of methacrylic acid, 126.5 mg (0.58 mmol, LR) of CTA 2, 42 mg (0.15 mmol, 0.25 mol. eq.) of ABCV and 30 mL of dry methanol were charged to the reaction flask. The flask was deoxygenated with four freeze-pump-thaw cycles under argon before heating to 60 ºC for 10 hours. The polymer formed was precipitated into a 10 fold volume excess of cold diethyl ether. Yield: 1.28 g (25%). The product was characterised by ^{1}H-NMR (250 MHz, MeOD) δ: 1.11 (3H, br m), 1.90 (2H, br m).

2.4.5 Synthesis of P(*t*BMA) with CTA3

15 mg (0.089 mmol, LR) of 2,2'-azobis(2-methylpropionitrile) (AIBN) was charged to the reaction flask and deoxygenated by five vacuum-nitrogen purge cycles. In a separate flask 6.3 g (44.25 mmol, 500 molar eq.) of *t*BMA, 0.122 g (0.35 mmol, 4 molar eq.) CTA3 and 10 mL of 1,4 dioxane were purged with nitrogen for 30 minutes. This solution was charged to the reaction flask which was sealed and heated to 60 °C for 15 hours. The polymer was isolated as a yellow amorphous solid by precipitation into a 10 fold volume of cold methanol/water (1:1). Yield: 1.90 g (30%). The product was characterized by ^{1}H-NMR and

GPC: M_n: 6.1 kDa, M_w: 8.3 kDa, $Đ_M$: 1.36. ^{1}H-NMR (300 MHz, MeOD) δ: 0.96 (3H, br m), 1.38 (9H, br s), 1.78 (2H, br m), 3.31 ppm (2H, t).

2.4.6 Synthesis of PNIPAm in 1,4 dioxane with CTA3

15 mg (0.089 mmol LR) of AIBN and 1 g (8.9 mmol, 100 molar eq.) of NIPAm were charged to the reaction flask and deoxygenated by five vacuum-nitrogen purge cycles. In a separate flask 0.122 g (0.35 mmol, 4 molar eq.) of CTA3 and 10 mL of 1,4 dioxane were purged with argon for 30 minutes. This solution was charged to the reaction flask which was sealed and heated to 60 °C for 56 hours. Samples were taken at periodic intervals using an argon flushed syringe and quenched in ice. The samples were analysed without any purification step by ^{1}H-NMR for % conversion and by GPC for chain length and distribution. 1H-NMR (400 MHz, MeOD) δ: 1.17 (6H, br m), 1.61 (2H, br m), 1.88 (1H, br m), 3.46 (2H, m), 3.99 ppm (1H br m).

2.4.7 Synthesis of PNIPAm in DMSO with CTA3

15 mg (0.089 mmol LR) of AIBN and 1 g (8.9 mmol, 100 molar eq.) of NIPAm were charged to the reaction flask and deoxygenated by five vacuum-nitrogen purge cycles. In a separate flask 0.122 g (0.35 mmol, 4 molar eq.) of CTA3 and 10 mL of dry DMSO (dried with 4 Å molecular sieves) were purged with argon for 30 minutes. This solution was charged to the reaction flask which was sealed and heated to 70 °C for 5 hours. Samples were taken at periodic intervals using an argon flushed syringe and quenched in ice. The samples were analysed without any purification step by ^{1}H-NMR for % conversion and by GPC for chain length and distribution. ^{1}H-NMR (300 MHz, DMSO-*d6*) δ: 1.03 (6H, br m), 1.22 (2H, br m), 1.97 (1H, br m), 3.47 (2H, m), 3.84 ppm (1H, br m).

2.4.8 Synthesis of P(*t*BMA-b-NIPAm) with CTA3

3.5 mg (0.01 mmol, LR) of AIBN, 0.5 g (M_n: 6154, 0.08 mmol, 8 molar eq.) of macro-RAFT agent (P*t*BMA) and 2.23 g (20 mmol, 1000 molar

eq.) of NIPAm were charged to the reaction flask and deoxygenated by five vacuum-nitrogen cycles. In a separate flask 10 mL of 1,4 dioxane was purged with nitrogen for 30 minutes, then charged to the reaction flask which was sealed and the reaction heated to 60 °C for 20 hours. When the chain length was monitored with reaction time, the reaction was inerted under argon and samples were taken from the reaction using an argon flushed syringe, quenched by cooling in ice and opening to the air. The diblock copolymer was isolated as a pale yellow amorphous solid by precipitation into a 10 fold volume of cold methanol/water (1:1). Yield: 2.2 g (80%). The product was characterized by ^{1}H-NMR and GPC: M_n: 9.5 kDa, M_w: 12.5 kDa, $Đ_M$: 1.31. ^{1}H-NMR (400 MHz, MeOD) δ: 1.08 (3H, br m), 1.17 (6H, br m), 1.31 (br m), 1.49 (9H, br s), 1.60, (2H, br m), 1.87 (1H br m), 2.11 (2H, br m), 3.46 (2H, m), 3.99 ppm (1H, br m).

2.4.9 Synthesis of P(*t*BMA-b-NIPAm-b-*t*BMA) with CTA3

4 mg (0.01 mmol, LR) of AIBN, 0.5 g (M_n: 10666, 0.05 mmol, 4 molar eq.) of macro-RAFT agent (P(*t*BMA-b-NIPAm)) and 1.67 g (12 mmol, 1000 molar eq.) of *t*BMA were charged to the reaction flask and deoxygenated by five vacuum-nitrogen cycles. In a separate flask 10 mL of 1,4 dioxane was purged with nitrogen for 30 minutes, then charged to the reaction flask which was sealed and the reaction heated to 60 °C for 17 hours. Yield: 30 mg (1.4%). The product was characterised by ^{1}H-NMR and GPC: M_n: 17.9 kDa, M_w: 23.3 kDa, $Đ_M$: 1.30. ^{1}H-NMR (250 MHz, MeOD) δ: 0.93 (3H, br m), 1.18 (6H, br m), 1.50 (9H, br s), 1.60 (2H, br m), 1.90 (1H, br m), 2.10 (2H, br m), 3.99 ppm (1H, br m).

2.4.10 Hydrolysis of P(*t*BMA-b-NIPAm)

1.5 g (M_n = 9543, 0.16 mmol, P*t*BMA DP: 43) of P(*t*BMA-b-NIPAm) was dissolved in 25 mL of DCM. 5 mL (65 mmol, 9.5 molar eq.) of Trifluoroacetic acid was added dropwise to the solution whilst stirring. The solution was heated to 40 °C (reflux) for 4.5 hours. The DCM was then removed under vacuum and the resulting polymer was

dissolved in alkaline aqueous solution. The polymer was recovered by heating the solution to 50 °C and acidifying to form a precipitate. The precipitate was filtered and dried under a vacuum. Yield: 0.56 g (41%). The % conversion of the tBMA groups on the polymer was characterised by ^{1}H-NMR. ^{1}H-NMR (400 MHz, MeOD) δ: 1.16 (6H, br m), 1.45 (9H, br s), 1.60 (2H, br m), 1.92 (1H, br m), 2.10 (2H br m), 3.99 ppm (1H, br m).

2.4.11 Thiolation of P(MA-b-NIPAm)

0.5 g (M_n^{th} = 7479, 2.4 mmol of MA groups) of P(MA-b-NIPAm) was dissolved in 10 mL of pH 7 phosphate buffer with 0.07 mL (0.42 mmol, 0.2 mol. eq.) of N-(3-dimethylaminopropyl-N'-ethylcarbodiimide) (EDC) and 0.05 g (0.042 mmol, 0.2 mol eq) N-hydroxysuccinimide (NHS) and allowed to stir at room temperature for 15 minutes. 0.38 g (3.34 mmol, 1.5 mol. eq.) of cysteamine HCl was added and the solution was stirred at room temperature for 7 days. The thiolated polymer was isolated by removing the aqueous liquors under vacuum. The polymer was then re-dissolved in methanol and the insoluble buffer salts were removed by filtration. The polymer was purified by precipitation from methanol into deionised water at 80 ºC. The precipitate was collected and dried in an oven overnight at 40 ºC. Yield: 0.21 g (42%). The LCST was measured using melting point apparatus and a 10 mg/mL solution of polymer in pH 7 100 mM phosphate buffer. The LCST of the sample synthesised was 37 ºC. ^{1}H-NMR (400 MHz, D_2O) δ: 0.89 (3H, br m), 1.06 (6H, br m), 1.63 (2H, br m), 1.82 (1H br m), 1.93 (2H, br m), 2.75 (t), 2.79 (2H, br t), 2.94 (t), 3.012 (m), 3.13 (2H br t), 3.32 (t), 3.82 (1H, br m).

2.4.12 Response of P(MA_{SH}-b-NIPAm) microspheres to heating above the LCST, measured by optical microscopy

The microspheres were formed according to the method described in section 2.1.14 but using the prepared P(MA_{SH}-NIPAm). A sample of microspheres was imaged by optical microscopy. The sample on the

microscope slide was then heated to 40 ºC on a hot plate for 10 minutes before viewing under the microscope again, and then a further 20 minutes before the final image was taken. The same sequence of images were taken of a sample of PMA_{SH} microspheres prepared in an identical manner.

2.4.13 Response of P(MA_{SH}-b-NIPAm) microspheres to heating above the LCST, measured by LSCM.

The microspheres were formed according to the method described in section 2.1.14 using nile red saturated tetradecane and the prepared P(MA_{SH}-b-NIPAm). A sample of microspheres was placed in a sample holder for the confocal microscope and a chosen region was imaged using the laser scanning mode. The sample was then heated to 43 ºC *in situ* using a heated stage and chamber. The same region of the sample was imaged at regular time intervals during the heating process. For comparison a sample from the same batch of microspheres was imaged over a comparable time period without heating.

2.4.14 5FU release study

Microsphere samples were prepared from a w/o emulsion using the method described in section 2.3.4 but with the prepared P(MA_{SH}-b-NIPAm). The dialysis system described in section 2.3.8 was set up to facilitate measurement of release. Release in the case of dialysis heated to 40 ºC was compared to release during dialysis at 21 ºC. The concentration of 5FU in the receptor was quantified by HPLC as described in section 2.3.8.

3 Lysozyme and poly(methacrylic acid) microspheres

Sonochemically produced lysozyme microspheres have been well researched by our collaborators at the University of Melbourne[7;8;47]. Initial work carried out with Zhou *et al*. was used as a basis from which to further develop the sonochemical methodology in our laboratories at Bath. This chapter reports optimisation of the sonochemical method for lysozyme and thiolated poly(methacrylic acid) (PMA_{SH}). The chosen conditions were used as a basis for the work reported in chapters 4 and 5.

3.1 Lysozyme microspheres

3.1.1 Optimisation and characterisation: Air filled microspheres

The experimental equipment used is described in section 2.1. Two ultrasound generators were used; a 20 kHz/400 W Branson generator (generator A) and a 23 kHz/600 W Sonics and Materials generator (generator B), both were fitted with a 3 mm diameter microtip to allow experiments to be carried out on a small scale.

In the initial study the optimised conditions[7] using generator A were used to form air filled microspheres. The ultrasound intensity and sonication time were the varied in order to understand the effect of these parameters on the microspheres' size distribution. Figure 3.1 shows examples the microscopy that was used to characterise the

microspheres formed; optical microscopy provides a simple, quick method to gauge the size distribution of microspheres in solution and when used with a mercury lamp can be used to observe a fluorescent marker bound to the protein shell. Scanning electron microscopy (SEM) provides additional information on the morphology of the protein shells, albeit in a dried state.

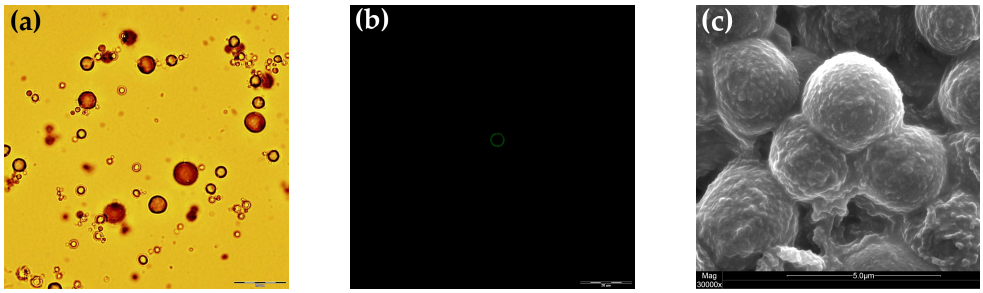

Figure 3.1: Air-filled lysozyme microspheres imaged in suspension by optical transmission microscopy, scale bar: 20 μm (a) and fluorescence transmission microscopy (fluorescent stain Fluorescein isothiocyanate excited by emission from mercury lamp), scale bar: 20 μm (b). Dried microspheres imaged by scanning electron microscopy, scale bar: 5.0 μm (c).

When varying sonication time and intensity the experimental protocol described in section 2.1.2 was kept constant. Prior to sonication the lysozyme in solution was denatured, in order to expose eight thiol groups, by incubating with DL-Dithiolthreitol (DTT) for two minutes at room temperature. After the sonication step the microspheres produced were washed by dilution with deionised water. This methodology can be adapted to form oil-filled microspheres which will be discussed in section 3.1.3. The first parameter to be varied was ultrasound intensity. Increasing the applied intensity of an ultrasonic system increases the energy output of the horn which in turn increases the amplitude of the tip motion. With generator A this was seen to increase the mean diameter (measured by image analysis of optical micrographs, see section 2.1) of the microspheres produced from ~2 μm at 10% power to 4-5 μm at 50% power (Figure 3.2) accompanied by an increase in the standard deviation implying a broader size distribution. Similarly increasing the sonication time results in an increase in the mean diameter of the microspheres produced at a given ultrasound intensity.

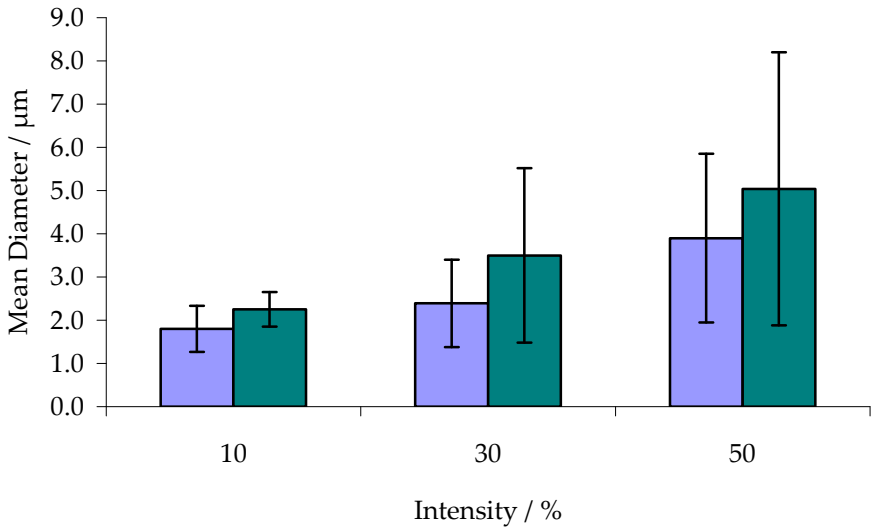

Figure 3.2: Change in mean diameter of air filled lysozyme microspheres with intensity for generator A (% of 400 W output of the generator). Blue: 15 s sonication; green: 30 s sonication (error bars correspond to one standard deviation from the mean).

The SEM images shown in Figure 3.3 have been taken from samples produced at the ultrasound intensities and sonication times included in Figure 3.2. As the ultrasound intensity increases the walls of the microspheres appear to become smoother suggesting a lower density of lysozyme aggregation on the surface of the air bubbles during shell formation. The shells of the microspheres formed at 50% power pucker under the electron beam, suggesting that shells formed at higher intensities are thinner and have less structural integrity than those formed at lower intensities. When the samples were produced at 50% power some sediment was observed in the tubes after sonication. This suggests that some of the microspheres had been broken open by the higher intensity sonication causing them to collapse and sink. Increasing the intensity results in more cavitation bubbles and emulsion bubbles being produced, which may lead to less protein aggregation on each individual air bubble, although it is not clear as to why this has the effect of increasing the size of the microspheres. These results are however useful in determining the requirement for low to moderate power output in order to form robust microspheres in a size range which is relevant to medical applications[99].

Referring to Figure 3.2 it can be seen that increasing the sonication time has a similar effect on the mean as increasing the power. This suggests that generating cavitation bubbles at the same rate for a longer period of time has the same effect on microsphere morphology as generating more cavitation within a set time period. The observations from the SEM images (Figure 3.3) show the same trend in morphology as was seen with increasing power. These results are in agreement with the work conducted by Zhou *et al*.[47] using the same generator.

The mean diameters of microspheres formed with generator B show a similar increase in mean diameter with increasing intensity but the trend is not well pronounced due to the breadth of the size distributions. The mean diameter only varies over a range of approximately 1 μm unlike with generator A (Figure 3.4).

In the box plot (Figure 3.4) the mean diameter is represented by the dotted line whilst the median is shown by the black line within the grey box. The grey box defines the interquartile range, bounded by the upper and lower quartiles, the whiskers the 5 and 95 percentiles and the dots represent outliers. (Outliers are defined as values within the sample population that are more than '1.5 times the interquartile range' greater than the lower quartile or less than the upper quartile.) This allows the shape of the size distribution to be assessed in each case. If the quartiles are considered, the lower powers appear to give a narrower size distribution as expected from previous results with generator A (Figure 3.2). In all cases it appears that the 5 and 95 percentiles are widely spread indicating that the system is not very well controlled and that some method of fractionation or filtering would be necessary if a narrow size distribution were required.

The trend in mean diameter with sonication time for samples produced with generator B is not as well defined (Figure 3.5). The sample at 15 s of sonication shows a highly symmetrical distribution but between 15 and 45 s there is no trend in increasing diameter with the distributions covering approximately the same range. It is interesting to note that the sample formed at 60 s of sonication has a much broader distribution of diameters and a significantly larger mean diameter, suggesting that there is a threshold sonication time between 45 and 60 s above which significantly larger microspheres start to be formed.

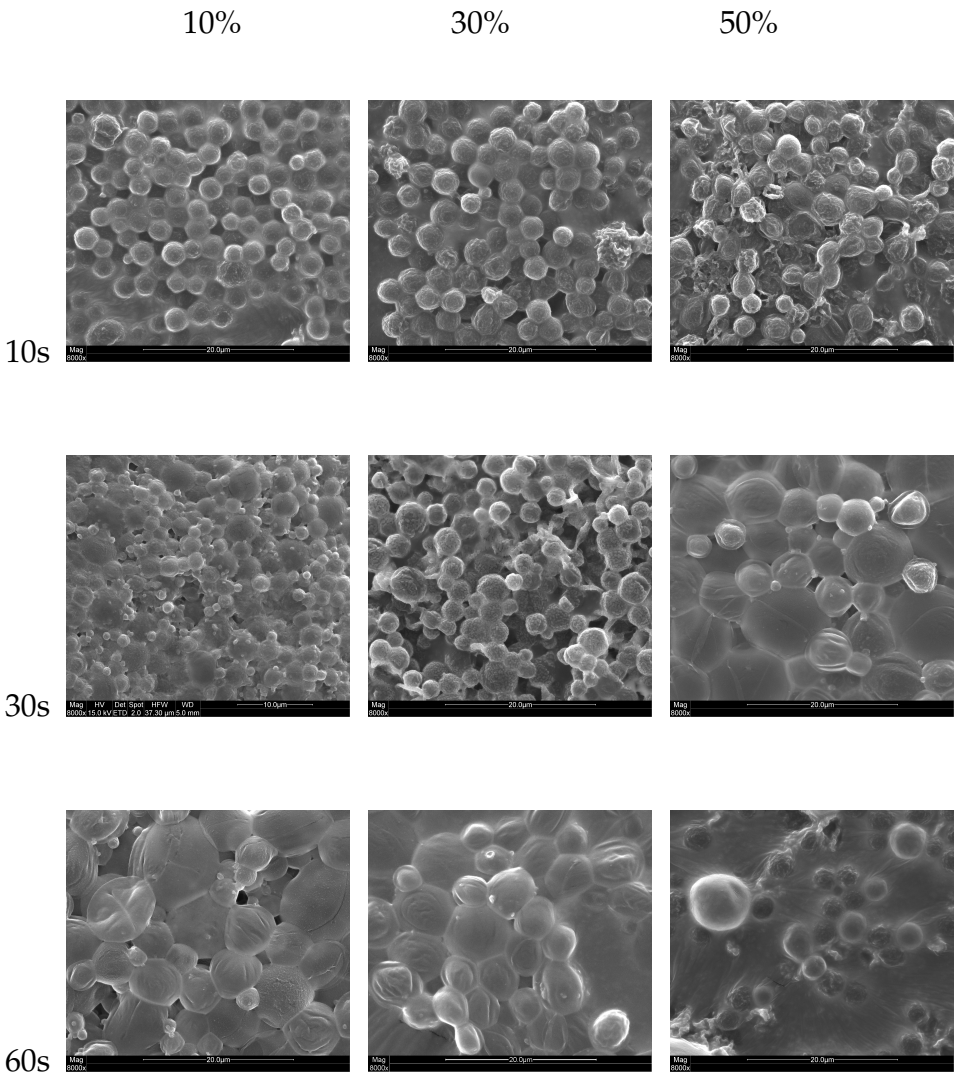

Figure 3.3: SEM Images demonstrating the observed change in air filled lysozyme microsphere morphology with intensity (% of 400 W generator A output) and sonication time, Scale bar: 20.0 μm.

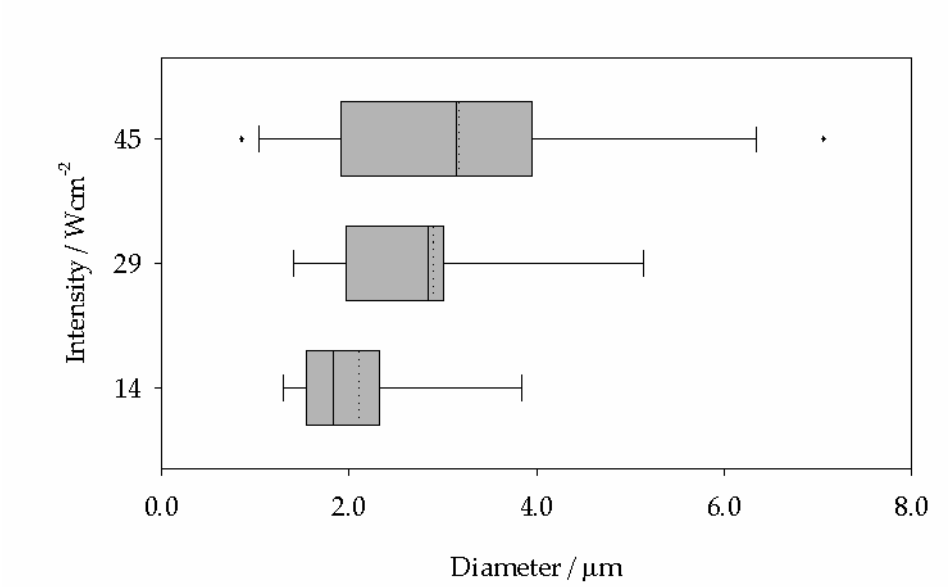

Figure 3.4: Change in size distribution of air filled lysozyme microspheres with intensity for generator B (sonication time 30 s). (The mean diameter is represented by the dotted line whilst the median is shown by the black line within the grey box. The grey boxes define the upper and lower quartiles, the whiskers the 5 and 95 percentiles and the dots represent outliers.)

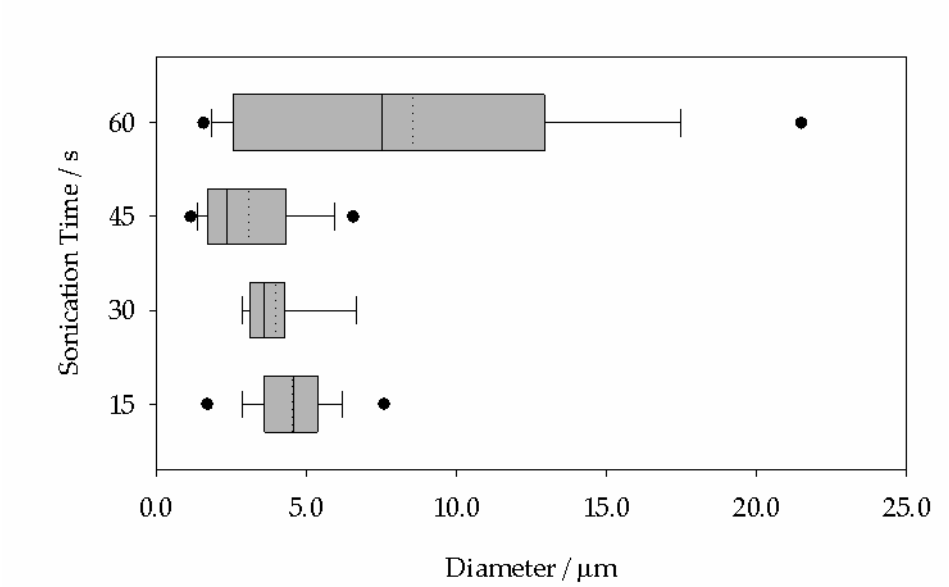

Figure 3.5: Change in size distribution of air filled lysozyme microspheres with sonication time for generator B (intensity 14 W cm^{-2}).

3.1.2 Evidence for disulfide cross linking in shell

It has been shown by Gedanken *et. al.*[16] that it is possible to form hollow microspheres without the need for intermolecular disulfide bonds. However denatured lysozyme contains thiol groups capable of cross linking and therefore it is expected that disulfide cross linked microspheres should form. This is favourable as it has been reported that microspheres stabilised by covalent cross links have a longer shelf life than microspheres formed without disulfide cross links, which are only stable for a matter of hours at room temperature[16]. Therefore as part of this investigation a number of control experiments have been carried out, based on Suslick's early work[1], in order to demonstrate that the lysozyme microspheres reported herein are stabilised by disulfide cross linking.

If no denaturation reaction is carried out to expose the thiol groups prior to sonication microspheres do not form supporting the case for disulfide bonds playing an important role in microsphere stability. Incubation of air filled lysozyme microspheres with 60 mg/mL of DTT, a disulfide cleavage agent (Figure 3.6), overnight led to collapse of the microspheres. After incubation the microspheres were no longer floating on the surface of the solution, but had ruptured and sunk to form a sediment at the bottom of the tube. This suggests that disulfide crosslinks were a key factor in the stabilisation of the lysozyme microspheres. Incubation with DTT is reported in later chapters as a means to trigger release of microsphere contents.

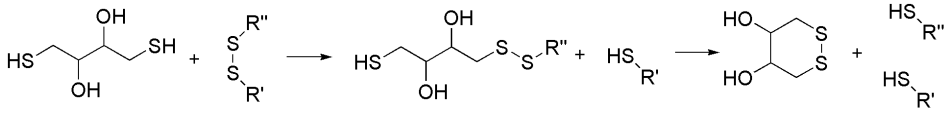

Figure 3.6: Mechanism for DTT mediated disulfide cleavage[120].

Further evidence for disulfide bond formation can be provided by radical trapping experiments. Super oxide radicals are required to facilitate sonochemical disulfide bonding, therefore trapping these radicals should inhibit microsphere formation[1;42]. Initially the well known radical scavenger, *tert*-butanol[121] was added during the microsphere production protocol (described in section 2.1.9) which completely prevented the formation of microspheres, providing evidence for

radical driven stabilisation of the lysozyme microspheres. When high speed homogenisation (section 2.1.8) was used in place of sonication to provide extensive emulsification without any sonochemical radical production, then a stable foam formed which lasted for approximately 48 hours but no microspheres were observed.

Superoxide dismutase (SOD) provides a more specific radical trap which targets super oxide radicals in particular[122]. SOD acts by catalysing the conversion of superoxide radicals to hydrogen peroxide and oxygen:

$$2O_2^- + 2H^+ \rightarrow O_2 + H_2O_2 \tag{3.1}$$

It was found that when the sonochemical protocol was carried out with 120 units/mL of SOD added to the lysozyme solution (see section 2.1.10) the yield of microspheres was reduced to 0-3% significantly less than the 8-20% yield observed in the standard reaction (Table 3.1), although microsphere formation was inhibited by the presence of SOD the results were variable and do not show a conclusive trend with SOD concentration.

SOD units/mL	% Yield of microspheres
0	8-20
37	7
69	0-9
120	0-3

Table 3.1: Yields of lysozyme microspheres in the presence of SOD. NB: experiments were carried out in triplicate for each SOD concentration. Yield defined as the dry mass of microspheres formed (after washing) expressed as a percentage of the mass of lysozyme added to the solution before sonication.

SOD contains one intramolecular disulfide bridge which may be denatured by DTT. Efforts were made in the experimental protocol to prevent denaturation of the SOD by adding the SOD immediately before sonication. However it is still possible that a small amount of denaturation may have occurred and contributed to the variable results observed.

The indirect evidence provided by these experiments gives strong support for the case that sonochemical lysozyme molecules are stabilised by disulfide bonding, although they do not discount the possibility that some additional stabilisation may be contributed by a hydrophobic mechanism.

3.1.3 Evidence of air and tetradecane encapsulation

The air filled lysozyme microspheres produced in the experiments discussed above float at the surface of the aqueous solution that they are stored in, indicating that their cores are less dense than the surrounding solution. This suggests that the microspheres have encapsulated air bubbles formed in the foam, in line with the proposed mechanism. The hollow nature of the microspheres can be demonstrated by rupturing the microspheres with a sharp blade *in situ* on the SEM stub before viewing them by SEM (Figure 3.7).

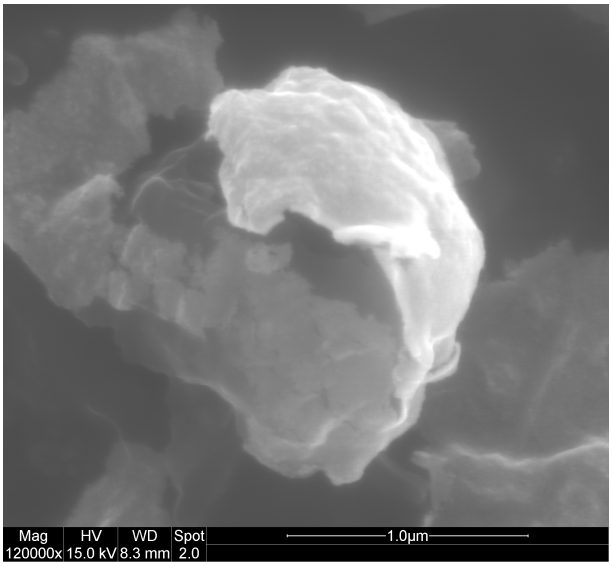

Figure 3.7: Example of an air filled microsphere (produced according to the protocol in section 2.1.2 using generator A) that has been mechanically ruptured after sample preparation on the SEM plate.

Further evidence for air encapsulation can be gained by measuring the multi bubble sonoluminescence (MBSL) produced on ultrasonic rupture of a suspension of air filled microspheres. MBSL is light produced as a result of the cavitational collapse of clouds of bubbles

in a solution under ultrasonic irradiation. The light is thought to be produced by radicals, formed as a result of the collapse, recombining[123]. Sonoluminescence is a useful tool for mapping cavitation but is very faint so must be observed using a photomultiplier tube. Alternatively it can be enhanced, for example by sonicating a solution of luminol[38] to give sonochemiluminescence which is sufficiently bright to be detected by long exposure photography in a dark box (protocol in section 2.1.11). Figure 3.8 shows an example of how cavitation can be mapped by capturing sonochemiluminescence. It can clearly be seen from these images that the distribution of cavitation in the luminol solution is changed when the horn tip is placed at the air:water interface as opposed to being fully submerged in solution.

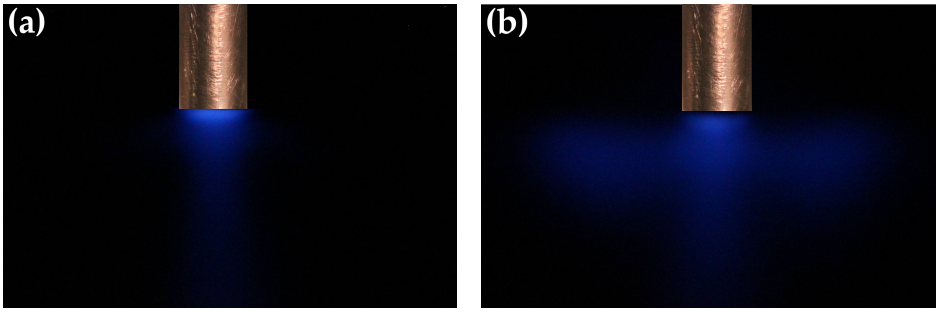

Figure 3.8: Sonochemiluminescence observed in an aqueous luminol solution when irradiated with ultrasound from generator B fitted with a 3 mm micro-tip (a) submerged in solution and (b) positioned at the air:water interface.

By irradiating water with pulsed ultrasound (from a plate transducer) and detecting the light produced with a photomultiplier tube connected to an oscilloscope it is possible to monitor the change in the sonoluminescence produced over time[119] (see section 2.1.12 for a detailed description of the experimental equipment and protocol designed by Lee *et al.* at the University of Melbourne[119]). In air saturated water a characteristic plot is generated with an initial growth in the intensity of sonoluminescence followed by a steady state phase (Figure 3.9). This initial period of increasing light intensity is associated with a build up of transient nuclei produced by ultrasound irradiation, resulting in increased cavitation and sonoluminescence[119]. In water that has been degassed under a vacuum there is insufficient dissolved gas to allow cavitation bubbles to form and hence sonoluminescence cannot occur meaning that no peaks are seen in the plot (Figure 3.10).

If a suspension of air filled microspheres is added to the degassed water the microspheres will rupture upon irradiation with ultrasound and the encapsulated air will be released into the water facilitating cavitation. As a result a small amount of sonoluminescence can be observed from the suspension of microspheres in degassed water (Figure 3.11). The sonoluminescence has a much lower intensity than that observed in the case of air saturated water because the volume of air held in the microspheres is very small and the suspension used was very dilute.

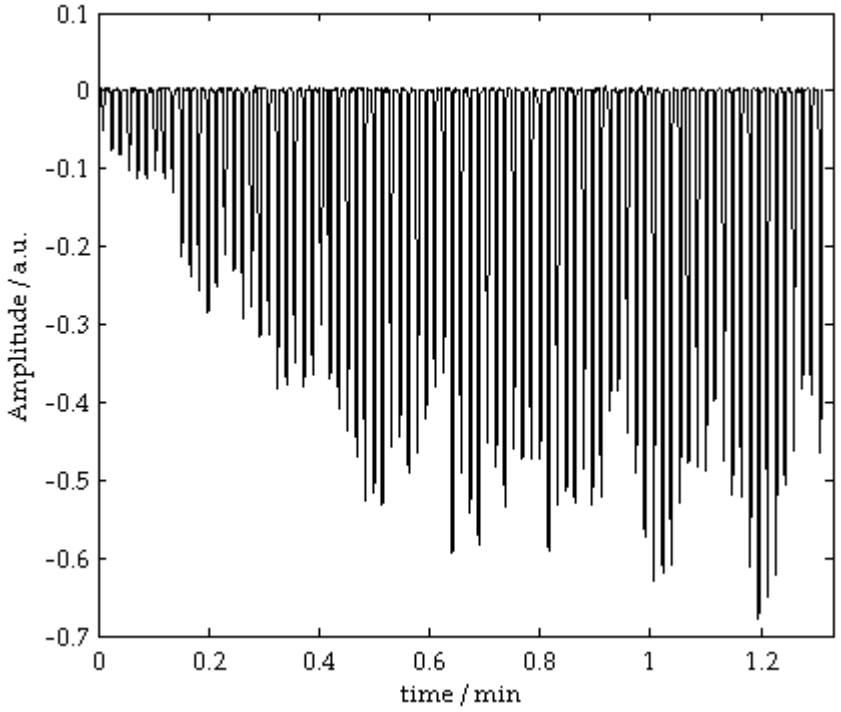

Figure 3.9: Sonoluminescence plot recorded by a photomultiplier tube and oscilloscope in pulsed mode for air saturated water.

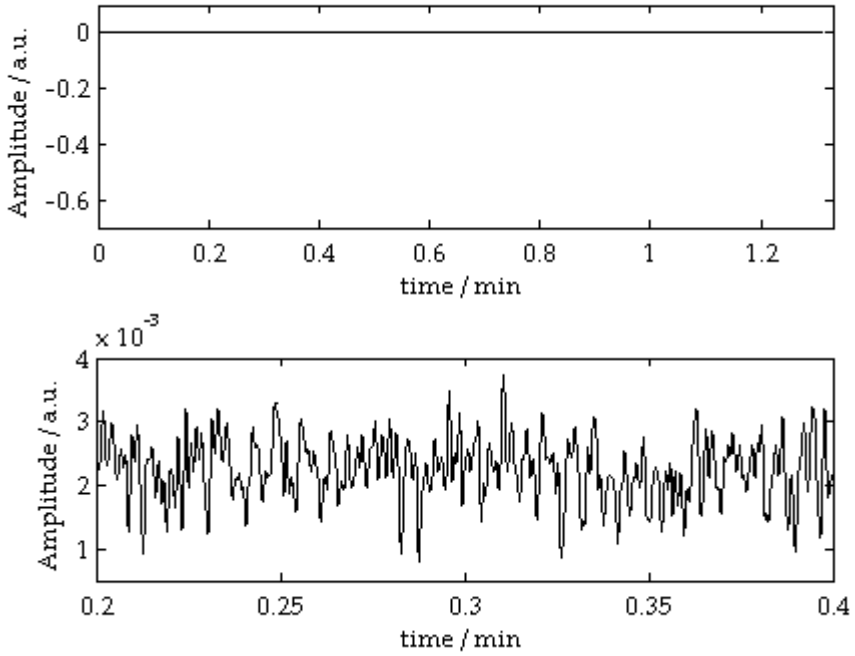

Figure 3.10: Sonoluminescence plot recorded by a photomultiplier tube and oscilloscope in pulsed mode for degassed water.

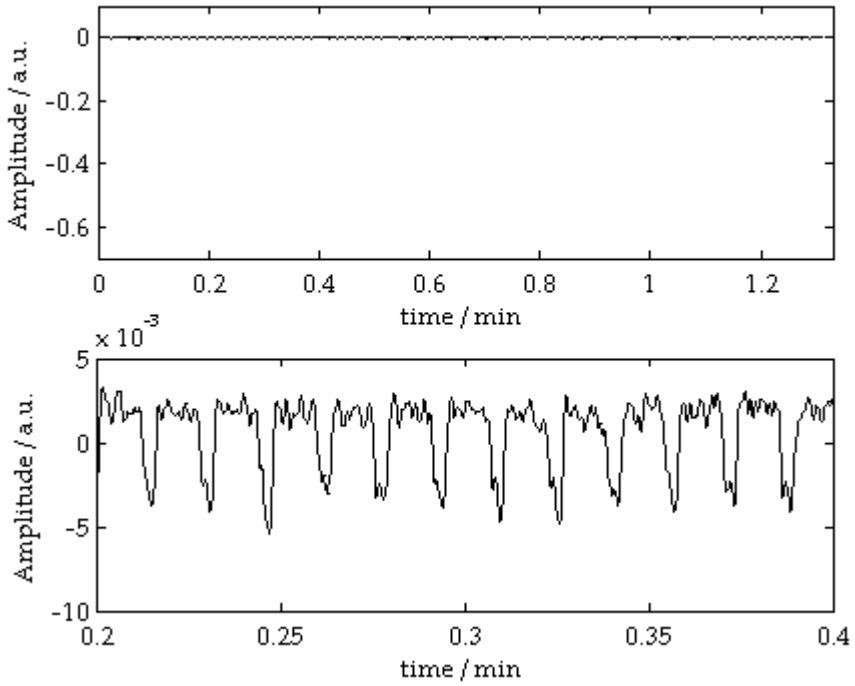

Figure 3.11: Sonoluminescence plot recorded by a photomultiplier tube and oscilloscope in pulsed mode for degassed water containing lysozyme microspheres with an air core.

In addition to air filled microspheres, oil filled microspheres can be formed by adapting the sonochemical protocol described above. After denaturing the lysozyme but prior to sonication 100 μL of oil was layered on the surface of the lysozyme solution. The sonicator tip was then placed at the oil : water interface. The oil chosen for this study was tetradecane, because it has been shown to work well with lysozyme and give microspheres in a size range that is useful for medical applications[8]. In a tetradecane/lysozyme system an emulsion is formed sonochemically between the aqueous solution and the tetradecane. The lysozyme molecules aggregate and crosslink on the surface of the tetradecane droplets encapsulating them and forming tetradecane filled microspheres.

An estimated yield of 2.22×10^8 microspheres can be produced from 1 mL of lysozyme solution with 100 μL of tetradecane, corresponding to quantitative encapsulation of the oil phase (the estimate was calculated from image analysis of micrographs of a known volume of the microsphere suspension, see section 2.1.3).

The microspheres formed in the tetradecane emulsion are significantly smaller than those formed in the air filled microsphere system when produced under the same conditions (Figure 3.12). This may be due to the lower interfacial tension at the tetradecane:water interface (52.2 mN/m at 20 °C)[124] compared to the air:water interface (72.8 mN/m at 20 °C)[124] which allows the tetradecane droplets to be smaller than the air bubbles resulting in smaller microspheres. The distribution of sizes is also smaller suggesting in turn that the tetradecane emulsion is less polydisperse than the foam formed in the air filled system.

The SEM images for tetradecane filled microspheres are quite different to those observed for air filled microspheres (Figure 3.13). The microspheres collapse under the vacuum used during the sample preparation to leave a honeycomb pattern on the plate. This suggests that the shells of the microspheres are porous allowing the encapsulated tetradecane to evaporate and escape from the microspheres under reduced pressure. It also indicates that the oil-filled shells have less structural integrity than the those in air filled microspheres. This collapse implies loss of a liquid core but does not provide direct evidence for oil encapsulation, in order to achieve this alternative microscopy methods must be used.

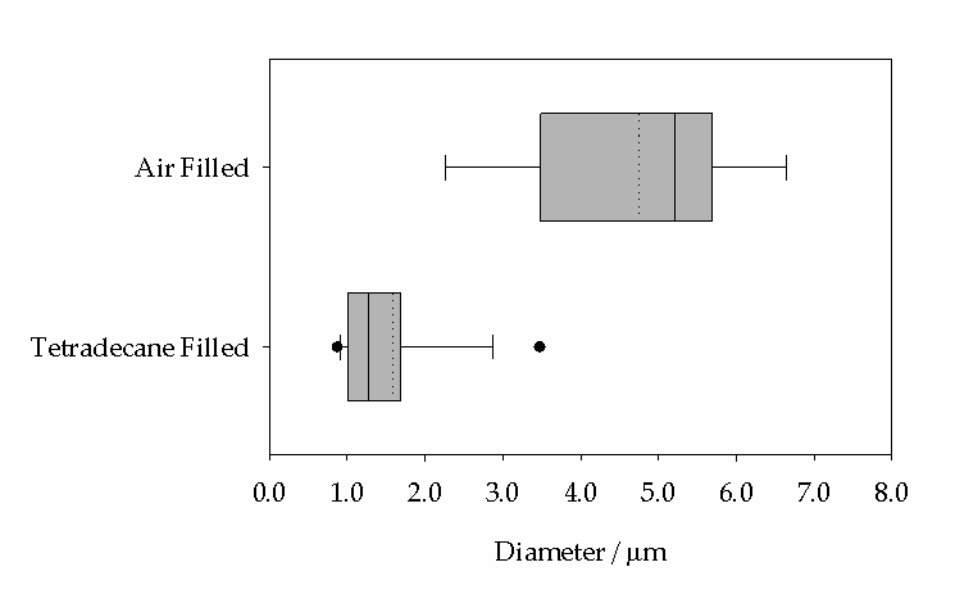

Figure 3.12: Size distributions of air filled and tetradecane filled lysozyme microspheres produced using generator B. Conditions: 29 $Wcm^{-2}$for 30 s sonication. (The mean diameter is represented by the dotted line whilst the median is shown by the black line within the grey box. The grey boxes define the upper and lower quartiles, the whiskers the 5 and 95 percentiles and the dots represent outliers.)

Imaging of the microsphere core can be achieved by adding a fluorescent species to the tetradecane prior to forming the microspheres. Nile red was chosen as a suitable lipophilic dye because it is has a broad absorption range, 400-600 nm and emits in the green to red region of the visible spectrum, 500-800 nm when dissolved in an alkane[125;126]. This allowed the microspheres to be imaged both by optical microscopy under irradiation from a mercury lamp and by laser scanning confocal microscopy using a green laser (543 nm). When tetradecane filled microspheres containing nile red are viewed by transmission optical microscopy with a mercury lamp they can be seen to fluoresce throughout the core (Figure 3.14a). The fluorescence is brightest at the centre of the microspheres where the depth of tetradecane is greatest. This can be compared with an air filled microsphere stained after formation using fluorescein isothiocyanate (Figure 3.14b). In this case the fluorescent molecules are present only in the thin shell. This means that the fluorescence is only bright enough to be visible from the 'side walls' of the sphere where there is

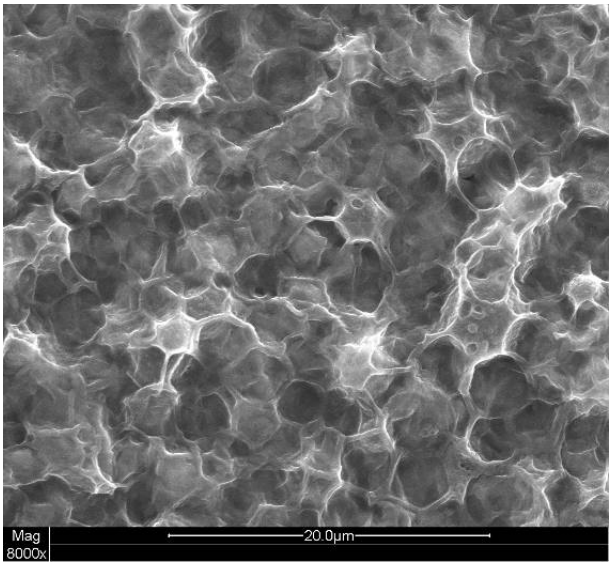

Figure 3.13: SEM Image of tetradecane filled microspheres, the microspheres collapsed under the vacuum used during sample preparation to leave a honeycomb pattern on the SEM stub. Scale bar 50 μm.

sufficient depth of shell wall to give a visible intensity. This causes the 3-dimensional microspheres to look like 2-dimensional empty rings, a stark contrast to when the microspheres are tetradecane filled.

Laser scanning confocal microscopy (LSCM) can be used to image an optical slice through the centre of the microspheres. This type of microscopy is useful in obtaining evidence for what resides in the internal structure of a microscopic structure. A 543 nm laser was used to excite red fluorescence from the nile red dissolved in the tetradecane and a 1 μm slice through the centre of a microsphere was imaged, Figure 3.15. The 1 μm optical slice imaged is thinner than the diameter of the microsphere, hence the red fluorescence seen in the core of the microsphere is as a result of nile red dissolved in the tetradecane encapsulated within the shell. The homogeneous distribution of red within the core is evidence of encapsulation of nile red and successful formation of oil filled lysozyme microspheres[a].

[a]The author wishes to acknowledge the kind assistance of Dr Adrian Rogers, at the University of Bath Microscopy and Analysis Suite, in collecting the confocal micrographs presented in this thesis.

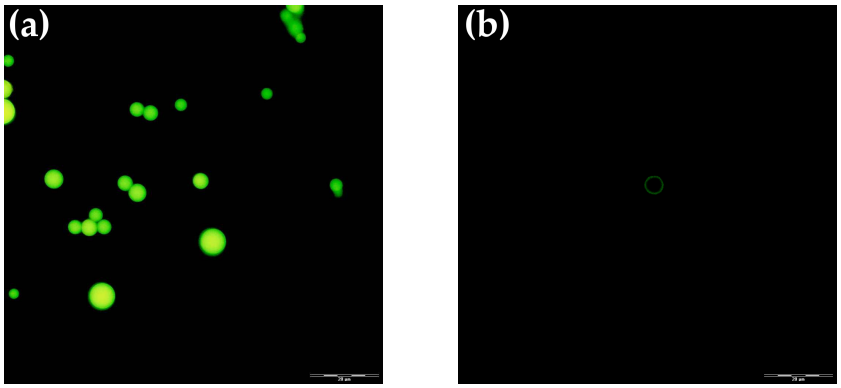

Figure 3.14: (a) Tetradecane filled microspheres, formed from tetradecane saturated with nile red, (b) fluorescein isothiocyanate stained air filled microspheres. Both samples were viewed in aqueous suspension by optical microscopy under irradiation from a mercury lamp, scale bar 20 μm.

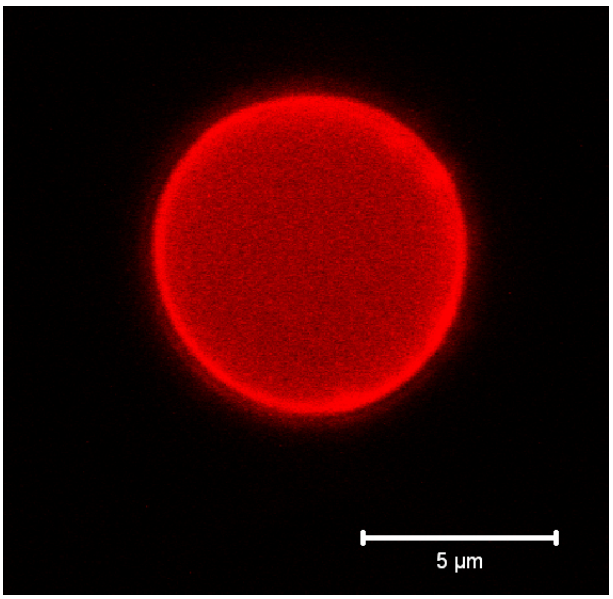

Figure 3.15: LSCM confocal micrograph of a 1 μm thick optical slice through a tetradecane filled microsphere containing nile red saturated tetradecane, viewed in aqueous suspension.

As an interesting aside to the experimental protocol, high speed video imaging was used to capture images of the lysozyme solution during sonication[b]. The imaging, which was conducted at a frame rate of 1000 frames per second (fps), allowed clusters of air bubbles/oil droplets to be observed in both the air filled and the oil filled protocols (Figures 3.16 and 3.17). These clusters were not observed when deionised water was sonicated under the same conditions (Figure 3.18) suggesting that the clusters are stabilised by lysozyme. It is likely that the microspheres formed from this protocol are formed in these clusters. When the ultrasound is switched off the clusters disintegrate and what appears to be individual bubbles are seen rising to the surface. These bubbles are too large to be microspheres and are likely to be simple foam bubbles. The microspheres can be observed as a turbid phase which creams to the surface over a period of hours after sonication. The clusters seen in the video stills provide some illustrative evidence for the proposed formation mechanism discussed in chapter 1. However more detailed empirical studies, outside the scope of this project, need to be carried out in order to fully understand the aggregation processes which occur in the formation of microsphere shells.

[b]The author wishes to acknowledge the kind assistance of Dr Timm Joyce Tiong in providing access to and assistance in operating the high speed video equipment.

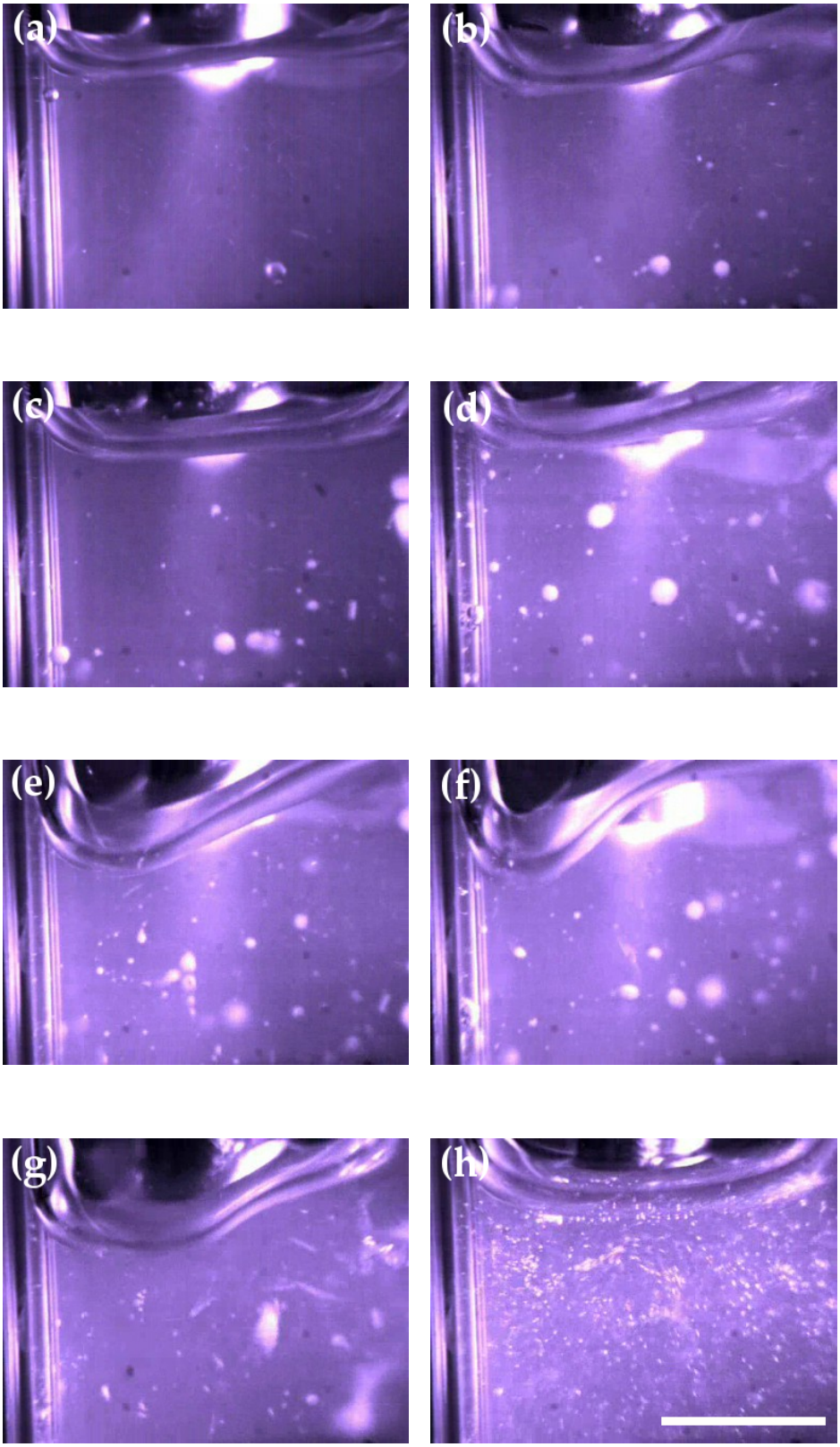

Figure 3.16: Stills taken from high speed video footage (1000 fps) of the lysozyme solution being sonicated during the production of air filled microspheres, (a-f) during sonication and (g-h) immediately after the sonicator was switched off. Scale bar 3 mm.

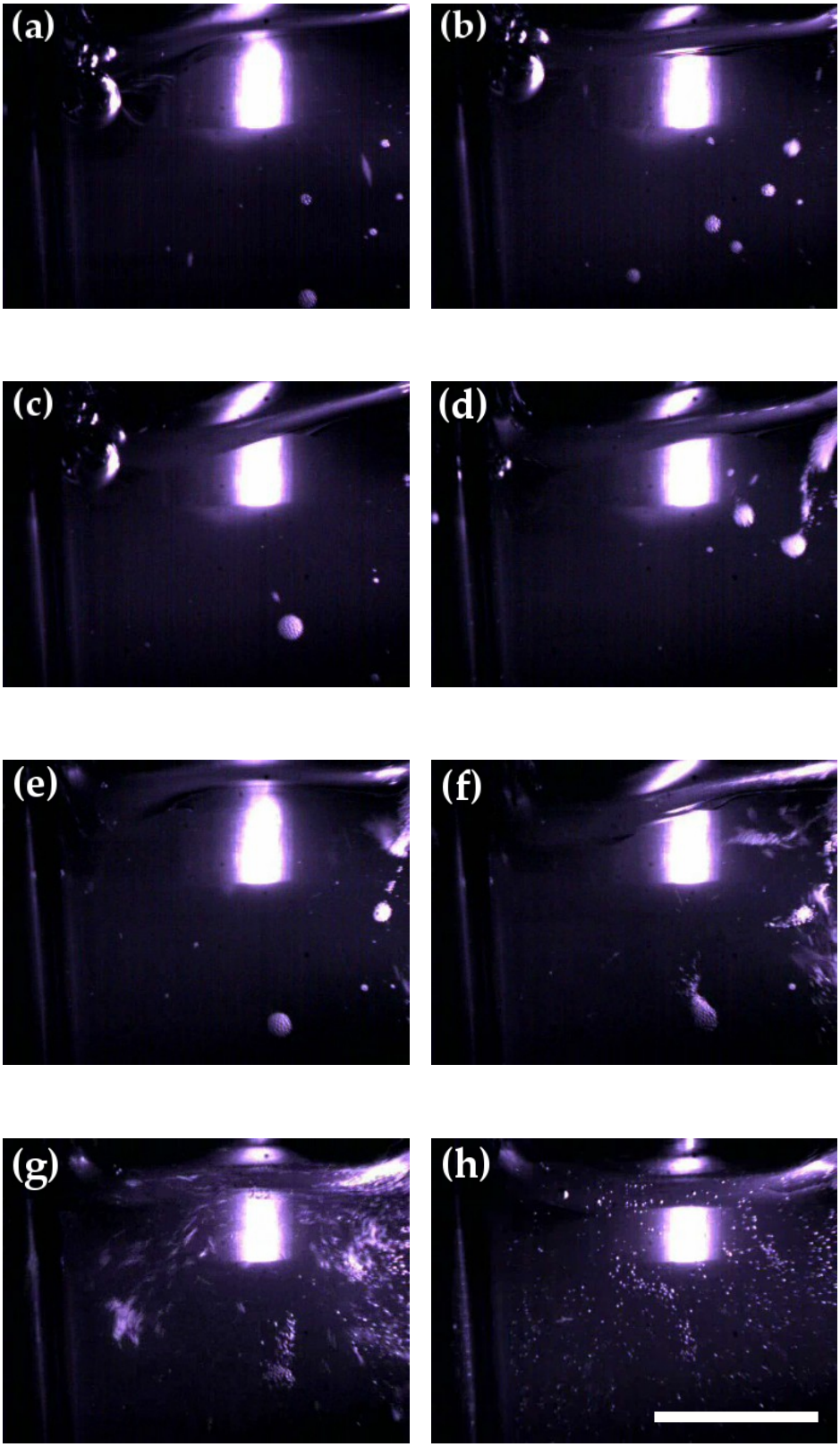

Figure 3.17: Stills taken from high speed video footage (1000 fps) of the lysozyme solution being sonicated during the production of tetradecane filled microspheres, (a-e) during sonication and (f-h) immediately after the sonicator was switched off. Scale bar 3 mm.

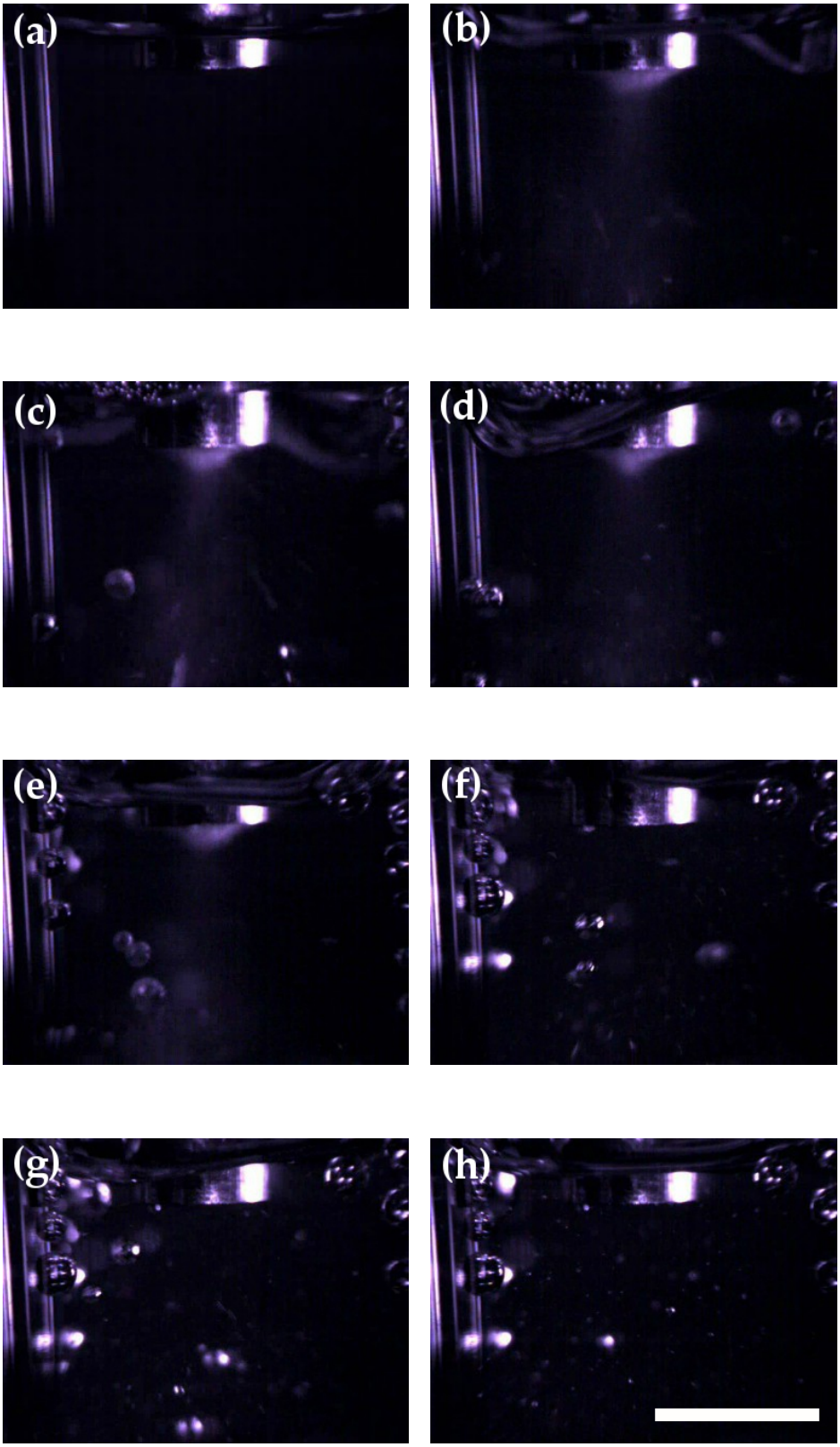

Figure 3.18: Stills taken from high speed video footage (1000 fps) of water sonicated under identical conditions to Figures 3.16 and 3.17, (a) taken before sonicating, , (b-e) during sonication and (f-h) immediately after the sonicator was switched off. Scale bar 3 mm.

3.2 PMA_{SH} microspheres

3.2.1 Synthetic route to PMA_{SH}

Poly(methacrylic acid) (PMA) was chosen as a suitable polymer to use in the initial stages of an investigation into polymer disulfide cross linked microspheres because it is biocompatible[127], water soluble and can be functionalised via the carboxylic acid groups on the chain to form pendant thiol groups[128]. In addition the surface activity of this polyelectrolyte can be tuned by adjusting the solution pH relative to its pKa (7.5)[129]. As such PMA_{SH} can fulfil the two main criteria for sonochemical microsphere production; it can aggregate on the oil:water interface and it can undergo disulfide crosslinking. A synthetic route for the functionalisation of PMA with cysteamine to form PMA_{SH} is reported in the literature[128] and is shown in Figure 3.19. This was our chosen synthetic route for the production of PMA_{SH}.

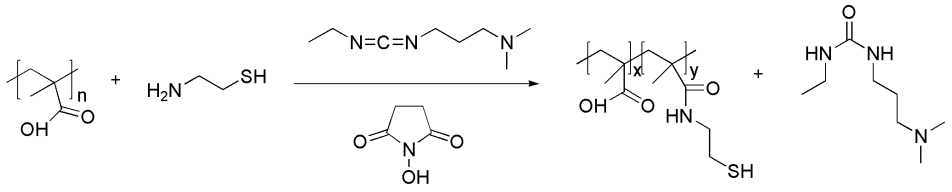

Figure 3.19: Reaction scheme for the functionalisation of PMA to form PMA_{SH}, carried out at 22 ºC for 24 hours.

Characterisation to establish the extent of functionalisation and to confirm the successful attachment of pendant thiol groups was conducted via ^{1}H-NMR. The two CH_2 peaks for cysteamine shifted from 3.15 and 2.79 ppm to 3.55 and 2.92 ppm corresponding to a change from being adjacent to an amine to being adjacent to amide. Percentage functionalisation was estimated by comparing the integral of the peak at 3.55 ppm to the integral of the PMA peak at 1.56 ppm. The PMA_{SH} used in this study had a thiol functionalisation of 33 mol%, corresponding to 15-16 thiolated units per PMA chain (DP:47). It was shown by Zhou *et al.*[17] that 5-30 mol% functionalisation, in their case corresponding to 9 - 52 thiol units per PMA chain (DP: 174), was sufficient to achieve adequate crosslinking and produce stable oil filled microspheres.

Diffusion ordered NMR spectroscopy (DOSY) was used to provide further evidence in support of the argument that the cysteamine was attached to the polymer chain, removing the possibility that the cysteamine was present as a separate molecular species in the sample, the theoretical background to DOSY NMR is discussed in Chapter 5. Some side products were also observed which were shown by DOSY to be attached to the chain.

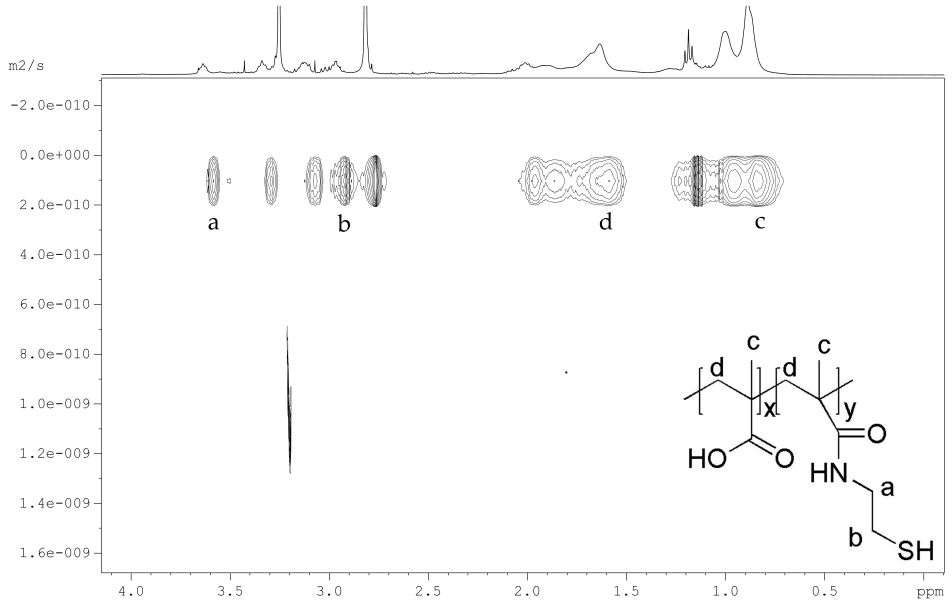

Figure 3.20: DOSY NMR spectrum of dried PMA_{SH} in D_2O at 25 ºC.

The FTIR and Raman spectra of the PMA_{SH} formed (Figure 3.21) were measured from the same dried sample of PMA_{SH} (see section 2.1 for details) and do not show strong S-H peaks, however peaks at 599 and 635 cm^{-1} can be observed in the Raman spectrum which can be attributed to S-S and C-S stretches respectively. These peaks were not observed in the PMA IR or Raman spectrum (Figure 3.22) which is an accurate match to that previously reported[130]. The spectra were collected after a significant period of storage under air so it may be that the samples had partially oxidised to form S-S cross links.

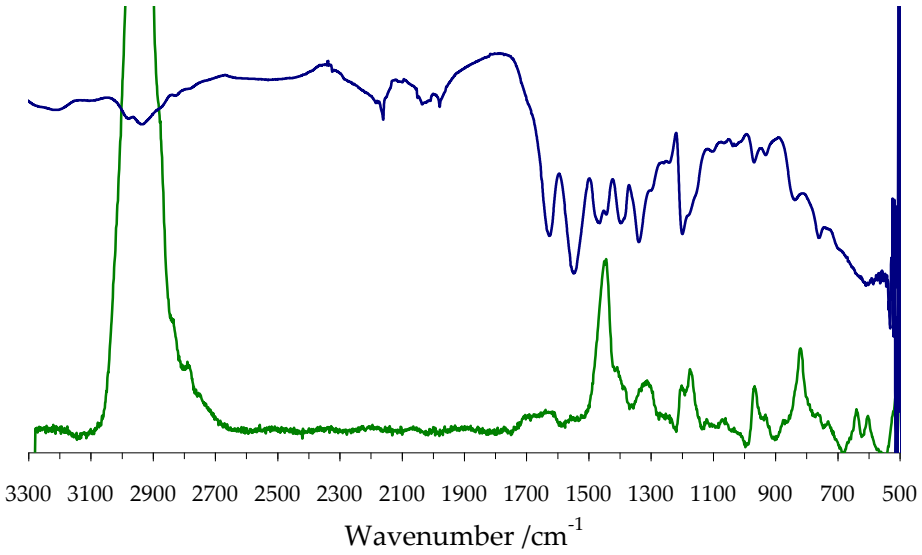

Figure 3.21: FTIR (blue) and Raman (green) spectra of PMA_{SH} (33% functionalisation).

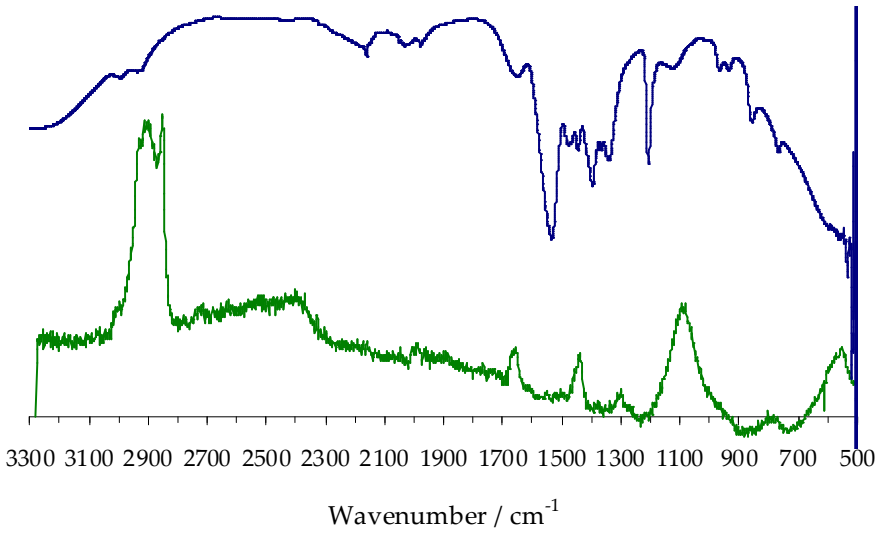

Figure 3.22: FTIR (blue) and Raman (green) spectra of dried PMA.

3.2.2 Microsphere production and characterisation

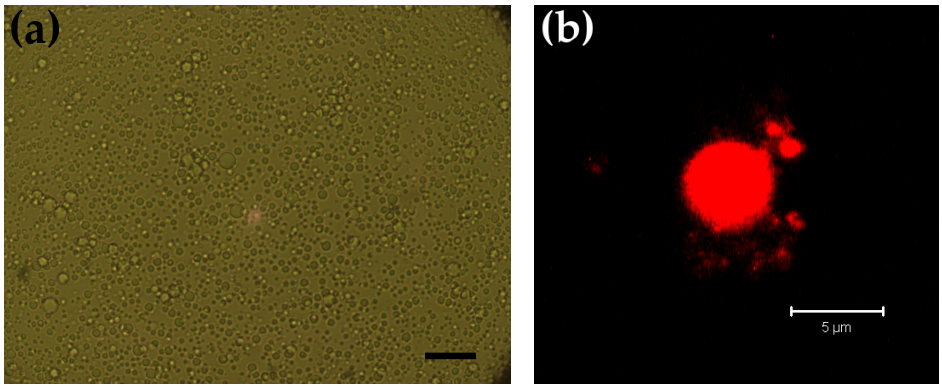

Figure 3.23: Optical transmission micrograph (scale bar: 20 μm) (a) and confocal micrograph (b) of tetradecane filled PMA_{SH} microspheres, the microspheres were imaged in suspension and the tetradecane was saturated with nile red.

Microspheres containing tetradecane can be formed from PMA_{SH} by using a version of the sonochemical procedure discussed above in section 3.1. In the case of PMA_{SH} microspheres no denaturation step is required as the thiol groups are already exposed. Instead the PMA_{SH} solution is slightly acidified prior to sonication, resulting in a small amount of precipitation, similar to that observed when lysozyme is denatured. It is thought that these precipitates aggregate on the oil droplets during microsphere formation. Figure 3.23 shows optical transmission and confocal images of PMA_{SH} microspheres formed with a nile red saturated tetradecane core. The red core observed in the confocal image is the result of fluorescence from the saturated nile red solution and, as with the lysozyme case, demonstrates that the tetradecane has been successfully encapsulated.

The morphology of the microspheres formed is very similar to that seen with lysozyme. The PMA_{SH} microspheres have a mean diameter of 2.1 μm, which is similar to that of lysozyme microspheres formed under the same conditions (2.2 μm). However the PMA_{SH} microspheres formed have a narrower size distribution with a standard deviation of 0.7 compared to 1.1 in the case of lysozyme microspheres, this is illustrated in Figure 3.24. An estimated yield of 1.24×10^9 microspheres can be produced from 1 mL of PMA_{SH} solution with 100 μL of tetradecane, corresponding to quantitative encapsulation

of the oil phase (the estimate was calculated from image analysis of micrographs of a known volume of the suspension produced after sonication, see section 2.1.3). Perfluorohexane can be encapsulated as an alternative, more biocompatible oil[131]. The microspheres produced have a smaller mean diameter (1.36 μm) and narrower size distribution, standard deviation: 0.42 (Figure 3.24).

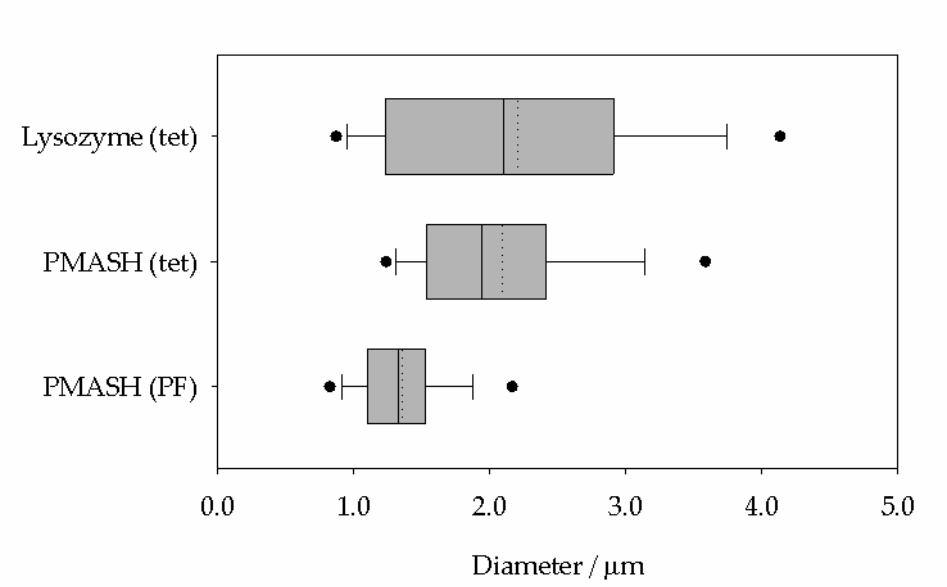

Figure 3.24: Size distributions of tetradecane filled lysozyme microspheres, tetradecane filled PMA_{SH} microspheres and perfluorohexane filled PMA_{SH} microspheres formed using 14 Wcm^{-2} ultrasound for 60 s. (The mean diameter is represented by the dotted line whilst the median is shown by the black line within the grey box. The grey boxes define the upper and lower quartiles, the whiskers the 5 and 95 percentiles and the dots represent outliers.)

Unlike lysozyme however PMA_{SH} microspheres containing a gaseous core cannot be formed using the current method. It was suspected that this was due to a reduced affinity for the air:water interface in the case of PMA_{SH} which would inhibit the aggregation required for effective shell formation. In order to test this theory the surface tensions (γ) of lysozyme and PMA_{SH} solutions were measured using a tensiometer fitted with a Du Noüy ring (section 2.1.16). As can be seen from Table 3.2 the use of tris buffer in place of deionised water slightly reduces the surface tension but its use was necessary to reflect the conditions used during microsphere production. At pH 8 there is not

a large difference between the surface tensions of the PMA_{SH} (60.3 mN/m) and lysozyme solutions (61.5 mN/m). In order to gain a more accurate reflection of the experimental conditions for microsphere production a second lysozyme solution was treated with DTT prior to measurement which increased the surface activity of the lysozyme resulting in a much lower surface tension (30-40 mN/m). However the denatured lysozyme gelled rapidly preventing accurate measurement of the surface tension. For comparison, the surface tension of a PMA_{SH} solution at buffered at pH 5 was measured and found to be only 10 mN/m lower than that of the buffer. At pH 5 the acid groups on the PMA_{SH} chains are fully protonated, which should result in a more surface active polymer. Unfortunately the acidic pH resulted in precipitation of some PMA_{SH} during the measurement depleting the solution concentration. As a result the conclusions drawn from this experiment are limited, surface activity may be a key factor in microsphere production but further measurements would be required to support this argument.

Solution	γ / mN/m
Deionised water	72.3
Tris buffer, pH 8.0	68.6
Acetate buffer, pH 5.0	60.7
Native lysozyme solution, pH 8.0	61.5
PMA_{SH} solution, pH 8.0	60.3
PMA_{SH} solution, pH 5.0	50.6

Table 3.2: Surface tension (γ) data collected using a tensionometer fitted with a Du Noüy ring. All solutions used MilliQ (18.2 MΩ·cm) deionised water, [tris]: 50 mM, [acetate]: 100 mM, [lysozyme]&[PMA_{SH}]: 0.34 mM.

FTIR spectra of dried tetradecane filled microspheres confirm the identity of the shells as PMA_{SH}. Comparison between the PMA_{SH} IR spectrum and the microspheres' IR spectrum (Figures 3.21 and 3.25) shows an increase in the intensity of the peak at 599 cm^{-1} which corresponds to a disulfide bond stretch. In the Raman spectrum the peak at 599 cm^{-1}, associated with the S-S bond stretch is taller than the adjacent C-S peak, in contrast to the PMA_{SH} Raman spectrum, providing further evidence for the formation of disulfide bonds in the shell. Further evidence for stabilisation of the microspheres by disulfide bonding is provided in the release studies reported below

and in Chapter 4 where DTT is used to stimulate release by cleaving disulfide bonds and disrupting the structure of the shell. In addition a new peak is observed in the carbonyl region of the FTIR spectrum at 1712 cm^{-1} and a two strong peaks are seen at 1059 and 1056 cm^{-1} respectively. These peaks are in bands corresponding to C=O and C-O bonds in a carboxylic acid group, which typically displays strong peaks. The carbonyl peak is shifted away from the wavenumber associated with PMA (1665 cm^{-1}). This indicates that a different carboxylic acid group has formed during the sonication carried out during microsphere production. The double peak at 1059/1056 cm^{-1} indicates that two functional groups have been formed it is suggested that the other is a C-O stretch associated with an alcohol group. The Raman spectrum shows two peaks in the O-H band, 3100-3300 cm^{-1}, which correspond to the alcohol and carboxylic acid groups but which could not be conclusively identified in the IR spectrum due to the presence of water. Similar peaks are seen in the FTIR spectrum of PMA_{ene} microspheres (Figure 3.36, section 3.3) and diblock copolymer microspheres (Figure 5.26, section 5.5) indicating that the alcohol groups are formed by reduction of the PMA carboxylic acid groups during sonication in all three cases.

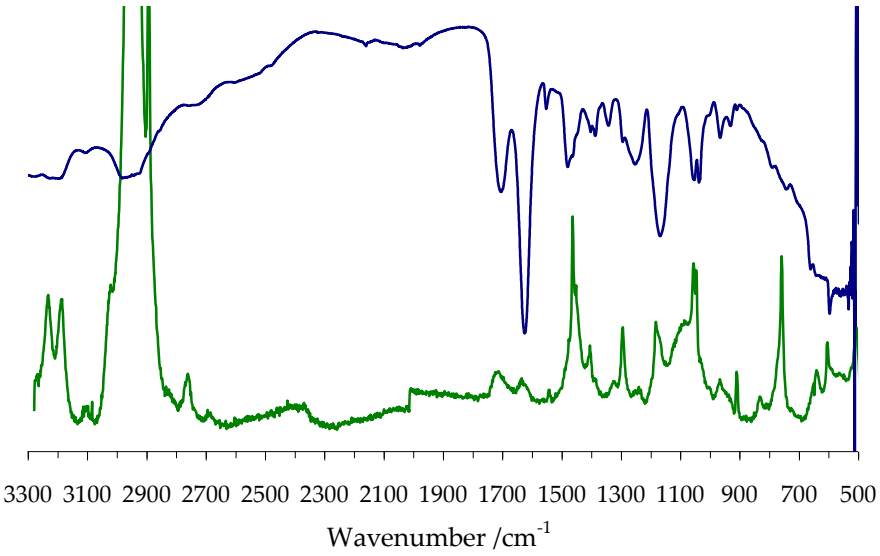

Figure 3.25: FTIR (blue) and Raman (green) spectra of dried tetradecane filled PMA_{SH} microspheres.

The short term stability of the microspheres was investigated by varying to the external pH of the bulk solution in a PMA_{SH} microsphere suspension (Figure 3.26). At acidic pH's the microspheres aggregate, however at pH 6 and above the microspheres remain discretely distributed. Below the pKa 7.5 of PMA[129] the acid groups will be protonated, increasing the overall hydrophobicity of the polymer chains. As a result the microspheres aggregate with one another. At higher pH's the PMA in the shells is ionised meaning that the microspheres are stable towards aggregation.

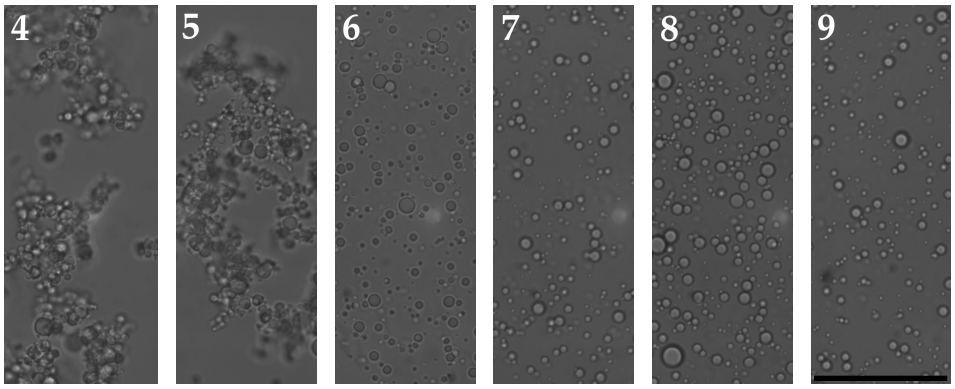

Figure 3.26: PMA_{SH} microspheres incubated at pH 4,5,6,7,8 and 9 in 100 mM phosphate buffer at 22 °C for 2 hours (scale bar: 50 μm).

3.2.3 Release of lipophilic dyes

The successful encapsulation of an oil phase containing nile red has been demonstrated by transmission and confocal microscopy for both lysozyme and PMA_{SH} microspheres. With delivery applications in mind it was interesting to develop a method which would allow the extent of release from the core to be measured under different circumstances. Nile red is highly lipophilic (logP: 3.441 ± 1.435[c]) and therefore very poorly soluble in water (maximum solubility: 0.018 μg/mL)[132]. Nile red containing microspheres were destroyed with 40 Wcm^{-2} ultrasound. However, due to its poor solubility, the quantity of nile red released into the aqueous phase was below the limit of detection by fluorescence spectroscopy, even after freeze drying and re-dissolution in DMSO (the fluorescence intensity of nile red in DMSO is 250 fold more intense than in water[133]).

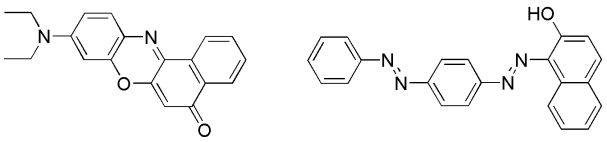

Figure 3.27: Nile red and sudan III

In order to establish the quantity of nile red that could be recovered upon complete destruction of the microspheres, a sample of microspheres was soaked in DMSO. DMSO is a much better solvent for nile red than water[126]. Addition of DMSO to a suspension of microspheres which had been mechanically disrupted by 2 minutes of sonication at 40 Wcm^{-2} allowed the nile red that had been released to be harvested. It was calculated from fluorescence measurements that 6-7% of the nile red initially added during microsphere production was recovered after destruction of the microspheres. This was lower than expected, as the microsphere population estimated in section 3.1.3 suggested 100% encapsulation of the tetradecane. In a control reaction, sonicating 100 μL of tetradecane saturated with nile red in DMSO resulted in 7% release. This suggests that the low release observed in the microsphere case was unlikely to be due to binding of nile red to protein shell fragments and was instead due to limited transfer of nile red from

[c]Calculated using Advanced Chemistry Development (ACD/labs) software V11.02 © 1994-2013 ACD/labs.

the tetradecane phase to the DMSO phase. Therefore in order to gain a better estimation of the extent of release that can be achieved when microspheres are ruptured the methodology was changed to utilise a more lipophilic receptor solvent.

Isopropyl myristate (IPM) is a lipophilic solvent which is used for *in vitro* release studies to mimic the solvency properties of skin[132]. The encapsulated dye was changed from nile red to another red dye, sudan III (SIII)[89] (Figure 3.27). SIII is a highly lipophilic dye (logP: 4.62)[134], it has a stronger absorbance in the visible spectrum than nile red and can therefore be detected at lower concentrations by UV/VIS spectroscopy. PMA_{SH} microspheres were formed from a saturated solution of SIII in tetradecane. Once formed the microspheres were treated in a variety of ways to rupture their shells; incubation with DTT, sonication at 40 Wcm^{-2} for 2 minutes, incubation at pH 1 and incubation at pH 14. After treatment the microsphere suspensions were gently shaken with IPM in order to collect the SIII.

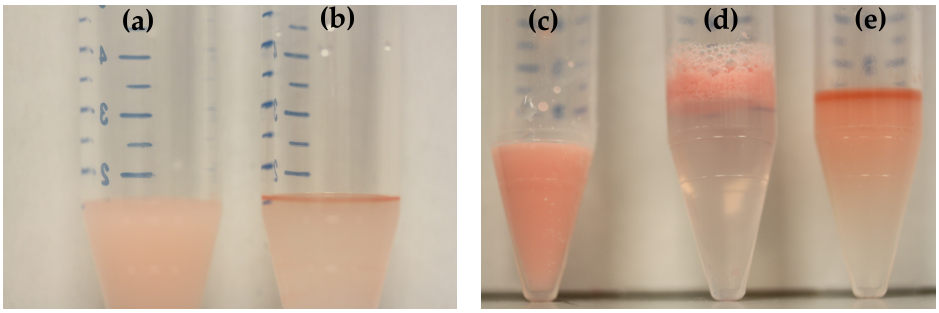

Figure 3.28: Release of sudan III saturated tetradecane phase from PMA_{SH} microspheres; (a) no treatment (30 mins), (b) incubated with 60 mg/mL DTT at 22 °C (30 mins), (c) no treatment (60 mins), (d) incubated at pH 1 (60 mins) and (e) incubated at pH 14 (60 mins).

Prior to solvent extraction with IPM the effects of the various treatments could be observed with the naked eye. In Figure 3.28 tubes (a) and (b) show a comparison between an untreated batch of PMA_{SH} microspheres and a batch that has been incubated with 60 mg/mL DTT at room temperature. The red oil which has been released on rupture of the PMA_{SH} shells by DTT can be clearly seen as a layer on the surface of the solution, whereas no oil layer is visible in tube (a). Solvent extraction of these samples into 2 mL of IPM allowed the quantity of SIII released to be measured by UV/VIS

spectroscopy and hence the extent of release could be calculated. The quantity of SIII harvested from an untreated sample of microspheres that had been allowed to stand for 60 minutes corresponded to 12% release (Table 3.3). This indicates that the encapsulation efficiency of tetradecane/SIII in PMA_{SH} microspheres was 88%. By comparison incubation with 60 mg/mL of DTT over a 60 minute period resulted in 70% release. Sonication of the microspheres at 40 Wcm^{-2} for two minutes did not cause such extensive release (17% compared to 12% in the untreated case). However, when the same sample of microspheres was sonicated for a second time with a small amount of residual IPM a further 35% of the encapsulated SIII was released. It is suggested that the presence of the lipophilic phase aided the disruption of the shell and the rate of release of the oil core. For comparison a control experiment was carried out in which the oil phase alone was sonicated in buffer and solvent extracted into IPM, quantitative release was observed.

	% release
PMA_{SH} MSs	12 ± 4
PMA_{SH} MSs incubated with DTT	70 ± 9
PMA_{SH} MSs sonicated for 2 mins	17 ± 2
PMA_{SH} MSs sonicated for a further 2 mins*	35 ± 8

Table 3.3: Quantity of sudan III recovered in IPM solvent extraction as a percentage of the total amount of sudan III added during microsphere production. (Microspheres (MSs) incubated for 1 hour with 60 mg/mL of DTT or sonicated at 40 Wcm^{-2}, *with residual IPM).

It can be seen from the photographs in Figure 3.28 that incubation with NaOH for 1 hour results in release of the red oil phase. This suggests that the microspheres are less stable at highly alkaline pH, however the extent of release could not be quantified because the alkaline solution formed a stable emulsion with IPM. In the acidic case the microspheres can be seen to have aggregated, as expected from the micrographs discussed in section 3.2.2, but no separated oil phase is visible. Again an emulsion formed with IPM which prevented quantification of release.

Hence it can be seen that tetradecane filled PMA_{SH} and lysozyme microspheres can be formed using the sonochemical method and

loaded with a dye (as a model for drug molecules). The PMA_{SH} and lysozyme microspheres formed are similar in size to those reported by Zhou *et al.*[7;8;47]. The size of the microspheres produced can be controlled by altering the sonication intensity or time in a similar manner to that reported by Zhou *et al.*[47]. The microspheres formed are stabilised by disulfide bonding, as evidenced by radical trapping experiments, FTIR, and Raman spectroscopy. The release experiments conducted demonstrate that release of dye loaded into the PMA_{SH} microspheres can be achieved if the microsphere shell is disrupted prior to solvent extraction into a lipophilic solvent. This demonstrates potential for these microspheres to be used in release applications within the body where the external receptor is lipophilic. Later chapters will discuss adaptions of the methodology explored in this chapter to facilitate encapsulation (and subsequent release) of hydrophilic species and temperature responsive release systems.

3.3 Thiol-ene Chemistry and PMA_{ene} microspheres

The thiol-ene reaction has been known since the early 1900s[135;136 137] but has gained more recent popularity, especially in materials chemistry applications, as a 'click' reaction[138]. The click class of reactions was first described by Sharpless et al.[139], a click reaction is defined as having the following characteristics:

> "a) high yields with by-products (if any) that are removable by non-chromatographic processes, b) regiospecificity and stereospecificity, c) insensitivity to oxygen or water, d) mild, solventless (or aqueous) reaction conditions, e) orthogonality with other common organic synthesis reactions, and f) amenability to a wide variety of readily available starting compounds."[138]

Thiol-ene reactions fulfil many of these criteria[138;140;141] particularly with respect to fast rates, near quantitative, regioselective yields, tolerance of water and oxygen and orthogonality across a wide range of alkenes and thiols[138]. This makes the thiol-ene reaction ideal for applications in materials chemistry[141–143]. Thiol-ene reactions can go via a free radical mechanism or a Michael addition, in this investigation we focussed on the free radical mechanism, Figure 3.29. This reaction can be initiated either thermally or via UV with the help of an added initiator[144]. UV initiation is the more popular initiation method giving fast rates of reaction and clean reaction profiles[145;146].

Sonochemistry offers an alternative radical source that could be used[147;148] but which has not yet been applied to thiol-ene chemistry. Large quantities of radicals can be produced either by thermolysis of the solvent[149;150] or by accelerated breakdown of initiators. As ultrasound is used to produce microspheres it was of interest to establish whether thiolene reactions could be initiated sonochemically. This could provide additional utility to the sonochemical microsphere protocol by providing the opportunity to cross link the microspheres via thiol-ene chemistry instead of disulfide crosslinking, or functionalise the shell with marker or biorecognition molecules in a one pot procedure during microsphere production.

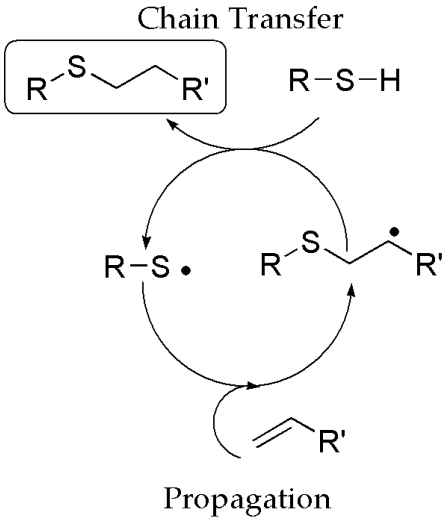

Figure 3.29: General free radical thiol-ene mechanism[140].

In order to establish whether typical thiol-ene reactions could be initiated sonochemically, thiol-ene reactions of a number of small molecule alkenes with 1-butanethiol were carried out. Prior to running the reactions the rate of radical production was measured under thermal conditions typical for thiol-ene reactions and under sonochemical conditions in order to establish thermal and sonochemical conditions which gave similar rates of radical production. A radical trap 2,2-diphenyl-1-picrylhydrazyl[149;151] (DPPH) was used to quantify the radical production in each system with toluene as the reaction solvent and Azobisisobutyronitrile (AIBN) as an initiator[152]. The change in absorbance at 520 nm was measured as the purple DPPH changed to orange $DPPH_2$ as a result of reaction with radicals (Figure 3.30).

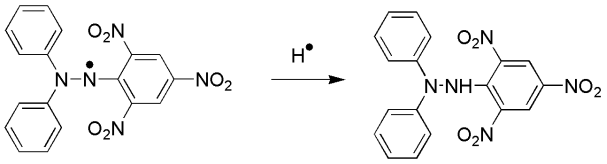

Figure 3.30: Conversion of DPPH to $DPPH_2$ by radical trapping[152].

Zero order kinetics were observed indicating that radical production was the rate determining step rather than the reaction of radicals with DPPH. It was found that by using an ultrasonic horn at 17 Wcm^{-2} with 10-20 mM AIBN a rate of reaction could be achieved at 24 ºC that was comparable to that with a 5 mM solution of AIBN at 50 ºC

without ultrasound (Table 3.4). Without ultrasound the rate of AIBN decomposition at 24 ºC is too slow to be adequately measured by radical trapping. However extrapolation from measurements made at higher temperatures[153] suggests that the rate should be approximately 2 x 10^{-8} s^{-1}. It can therefore be concluded that ultrasound accelerates the rate of AIBN decomposition at room temperature. Based upon the results of these radical trapping experiments it can be suggested that these sonochemical conditions can be used to carry out thiol-ene coupling at room temperature.

Initiation	[AIBN] mM	T /°C	k /10^{-4}mol dm^{-3} s^{-1}
Thermal	20	50 ± 2	15.0 ± 2.6
	10		6.8 ± 0.4
	5		3.3 ± 0.4
	0		0.0
23 kHz ultrasound, 17 Wcm^{-2}	20	24 ± 2	3.8 ± 0.4
	10		3.0 ± 0.4
	5		2.2 ± 0.2
	0		0.62 ± 0.03

Table 3.4: Rate constants for DPPH radical trapping in 0.08 mM toluene solutions.

The conditions chosen were applied to thiol-ene reactions between 1-butanethiol and a range of alkenes listed in Table 3.5 (see sections 2.2.3-5). Good conversions were seen under sonochemical conditions with AIBN for norbornene and N-isopropylacrylamide (NIPAm). It is reported in the literature[140] that alkene reactivity in thiolene coupling decreases as the electron density in the double bond decreases. This trend is followed in both the sonochemical and thermal systems implying that the mechanism is similar in both systems.

In spite of comparable rates of radical production in the two systems the thermal reactions can be seen to achieve much higher conversions, which is perhaps due to competing side reactions in the sonochemical case. Gas chromatography coupled with mass spectrometry (GC-MS) was used to confirm the identity of the major product in each case but no significant side products were observed. Thioether bonds are susceptible to sonolysis in organic solvents[154]. This may result in some loss of product and the radicals produced would be capable of forming a variety of compounds whilst acting as a radical trap, therefore

Alkene	))))* 24 °C	)))) 24°C	Δ* 50 °C	Δ 50 °C
norbornene	63	14	99	0
N-isopropyl acrylamide	42	0	100	0
butyl vinyl ether	30	2	8	0
1-heptene	15	0	24	0
1-pentene	0.3	0.5	0	0
allyl butyl ether	0	0	0	0
allyl amine	0	0	0	0

Table 3.5: % conversion at 2 hours for thiol-ene reaction of alkenes with 1-butanethiol in toluene under inert conditions (* with 20 mM AIBN in the ultrasound reaction and 5 mM AIBN in the thermal reaction).

reducing the concentration of radicals available to initiate further thiol-ene reactions. An improvement to the sonochemical conversion can be achieved by extending the reaction time, increasing the ultrasound power, increasing the concentration of AIBN or increasing the number of thiol equivalents. For example in the case of butyl vinyl ether 88% conversion was achieved over 4 hours by increasing the concentration of AIBN to 60 mM, using 5 equivalents of thiol and using an ultrasound intensity of 21 Wcm^{-2} (simply extending the reaction time to 4 hours gave a conversion of 45%). These conditions would be less appropriate on a larger scale.

Electron deficient alkenes allyl amine and allyl butyl ether did not show any reaction in either system, neither did 1-pentene under thermal conditions and its sonochemical reaction was negligible. In the case of these electron deficient alkenes significantly higher radical production would be required to facilitate a reaction. As expected no reaction was seen with any alkene thermally in the absence of initiator. In the sonochemical system the more reactive alkenes did show some small conversions without initiator present. This shows the benefit of the sonochemical system; an initiator is not necessary for radical production. This is useful in several applications, for example in polymer cross linking where added initiator may cause problems with discolouration or biocompatibility, especially as in the case of polymer cross linking quantitative conversions are not required for efficient cross linking.

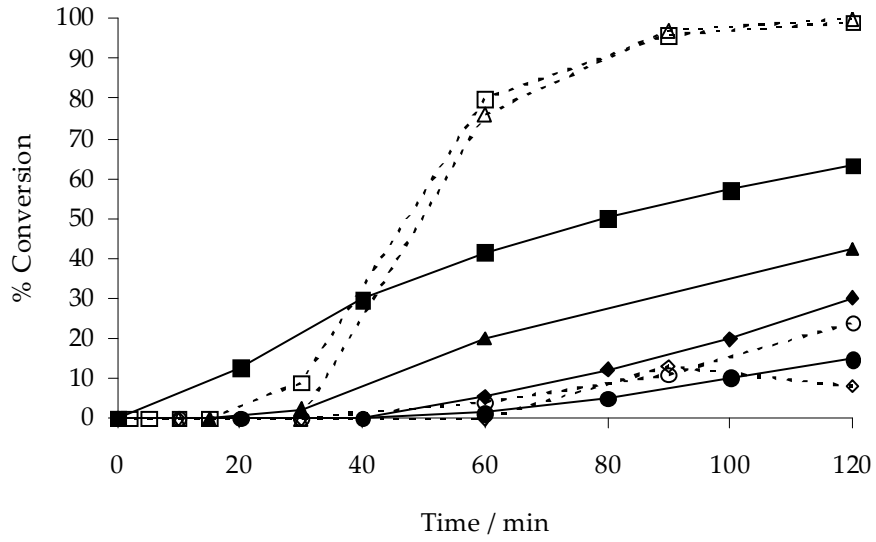

Figure 3.31: Reaction profiles in toluene, filled shapes: sonochemical conditions, empty shapes: thermal conditions, squares: norbornene, triangles: NIPAm, diamonds: butyl vinyl ether, circles: 1-heptene.

The reaction profiles of the four most reactive alkenes in their reactions with AIBN present are shown in Figure 3.31. In the sonochemical system there is a steady decline in reactivity as the alkenes become more electron deficient, the same trend is followed in the thermal case but with a much wider difference. Some inhibition is observed in the thermal cases, this is probably due to residual oxygen. No inhibition is seen in the sonochemical reaction profile due to effective degassing by the ultrasound.

Having demonstrated that it is possible to carry out sonochemically initiated thiol-ene chemistry in inert organic conditions it was interesting to transfer the methodology into water without any inertion as these conditions more closely resemble those used in the microsphere protocol. Potassium persulfate was used as a water soluble initiator with the water soluble thiol, cysteamine HCl. The number of thiol equivalents used was increased from 1.5 to 5 in light of the results of the first investigation and in order to supress any competing polymerisation reactions in the cases of NIPAm and acrylamide[155].

Dosimetry experiments were carried out with terephthalic acid[156] (TA) which traps $HO^{\bullet}$, to estimate radical production and determine condi-

tions where the same concentration of initiator could be used in both the thermal and the sonochemical systems to produce comparable rates of radical production. This was achieved by measuring the rate of increase in fluorescence intensity over an hour as fluorescent hydroxyterephthalic acid (HTA) was formed from reaction between TA and a hydroxyl radical (Figure 3.32). Table 3.6 shows the results of these experiments and again ultrasound shows evidence of radical production without initiator whereas the thermal system does not.

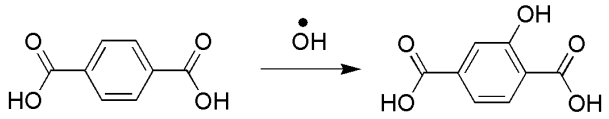

Figure 3.32: Conversion of TA to HTA through reaction with a hydroxyl radical.

Initiation	$[K_2S_2O_4]$ /mM	T /°C	Rate of change of fluorescence at 410 nm (au/min)
Thermal	1.75	45 ± 2	2383 ± 724
	0		No rxn.
23 kHz	1.75	24 ± 2	1763 ± 113
Ultrasound	0		1296 ± 74

Table 3.6: Rate of change of fluorescence for radical trapping by TA in a 0.2 mM aqueous solution.

The more reactive alkenes that do not polymerise show quantitative conversion after one hour in both the sonochemical system and the thermal system (Table 3.7). As with the organic system there are reports of aqueous sonolysis in the literature[157] but these results show that it is not a significant problem in this aqueous system in the way it is in the organic system under similar conditions. For both NIPAm and acrylamide some polymerisation is observed to compete with the thiolene reaction, 16% and 50% conversion to polymer is observed in each respectively. It was also observed that acrylamide underwent some reaction to form thioether in the absence of initiator. In this case it seems that thermal decomposition of acrylamide at 45 ºC provides sufficient radicals to initiate the thiol-ene reaction. As with the organic case there is some sonochemical reaction in the absence of initiator due to sonochemical radical production. Indeed pentenoic acid is

seen to react to 100% conversion sonochemically without any initiator present. These results present the opportunity to use ultrasound to initiate a thiol-ene reaction without any initiator present, ideal in cases where thermal lability of the reagents may prevent the use of thermal conditions or the use of an initiator is not appropriate, for the reasons discussed above. Indeed in the case of this project initiating the thiolene reaction sonochemically without any initiator is ideal for the microsphere protocol, especially as quantitative conversion is not essential for cross linking reactions.

Alkene	))))* 24 °C	)))) 24 °C	Δ* 45 °C	Δ 45 °C
4-Pentenoic acid	100	100	100	0
3-Allyloxy-2-hydroxy-1-propanesulfonic acid	100	5	100	0
N-isopropyl acrylamide	69	0	62	0
Allyl alcohol	100	30	77	0
Acrylamide	35	12	41	28
Allyl amine	33	8	14	0

Table 3.7: % conversion at 1 hour for thiol-ene reaction of alkenes with cysteamine hydrochloride in water under ambient conditions (* with 1.75 mM $K_2S_2O_4$in both cases).

Again the reaction profiles for the four most reactive alkenes were studied, Figure 3.33. For the more reactive alkenes quantitative conversion can be achieved within 10-30 minutes with both the sonochemical and thermal conditions. As with the organic case the thermal reactions are slightly faster but the longer reaction time required for the sonochemical system is not inconvenient.

The high conversions observed in the aqueous system demonstrate that thiol-ene reactions can be carried out efficiently with ultrasound in place of thermal initiation and extend the scope of thiol-ene reactions to encompass a system where a chemical initiator is not required. These reaction conditions do not fulfil all of the requirements of a 'click' reaction discussed above but do provide an effective reaction system with which to approach applications in polymer crosslinking at room temperature.

With this in mind this reaction was applied to the sonochemical production of microspheres by using an olefinic analogue of PMA_{SH},

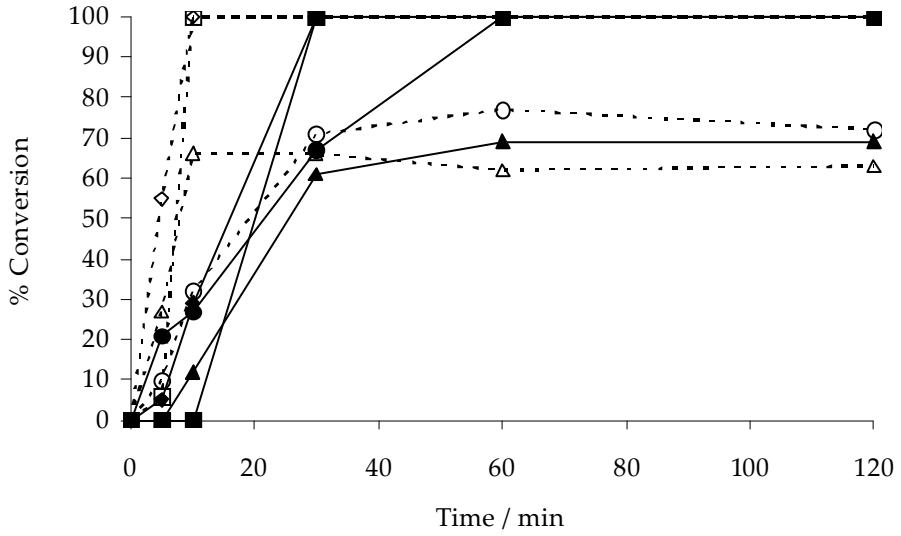

Figure 3.33: Reaction profiles in water, filled shapes: sonochemical conditions, empty shapes: thermal conditions, diamonds: pentenoic acid, squares: 3-allyloxy-2-hydroxyl-1-propanesulfonic acid, triangles: NIPAm and circles: allyl alcohol.

PMA_{ene} and DTT as a crosslinking agent. This system was designed to provide a simple model to establish whether thiol-ene chemistry could be used to crosslink PMA in the microsphere shells with a view to developing the system towards more complex crosslinkers which contain, for example a biodegradable or photo labile linkage. Such linkages could provide an alternative route to externally triggered breakdown of the microsphere shell to that based on the polymer behaviour discussed in Chapter 5. By using a degradation route which utilises the crosslinker there is potential to design dual responsive microspheres that contain a responsive block co-polymer and degradable linkages. This sonochemical thiol-ene chemistry also provides a route to 'one-pot' surface functionalisation of the microsphere shell by adding an alkene based ligand or marker molecule to a standard microsphere protocol, although this option has not been explored in this project.

In order to achieve a 'proof of principle' for thiol-ene crosslinking in microsphere production, as an alternative to disulfide crosslinking, PMA_{ene} was synthesised in a similar manner to PMA_{SH}, Figure

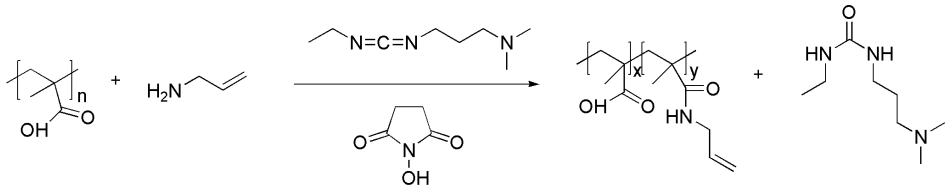

Figure 3.34: Reaction scheme for the functionalisation of PMA to form PMA_{ene}, carried out at 22 ºC for 24 hours.

3.34. In the case of PMA_{ene} 15% functionalisation was achieved, corresponding to 7 alkene units per PMA chain (DP: 47), confirmed by DOSY NMR. The PMA_{ene} produced was used in the sonochemical protocol together with two molar equivalents of DTT as a dithiol cross linker. The tetradecane filled microspheres formed are shown in Figure 3.35. In order to establish whether the shells contained thioether linkages the microspheres produced were dried and analysed using FTIR (Figure 3.35). The broad peak at 616 cm^{-1}suggests a C-S stretch consistent with thiol-ene crosslinking. However further characterisation is required to provide more substantial evidence for thiol-ene crosslinking of the microsphere shell.

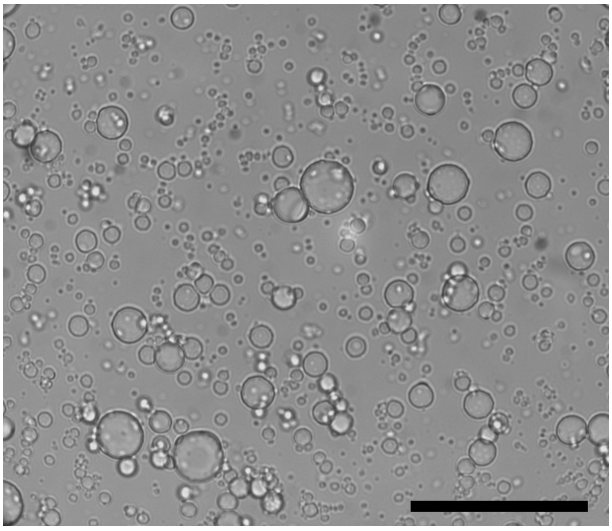

Figure 3.35: Optical micrograph of PMAene microspheres crosslinked with DTT in aqueous suspension, scale bar: 50 μm

These results demonstrate that the sonochemically initiated thiol-ene reaction is a viable alternative to its thermally initiated analog. The reaction rates in the aqueous system were particularly favourable, achieving high conversions in short reaction times. The initiator free

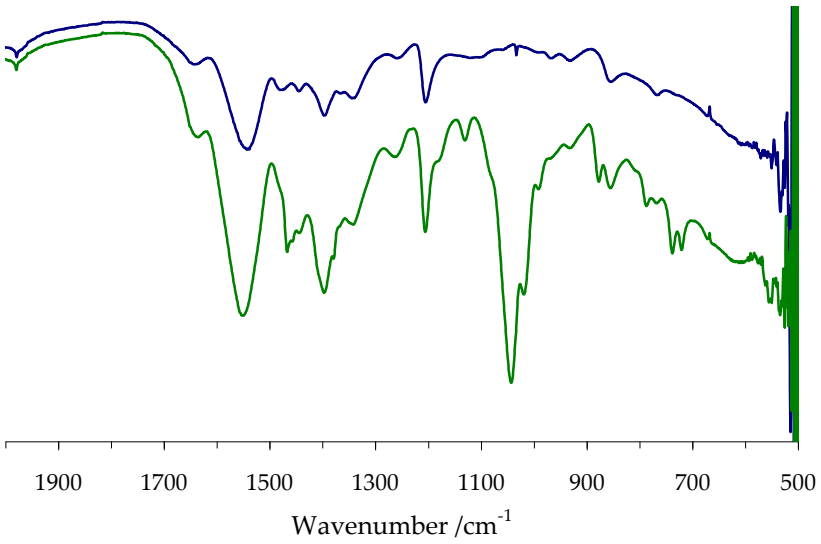

Figure 3.36: FTIR Spectra of dried PMAene (blue) and dried PMAene/DTT tetradecane filled microspheres (green)

sonochemical thiol-ene reaction can be transferred to the sonochemical microsphere protocol in order to form PMA_{ene} microspheres with the aid of a cross linker. This utility provides potential for future applications of sonochemical microspheres through the use of degradable cross linkers.

4 Water in oil emulsion filled microspheres

Beyond sonochemical encapsulation of an oil phase within a protein or polymer shell, discussed in chapter 3, it is of interest to explore the potential to encapsulate an aqueous phase using the sonochemical method. The presence of an aqueous phase within the core of sonochemically produced microspheres opens up the opportunity to deliver hydrophilic species in addition to lipophilic species.

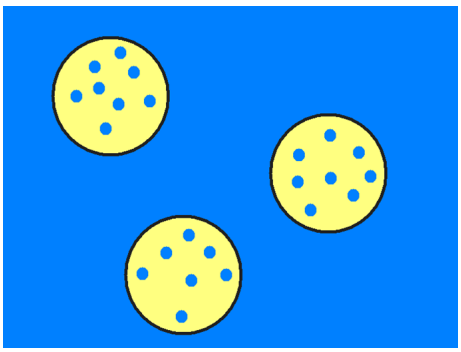

Figure 4.1: Schematic of ideal w/o emulsion filled microsphere structure, blue: aqueous phase, yellow: oil phase and grey: lysozyme shell.

The formation of oil filled protein and polymer microspheres via the sonochemical method is dependent upon the emulsification that occurs during the sonication step. In order to facilitate both emulsification and encapsulation of an aqueous phase, formation of a triple emulsion was proposed. It was thought that by forming a water in oil (w/o) emulsion phase which could then be emulsified in a second oil in water (o/w) emulsion during microsphere production a water in oil in water (w/o/w) emulsion stabilised by the protein shell could be formed. Figure 4.1 shows an idealised schematic version of the structures proposed. Formation of these w/o emulsion microspheres

should facilitate encapsulation of hydrophilic species in addition to lipophilic species, broadening the scope of sonochemically produced microspheres for drug delivery.

4.1 Water in oil and water in oil in water emulsions

In order to design a w/o emulsion that is sufficiently stable to undergo sonication with a protein solution to form w/o emulsion filled microspheres an understanding of the theory behind emulsion production and stability is required. Emulsions are inherently thermodynamically unstable due to the high surface energy of the dispersed phase[158]. As a result a large input of energy is required to form an emulsion, this can be provided by mechanical means, for example via a homogeniser or an ultrasonic transducer[159]. The emulsion can be stabilised by using surface active species (often a surfactant) to reduce the interfacial tension between the droplets and the continuous phase[160]. When emulsifying oil and water either an o/w or a w/o emulsion can be formed, determined largely by whether the surfactant chosen is more soluble in the water or oil phase[158]. In this study our interest is in forming a w/o emulsion that is stable enough to undergo a second emulsification step to form a w/o/w double emulsion which is then stabilised by a protein or polymer shell.

Emulsion droplets tend to adopt a spherical shape in order to minimise their surface area and therefore their surface energy. Interfacial tension (γ Nm^{-1}) is a proportionality constant describing the change in Gibbs free energy (∂G) with changing surface area ($\partial \sigma$)[161]:

$$\gamma = \left(\frac{\partial G}{\partial \sigma} \right)_{T,p} \tag{4.1}$$

The pressures exerted on the curved interface of the droplet are determined by the Laplace equation which states that the pressure on

the concave face of the interface (P_{in}) will always be greater than that on the convex face (P_{out})[160].

$$P_{in} = P_{out} + \left(\frac{2\gamma}{r}\right) \tag{4.2}$$

This difference in pressure across the interface decreases, eventually to zero, as the radius of curvature (r) increases, eventually to infinity for a flat interface[160]. The small droplets formed in emulsions have a small radius of curvature and therefore the pressure gradient across the interface is large. The pressure gradient is also influenced by the interfacial tension at the bubble surface. Hence an emulsion can be stabilised by a surfactant which reduces the interfacial tension.

Several processes can contribute to the breakdown of an emulsion:

- Ostwald ripening: This is a thermodynamically driven process in polydisperse emulsions that results in an increase in the average droplet size of an emulsion[162]. Small droplets have a higher surface energy than large droplets due to their larger surface area to volume ratio. As a result small droplets dissolve into the continuous phase more rapidly than large droplets. The dissolved molecules diffuse through the continuous phase and join the larger droplets[162;163]. The overall result of this process is a decrease in the free energy of the emulsion and eventual phase separation. In a w/o emulsion this phenomenon can be described as an osmotic process, water molecules from the dispersed droplets pass through the continuous oil phase as if it were a partially permeable membrane[164].

- Droplet coalescence: If the energy barrier to coalescence between two adjacent droplets is not sufficiently large then a single larger droplet with a lower surface energy will form. The presence of an interfacial membrane of surfactant molecules prevents coalescence by reducing the interfacial tension of the individual droplets whilst providing a physical barrier[158].

- Sedimentation and creaming: Inverse (w/o) emulsions are prone to sedimentation, whilst oil droplets in an o/w emulsion tend to cream at the surface. Inverse emulsions can be stabilised towards

sedimentation by reducing the droplet size, as small droplets have greater kinetic stability[165].

Sonochemical emulsification

Mechanical emulsification works by creating shear which disrupts the interface between two phases resulting in droplet formation[159;166]. In this study ultrasound will be used as the method of emulsification. The exact mechanism of droplet disruption by ultrasound is not yet fully understood, however the following three mechanisms are known to contribute to droplet formation[35]:

- Unstable oscillations at the water:oil interface (capillary waves) disrupt the interface resulting in the formation of droplets. This mechanism only makes an important contribution if the wavelength of the capillary waves is significantly shorter than the diameter of the initial droplet. The wavelength of the capillary waves at 20 kHz is typically 10 μm so this mechanism is only of significant importance at the start of the emulsification process[167].

- Oscillation of whole droplets followed by disruption will occur with droplets which have a diameter matching the wavelength of the sound wave, which at 20 kHz is 10 μm. This mechanism makes a limited contribution to the overall emulsification process due to the polydisperse nature of the system[168].

- Cavitation is thought to be the dominant emulsifying mechanism and it has been observed empirically that parameters which enhance cavitation also enhance emulsification resulting in smaller droplet diameters. Upon cavitational collapse micro jets are generated which are thought to cause extensive droplet disruption, although this mechanism has not yet been proven[35;159;166].

It has been demonstrated that the droplet size in w/o emulsions decreases with increasing energy density in ultrasound systems[165]. Emulsions generated by sonication have dispersed droplets with a smaller average diameter than those generated in high pressure homogenizers and are therefore more stable[35].

The purpose of this study is to create encapsulated w/o/w droplets using a two step process. The cross-linked lysozyme shell should

stabilise the secondary emulsion by providing a physical barrier to coalescence. As a result the main challenges in the design of the system are in creating a w/o emulsion that is sufficiently stable to undergo the second emulsification step, and in maintaining the integrity of the internal water droplets after formation of the double emulsion. The surfactant chosen to stabilise the dispersed water droplets is sorbitan monooleate (Span 80®) (Figure 4.2), an emulsifier commonly used in food products such as cakes, icings and artificial whipped cream[169]. Span 80® has a Hydrophile Lipophile Balance (HLB) value of 4.3 meaning that it has a greater affinity for the oil phase than the aqueous phase[169]. This makes it a suitable surfactant for a w/o emulsion as it is has been shown to be favourable to emulsion stability if the emulsifier has a higher affinity for the continuous phase than the dispersed phase[169].

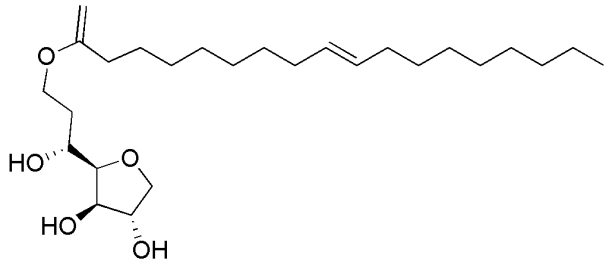

Figure 4.2: Span 80®

There are a number of factors that affect the stability of w/o and w/o/w emulsions, below is a brief summary discussing these factors in the context of Span® surfactants and how they can be manipulated in order to achieve desired emulsion characteristics. The two key factors that concern this study are emulsion stability which should be maximised and droplet size which should be minimised.

Choice of oil: There is very little comment in the literature regarding the properties of oils used in w/o emulsions. However it was noted by Capdevila *et al.*[170] that long alkyl chain oils give more stable emulsions than those oils with short alkyl chains. Water molecules are thought to become less soluble in the oil phase as the length of the alkyl chains increases and therefore Ostwald ripening is inhibited in emulsions formed with long alkyl chains[170]. This supports the case for using tetradecane, the oil phase utilised in chapter 3, in the emulsions produced for encapsulation. In a study of ultrasound

assisted emulsification it was noted by the authors that oil viscosity did not affect the resulting size distribution of the water droplets formed[166].

Surfactant concentration: Double emulsions are often stabilised by two surfactants, one in the oil phase which stabilises the internal water droplets and one in the continuous water phase which stabilises the secondary oil droplets, for example Span 80® with Tween 80®[171]. In our case we have chosen to replace the surfactant in the aqueous phase with lysozyme which will stabilise the secondary oil droplets by forming a cross linked shell. This has the benefit that unfavourable surfactant interactions can be removed from the system, for example; Tween 80® is able to solubilise Span 80® in micelles removing it from the oil phase to the bulk aqueous phase, destabilising the w/o phase[171]. Increasing the concentration of surfactant in the oil phase decreases the internal water droplet size and decreases the w/o/w droplet size[171 169]. This results in greater kinetic stability to coalescence. However if the surfactant concentration is increased beyond the critical micelle concentration (cmc) then the rate of Ostwald ripening will increase because the transport of water molecules through the continuous oil phase will be aided by the presence of inverse micelles[172]. The effect of Span 80® concentration on the diameter of the internal water droplets in the emulsions produced for the w/o emulsion microspheres discussed in section 4.2 will be considered, whilst optimising the emulsion production conditions.

Sonochemical w/o/w microspheres

There are several reports of w/o/w emulsions formed under ultrasound irradiation and stabilised by polymer coatings[173;174], however in these cases the ultrasound is used only for emulsification and not for sonochemical purposes. One report describes the self assembly of egg white proteins around a benzotrifluoride oil phase, whilst under sonication in a 35 kHz ultrasound bath for 1- 60 minutes, to form w/o/w capsule structures[175]. The structures formed in this system are based on pickering emulsions formed in an initial emulsification step. These emulsions are simple o/w emulsions which are not particularly stable. However when these emulsions are sonicated,

w/o/w structures are formed which are more stable. It is suggested by the authors that the unexpected w/o/w structure is formed as a result of deformation of the protein shells during sonication resulting in pinching of water droplets into the internal oil phase[175]. The result is a structure made up of capsules within capsules. This system is based on a mixture of proteins, including lysozyme, which will have contributed in part to the formation of complex w/o/w capsules and are likely to have undergone some sonochemical denaturation.

Characterisation of encapsulation and release

In order to use these w/o/w systems for drug delivery applications it is necessary to characterise the encapsulation of solute within the inner aqueous phase and also the release profile, both under storage conditions and also as a result of triggered release. In order to achieve this the following definitions were used:

Encapsulation efficiency[176]: "The amount of aqueous phase marker that remains entrapped in the inner aqueous phase during manufacture of the w/o/w double emulsion".

Encapsulation stability[176]: "The amount of aqueous phase marker which remains entrapped in the inner aqueous phase during storage or stresses".

Released markers can be separated from the emulsion phase (in this case microspheres) either by centrifugation or dialysis prior to measurement. In order to accurately quantify the encapsulation efficiency and the encapsulation stability the chosen marker molecule must not be degraded during production of the w/o/w system or afterwards in release. A range of different markers and detection methods have been reported including: vitamin B12, methylene blue and glucose, all detected by UV/VIS spectroscopy[176;177]; vitamin B1 release was detected by electrochemical methods[178]; release of salt can be characterised by conductivity[179;180] and finally release can be monitored by measuring the fluorescence from fluorophores or fluorescently labelled proteins[181;182]. In the following discussion fluorescence, conductivity and UV/VIS (via HPLC) are used to detect release of 5,6-carboxyfluorescein, sodium chloride and 5-fluorouracil respectively.

Results and Discussion

Encapsulation of lipophilic components dissolved in oil phases within the microspheres is accomplished by floating a small amount of the oil solution on the surface of the protein solution and sonicating for a short time with the tip of the ultrasound horn at the oil:water interface (as described in chapter 3). This methodology was modified here by replacing the organic component with a water-in-oil emulsion, using a continuous oil phase known to facilitate microsphere formation. The challenges in this investigation were; to prepare a stable w/o emulsion which could be layered on the surface of the lysozyme solution, to maximise the quantity of aqueous phase within the inverse emulsion and to develop the sonochemical methodology described in chapter 3 so that the emulsion maintained its internal structure once formed into microspheres.

4.2 Inverse emulsion optimisation

The first step undertaken in the development of w/o emulsion microspheres was to find the optimum conditions for formation of a w/o emulsion using our ultrasonic transducer. Ultrasonic emulsification was carried out as a convenient and efficient means of forming a finely dispersed emulsion. It was not possible to form a stable w/o emulsion by sonicating water and tetradecane alone, instead a two phase system formed containing an o/w emulsion phase and an excess of tetradecane.

Djenouhat *et al.*[183] report using Span 80® to stabilise a water in oil emulsion made up of sulfuric acid in hexane. Span 80® is soluble in the continuous hexane phase and stabilises the water droplets as inverse micelles, reducing the interfacial energy and facilitating w/o emulsion formation. Reproducing the optimised conditions reported by Djenouhat *et al.* (three minutes sonication time, 5 w/w% Span 80®, 0.5 M sulfuric acid and an aqueous:hexane ratio of 1:1) using generator B at an intensity of 45 W cm^{-2} a w/o emulsion was formed. The hexane w/o emulsion was used in the sonochemical microsphere protocol but no microspheres containing an emulsion phase were formed. It

was clear that the emulsion was not sufficiently stable to survive the sonication used to form microspheres. However substituting tetradecane in place of hexane resulted in a w/o emulsion that could be used to form w/o emulsion microspheres. The w/o emulsion in the microspheres can be clearly discerned by optical microscopy (Figure 4.3).

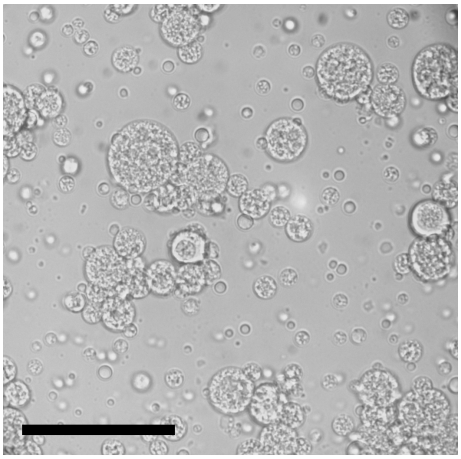

Figure 4.3: Optical micrograph of w/o emulsion microspheres formed from a 40 wt% (0.5 M sulfuric acid$_{(aq)}$: tetradecane containing 5 wt% Span 80®) w/o emulsion according to the sonochemical method (section 2.3.2), scale bar 50 μm.

In order to optimise the conditions used to form the w/o tetradecane emulsion the effect of varying the concentration of Span 80®, sonication time and salt concentration on the dispersed aqueous droplet diameters were studied. The emulsions formed in each case were diluted in tetradecane containing a matching concentration of Span 80®, to allow the droplet diameter distribution to be measured by dynamic light scattering (DLS). The aim was to minimise the droplet diameter in order to form a well controlled, finely dispersed emulsion that could be encapsulated reproducibly within protein microspheres.

Figure 4.4 shows the z-average droplet diameters, measured by DLS, formed with different concentrations of Span 80® in the tetradecane phase. The z-average diameter is defined as an average of the droplet population's hydrodynamic diameters weighted with the square of the particle mass[184]. It can be seen that between 0.5 and 4 wt% increasing the Span 80® concentration reduces the z-average diameter of the water droplets in the emulsion. However 4 wt% is the optimum Span

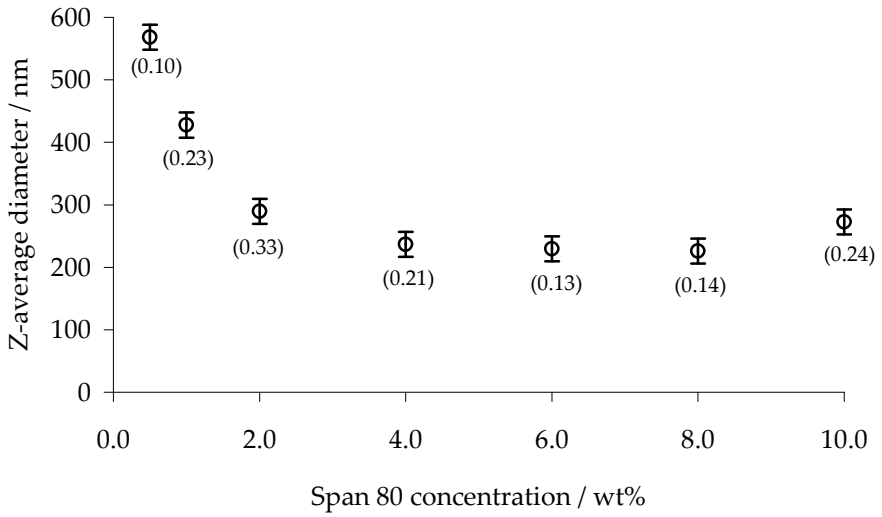

Figure 4.4: Effect of surfactant concentration on droplet diameter in a 40% v/v tetradecane emulsion measured by DLS (sample dispersities displayed in brackets). (6 M $NaCl_{(aq)}$, 5 min sonication; 45 Wcm^{-2})

80® concentration, as at higher concentrations no change in water droplet diameter is observed. Early studies also showed that whilst w/o microspheres could be successfully formed from 4 wt% Span 80® emulsions, w/o microspheres could not be formed from 0.5 wt% Span 80® emulsions. Hence 4 wt% was chosen as the best Span 80® concentration for ongoing investigations.

The second parameter considered was sonication time. The z-average diameter of water droplets in emulsions formed by sonication over different time periods are shown in Figure 4.5. Intuitively it would be expected that the diameter of the water droplets formed would decrease with increasing sonication time as more cavitation events are allowed to occur. This is consistent with the results collected. Between one and ten minutes, increasing the sonication time results in a decrease in water droplet diameter. However after ten minutes the change in diameter with respect to sonication time plateaus. Five minutes was chosen as the optimum sonication time as the small decrease in diameter between five and ten minutes did not warrant doubling the sonication time.

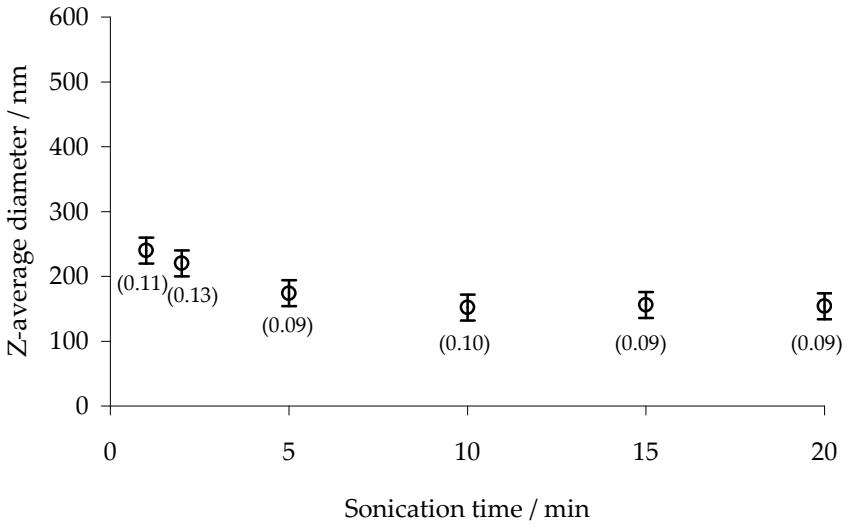

Figure 4.5: Effect of sonication time on droplet diameter in a 40% v/v tetradecane emulsion measured by DLS (sample dispersities displayed in brackets). (4 wt% Span 80®, 0.06 M NaCl, 45 W cm^{-2})

The final parameter investigated was salt concentration. Early scoping experiments discussed at the start of this section were carried out using 0.5 M sulfuric acid as the aqueous phase. Sulfuric acid was not deemed appropriate for the desired application due to the risk that acid hydrolysis may result in degradation of drug or dye molecules encapsulated in the aqueous phase. A stable emulsion can be formed, with a mean droplet size of 234 nm (SD: 6 nm), using the conditions chosen above with pure water as a dispersed phase, Figure 4.6. However when the emulsion was used to form microspheres the emulsion is degraded to a much coarser emulsion with a mean droplet diameter of 2292 nm (SD: 1537 nm) (Figure 4.7a). This in turn resulted in a very polydisperse size distribution of microspheres with varied water loadings.

It was found that adding salt (NaCl) to the aqueous phase did not significantly change the z-average diameter of the dispersed water droplets in the initial emulsion, Figure 4.6. However the emulsion was significantly more stable to coarsening during microsphere formation (Figure 4.7). It was found that when a salt concentration of 0.5 M or higher was used in the dispersed water phase a fine emulsion structure

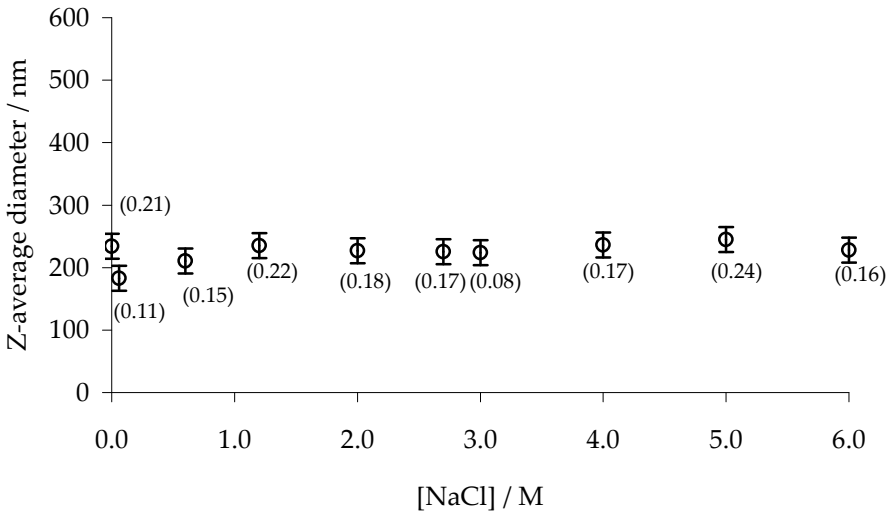

Figure 4.6: Effect of salt concentration on droplet diameter in a 40% v/v tetradecane emulsion measured by DLS (sample dispersities displayed in brackets). (4 wt% Span 80®, 5 min sonication; 45 Wcm^{-2})

was retained in the microspheres formed. This was preferable to the case with 0.06 M salt solution (Figure 4.7b) or pure water because the fine emulsion meant that the volume percentage of water was consistent from microsphere to microsphere. It was also observed that, unlike the samples formed with a salt concentration of 0.5 M or greater, in the case of pure water and 0.06 M salt solution oil filled microspheres were formed in addition to w/o emulsion microspheres. This indicates that significant breakdown of the emulsion occurred releasing oil into the bulk aqueous phase during microsphere production.

There have been a number of studies reported which address the effect of salt in the internal water phase on w/o emulsion stability[164;171;185;186]. From these it seems that the most important effect of a hypertonic internal aqueous phase is the osmotic pressure gradient that is created. It has been reported that the osmotic pressure created by a hypertonic internal water phase counterbalances the Laplace curvature pressure, stabilising the emulsion by reducing Ostwald ripening[164;171;185]. This effect was demonstrated in a study carried out on w/o emulsions of NaCl in hydrocarbon oil stabilised by

Span 80®[186]. It was shown that the ionic strength of the solution could be used to control the rate at which Ostwald ripening occurred and therefore the stability of the w/o emulsion. It was reported that emulsions containing a dispersed aqueous phase with a salt concentration greater than 0.012 M were stable towards Ostwald ripening and coalescence[186].

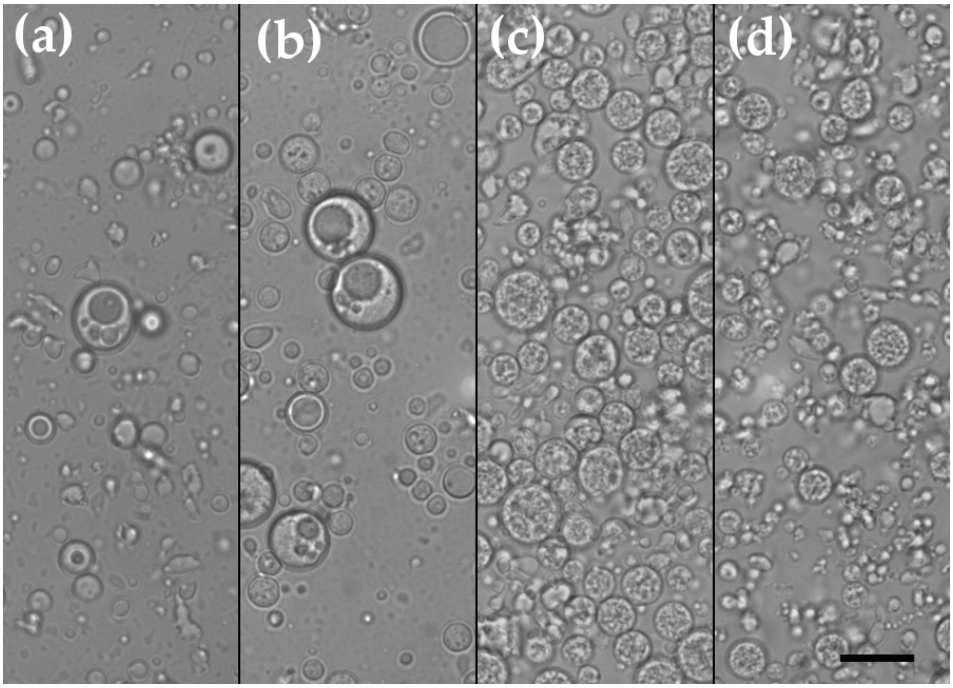

Figure 4.7: Effect of [NaCl] in the w/o aqueous phase on the microspheres' internal emulsion morphology. (a) DI water, (b) 0.06 M, (c) 0.5 M and (d) 3 M NaCl solutions respectively. Scale bar: 10 μm.

An emulsion with a 40 vol% dispersed aqueous phase (1 M $NaCl_{(aq)}$) was produced using the optimised conditions chosen above (emulsion: tetradecane with 4 wt% Span 80®, five minutes sonication at 40 Wcm^{-2}). When this emulsion was used to form microspheres (30 s sonication at 14 Wcm^{-2}) the microspheres produced had a mean diameter of 5.0 μm (SD 1.5 μm), not dissimilar to the lysozyme tetradecane filled microspheres produced under comparable sonochemical conditions; mean diameter 4.5 μm (SD: 1.5 μm).

In order to maximise the loading of hydrophilic species in the final microspheres the effect of varying the emulsion proportions was investigated (Figure 4.8). Emulsions were formed containing 20, 40, 60 and 80 vol% dispersed aqueous phase (1 M NaCl), these emulsions

were then used in the microsphere production protocol. Emulsion microspheres could be formed from the 20 and 40 vol% emulsions (Figure 4.8a,b), however in the case of 60 and 80 vol% aqueous phase microsphere production was less successful and a mixture of oil filled microspheres and protein aggregates were formed (Figure 4.8c,d). The microspheres formed from the 40 vol% emulsion have a finer internal structure than those formed from the 20 vol% emulsion. As such the emulsion with 40 vol% dispersed aqueous phase was chosen as the optimum emulsion for future microsphere production.

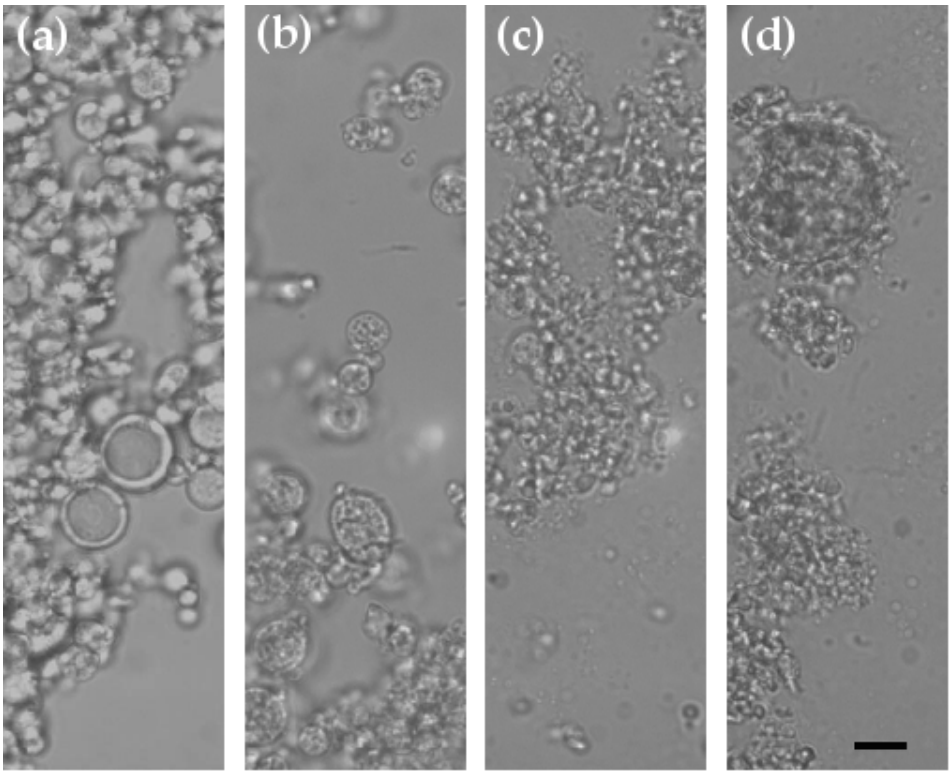

Figure 4.8: Microspheres formed from w/o emulsions with varying aqueous:oil ratios. (a) 20 v/v%, (b) 40 v/v%, (c) 60 v/v% and (d) 80 v/v% aqueous phase (1 M NaCl solution). Scale bar: 10 μm.

Hence the final optimised conditions chosen for w/o emulsion filled microsphere production were as follows: For the primary emulsion; 40 wt% aqueous phase, 1 M NaCl, 4 wt% Span 80® in tetradecane, sonication for 5 minutes at 40 W cm^{-2}. For the microspheres; 100 μL of preformed w/o emulsion was sonicated with 1 mL of 50 mg/mL lysozyme solution at 14 W cm^{-2} for 30 s. These conditions were used when studying encapsulation of hydrophilic and lipophilic dyes and

characterising the release of hydrophilic species, which is discussed in the next section.

4.3 Encapsulation of hydrophilic and lipophilic species

Laser scanning confocal microscopy (LSCM) was used to demonstrate encapsulation of both lipophilic and hydrophilic dyes within emulsion microspheres. Fluorescent dyes 5,6 carboxyfluorescein and nile red were added to the aqueous and oil phase respectively prior to formation of the w/o emulsions. Once formed, the microspheres were imaged using a 488 nm laser to excite green fluorescence from the 5,6-carboxyfluorescein aqueous solution and a 543 nm laser to excite red fluorescence from the nile red oil solution.

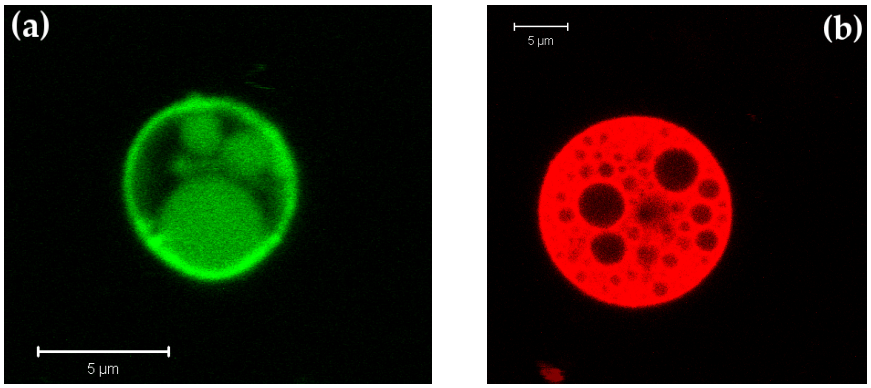

Figure 4.9: LSCM image of w/o emulsion filled lysozyme microspheres in suspension. (a) Internal aqueous phase: 1 mM 5,6-carboxyfluorescein in 10 mM HEPEs buffer, oil phase: 4 wt% Span 80® in tetradecane, external aqueous phase: 3.3 mM tris buffer, viewed under 488 nm laser. (b) Internal aqueous phase: 1 M NaCl(aq), oil phase: 4 wt% Span 80® in nile red saturated tetradecane, external aqueous phase: 3.3 mM tris buffer, viewed under 543 nm laser.

Figure 4.9a shows a 1 μm optical slice through a microsphere containing 5,6 carboxyfluorescein in the internal aqueous phase of the encapsulated emulsion and Figure 4.9b a 1 μm slice through a microsphere containing nile red in the oil phase. In each case the emulsion structure can be clearly observed with the green dye highlighting the dispersed water droplets and the red dye showing the continuous oil phase. In Figure 4.9a, in addition to the dye in the encapsulated aqueous phase, some carboxyfluorescein can also be seen to be trapped in/bound to the lysozyme shell. This indicates that some degradation of the emulsion has occurred during production

resulting in release of the dye from the internal aqueous phase. The released dye has bound to the lysozyme shell resulting in the green ring observed. These images provide evidence for successful encapsulation of the emulsion phase within lysozyme microspheres and demonstrate that large dye molecules can be encapsulated and retained.

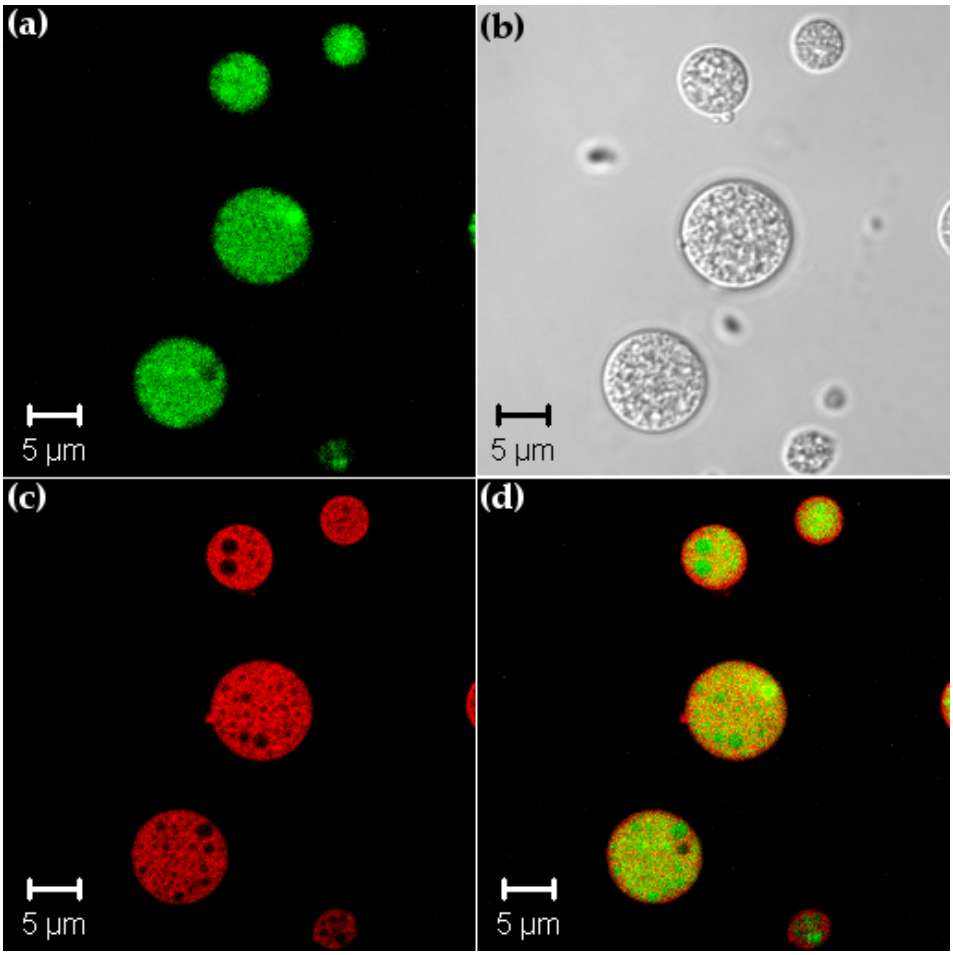

Figure 4.10: LSCM image of w/o emulsion filled lysozyme microspheres in suspension. Internal aqueous phase: 1 mM 5,6-carboxyfluorescein and 1 M NaCl in 10 mM HEPEs buffer, oil phase: 4 wt% Span 80® in nile red saturated tetradecane, external aqueous phase: 3.3 mM tris buffer. (a) viewed under 488 nm laser, (b) white light optical transmission image, (c) viewed under 543 nm laser, (d) viewed under both 488 nm and 543 nm lasers.

More compelling evidence for the enhanced utility of these microspheres beyond that of simple oil filled microspheres can be achieved by adding dyes to the oil and water phases simultaneously. The

resulting LSCM images are shown in Figure 4.10 where it can be seen that the green regions associated with the aqueous phase (Figure 4.10a) correspond to the dark regions in the red image (Figure 4.10c). When the two channels are overlaid the green regions fit exactly into the dark regions left by the red image (Figure 4.10d). This confirms that successful encapsulation of an intact emulsion phase has been achieved and that 5,6-carboxyfluorescein and nile red are encapsulated in the two domains of the emulsion.

Yellow regions in the overlaid image (Figure 4.10d) correspond to parts of the emulsion where the aqueous droplets are less than 1 μm in diameter. The optical slice imaged is 1 μm thick, therefore when the encapsulated aqueous droplets are less than 1μm in diameter the green aqueous phase and the red oil phase overlap within the slice. Figure 4.11 shows the same image with the co-localised pixels removed. In this image the larger water droplets can be seen as distinct green circles, confirming the clearly defined regions of the encapsulated emulsion.

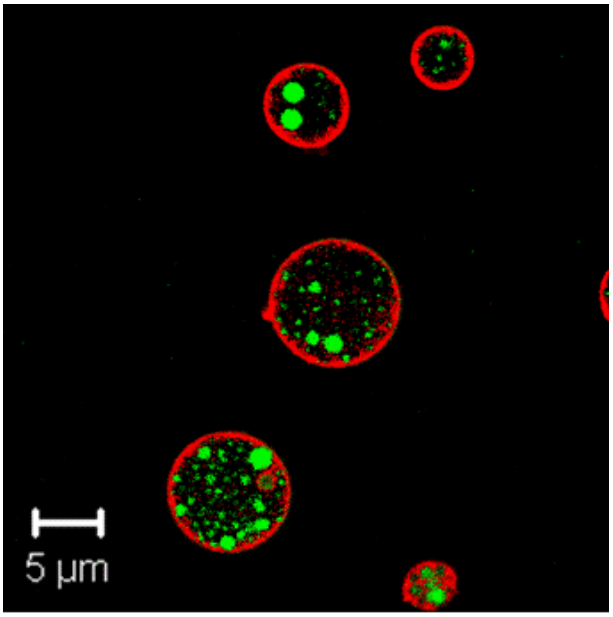

Figure 4.11: LSCM image of w/o emulsion filled lysozyme microspheres in suspension as in Figure 4.10d but with colocalised pixels removed, a pixel was defined as colocalised when both channels (488 and 543 nm) had an intensity of greater than 100 gray[187].

4.4 Release of hydrophilic species from w/o emulsion filled microspheres: Lysozyme microspheres

Having demonstrated that w/o emulsion filled microspheres could be successfully formed using the sonochemical method and that hydrophilic species could be encapsulated it was interesting to investigate the release profiles for hydrophilic species from these microspheres.

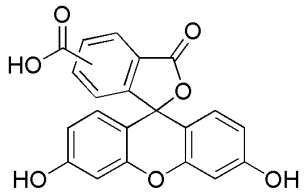

Figure 4.12: 5,6-Carboxyfluorescein

5,6-carboxyfluorescein was chosen as a suitable marker for release because its tendency to dimerise at high concentrations results in self quenching of its fluorescence[188;189]. Hence release can be measured by encapsulating a quenched concentration of 5,6-carboxyfluorescein as the internal aqueous phase and monitoring the increase in fluorescence as the 5,6-carboxyfluorescein is released from the microspheres and diluted into the external aqueous phase[190]. Release of 5,6-carboxyfluorescein was triggered using DTT as a disulfide cleavage agent. It was hoped that cleaving the stabilising disulfide bonds in the shell would provide a crude mimic of the shell degradation that would occur within the reductive environment of a cell subsequent to uptake of a microsphere[90]. A 50 μL portion of microspheres in aqueous suspension was diluted into 2 mL of HEPEs buffer and shaken at 37 °C. The fluorescence emitted by microsphere suspensions incubated with different concentrations of DTT was monitored over a six hour period and the resulting release curves are shown in Figure 4.13.

In the absence of DTT, lysozyme w/o emulsion filled microspheres are stable to 5,6-carboxyfluorescein release over a six hour period (in fact the untreated microspheres remained stable over a 12 hour period). It can be seen from Figure 4.13 that the rate of increase in fluorescence, and hence the rate of release of 5,6-carboxyfluorescein, is

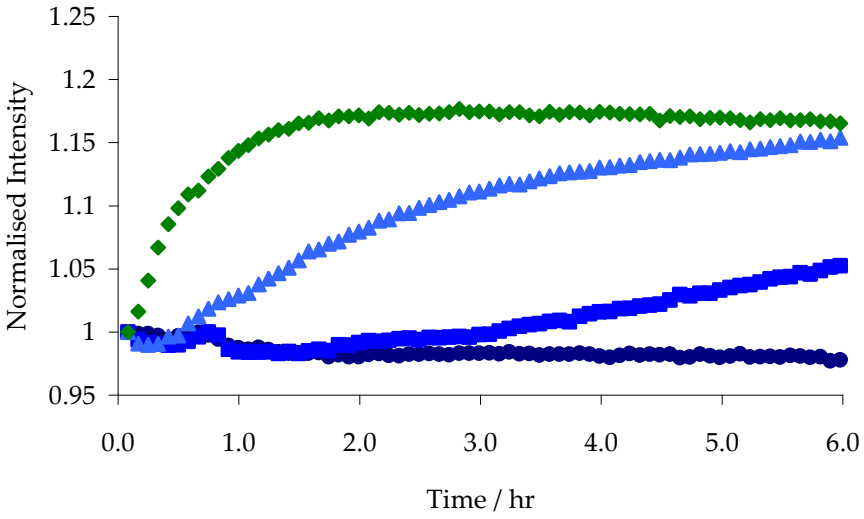

Figure 4.13: Change in solution fluorescence on breakdown of w/o emulsion filled lysozyme microspheres containing 50 mM 5(6)-carboxyfluorescein dispersed in tetradecane on incubation at 37 ºC with DTT. Green diamonds: 60 mg/mL DTT, pale blue triangles: 30 mg/mL DTT, bright blue squares: 12 mg/mL DTT, navy blue circles: no DTT.

dependent on the DTT concentration. The microspheres in 60 mg/mL DTT solution achieved maximum release after two hours compared to six hours in the case of microspheres in the 30 mg/mL DTT solution. DTT destabilises the microsphere shells by cleaving disulfide bonds and the concentration dependence indicates that the disulfide bonds are crucial to the integrity of the protein shell. The DTT dependent loss of the protein shell resulting in 5,6-carboxyfluorescein release also demonstrates that the continuous tetradecane phase alone is insufficient to prevent leakages, so release can be triggered by breakdown of the protein shell. Breakdown of the microspheres and release of the internal water phase can be confirmed by viewing the microspheres under a microscope before and after treatment with DTT (Figure 4.14a,b). After treatment only small oil filled microspheres and protein fragments remain.

In addition to chemical breakdown of the microsphere shells, release triggered by mechanical breakdown of the microsphere shells was investigated. A suspension of microspheres was sonicated at 45 Wcm^{-2} using ultrasound from generator B over a 4 minute period. Release

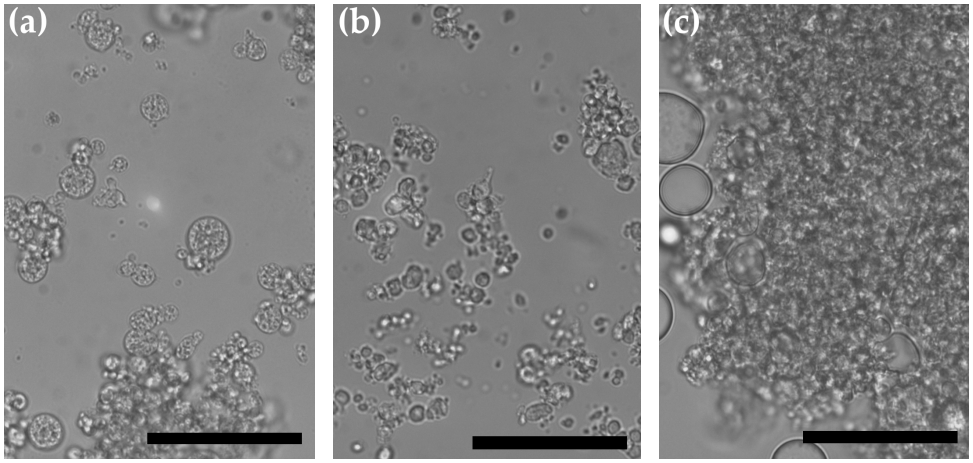

Figure 4.14: Optical micrographs of lysozyme microspheres in suspension taken before (a), after 12 hrs with DTT incubation (b) and after four minutes sonication (c), scale bar: 50μm

was monitored over this period (Figure 4.15) and the maximum fluorescence was observed after 60 s sonication. The fluorescence intensity at 60 s corresponds to the fluorescence intensity after 2 hours incubation with 60 mg/mL DTT. Unfortunately the nature of the experimental method and the fact that the suspension concentration of microspheres cannot be accurately defined, means that the extent of release cannot be expressed as a percentage of the quantity encapsulated. Hence the results in the DTT incubation and sonication experiments were normalised to the fluorescence at 'time zero'. Again breakdown of the microspheres was confirmed from micrographs taken after sonication (Figure 4.14c), in this case all that remained were large protein aggregates and oil droplets.

Subsequent to monitoring dye release, the release of NaCl, used to enhance the stability of the w/o emulsion phase, from emulsion microspheres in suspension was measured. Salt release from the microspheres was estimated by measuring the conductivity of a suspension of microspheres before and after sonicating at 45 Wcm^{-2} for 2 minutes. The change in conductivity resulting from mechanical breakdown of the microspheres during sonication is shown in Figure 4.16 for three different scenarios.

In Figure 4.16a w/o emulsion microspheres containing 6 M NaCl in the dispersed aqueous phase were broken down by sonication. The resulting increase in conductivity indicates that as a result of this

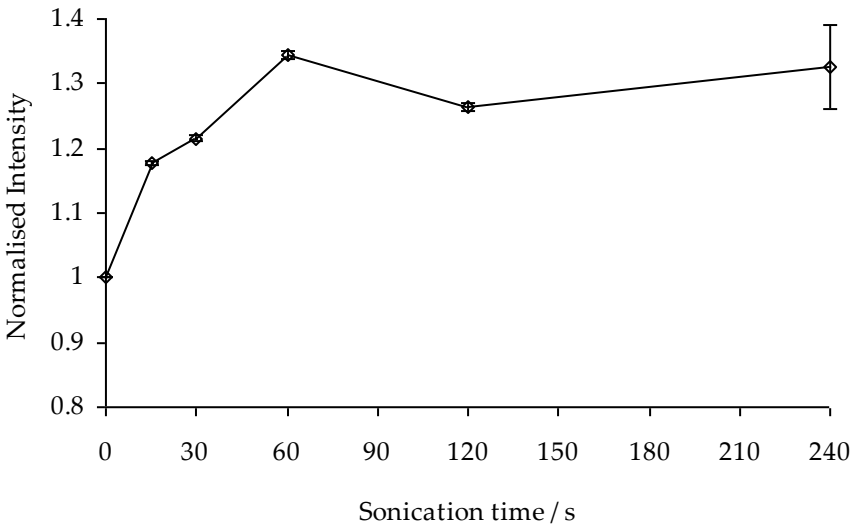

Figure 4.15: Change in fluorescence due to release of carboxyfluorescein on ultrasonic breakdown of w/o emulsion filled microspheres with 50 mM 5,6-carboxyfluorescein as the internal aqueous phase.

breakdown salt is released from the internal aqueous phase, as would be expected. In comparison when oil filled microspheres are sonicated there is only a very small increase in conductivity (Figure 4.16b). There is no salt present in the internal phase in this case so it is suggested that this small increase in conductivity is a result of small charged protein fragments being released from the broken shell. Figure 4.16c shows the control experiment in which an aliquot of salt solution equivalent to 100 % release of the internal aqueous phase in (a) was added to a suspension of oil filled microspheres prior to sonication. A decrease in conductivity was seen after sonication which may be attributed to binding of the salt ions to fragments of the broken protein shells. The observed increase in conductivity in Figure 4.16(a) and the observed decrease in conductivity in Figure 4.16(c) support the case for salt release from the internal aqueous phase.

Whilst studying the release of dye molecules and salt is experimentally amenable and enlightening as to the release mechanisms that occur, when considering developing polymer microspheres for drug delivery applications it is interesting to study the release profile of an actual drug molecule. 5-Fluorouracil (5FU) (Figure 4.17) is a cytostatic drug

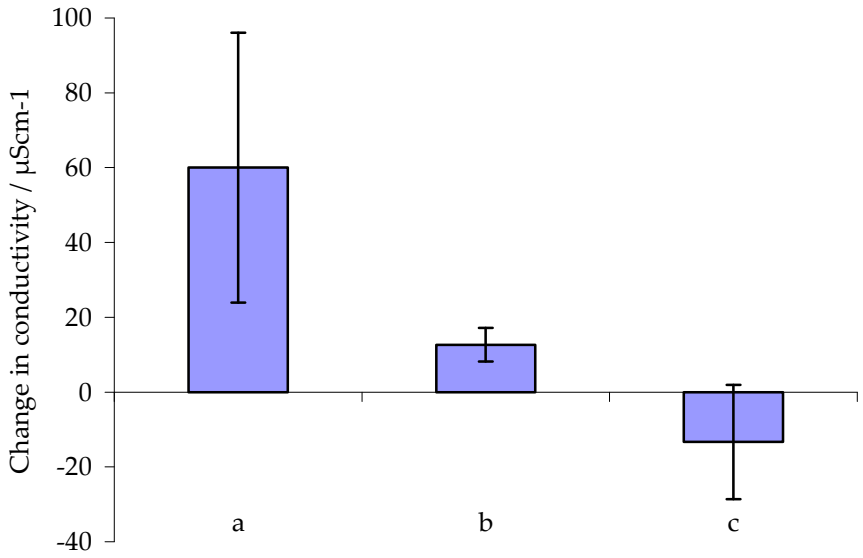

Figure 4.16: Mean change in solution conductivity at 25 ºC upon ultrasonic breakdown of microsphere suspensions: (a) microspheres containing a 6.1 M NaCl solution as the aqueous phase suspended in water; (b) microspheres containing only tetradecane suspended in water; (c) microspheres containing only tetradecane suspended in NaCl solution.

used extensively in cancer therapies, particularly in the treatment of colorectal cancers, breast cancers and cancers in the aerodigestive tract[80]. It acts by replacing uracil in RNA thereby inhibiting vital biosynthetic processes from occurring in the treated cells[80]. Due to the non-specific action of the drug a number of severe side effects are felt by patients including diarrhoea, nausea, vomiting, hair loss and cardiotoxicity[191 192]. One of the key motivators in developing drug delivery vehicles is to reduce these side effects by achieving targeted delivery of the drug to the disease site, minimising systemic toxicity.

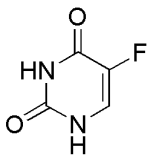

Figure 4.17: 5-Fluorouracil (5FU)

In order to test lysozyme microspheres as carriers for 5FU, a saturated solution of 5FU (0.1 M) in a 1 M sodium chloride solution

was used as the dispersed aqueous phase in the w/o emulsion. Emulsion filled lysozyme microspheres were formed according to the standard procedure discussed above. Once formed, the microsphere suspensions were transferred to a container sealed with a partially permeable membrane for dialysis. Deionised water (MilliQ, 18.2 MΩ·cm) was used as the dialysis receptor. The design of this system meant that two processes occurred in the transfer of 5FU from the interior of the microspheres to the receptor (from which samples were taken); rupture of the microsphere shells and release of the microsphere's internal phase followed by transfer of 5FU across the dialysis membrane. However the initial release of 5FU was deemed to be the rate determining step and the use of a dialysis membrane facilitated precise sampling of the 5FU in the receptor. The concentration of 5FU in the dialysis receptor was measured at chosen time intervals by High Pressure Liquid Chromatography (HPLC) of undiluted samples [a]. (Full experimental details given in section 2.3.8).

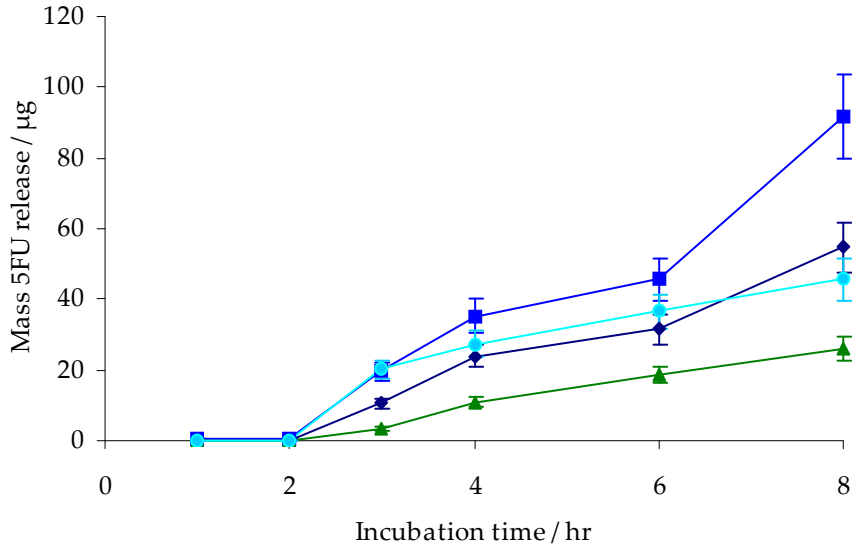

Figure 4.18: Release of 5FU from w/o emulsion filled lysozyme microspheres as a result of incubation in aqueous suspension at 22 °C with 12 mg/mL DTT (blue squares), 30 mg/mL DTT (green triangles), 60 mg/mL DTT (light blue circles) and without DTT (dark blue diamonds).

[a]The author wishes to acknowledge the kind assistance of Wing Sin Chiu in developing the HPLC method used and processing the results collected.

The w/o filled microspheres were incubated with DTT in order to measure the extent of 5FU release in response to cleavage of the disulfide crosslinking in the microsphere shell. The microspheres were incubated with the same concentrations of DTT used when studying release of 5,6-carboxyfluorescein (Figure 4.13), to allow the release profiles of the two molecules to be compared. Figure 4.18 shows the release profiles for w/o emulsion filled microspheres loaded with 5FU. In all cases the microspheres were stable to release over a two hour period. Between two and eight hours release occurred in all four systems but there was no trend apparent with increasing DTT concentration. After eight hours incubation, the microspheres that were untreated had released 54.7 μg of 5FU, corresponding to 18.6% of that initially encapsulated, compared to 45.6 μg (15.5% release) when an identical batch of microspheres were incubated with 60 mg/mL of DTT. Incubation with 12 mg/mL DTT and 30 mg/mL DTT resulted in 31.1% and 8.8% release respectively. Unlike release of 5,6-carboxyfluorescein from w/o filled microspheres, where increasing DTT concentrations resulted in faster rates of release, it appears that when w/o emulsion filled microspheres are loaded with 5FU and stored in aqueous suspension the extent of leakage/release is independent of DTT concentration. 5FU is a significantly smaller molecule than 5,6-carboxyfluorescein so it may be that the extent of cross linking achieved in these lysozyme microspheres is not sufficient prevent leakage from the internal aqueous phase when stored over a period of hours.

Sonication was used as an alternative means to trigger release of 5FU, mechanical disruption had been shown to trigger release of 5,6-carboxyfluorescein and sodium chloride. In this case three samples of microspheres were dialysed for 30 minutes before sonication and then for a further 30 minutes after each period sonication. The concentration of 5FU in the dialysis receptors was measured by HPLC after each period of dialysis and the cumulative release observed is plotted against total sonication time in Figure 4.19. From the concentration of 5FU in the dialysis receptor before the first period of sonication the encapsulation efficiency of the lysozyme microspheres was estimated to be 99.3%. The total dialysis time was 2.5 hours, from Figure 4.18 it can be seen that untreated microspheres are stable to

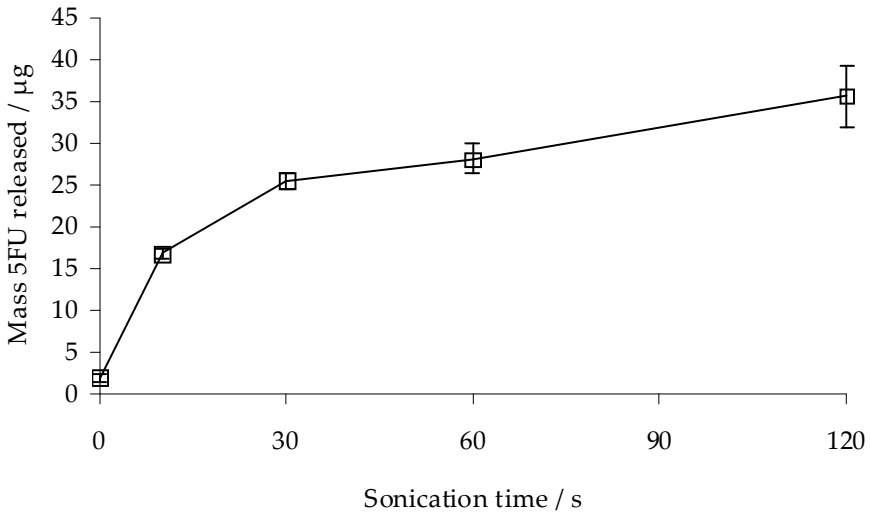

Figure 4.19: Mean release of 5FU from w/o emulsion filled lysozyme microspheres as a result of sonication in aqueous suspension at 40 Wcm^{-2} over a two minute period.

release over this time period and therefore it can be concluded that the mean release of 5FU observed after 2 minutes of sonication (35.7 μg, 12.2%) is due to mechanical disruption of the microsphere shells and encapsulated w/o emulsion phase.

4.5 Release of hydrophilic species from w/o emulsion filled microspheres: PMA_{SH} microspheres

Emulsion containing PMA_{SH} microspheres were formed using an adaptation of the sonochemical method described above. As with tetradecane filled PMA_{SH} microspheres the denaturation step was removed and replaced with an acidification step prior to sonication. It was found that the the optimised conditions chosen for the lysozyme system above could be used to produce microspheres containing a fine emulsion in a reproducible manner from PMA_{SH}. Figure 4.20a provides evidence for successful encapsulation of intact w/o emulsion droplets, the microspheres formed are very similar in morphology to those produced from lysozyme. Figure 4.20b shows a 1 μm thick optical slice through a w/o emulsion containing PMA_{SH} microsphere containing nile red in tetradecane taken using LSCM. As with the lysozyme w/o emulsion filled microspheres the encapsulated emulsion structure can be clearly discerned.

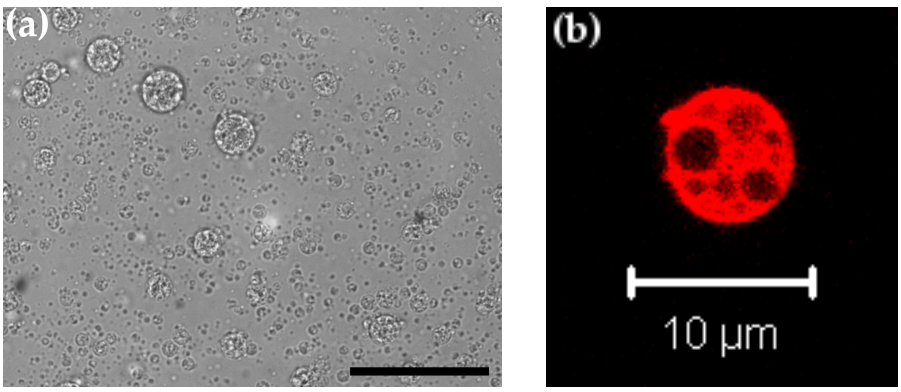

Figure 4.20: PMA_{SH} w/o emulsion filled microspheres in aqueous suspension (a) optical micrograph, scale bar 50 μm (b) confocal micrograph, viewed under the 543 nm laser, showing fluorescence from the encapsulated nile red/tetradecane solution.

PMA_{SH} microspheres are of interest because they are a model and starting point for the microspheres formed from responsive block co-polymers, discussed in the next chapter. It was therefore interesting to characterise the stability of the PMA_{SH} microspheres towards

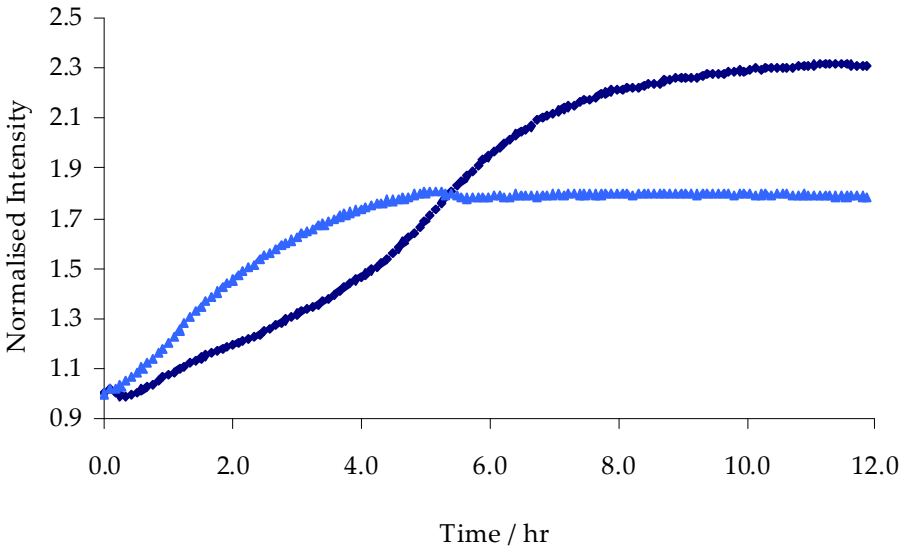

Figure 4.21: Change in solution fluorescence on breakdown of w/o emulsion filled PMA_{SH} microspheres containing 50 mM 5(6)-carboxyfluorescein dispersed in tetradecane on incubation at 37 °C with DTT. Dark blue: No DTT, bright blue: 30 mg/mL DTT.

release of hydrophilic species loaded in the internal aqueous phase. To allow a comparison to be drawn with the lysozyme microsphere system the release of 5,6-carboxyfluorescein *in vitro* was measured using the same experimental conditions as with the lysozyme system above. The resulting release profiles are shown in Figure 4.21. It can be seen that in the absence of DTT, unlike the lysozyme microspheres, PMA_{SH} microspheres are not stable over a 12 hour period. There are two distinct regions in the release profile corresponding to two modes of release. The initial release, between 0 and 4 hours can be attributed to loss of 5,6-carboxyfluorescein trapped in and adsorbed to the PMA_{SH} shell. At 4 hours the rate of release increases before starting to plateau after 8 hours. This second phase of release is caused by loss of integrity of the PMA_{SH} shells resulting in burst release of the contents which are rapidly mixed into the external buffer. This shell rupture can be attributed to insufficient cross linking in the shell which can only prevent leakage from the internal water phase over a short time period.

Incubation with DTT causes accelerated release of the microsphere's contents (Figure 4.21). Maximum release is achieved at 5 hours after which the fluorescent intensity remains constant indicating that no further release has occurred. This provides evidence for the role of the disulfide bonds in the PMA_{SH} shell in stabilising the internal core against release. It is suggested that increasing the extent of PMA_{SH} functionalisation would facilitate a greater degree of crosslinking in the shell which in turn would extend the lifetime of the PMA_{SH} microspheres for storage. The overall extent of release compared to the initial measured fluorescence in the case with DTT incubation is lower than the case without DTT. Due to experimental constraints there was a delay of 5-10 minutes between adding the DTT and starting the fluorescent measurement. It was observed that in this time the samples incubated with DTT took on a stronger colour than those without DTT. It is suggested that incubation with DTT caused very rapid release of dye molecules that were adsorbed onto or trapped within the PMA_{SH} shells prior to the start of the measurement. As a result the measured change in observed fluorescence is smaller than it should be.

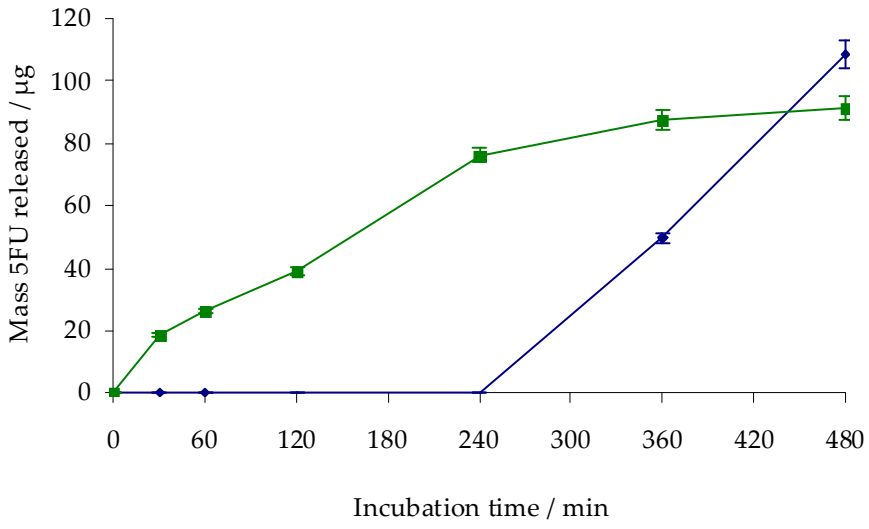

Figure 4.22: Release of 5FU from w/o emulsion filled PMA_{SH} microspheres as a result of incubation in aqueous suspension at 22 ºC with 30 mg/mL DTT (green squares), and without DTT (dark blue diamonds).

As with lysozyme microspheres it was of interest to study the release characteristics of the drug molecule 5FU from the w/o emulsion

filled PMA_{SH} microspheres. In the first instance release of 5FU from untreated microspheres and microspheres incubated with 30 mg/mL DTT was monitored over an eight hour period, Figure 4.22. The same batch of PMA_{SH} was used to produce the microspheres as in the 5,6-carboxyfluorescein experiment described above. In common with the previous experiment untreated microspheres are seen to lose their integrity between 4 and 6 hours leading to a rapid burst release profile and 37.1% release (109.04 μg of 5FU) at 8 hours. However no leakage from the shell prior to this release is apparent. Treatment with DTT triggers breakdown of the shell and immediate release of 5FU, 26.1% release (76.6 μg) had occurred after 4 hours incubation, compared to 0.1% release (0.3 μg) in the untreated case. After 8 hours 31.2% (91.8 μg) of the 5FU loaded into the microspheres incubated with DTT had been released and the release rate had plateaued. As in the case of 5,6-carboxyfluorescein above the extent of release at eight hours was greater from untreated microspheres than those incubated with DTT. Whilst this discrepancy is seen in both release experiments carried out on w/o emulsion filled PMA_{SH} microspheres it was not observed in the experiments carried out with w/o emulsion filled lysozyme microspheres.

Figure 4.23 shows optical micrographs of PMA_{SH} emulsion microspheres before and after dialysis, with and without DTT. Destruction of the microspheres is clear in both cases. The untreated microspheres appear to have undergone rupture without forming into larger structures whereas the microspheres treated with DTT have merged to form larger emulsion droplets. Incomplete destruction of the emulsion in both cases is consistent with the incomplete release observed in Figure 4.22. The existence of these large 'intact' emulsion droplets in the DTT treated sample may go some way to explaining why release plateaued after four to eight hours of incubation with DTT, however the reason for the formation of these droplets is not clear.

Sonication was used to mechanically rupture w/o emulsion filled PMA_{SH} microspheres loaded with 5FU. The experiment was carried out in an identical manner to that described with w/o emulsion filled lysozyme microspheres described above. After a total of 6 minutes sonication the cumulative release of 5FU from the microspheres amounted to 83.5 μg (28.4 % of the 5FU initially encapsulated). The

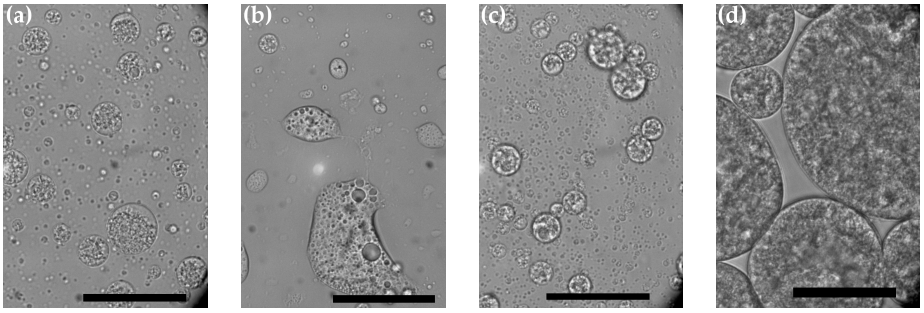

Figure 4.23: Optical micrographs of PMA_{SH} microspheres taken before and after 24hrs in suspension (a,b), before and after 24hrs in suspension with DTT incubation (c,d), scale bar: 50μm

encapsulation efficiency for the w/o emulsion filled PMA_{SH} microspheres, estimated from the 5FU present in the dialysis receptor prior to sonication, was 99.98%. It is known from the release experiment carried out with DTT, Figure 4.22, that untreated microspheres are stable to release for four hours. The sonochemical release experiment was carried out over a 3.5 hour period so it can be concluded that the release of 5FU observed is as a result of sonochemical disruption of the PMA_{SH} shell and internal emulsion phase. Figure 4.25 shows micrographs taken before and after sonochemical treatment of the w/o emulsion filled microspheres, confirming destruction of the microspheres.

Therefore it can be concluded that the sonochemical method can be used to form w/o emulsion filled protein and polymer microspheres. These microspheres can be used to encapsulate both hydrophilic and lipophilic species within the internal emulsion phase, as demonstrated in the confocal micrographs collected. Release of encapsulated hydrophilic species including 5,6 carboxyfluorescein, sodium chloride and 5-fluorouracil has been demonstrated providing evidence (*in vitro*) supporting the case for the use of w/o emulsion filled microspheres as drug carriers. It was observed in the case of w/o emulsion filled lysozyme microspheres that the small drug molecule 5FU leaked freely from the microspheres during dialysis, which was not the case for the larger dye molecule 5,6-carboxyfluorescein. PMA_{SH} microspheres were more robust to 5FU leakage, perhaps due to a greater extent of crosslinking (the PMA_{SH} used had 15-16 thiol groups per chain, compared to a maximum of eight on lysozyme.) Further studies could

be conducted in the future to further characterise the effect of shell crosslinking on 5FU and 5,6-carboxyfluorescein release.

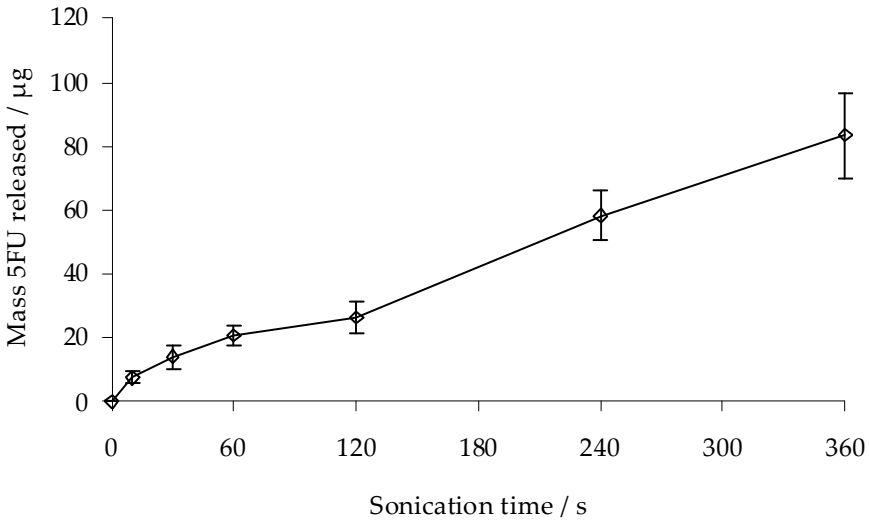

Figure 4.24: Release of 5FU from w/o emulsion filled PMA_{SH} microspheres as a result of sonication in aqueous suspension at 40 Wcm^{-2} over a six minute period.

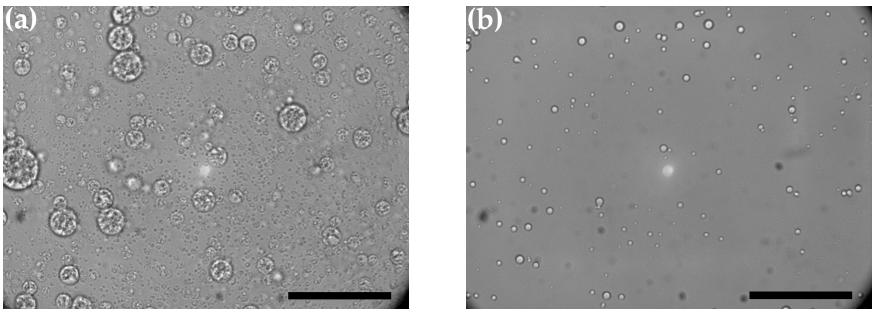

Figure 4.25: Optical micrographs of PMA_{SH} microspheres taken before (a) and after (b) sonochemical breakdown, scale bar: 50μm.

5 Responsive polymers and microspheres

It was demonstrated in chapters 3 and 4 that it is possible to encapsulate both hydrophilic and lipophilic molecules in the core of sonochemically produced microspheres. Release of these molecules has been triggered via mechanical or chemical breakdown of the microsphere shell. It would be of greater use to applications in drug delivery if release could be initiated by a stimulus integral to the environment *in vivo*, for example a change in temperature or pH. Stimulus responsive polymer capsules are a topic of intense research, many different release mechanisms are under investigation, including biological, chemical, photo, thermal, electrical and magnetic stimuli[193]. To date the sonochemical method has not been used to produce responsive polymeric microspheres.

This chapter describes a strategy which utilises the sonochemical method described above to form hollow polymer microspheres which have shells that respond to a change in temperature. In order to achieve this a block copolymer of PMA_{SH} with N-isopropylacrylamide (NIPAm) has been produced. PNIPAM was chosen as an appropriate stimulus responsive block due to its well known coil-globule transition at the lower critical solution temperature (LCST) which occurs close to physiological temperature. The behaviour of PNIPAm in aqueous solution is discussed further below. A block copolymer was favoured over a random copolymer as it is known that the LCST of PNIPAm is changed by its block length so a well characterised block length will give a well controlled LCST[194].

Following the work discussed in chapter 3, PMA_{SH} was chosen as the structural cross linking block as its ability to form oil filled microspheres under sonochemical conditions is now well understood.

It was proposed that by forming microspheres from an ABA triblock of PMA_{SH} and PNIPAm the cross linked sections would incorporate the PNIPAm into the microsphere shell such that upon heating through the LCST, the coil to globule phase change in the PNIPAm block would trigger a change in morphology of the microsphere shell, either to open pores in the shell or rupture the shell completely (Figure 5.1). It is proposed that either of these responses would facilitate temperature responsive release of the microsphere's contents. Such behaviour would widen the utility of sonochemically produced polymeric microspheres in drug delivery.

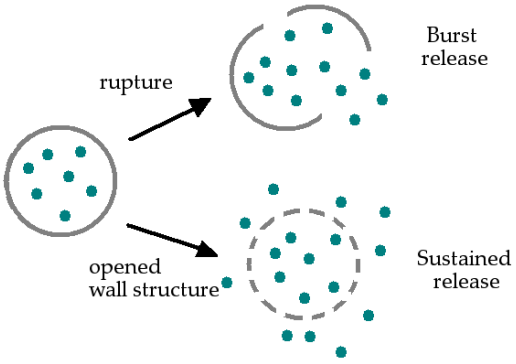

Figure 5.1: Possible release mechanisms, triggered by heating above the LCST, for block copolymer microspheres containing PNIPAm within the shell structure.

The following chapter discusses the controlled radical polymerisation strategy used to produce the block copolymers in question and their use in microsphere production. Evidence is also presented as a proof of principle to support the proposal that these microspheres could be used for temperature responsive release of an active species. Prior to presenting experimental results the theory of PNIPAm's LCST behaviour and controlled radical polymerisation is discussed.

5.1 Poly(N-isopropylacrylamide)

Poly(N-isopropylacrylamide) (PNIPAm) is very widely used in the field of responsive drug delivery devices because it undergoes a well defined phase transition typically in the region of 30-35 ºC[195] however transitions at temperatures as high as 43 ºC have been observed for low molecular weight samples[194]. Hence when incorporated into a drug carrier PNIPAm can be used to trigger release at around physiological temperature[196–201].

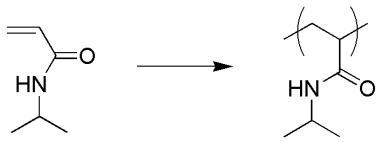

Figure 5.2: N-isopropylacrylamide and poly(N-isopropylacrylamide)

PNIPAm is one of a family polymers which display inverse solubility behaviour in response to increasing temperature. These polymers are partially hydrophobic, therefore in order to dissolve in an aqueous medium the polymer chains fold to protect the hydrophobic portions. The water molecules surrounding each polymer chain become highly ordered in order to hydrogen bond with the hydrophilic portions of the chain, solubilising the polymer[195]. This phenomenon is commonly known as the 'hydrophobic effect'[195] and is associated with a decrease in entropy. As a result increasing the solution temperature above a threshold causes the free energy of mixing to become positive and the polymer to precipitate out of solution. This threshold is the Lower Critical Solution Temperature (LCST) and can often be observed macroscopically as the cloud point of the solution.

The LCST varies with a number of factors including; the identity of the temperature responsive block, chain length, tacticity and the presence of copolymers. In principle the LCST can be anywhere between 0 °C and 100 °C, more hydrophilic analogs of PNIPAm have higher LCSTs, resulting from more favourable polymer-solvent interactions, and more hydrophobic analogs of PNIPAm have lower LCSTs[195].

The mechanism of the solubility transition that occurs at the LCST is not fully understood and is still the subject of active research[202]. Hydrogen bonding between the polymer chain and water molecules is

the main intermolecular interaction involved in solubilising PNIPAm. A recent computational study has provided evidence for the change in hydrogen bonding on heating a PNIPAm hydrogel through its LCST[202]. Three types of hydrogen bonding are defined in the study; polymer - polymer, polymer (donor) - water (acceptor) and water (donor) - polymer (acceptor). On heating through the LCST there is no significant change in the lifetime of the first two types of bonding but the water (donor) - polymer (acceptor) bonds were seen to break and not reform above the LCST. This suggests that it is these hydrogen bonds which are most fundamental to PNIPAm solubility and that the loss of these stabilising bonds is an important factor in the collapse of the polymer chains out of solution[202].

In a single chain system the PNIPAm chains can be observed to collapse individually before aggregating with nearby chains to form a macroscopic precipitate. In the case of a cross linked hydrogel a decrease in volume is observed and the LCST is referred to as the Volume Phase Transition Temperature (VPTT). Hydrogels with extensive crosslinking undergo a small change in volume at the VPTT compared to those with minimal crosslinking[198].

The LCST of PNIPAm can be tuned to a desired temperature to suit a chosen application, most simply, by varying the PNIPAm chain length. High molecular weight PNIPAm chains have a significantly lower LCST than low molecular weight samples (for example a 32.5 kDa chain exhibits a cloud point at 33 °C, whereas a 3.3 kDa polymer has a cloud point at 43 °C)[194]. This is likely to be a result of the larger quantity of polymer-solvent interactions in the case of longer polymer chains. This chain length dependence means that achieving a narrow $Đ_M$ is important in producing polymer samples that give well defined LCSTs. Alternatively incorporating hydrophilic or hydrophobic monomers will raise or lower the LCST accordingly[203]. In the case of low molecular weight polymers the presence of an end group (for example a controlled radical polymerisation agent) can be used to achieve a similar effect[204].

In a crosslinked gel the inclusion of ionic groups, for example acidic comonomers, causes an increase in osmotic pressure within the gel. The gel is subject to a high degree of swelling below the VPTT and on heating through the VPTT undergoes a more abrupt volume

transition than observed for PNIPAm homopolymer hydrogels. If two thermosensitive segments are used with distinct LCSTs a two step phase transition can be achieved[205].

The tacticity of a sample of PNIPAm has a significant effect on both its solubility and LCST. Whilst atactic PNIPAm is freely soluble in cold water and has a typical LCST of 32 ºC[206,207], isotactic rich (> 72%) PNIPAm is insoluble in cold water[207]. Syndiotactic PNIPAm is soluble in cold water and, with comparable chain lengths, increasing the syndiotactic component from 53 to 71% causes an increase in the solution cloud point from 33.1 ºC to 35.9 ºC[207;208,206]. It was also observed that syndiotactic rich PNIPAm displayed a sharper phase transition with less hysterisis at the LCST than atactic PNIPAm[208].

5.2 Diffusion Ordered NMR Spectroscopy

Diffusion ordered (DOSY) NMR spectroscopy is a 2D ^{1}H-NMR experiment which can be used as a complimentary technique to Gel Permeation Chromatography (GPC) in the characterisation of block co-polymers. First developed in 1992[209] DOSY NMR correlates the diffusion of molecules in an NMR sample to their ^{1}H-NMR chemical shifts. The experiment involves measuring the exponential signal attenuation in a series of pulsed field gradient experiments. By fitting the decay curves, the diffusion coefficients of the molecules can be calculated[210] and displayed as a map of chemical shift *vs* diffusion coefficient, *D*. The size and shape of the molecules, solvent interactions and temperature will determine the rate of self diffusion described by the diffusion coefficient[211]. Therefore the diffusion coefficient can be used as a measure of polymer size in solution and hence chain length[212]. In the case of a mixture, diffusion coefficients corresponding to the chemical shifts of the different species in solution will be displayed in the map. This highlights a key benefit of DOSY NMR over GPC analysis; the identity of the polymers in solution can be established from their chemical shifts, a facility that is not provided by GPC.

There have been a number of reports of the use of DOSY NMR to measure polymer dispersities[211,212], characterise block copoly-

mers[213;214 215;216], resolve polymer mixtures[210], and recently to measure the Critical Micelle Concentration of amphiphilic block copolymers[217]. However DOSY NMR, used in its simplest form to produce single exponential 2D maps is not without its drawbacks. If DOSY NMR is used to monitor samples which contain overlapping signals, for example a mixture of a homopolymer macroRAFT agent or macroinitiator and the corresponding diblock, the diffusion coefficient for the peak associated with the overlapping chemical shifts will not be accurate[216]. If only diblock copolymer is present the diffusion coefficients of the chemical shifts associated with the two blocks will be identical and will reflect the true molecular mass of the diblock copolymer. If however a mixture is present the mathematical transformation used will result in a peak at a diffusion coefficient which corresponds to neither the diblock copolymer nor the homopolymer but rather an average of the two which has no meaning[216]. As a result DOSY NMR can be used as a tool to characterise the product of a block copolymerisation because peaks that do not correspond to the same diffusion coefficient will be evidence of an impure product. However care must be taken not to derive a M_n value from the spectra of such a sample.

In light of this and of the mathematical and empirical complexities of obtaining accurate molecular mass information from DOSY spectra the DOSY experiments discussed in sections 5.4 and 3.2 have been employed simply to confirm diblock copolymer formation.

5.3 Controlled radical polymerisation techniques

Controlled radical polymerisations (CRP) were first developed in the 1990's as a means of producing polymers with well controlled architectures[218]. Prior to the development of CRP, ionic polymerisations were used to form polymers with well defined chain lengths[219]. These polymerisations can also be described as 'living polymerisations':

"Living polymers are polymers that retain their ability to propagate and grow to a desired size while their degree of termination or chain transfer is still negligible."[219]

However the polymerisations required stringent inertion and were limited in the monomer functionalities that could be accommodated[220]. CRP allows access to controlled polymers from a much broader range of monomers[221].

There are a number of different methods which can be used to carry out a controlled radical polymerisation: Stable Free Radical Polymerisation (SFRP), a well known example of which is Nitroxide Mediated Polymerisation (NMP)[218], Atom Transfer Radical Polymerisation (ATRP)[222] and Reversible Addition-Fragmentation Chain Transfer Polymerisation (RAFT)[223]. Included within this list are two different mechanistic approaches to CRP, the first, which facilitates SFRP and ATRP, is the persistent radical effect[224]. This utilises termination reactions between growing polymer chains in the early stages of the polymerisation reaction to cause an accumulation of persistent radicals (X) (Figure 5.3). These radicals are unable to terminate by reaction with themselves but instead combine with the propagating chain radicals to form dormant radical adducts. This accumulation drives the initial equilibrium between dormant and active species resulting in a steady state of persistent radicals and dormant radical adducts facilitating controlled chain growth.

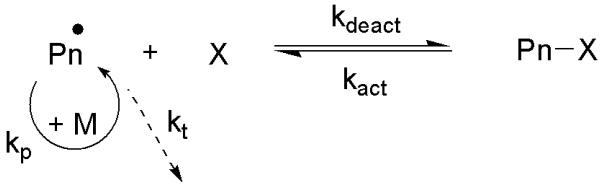

Figure 5.3: Controlled polymerisation mechanism mediated by the Persistent Radical Effect.[221].

In contrast, RAFT polymerisation occurs via a degenerative chain transfer equilibrium which is initiated in an analogous manner to simple radical polymerisations[221]. In this case control is achieved when the propagating chain radicals combine in a reversible manner with a RAFT agent to form a stable, dormant adduct. This dormant species exists in equilibrium with the active propagating radicals and

the RAFT agent is designed such that the rate of transfer is much faster than the rate of propagation, allowing control over the rate of monomer addition to be achieved[221] (Figure 5.4).

Common to both mechanisms is the formation of a dormant radical adduct in dynamic equilibrium with the propagating chain radicals. Propagating chain growth is limited by the fast deactivation rate, which in an ideal scenario limits the chain growth to one or two monomers at a time[218]. Formation of the dormant adduct also protects the polymer chain from competing termination and side reactions, for example back biting or branching reactions, which are common in radical polymerisations[218]. The polymers formed using these methods can be synthesised to meet a pre-determined chain length and have a very narrow dispersity (typically less than 1.3)[221].

Although controlled radical polymerisations do not fulfil the true definition of a living polymerisation a well designed reaction displays a number of characteristics which reflect the control achieved in a living polymerisation: chain growth is a linear function of monomer conversion, the total number of polymer molecules present remains constant and independent of conversion, the desired chain length can be controlled by reaction stochiometry, the polymers produced have narrow dispersities and subsequent monomer additions lead to chain extension or block formation[225]. The minimal termination/ undesired chain transfer reactions that occur in such systems mean that a very high proportion of the chains produced retain a living chain end which can be re-introduced into a second polymerisation in order to achieve further chain growth. It is by this method that block co-polymers with well defined architectures can be synthesised[221].

There are many examples of well defined complex polymer architectures which have been produced via RAFT polymerisation in the recent literature[226] and a few are highlighted here: Coupling a RAFT agent containing a N-hydroxysuccinimide group onto one of the amine groups in lysozyme[227], allows protein-polymer conjugates to be formed. Star copolymers can be formed by growing the polymer arms from the core outwards[226], either with the RAFT functionality on the outer end of each growing arm which facilitates further functionalisation, for example with proteins[228], or with the RAFT functionality in the core of the star, which reduces the risk of cross polymerisation

between stars[229]. Alternatively RAFT polymerisation can be used to form 'macroRAFT agents' which can be coupled together with a crosslinker to form a star, for example in the case reported by Zhu *et al.*[230] where polystyrene arms formed using an azide containing RAFT agent were subsequently 'clicked' together with a trialkyne crosslinker. Dendritic polymers formed by RAFT polymerisation have been reported[231] as have graft copolymers[232;233]. Graft copolymers can be formed by chain extension from RAFT groups attached to a polymer backbone[232]. Alternatively interesting structures such as a block-graft copolymer can be formed by using, for example, a polystyrene 'macroRAFT agent' with PEO macromonomers that had been end-functionalised with acrlyate monomer units to produce a toothbrush like structure with a polystyrene handle[233].

It is the ability to form well defined block copolymers that is of particular interest in the case of this project. The CRP method used was RAFT which is discussed in more detail below.

RAFT Polymerisation:

RAFT polymerisations display living characteristics as a result of a degenerative chain transfer equilibrium[218]. The equilibrium is so called because the reaction starts with a chain transfer agent and the product of the equilibrium is also a chain transfer agent, which in a well controlled reaction should have a similar activity to its precursor, Figure 5.4.

The addition - fragmentation equilibrium is controlled by a RAFT agent, which can have one of several structures, shown in Figure 5.5. The characteristics of the RAFT agent control not only the molecular weight but also the dispersity of the polymer formed and the activity of the polymer chain ends towards further transformations[234]. The key structural features which control the RAFT agent's activity can best be described by considering the R and Z groups separately (Figure 5.4). These structure-activity relationships are described below but first the overall RAFT mechanism must be considered.

The RAFT polymerisation mechanism is depicted in Figure 5.4. The reaction is initiated by a radical initiator in a similar way to a standard

(1) Initiation:

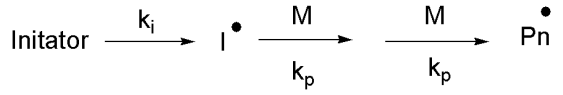

(2) Reversible chain transfer/propagation:

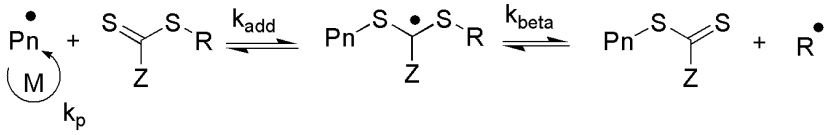

(3) Reinitiation:

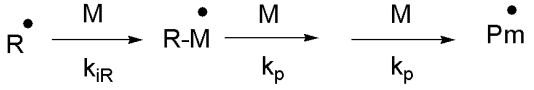

(4) Reversible (degenerate) chain transfer/propagation:

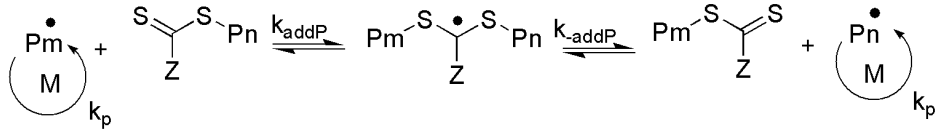

(5) Termination:

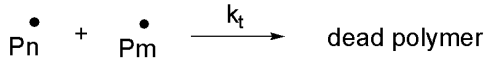

Figure 5.4: RAFT Mechanism[218]

free radical polymerisation (1), indeed in most cases the same initiator is used. Once a small number of macroradical species have formed the macroradicals and RAFT agent can undergo a reversible chain transfer reaction in an initial 'pre-equilibrium' (2). The intermediate radical formed in the reaction can either return to the starting materials via a β-scission reaction or the R group can be ejected in a similar β-scission reaction to form a new radical species and a dormant polymer chain[235]. The ejected R radical initiates new propagating polymer chains (3) and the main equilibrium is set up; a new macro radical can now react with the previously formed dormant chain forming a new radical intermediate (4). This intermediate can cleave to release either polymer chain, retaining the second in a dormant state (4). In order to obtain a high degree of control the RAFT agent is used in an excess to the initiator so that the majority of polymer chains produced are initiated by the R group from the RAFT agent[235]. It is the addition

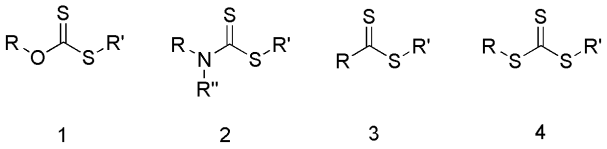

Figure 5.5: RAFT Agent classes: (1) Xanthate, (2) Dithiocarbamate, (3) Dithioester, (4) Trithiocarbonate[235].

- fragmentation equilibrium which controls the growth of polymer chains in a RAFT polymerisation. The chains in the intermediate have an equal probability of being released to become propagating macroradicals due to the symmetrical nature of the radical intermediate. This together with a rapid rate of transfer ensures that all the macroradicals grow at very similar rates yielding a polymer with a molecular weight that is controlled by the reaction stochiometry and has a narrow dispersity. Despite the pseudo-living characteristics observed for many RAFT polymerisations a small quantity of termination reactions occur (5), predominately as combination reactions between growing radical chains[218]. These termination reactions should be minimised, firstly in order to maintain control over chain length and dispersity but also in order to maintain 'living' RAFT end groups on the polymers produced. It is these RAFT end groups that, when retained, facilitate further block co-polymerisation reactions[235].

$$k_{tr} = k_{add}\left(\frac{k_{beta}}{k_{-add} + k_{beta}}\right) \tag{5.1}$$

The activity of a RAFT agent can be defined by its transfer constant, k_{tr}, which is a product of k_{add} and k_{beta}, see equation 5.1, compared to the rate of monomer propagation[235], k_p. In designing a RAFT polymerisation it is important to consider the transfer constant both for the initial RAFT agent and the macromolecular RAFT agent that is subsequently produced.

The Z group on the RAFT agent affects k_{tr} by influencing the reactivity of the C=S bond towards radical addition[223]. Dithioesters and trithiocarbonates are the most reactive RAFT agents[235] (Figure 5.5). As a general rule the transfer constant is increased when the Z group contains electron withdrawing groups which stabilise the intermediate

radical that forms leading to an overall increase in reactivity with respect to addition into the C=S bond[235]. However it should be noted that if the intermediate radical is too stable then the rate of fragmentation will be retarded and unwanted side reactions will prevail[235]. If the RAFT agent chosen contains a nitrogen or oxygen lone pair adjacent to the C=S bond then zwitterionic canonical forms will play a significant role, reducing the double bond character of the C=S bond and, in turn reducing its reactivity. The relative reactivities of several common Z groups are listed in Figure 5.6.

The reactivity of the RAFT agent C=S bond must be chosen to suit the monomer in question. Monomers can be put in order from more activated monomers to less activated monomers. The double bond in more activated monomers is conjugated into an aromatic ring or carbonyl group, examples of more activated monomers include styrene and methyl methacrylate. Less active monomers do not have conjugated double bonds, in these cases the double bond is located next to a saturated carbon or the heteroatom in a heteroaromatic ring, as is the case in N-vinylpyrrolidone[235]. Propagating radicals composed of more activated monomers are less active in radical addition so a more active RAFT agent is required for good control to be achieved. In contrast less activated monomers display poor homolytic cleavage from the radical intermediate so a less active RAFT agent is required in order to prevent rate retardation[235].

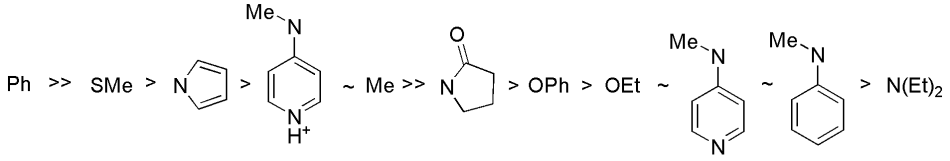

Figure 5.6: Variation of transfer constant with Z group substituents.[235].

It is the leaving group ability of the R fragment and hence the partitioning between the precursors and the products in the first addition-fragmentation equilibrium that defines the R group's contribution to the transfer constant[223]. Good control over dispersity is achieved when fragmentation is rapid so that side reactions are avoided and the reaction can proceed rapidly when the R group is released in favour of the macroradical. In the case of an R group that is a poor leaving group the polymerisation is likely to stall[235].

Characteristics general to leaving groups used in synthetic organic chemistry have a strong influence; steric and electronic effects that improve the stability of the R group radical will improve its leaving group characteristics. Hence R groups that form tertiary radicals and which contain delocalising or electron withdrawing groups are commonly used[235]. In addition to having good leaving group qualities the R group must also be efficient in re-initiating polymerisation; the rate of re-initiation must exceed the rate of propagation in order to achieve good control and prevent the R radicals from being consumed in side reactions. In the case of monomers with high propagation rate constants a primary or secondary R group may be favoured in order to achieve a rapid re-initiation rate[236]. Figure 5.7 lists a series of common R groups in order of their effect on the transfer constant.

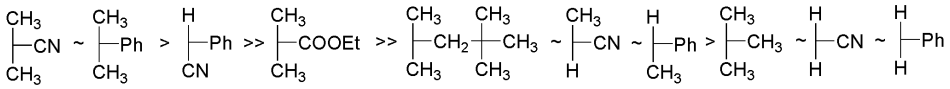

Figure 5.7: Variation of transfer constant with R group substituents.[235].

The following section discusses the current literature precedent for using RAFT to form PMA and PNIPAm copolymers, which was used as a basis for the following experimental work.

RAFT polymerisation of NIPAm, MA and related monomers

There have been a number of reports of using RAFT polymerisation to produce PNIPAm, PMA and their copolymers under controlled conditions. The two RAFT agent types most commonly used are dithioesters and trithiocarbonates (Figure 5.8). A dithiobenzoate (**2**) has been used to produce PNIPAm[237] and P(*t*BMA-b-NIPAm)[238]. In both cases the polymers produced had narrow size distributions but the rate of polymerisation was slow. It was suggested by the authors that slow re-initiation by the R group had retarded the rate of polymerisation. Yang *et al.*[239] report the use of a different dithiobenzoate RAFT agent (**1**) with a low transfer constant in the synthesis of P(NIPAm-MA-NIPAm), the low transfer constant favours tri-block formation as it results in a less labile RAFT end group on the

macro-RAFT agent, if the transfer constant of the propagating chain is similar to that of the RAFT precursor. As a result a larger proportion of polymer chains retain their RAFT functionality facilitating growth of the next block. However Yang *et al.* did report some breakdown of their RAFT agent during the reaction and as a result Pelet *et al.*[240] report using a RAFT agent (**3**) with an alternative tertiary R group in order achieve better control in the latter stages of the reaction.

Examples of polymers of methacrylic acid or methacrylates are also reported where dithiobenzoates have been used as RAFT agents[240–243](**3-5**). However the polymerisations were not trouble free. The RAFT agents used were subject to degradation, especially by hydrolysis in aqueous solvent[240]. Guillaneuf *et al.*[241] report the formation of dithiobenzoic acid from (**3**) as a side product in the polymerisation of methacrylic acid. Dithiobenzoic acid disrupts the addition - fragmentation equilibrium by acting as a pseudo-RAFT agent. As a result control over dispersity and chain length was reduced.

Trithiocarbonate RAFT agents offer an alternative to dithioesters in the polymerisation of NIPAm[244] (**6**), MA[245;246](**9**) and *t*BMA[247](**7**). The trithiocarbonates used display good control and do not degrade under the reaction conditions used. There is one example of successful diblock formation from a macroRAFT agent formed from NIPAm with a trithiocarbonate[248](**7**). Although these reactions display good control there are several reports of an inhibition period at the start of the polymerisations[246;249](**8,9**), attributed to slow reinitiation on the part of the tertiary R group.

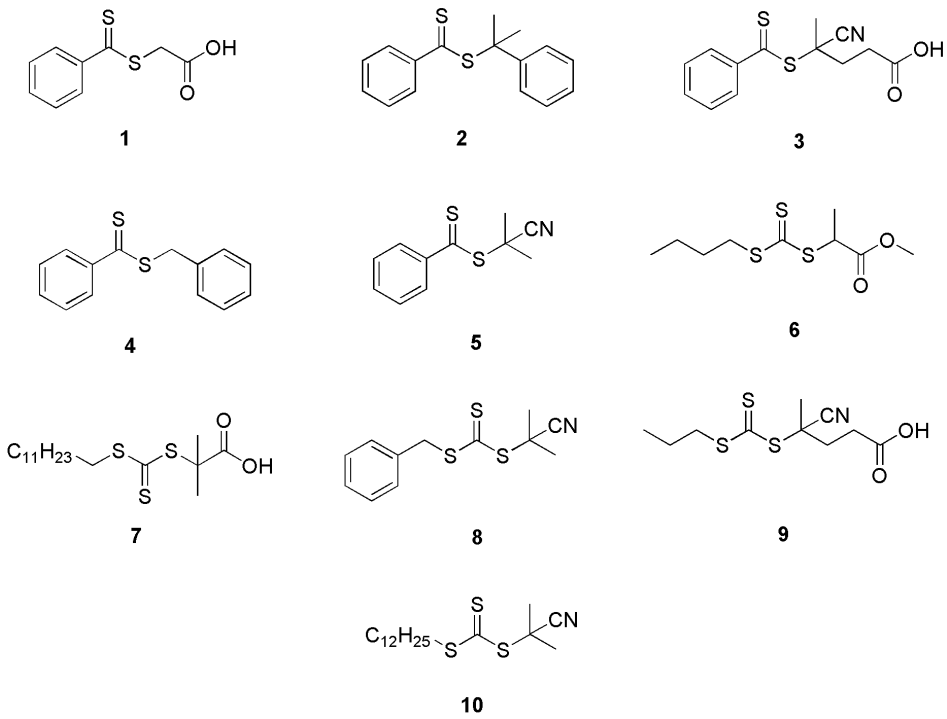

Figure 5.8: RAFT Agents

Results and Discussion

5.4 P*t*BMA macroRAFT agent synthesis

The block copolymer synthesis was carried out in a step-wise manner using a RAFT methodology similar to that described above. Early synthetic attempts used dithiobenzoate RAFT agents, 4-cyano-4-(phenyl carbonothioyl thio)pentanoic acid (**3**) and S-(Thiobenzoyl)thio glycolic acid (**1**) (Figure 5.8), with methacrylic acid (MA), tert-butylmethacrylate (t-BMA) and NIPAm. Homopolymers were successfully formed from all three monomers and their identity confirmed in each case by ^{1}H-NMR (section 2.4.1-4). The molecular weight distributions were measured by GPC, except in the case of PMA which is not soluble in the chosen GPC solvent, tetrahydrofuran (THF) (Table 5.1 entries 1-4). When the homopolymers that had been produced were used as macroRAFT agents no diblock copolymers were successfully formed.

#	RAFT Agent	Polymer	M_n (kDa)	*DP*	$Đ_M$
1	**3**	P*t*BMA	33.1	233	1.28
2	**3**	PNIPAm	3.2	28	1.67
3	**3**	PMA	n/a	n/a	n/a
4	**1**	PMA	n/a	n/a	n/a
5	**10**	PNIPAm	3.9	34	1.37
6	**10**	P*t*BMA	5.7	40	1.35
7	**10**	P(NIPAm-b-MA)	n/a	n/a	n/a
8	**10**	P(*t*BMA-b-NIPAm)	10.7	40+44	1.43
9	**10**	PMA	-	-	-

Table 5.1: Polymers formed with dithiobenzoate and trithiocarbonate RAFT agents in early studies (RAFT agent numbers link to the structures shown in Figure 5.5).

Based on the evidence in the literature for more effective use of trithiocarbonate RAFT agents in the synthesis of PMA and PNIPAm block copolymers, polymerisations with 2-cyano-2-propyl dodecyl trithiocarbonate (**10**) were trialled (Figure 5.8, Table 5.1 entries 5-8). Initial attempts showed that PNIPAm and P*t*BMA polymers could be produced readily with narrow dispersities ($Đ_M$). A diblock copolymer was successfully formed from a PNIPAm macroRAFT agent using

methacrylic acid as a comonomer. However the homopolymerisation of methacrylic acid with **10** was not successful.

The homopolymer formed from *t*BMA was successfully used to synthesise a diblock copolymer with NIPAm. In light of this and the poor PMA yields, P*t*BMA was chosen as a suitable substitute for PMA. The use of *t*BMA as a monomer had additional experimental benefits. The GPC equipment available used a THF solvent system, facilitating molecular weight characterisation of P*t*BMA and PNIPAm polymers but not PMA. Therefore block characterisation could be achieved more readily with P*t*BMA than PMA. Utilising *t*BMA, essentially as a protected methacrylic acid monomer, requires an additional hydrolysis step to give the required polymer; however varying the extent of hydrolysis gives an additional synthetic opportunity to adjust the hydrophobicity of the final polymer. In light of Gedanken's observations[53] it was thought that this additional flexibility would be beneficial in the future for designing microspheres. Hence the synthetic scheme shown in Figure 5.9 was chosen for the block copolymer synthesis (for full experimental details see section 2.4.5-9).

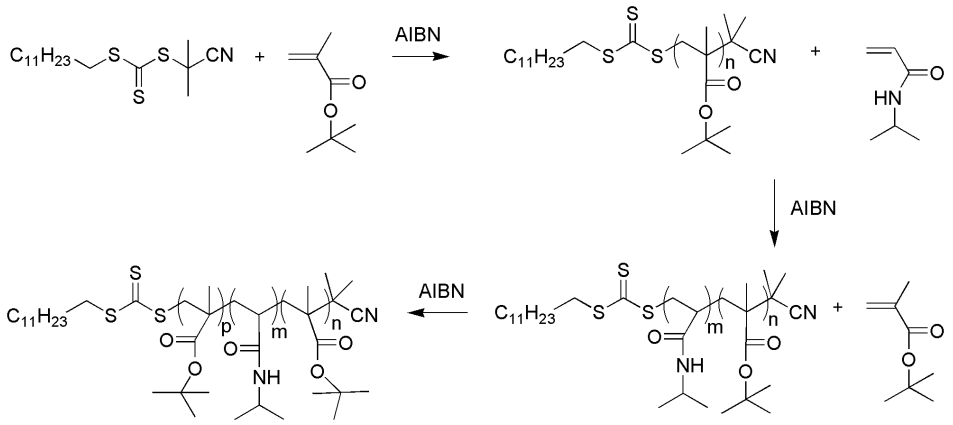

Figure 5.9: Synthetic scheme for block co-polymer synthesis chosen for the synthesis of P(*t*BMA-b-NIPAm-b-*t*BMA).

Dry dioxane was used as a solvent in all three steps but the polymers were isolated at each stage in order to prevent contamination of blocks with monomer from the preceding block. The polymers formed were characterised by ^{1}H-NMR and in each case the desired chain composition was confirmed, GPC was used to measure the molecular weight distribution of each polymer sample produced.

In the first instance a homopolymer of *t*BMA bearing a RAFT end group was required to act as a macroRAFT agent to the second block. In order to synthesise a clean sample of diblock copolymer, with no residual homopolymer, it was important to ensure that the number of 'dead' chains in the macroRAFT agent was minimised. This was achieved firstly by using a 4:1 ratio of RAFT agent to initiator (AIBN) when synthesising P*t*BMA, ensuring the vast majority of chains initiated were capped by the RAFT agent. Secondly the macroRAFT polymer was isolated at approximately 60% monomer conversion. Not running the reaction to high conversion reduced the extent to which termination reactions were likely to occur.

In order to demonstrate that the P*t*BMA synthesis was carried out under controlled conditions the chain growth and percentage conversion were monitored with respect to reaction time by GPC and ^{1}H-NMR respectively. Figure 5.10 shows P*t*BMA chain growth with respect to time and monomer conversion. It can be seen that the *t*BMA RAFT polymerisation displays controlled chain growth, linear with respect to percentage monomer conversion, as is expected from a CRP reaction. The linear profile indicates that the number of polymer chains is constant throughout the reaction and that competing termination reactions are negligible. Hence P*t*BMA produced under the reaction conditions chosen and isolated after 13-14 hours of reaction time will have retained a high percentage of RAFT end group functionality. The polymer produced under these conditions was a bright yellow powder and the anti-solvent used in the work up was colourless, indicative of a high degree of retention of RAFT end groups.

The presence of the RAFT end group was confirmed by ^{1}H-NMR using the marker peak at 3.3 ppm corresponding to the CH_2 adjacent to the trithiocarbonate group (Figure 5.12). The molecular weight distribution was measured by GPC, shown in Figure 5.11. There is some tailing in the distribution towards shorter chain lengths which indicates that some termination reactions occurred in the early stages of the polymerisation, perhaps as a result of residual oxygen or impurities in the reaction medium. The dispersity of the sample is 1.36 (Table 5.2), high for a RAFT polymerisation but still indicating a

good degree of control[225]. This polymer was used as the macroRAFT agent in the diblock copolymer synthesis.

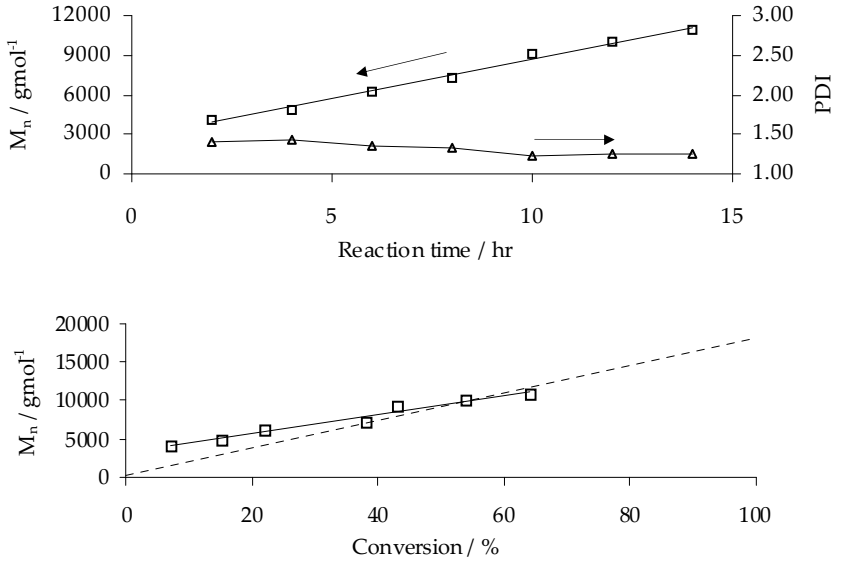

Figure 5.10: P*t*BMA chain growth with respect to time and monomer conversion, characterised by ^{1}H-NMR and GPC analysis of crude reaction samples taken at timed intervals over the course of the polymerisation. (Dashed line corresponds to the theoretical M_n, PDI = Đ).

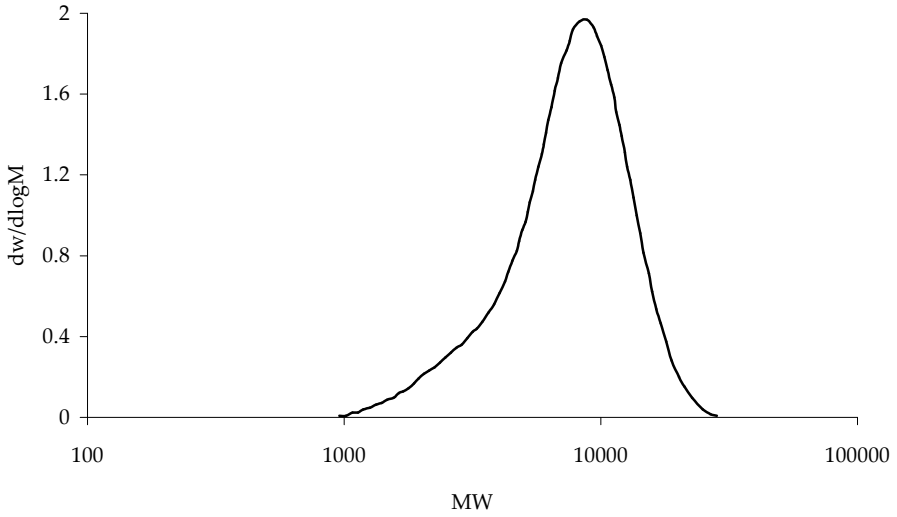

Figure 5.11: Molecular weight distribution of P*t*BMA macroRAFT agent. (Average molecular weight and $Đ_M$ listed in Table 5.2).

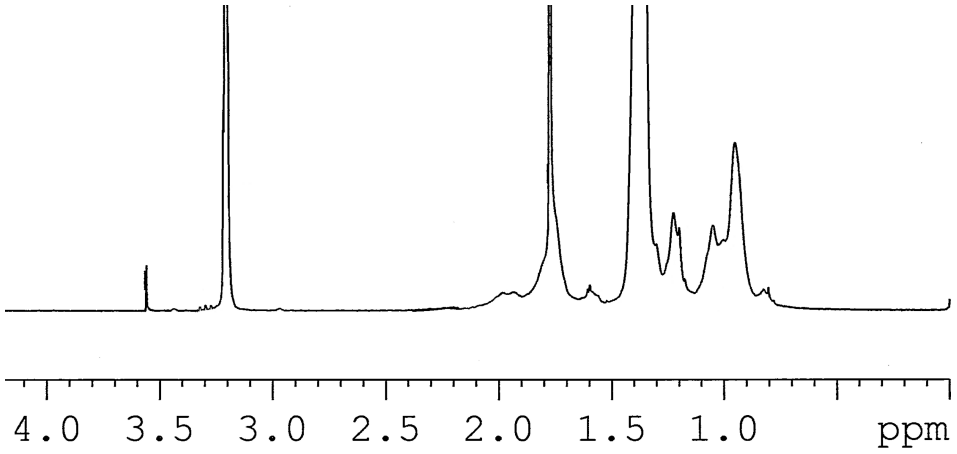

Figure 5.12: ^{1}H-NMR spectrum of P*t*BMA macroRAFT agent.

5.5 P(*t*BMA-b-NIPAm) synthesis

The NIPAm polymerisation was monitored in order to establish the degree of control that could be achieved with the chosen RAFT agent. A significant inhibition period was observed both in dry dioxane (Figure 5.13) and DMSO (Figure 5.14) although the overall reaction time was drastically shorter in DMSO. The reason for the inhibition period was thought to be due to a mismatch between the re-initiation rate of the R group on the RAFT agent and the propagation rate of NIPAm, resulting in a retarded addition-fragmentation reaction. In both cases the chain growth had a linear correlation with monomer conversion indicating a constant number of propagating chains and negligible termination reactions. Despite the long inhibition period, the conditions used in dioxane were used to successfully synthesise a diblock from the P(^{t}BMA) macroRAFT agent (dioxane was chosen because the macroRAFT agent had poor solubility in DMSO).

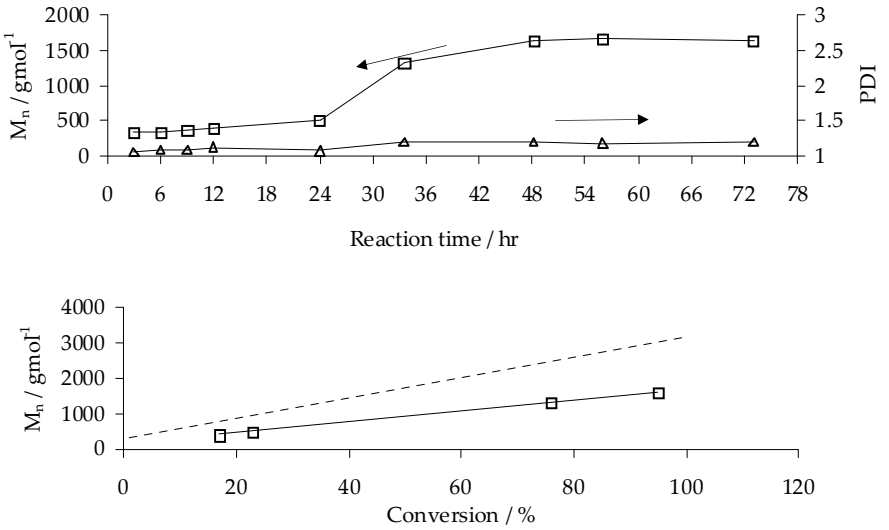

Figure 5.13: PNIPAm chain growth with respect to time and monomer conversion in dioxane, characterised by ^{1}H-NMR and GPC analysis of crude reaction samples taken at timed intervals over the course of the polymerisation. (Dashed line corresponds to the theoretical M_n, PDI = Đ).

$$M_n^{calc} = \frac{[m]_0 \times M_m \times \rho}{[CTA]_0} + M_{CTA} \tag{5.2}$$

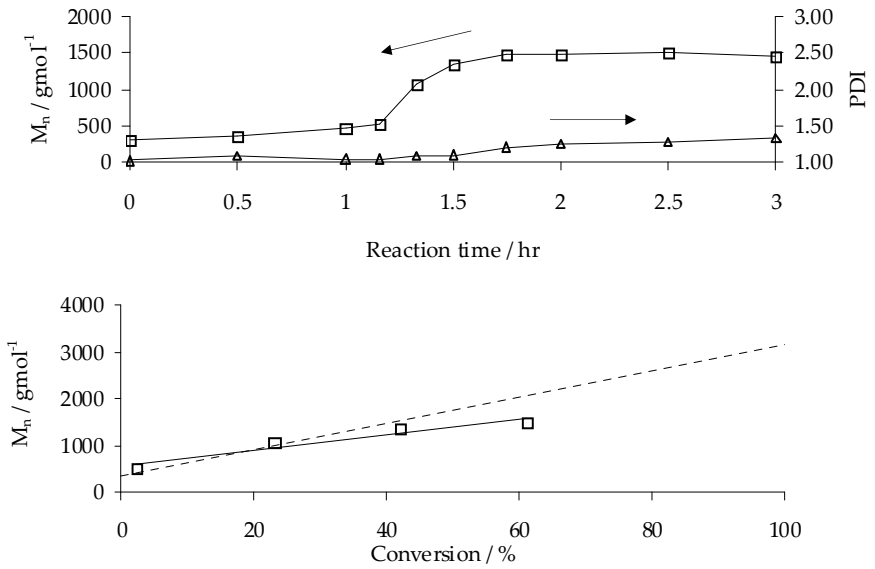

Figure 5.14: PNIPAm chain growth with respect to time and monomer conversion in DMSO, characterised by ^{1}H-NMR and GPC analysis of crude reaction samples taken at timed intervals over the course of the polymerisation. (Dashed line corresponds to the theoretical M_n, PDI = Đ).

	M_n^{calc} (kDa)	M_n (kDa)	$Đ_M$	*DP* (GPC)	*DP* (NMR)	*D* (x 10^{-10}m^{2}s^{-1})
P(*t*BMA)	5.6	6.2	1.36	43	79	2.063
DB	28.8	9.5	1.31	43+30	80+40	1.028

Table 5.2: Characterisation data for the macroRAFT agent and P(*t*BMA-b-NIPAm) (DB). (*D*: DOSY diffusion coefficient measured by DOSY NMR)

The expected number average molecular weight M_n^{calc} of each polymer was calculated according to equation 5.2[225] where $[m]_0$ is the initial monomer concentration, M_m is the monomer molecular mass, ρ is the fractional conversion, $[CTA]_0$ is the initial RAFT agent concentration and M_{CTA} is the molecular mass of the RAFT agent.

From the molecular weight distributions shown in Figure 5.17 (measured by GPC) it can be seen that the diblock sample has a higher M_n than the macroRAFT agent, corresponding to approximately 30 units of NIPAm in the second block. The composition of the diblock copolymer was confirmed by ^{1}H-NMR analysis (full ^{1}H-NMR assignments are listed in sections 2.4.5-11). PNIPAm has a characteristic broad peak

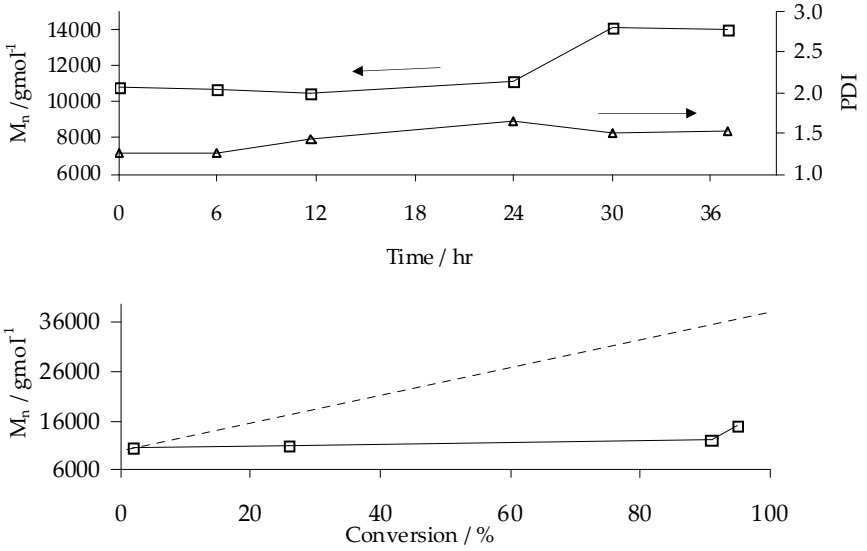

Figure 5.15: PNIPAm chain growth from macro-RAFT with respect to time and monomer conversion in dioxane, characterised by ^{1}H-NMR and GPC analysis of crude reaction samples taken at timed intervals over the course of the polymerisation. (Dashed line corresponds to the theoretical M_n, PDI = Đ).

at 3.9 ppm (in MeOD) corresponding to the single proton on the centre carbon of the isopropyl group which is clearly visible in the ^{1}H-NMR. In addition retention of the RAFT end group was confirmed by the marker peak at 3.4 ppm (Figure 5.16). The degree of polymerisation was estimated from the ratio of the RAFT marker peak to the polymer peaks for both the macroRAFT agent and the diblock copolymer (Table 5.2).

Figure 5.15 shows the chain growth of a PNIPAm block from the macroRAFT agent with respect to time and conversion. A long inhibition period is observed, as with homo-PNIPAm; however during the inhibition period the $Đ_M$ increases and the monomer is consumed. As a result there is not a linear relation between monomer conversion and block growth, rather, block growth occurs in the final stages of the reaction. This is due to a competing homopolymerisation reaction initiated by AIBN and not controlled by the RAFT agent. This was confirmed when both the diblock copolymer and PNIPAm homopolymer were isolated from the work up. It is the growth of this homo-PNIPAm that is responsible for the increase in $Đ_M$ and

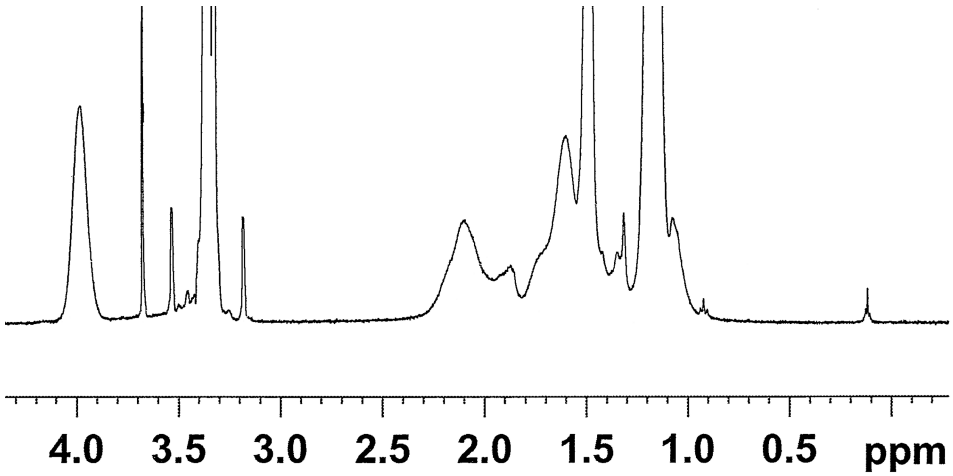

Figure 5.16: ^{1}H-NMR spectrum of Poly(*t*BMA-b-NIPAm).

monomer consumption prior to chain extension of the macroRAFT agent. This homopolymerisation may explain the mis-match between $M_n{}^{calc}$and the GPC M_n, however the agreement between the ^{1}H-NMR ratios and $M_n{}^{calc}$ suggest that the mismatch is in fact due to the diblock copolymer folding in the THF in such a way that the M_n is underestimated.

Although ^{1}H-NMR analysis shows that PNIPAm and P(*t*BMA) co-exist in the sample isolated this in itself is not evidence of a diblock copolymer, an identical ^{1}H-NMR spectrum could be produced from a blend of two homopolymers. The shape of the molecular weight distribution measured by GPC (Figure 5.17) is indicative of a diblock copolymer, there is no sign of a shoulder in the peak which would be expected for a blend of homopolymers. DOSY NMR can be used to measure the diffusion coefficients of individual peaks in the ^{1}H-NMR spectrum in order to provide supporting evidence for diblock copolymer formation.

The DOSY spectrum in Figure 5.18 is from the diblock copolymer sample characterised by GPC in Figure 5.17. The PNIPAm peaks share their diffusion coefficient with the *t*BMA peaks supporting the case for diblock copolymer formation. The diffusion coefficient for the diblock copolymer is slower than the macroRAFT agent, indicating that the polymer formed is indeed a larger molecule (Table 5.2).

In contrast the DOSY spectrum shown in Figure 5.19 gives an example of an unsuccessful triblock synthesis, the corresponding molecular

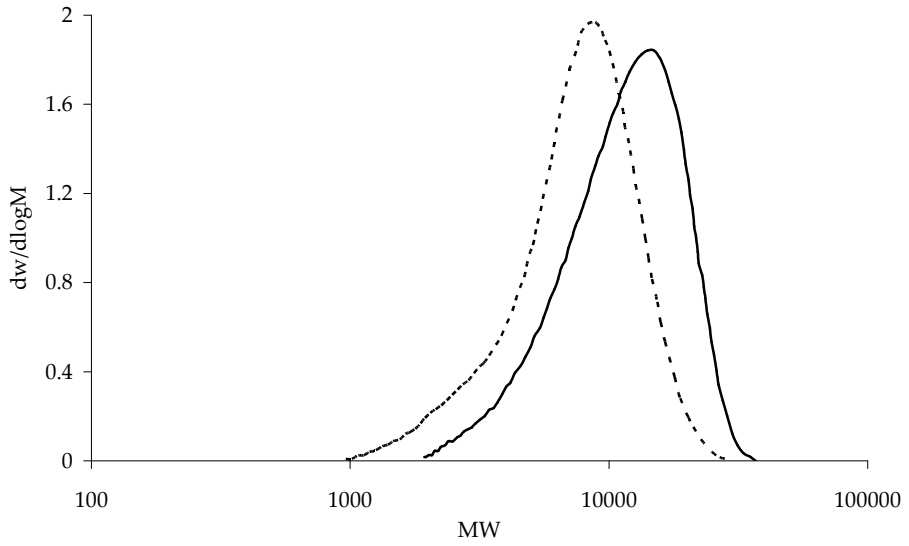

Figure 5.17: Molecular weight distributions determined by GPC for Poly(*t*BMA) macroRAFT agent (dotted line) and Poly(*t*BMA-b-NIPAm) (solid line). (Average molecular weight and $Đ_M$ listed in Table 5.2).

weight distribution determined by GPC is shown in Figure 5.20. Two peaks can clearly be seen in the GPC plot and the DOSY spectrum shows a mixture of diffusion coefficients. As discussed above the diffusion coefficients are meaningless where overlap occurs but the DOSY spectrum can be used to identify the diblock copolymer as the lower molecular weight species.

Based on the characterisation above it can be concluded that a diblock copolymer has been successfully formed and isolated from any additional PNIPAm homopolymer.

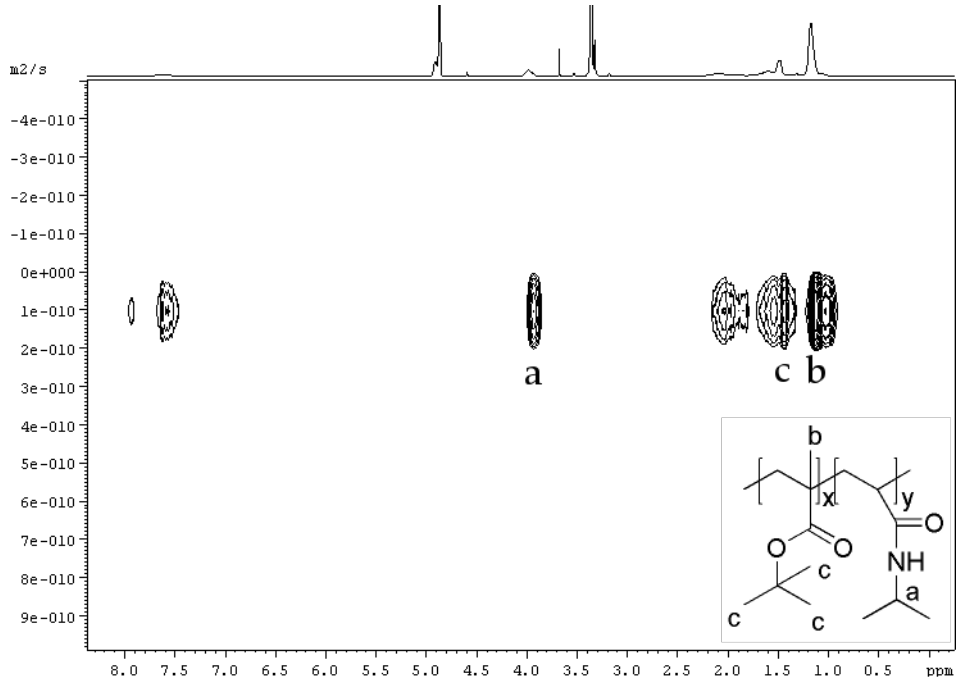

Figure 5.18: ^{1}H-NMR DOSY spectrum of P(*t*BMA-b-NIPAm) in deuterated methanol at 25 °C.)

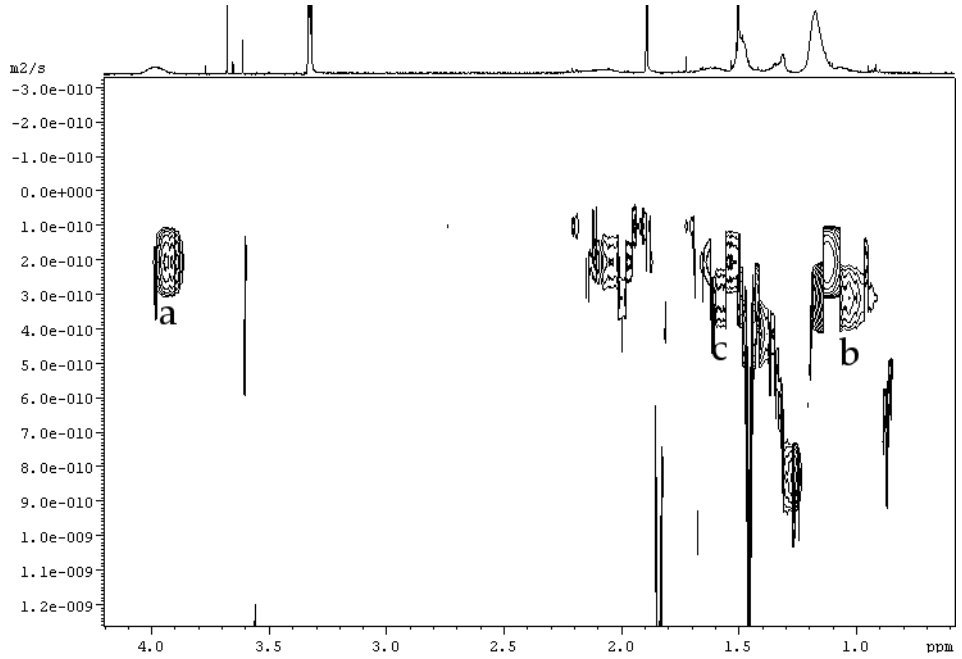

Figure 5.19: ^{1}H-NMR DOSY Spectrum of mixture of P(*t*BMA-b-NIPAm) and P(*t*BMA) in deuterated methanol at 25 °C. (Marker peak assignments correspond to Figure 5.18.)

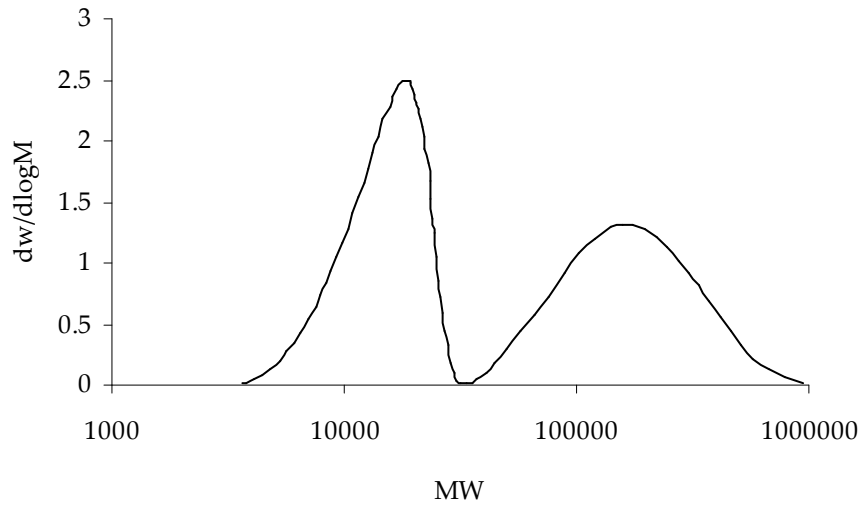

Figure 5.20: Molecular weight distribution determined by GPC for a mixture of P(*t*BMA-b-NIPAm) and P(*t*BMA).

5.6 P(*t*BMA-b-NIPAm-b-*t*BMA) Synthesis

The triblock copolymer synthesis was carried out using a diblock copolymer macroRAFT agent (see Table 5.3 for molecular weight information and Figure 5.23 for the ^{1}H-NMR spectrum). The triblock copolymer composition was confirmed by ^{1}H-NMR (Figure 5.24, Table 5.3) and the diffusion coefficient calculated from DOSY NMR indicated chain extension. Chain extension with *t*BMA was achieved whilst maintaining a low $Đ_M$ in the isolated triblock copolymer as shown by the molecular weight distributions measured by GPC (Figure 5.22, Table 5.3).

There were however significant issues with contamination from dead diblock copolymer chains and P*t*BMA homopolymer in all the batches synthesised and in this case the yield of clean triblock copolymer was 30 mg (1.4 %). The small extent of triblock formation was likely to be due in part to non-quantitative RAFT chain end retention on the diblock copolymer which reduced the number of triblock chains that could form. A subsequent result of this was a reduced ratio of RAFT agent to initiator, which contributed to the high degree of monomer consumption through P*t*BMA homopolymer formation.

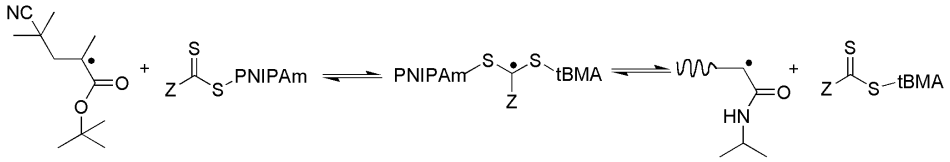

Figure 5.21: Schematic of RAFT pre-equilibrium between the a PNIPAm macroRAFT agent and *t*BMA.

Formation of a *t*BMA bock copolymer from a PNIPAm macroRAFT agent is challenging due to the relative reactivities of the two propagating radicals. As shown in Figure 5.21, the tertiary radical on the *t*BMA monomer is more stable than the secondary radical on the PNIPAm chain end. As a result the pre-equilibrium of the RAFT polymerisation in Figure 5.21 (corresponding to step 2 in Figure 5.4) will strongly favour the left hand side, in other words the *t*BMA monomer radical. The balance of this equilibrium will cause PNIPAm macroRAFT agent to remain capped and hence the RAFT polymerisation will be highly

unlikely to proceed. Instead the *t*BMA monomer radical will tend to polymerise to form a homopolymer via free radical polymerisation.

In light of the poor triblock copolymer yields achieved, the diblock copolymer was taken forward for hydrolysis and thiolation ready for use in the microsphere studies.

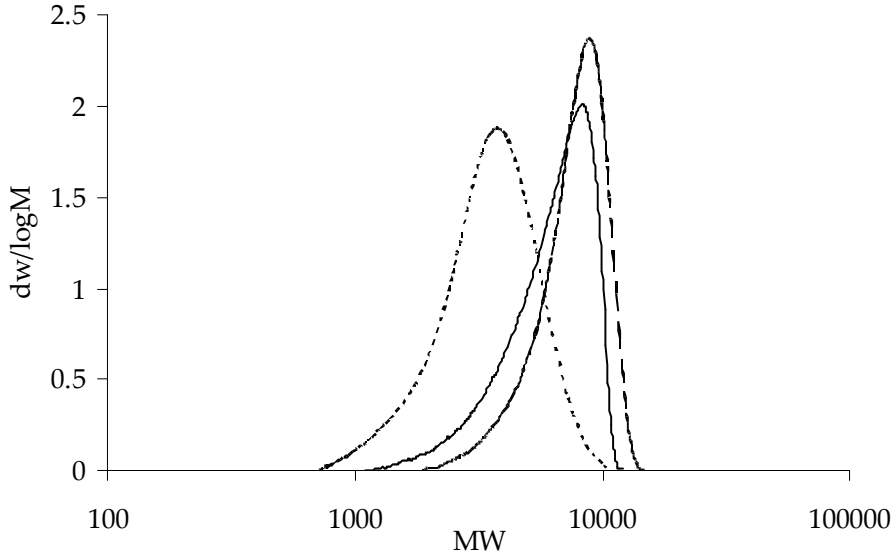

Figure 5.22: Molecular weight distributions determined by GPC for P*t*BMA macroRAFT agent (dotted line), P(*t*BMA-b-NIPAm) macroRAFT agent (solid line) and Poly(*t*BMA-b-NIPAm-b-*t*BMA) (dashed line), produced in sequential syntheses. (Average molecular weights and $Đ_M$ listed in Table 5.3).

	$M_n{}^{calc}$ (kDa)	M_n (kDa)	*DP* (GPC)	*DP* (NMR)	$Đ_M$	*D* (x $10^{-10}m^2s^{-1}$)
P(*t*BMA)	5.2	5.7	40	164	1.35	-
DB	22.7	10.7	40+44	164+218	1.43	7.780
TB	-	17.9	40+44+51	-	1.30	1.025

Table 5.3: Characterisation data for macroRAFT agent P(*t*BMA), P(*t*BMA-b-NIPAm) macroRAFT agent (DB) and P(*t*BMA-NIPAm-*t*BMA) triblock copolymer (TB). See Equation 5.2 for $M_n{}^{calc}$

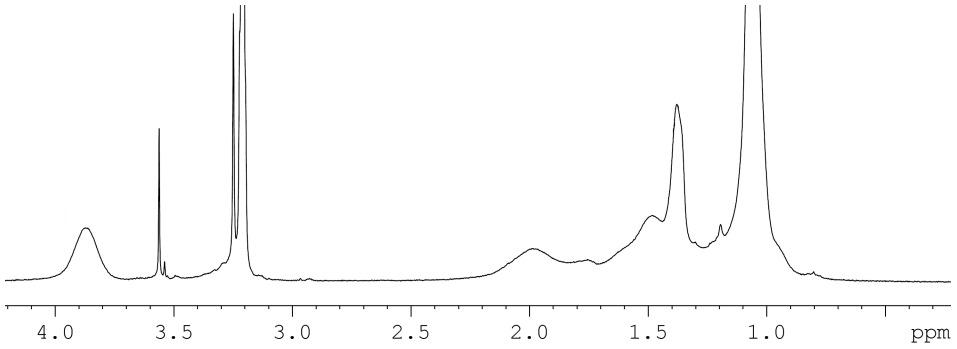

Figure 5.23: ^{1}H-NMR spectrum of Poly(*t*BMA-b-NIPAm) macroRAFT agent.

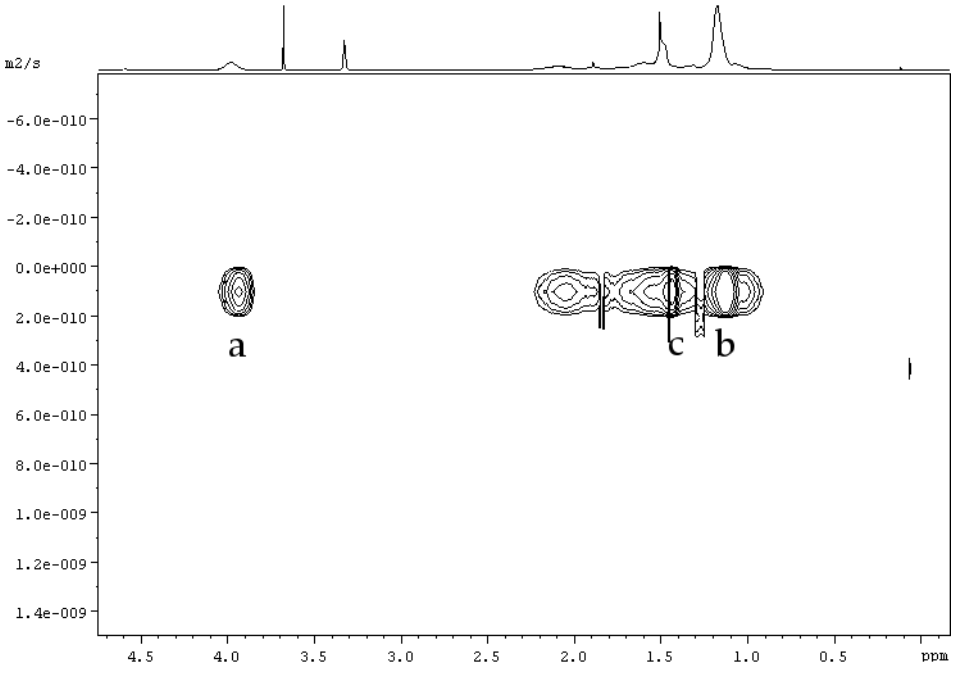

Figure 5.24: ^{1}H-NMR DOSY spectrum of P(*t*BMA-b-NIPAm-b-*t*BMA) in deuterated methanol at 25 ºC. (Marker peak assignments correspond to Figure 5.18).

5.7 Hydrolysis and Thiolation of P(*t*BMA-b-NIPAm)

The hydrolysis and thiolation methods used are already well known in the literature[17;200] and the synthetic scheme used in this investigation is shown in Figure 5.25.

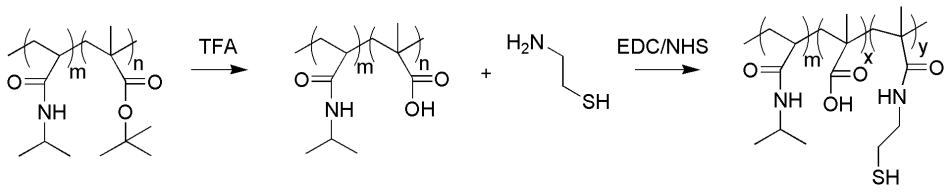

Figure 5.25: Synthetic scheme for hydrolysis and thiolation. (Full experimental details given in section 2.4.10 and 2.4.11).

The extent of hydrolysis of ester groups was monitored by following the loss of the t-butyl protons (1.5 ppm) in the ^{1}H-NMR spectrum, 84% conversion to acid groups was achieved. The product polymer was no longer THF soluble, preventing GPC analysis but DOSY NMR in deuterated methanol showed that the diffusion coefficient of the polymer had not changed, confirming that no block degradation had occurred (D = 1.028 x 10^{10}m^{2}s^{-1}). In addition it was observed during the work up that the polymer produced precipitated from an aqueous phase in response to both acidification and heating above 40 ºC, indicating the presence of both the PNIPAm and the PMA block. The loss of ester groups and the formation of carboxylic acid groups can be observed by FTIR spectroscopy (Figure 5.26). The carbonyl peak at 1719 cm^{-1} shifts to 1698 cm^{-1} suggesting formation of the polyacid.

The thiolation protocol used was analogous to that reported in Chapter 3 for the production of PMA_{SH}. In this case 5% thiolation was achieved (estimated from the ^{1}H-NMR spectrum, as in section 3.2.1). Attachment of the cysteamine functionalities onto the polymer chain was confirmed by DOSY NMR which showed the peaks corresponding to the two CH_2 groups at the same diffusion coefficient as the polymer peaks (D = 1.023 x 10^{10} m^{2}s^{-1}).

The structure of the polymer produced is shown in Figure 5.27. It is this polymer that was used to form microspheres in the following section. With a view to carrying out temperature response studies on

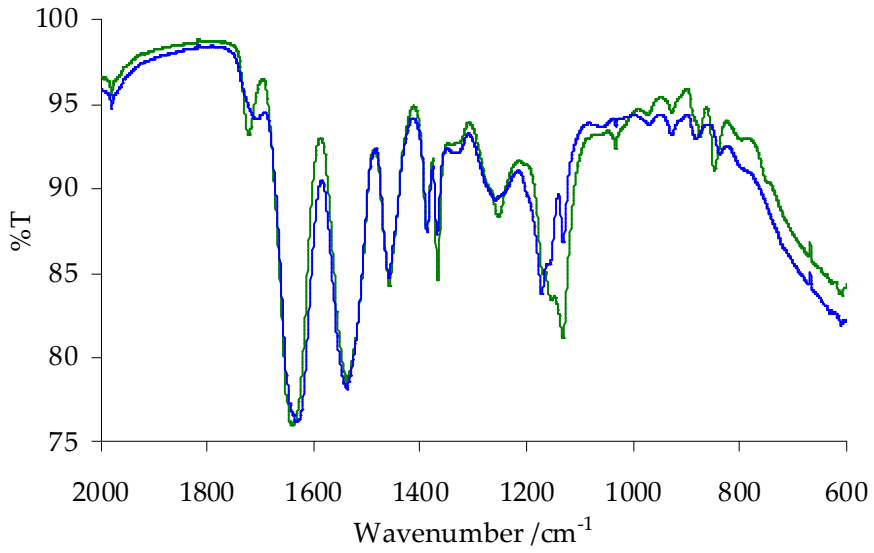

Figure 5.26: FTIR spectrum of P(*t*BMA-b-NIPAm) (green) and P(MA-b-NIPAm) (blue), both samples were dried prior to measurement.

the microspheres produced, the LCST was measured by observing the cloud point of a 10 mg/ml aqueous solution of polymer buffered at pH 7. The cloud point occurred at 37 °C and it is proposed that it is at or just above 37 °C that a change in microsphere morphology would occur.

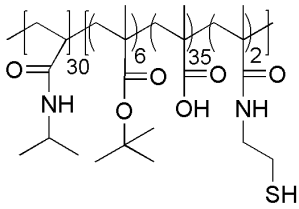

Figure 5.27: Functionalised diblock co-polymer structure used for microsphere production.

5.8 Formation of microspheres from P(MA_{SH}-b-NIPAm)

The thiolated diblock co-polymer, P(MA_{SH}-b-NIPAm) was used to investigate the scope for sonochemical microsphere production from synthetic block co-polymers. The anticipated end application of polymer microspheres of this type is drug delivery so the focus of this section is on oil filled and emulsion filled microspheres.

It was found that the sonochemical conditions described in Chapter 3 could be used to produce tetradecane filled microspheres from the diblock copolymer (see section 2.3.4). The mean diameter of the microspheres produced was 2.7 μm and the microspheres produced had a broader size distribution (standard deviation: 1.0) than those produced from PMA_{SH}(standard deviation: 0.7), illustrated in Figure 5.29. The microspheres had a very similar morphology to PMA_{SH} microspheres when viewed by optical microscopy (Figure 5.28a). Confocal microscopy showed that nile red dissolved within the tetradecane phase could be successfully encapsulated within the polymer shell (Figure 5.28b). This evidence indicates that it is possible to incorporate an additional block within the PMA_{SH} polymer whilst still maintaining the ability to form microspheres. Qualitative observations indicate that the microspheres formed are stable over at least a 6 week period in aqueous suspension at approximately 22 ºC.

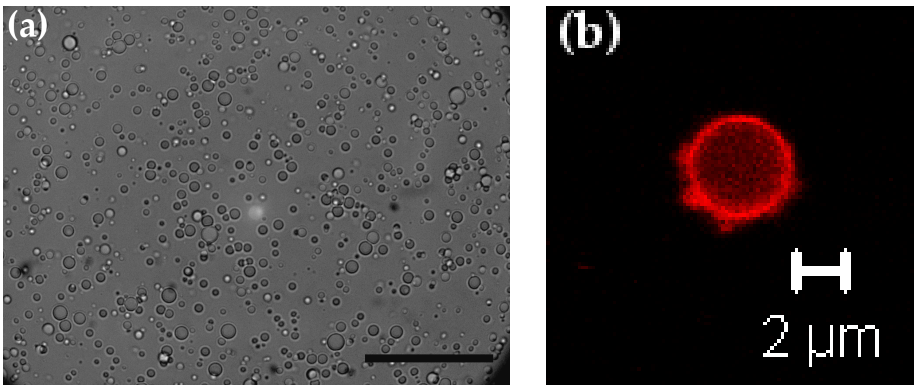

Figure 5.28: Optical micrograph (scale bar: 50 μm) (a) and confocal micrograph (b) of tetradecane filled P(MA_{SH}-b-NIPAm) microspheres formed using nile red saturated tetradecane.

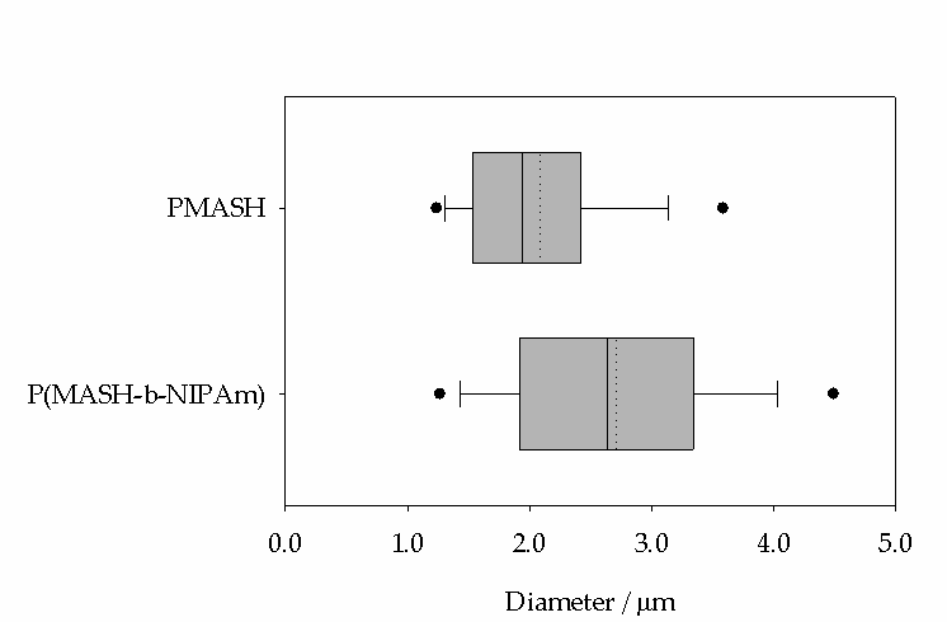

Figure 5.29: Size distributions of PMA_{SH} and P(MA_{SH}-b-NIPAm) microspheres formed under identical sonochemical conditions (60 s sonication at 14 Wcm^{-2} with generator B). (The mean diameter is represented by the dotted line whilst the median is shown by the black line within the grey box. The grey boxes define the upper and lower quartiles, the whiskers the 5 and 95 percentiles and the dots represent outliers.)

Figure 5.30 shows the FTIR spectra of both the diblock copolymer and the microspheres formed. The similarity of the spectra confirms that the diblock copolymer is forming the structural component of the microsphere shells. The peak at 545 cm^{-1} suggests disulfide cross linking in the microsphere shell. The peak at 1000 cm^{-1} was also seen in the PMA_{SH} microspheres reported in chapter 3.

In addition to forming tetradecane filled microspheres, encapsulation of a water-in-oil emulsion was also demonstrated using the methodology reported in Chapter 4 (experimental method detailed in section 2.3.4), an optical micrograph of the microspheres formed is shown in Figure 5.31. This enables the range of these P(MA_{SH}-b-NIPAm) microspheres to encompass encapsulation of both hydrophilic and lipophilic species.

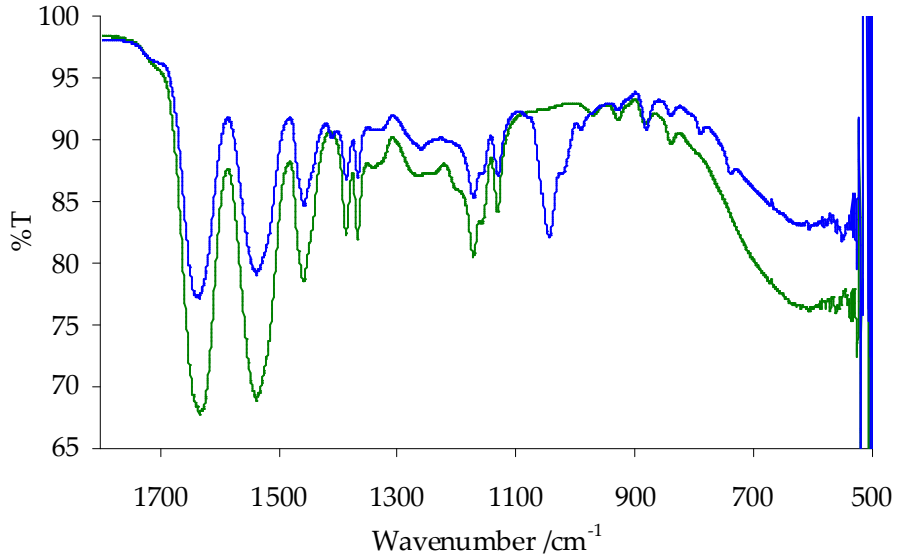

Figure 5.30: FTIR spectrum of the dried P(MA_{SH}-b-NIPAm) (green line) and dried tetradecane filled microspheres formed from P(MA_{SH}-b-NIPAm) (blue line).

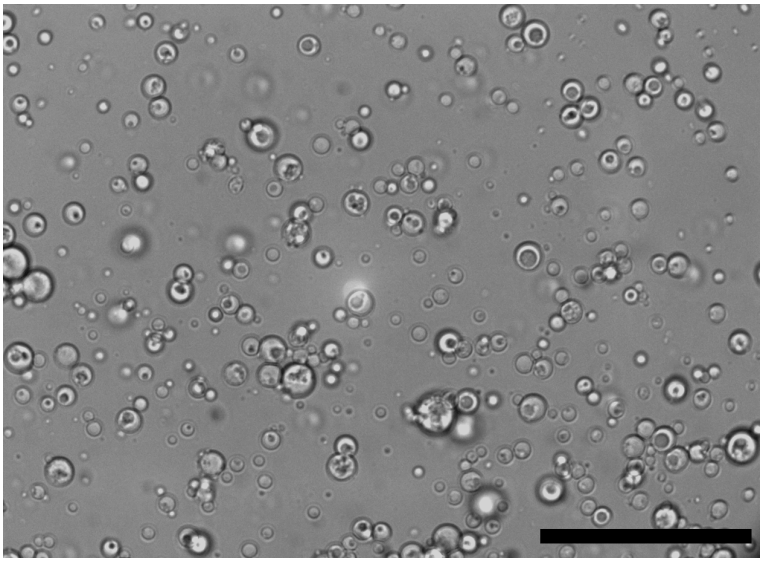

Figure 5.31: w/o emulsion filled P(MA_{SH}-b-NIPAm) microspheres in aqueous suspension, scale bar: 50 μm.

5.9 Temperature responsive behaviour of P(MA_{SH}-b-NIPAm) microspheres

The P(MA_{SH}-b-NIPAm) microspheres described above have been designed in order to fulfil the challenge of forming microspheres sonochemically that respond to an external stimulus, in this case an increase in the solution temperature above the LCST of the diblock copolymer (37 °C). At pH 8 (the pH used for sonochemical microsphere production) it is proposed that inter- and intra-molecular hydrogen bonding will occur between the two blocks in the polymer incorporated into the microsphere shell. The pKa of PMA[250] is estimated to be 7.5 therefore at pH 8 approximately 80% of the acid groups will be deprotonated. Therefore it is expected that at pH 8 the microsphere shell will be subject to a high degree of swelling and will behave somewhat like a hydrogel.

There is some evidence in the literature[251] for partitioning of blocks in a hydrogel as a result of hydrogen bonding which supports the case for partitioned portions of PNIPAm within the structure of the microsphere shell. It is proposed that upon heating through the LCST the PNIPAm blocks within the microsphere shell will collapse disrupting the hydrogen bonding network within the shell and resulting in rapid deswelling of the shell. This would either cause holes to open up in the shell between the disulfide crosslinked sections or collapse of the shell against the oil core would result in rupture of the shell and burst release of the contents.

In order to establish whether the microspheres produced change in response to a change in solution temperature, three experiments were carried out. In the first experiment a sample of tetradecane filled P(MA_{SH}-b-NIPAm) microspheres was placed under a coverslip on a microscope slide and heated to 40 °C on a hot plate over a period of 30 minutes. In order to provide a comparative control experiment a sample of tetradecane filled PMA_{SH} microspheres was treated in an identical manner. The micrographs in Figure 5.32 were taken before heating and then after 10 minutes and 30 minutes of heating respectively.

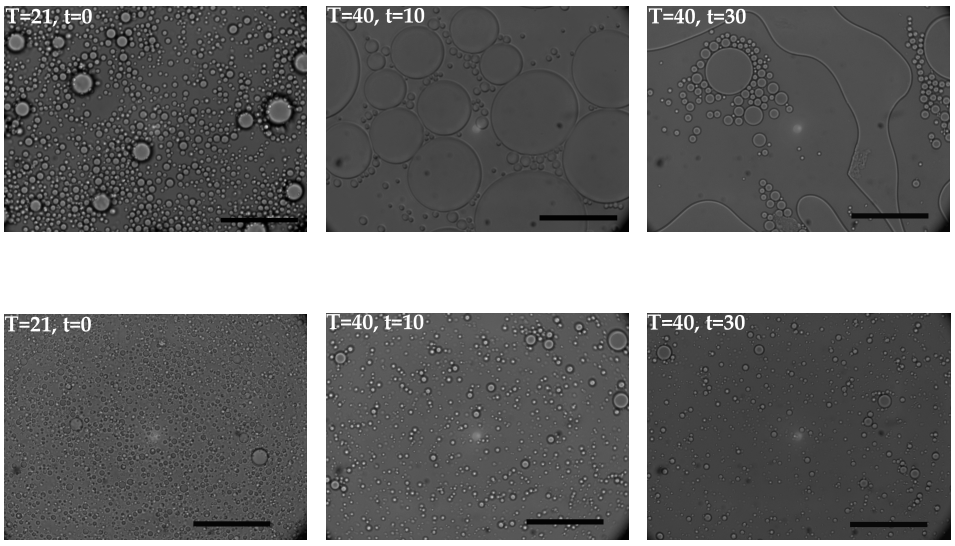

Figure 5.32: Optical micrographs of a sample of microspheres on a microscope slide heated above the phase transition temperature of PNIPAm on a hot plate. Top row: P(MA_{SH}-b-NIPAm) microspheres, bottom row: PMA_{SH} microspheres. T = temperature (°C), t = time (min). Scale bar: 50 μm.

Before heating, both samples contain discretely distributed microspheres typical of polymer microspheres made previously. Upon heating the PMA_{SH} microspheres are stable and show no significant change in morphology or size during the 30 minute period. However in the case of P(MA_{SH}-b-NIPAm) microspheres a significant change is seen to occur between t=0 and the micrograph taken after 30 minutes at 40 °C. After 10 minutes heating, some of the microspheres appear to have grown much larger. Alternatively adjacent microspheres have ruptured releasing oil which has coalesced into larger droplets. This hypothesis is born out in the micrograph taken at 30 minutes where large 'puddles' of oil can be observed. These regions of oil were not present in the sample at t=0 so it can be inferred that the oil which has formed the puddles has been released by the microspheres upon rupture. It can be seen that some small droplets/microspheres remain indicating that 30 minutes at 40 °C is an insufficient time period to achieve quantitative breakdown of the microspheres.

These micrographs indicate that whilst PMA_{SH} microspheres are stable at 40 °C, P(MA_{SH}-b-NIPAm) microspheres are not and heating

past the LCST of the diblock copolymer does result in rupture of the microspheres. However more compelling evidence can be collected by heating a sample of microspheres *in situ* on a microscope stage and imaging fluorescent nile red in the oil phase. This experiment was carried out using a laser scanning confocal microscope fitted with a heated stage and chamber. A chosen region of the sample was imaged over a 34 minute period, during which time the stage and chamber were heated from 25 °C to 44 °C (Figure 5.33).

Micrographs of the same region were taken at regular time intervals. This allowed the effect of heating above the LCST on a specific population of microspheres to be monitored. The heating rate achieved by the chamber and stage meant that the heating phase between 25 and 38 °C took 15 minutes. The effect of heating through 37 °C was seen immediately as some microspheres coalesced into a larger red puddle. Over the following 20 minutes the sample was held at 43-44 °C and breakdown of the individual microspheres can be observed as they coalesce to form larger puddles. The red fluorescence observed clearly indicates that the oil released originated from within the microspheres. As in the previous experiment the time period of the experiment was not sufficient to observe rupture of the entire population of microspheres; however it is proposed that incubation over a longer time period would result in rupture of all the microspheres in the population. In a control experiment a sample of microspheres taken from the same batch was observed over a 25 minute period at an ambient temperature of 25 °C (Figure 5.34). No change in morphology is observed indicating that the rupture observed in Figure 5.33 triggered by heating above the polymer's LCST.

The third experiment was conducted using dynamic light scattering (DLS) to look for shell fragments or collapsed P(MA_{SH}-b-NIPAm) globules from the microsphere shells after heating (Figure 5.35). Most of the microspheres formed from PMA_{SH} and P(MA_{SH}-b-NIPAm) are too large to allow the whole population to be characterised by DLS which can only detect radii up to 1500 nm. But the smaller microspheres in the distribution can be observed and, more importantly if P(MA_{SH}-b-NIPAm) polymer globules are formed from shell fragments upon collapse of the microspheres, these will be

detected. When the P(MA_{SH}-b-NIPAm) microspheres were heated to 40 ºC in the DLS chamber for 60 minutes a bimodal distribution formed (Figure 5.35b). It is suggested that the smaller peak at 258 nm corresponds to polymer globules formed on break down of the P(MA_{SH}-b-NIPAm) microspheres. As a control PMA_{SH} microspheres were heated to 40 °C in the DLS chamber for 45 minutes (Figure 5.35a). No significant change in the size distribution of observable microspheres was seen.

It can therefore be concluded that temperature responsive microspheres with a phase change in the region of 37 ºC can be formed from P(MA_{SH}-b-NIPAm) with an LCST of 37 ºC. RAFT polymerisation with 2-cyano-2-propyl dodecyl trithiocarbonate provides an effective means of producing P(*t*BMA-b-NIPAm) with a narrow dispersity which can be subsequently functionalised and used to produce these microspheres. Both tetradecane filled and w/o emulsion filled microspheres can be formed and coalescence of oil droplets released as a result of shell rupture on heating above the LCST can be observed by optical transmission and confocal microscopy.

Release of 5FU from w/o emulsion filled P(MA_{SH}-b-NIPAm) microspheres was measured (using the method described in Chapter 4) both at ambient temperature and after heating to 40 ºC for two hours. Release was negligible in both cases. By comparison 12.8 % release was achieved from PMA_{SH} microspheres heated over a two hour period at 40 ºC. The lack of leakage or temperature release from the P(MA_{SH}-b-NIPAm) microspheres does not corroborate the temperature responsive behaviour observed with tetradecane filled P(MA_{SH}-b-NIPAm) microspheres. Further investigation is required to understand the release mechanism and improve the microsphere shell design in order to achieve triggered release of hydrophilic and lipophilic species.

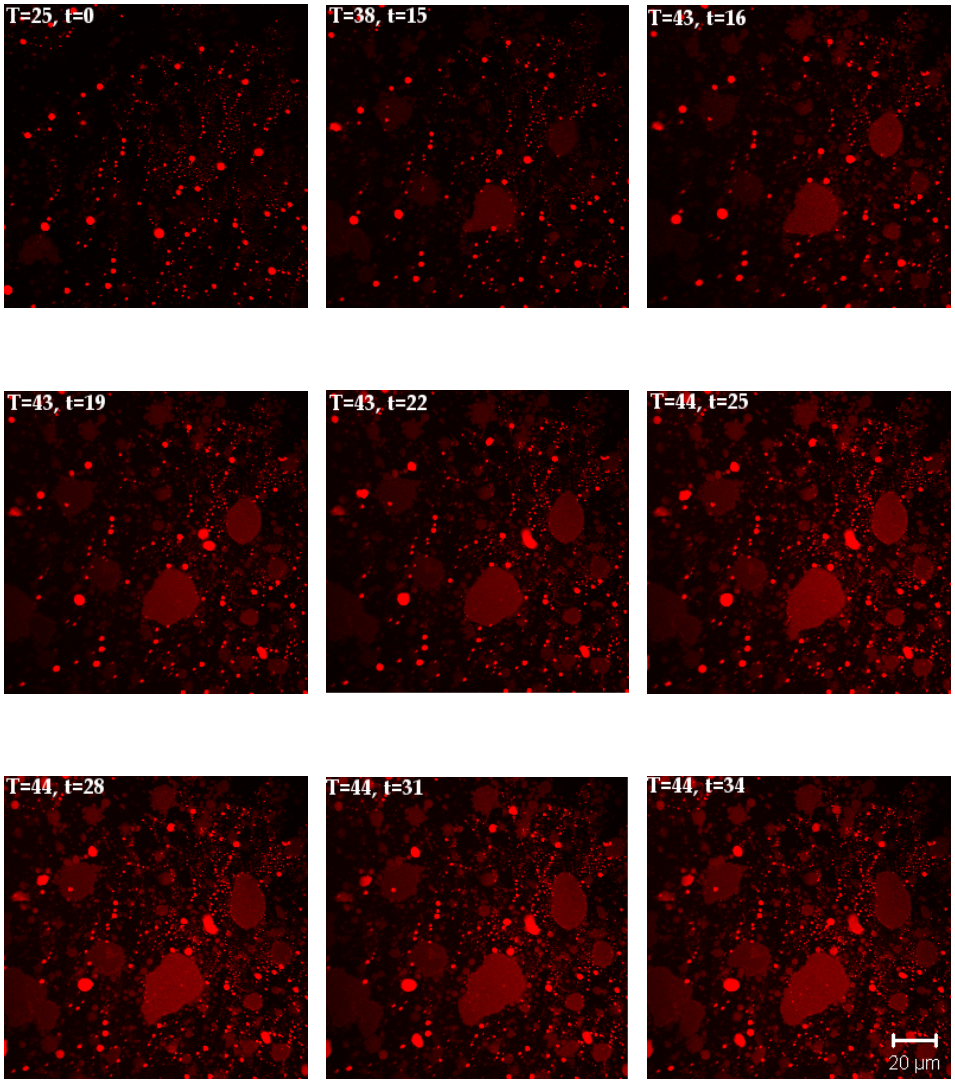

Figure 5.33: Confocal micrographs of an aqueous suspension of tetradecane filled P(MA_{SH}-b-NIPAm) microspheres containing nile red saturated tetradecane on a microscope slide heated above the phase transition temperature of P(MA_{SH}-b-NIPAm) on the microscope stage and viewed under a 543 nm laser. T = temperature (°C), t = time (min).

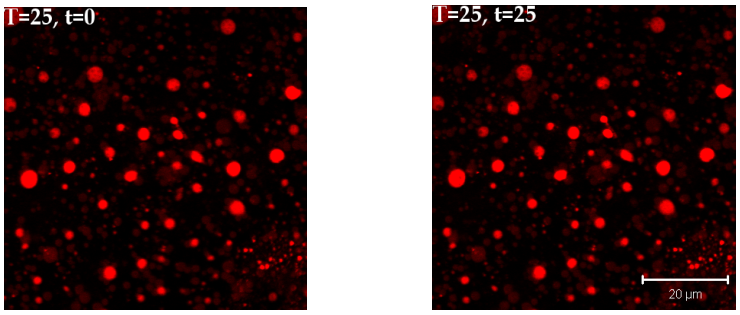

Figure 5.34: Confocal micrographs of an aqueous suspension of tetradecane filled P(MA_{SH}-b-NIPAm) microspheres containing nile red saturated tetradecane on a microscope slide held at ambient temperature and viewed under a 543 nm laser. T = temperature (°C), t = time (min).

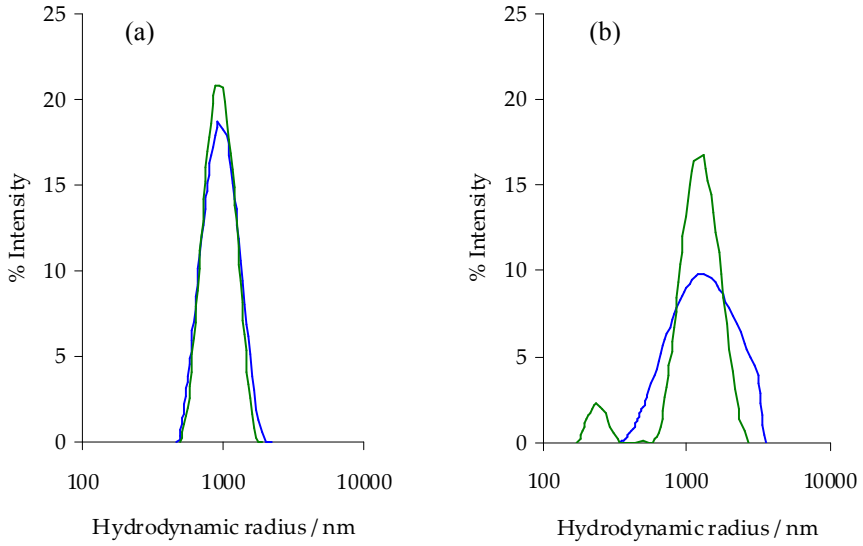

Figure 5.35: DLS trace for PMA_{SH} microspheres (a) and P(MA_{SH}-b-NIPAm) microspheres (b) in dilute aqueous solution at 25 ºC (blue) and 40 ºC (green).

6 Conclusions

The aims set out in Chapter 1 of this thesis were; to extend the scope of sonochemically produced microspheres for delivery applications by addressing the shell material, shell stabilisation/bonding and core composition.

In chapter 3 optimisation of the sonochemical method described by Suslick *et al.* and others[1;8;42;49] was set out, facilitating formation of microspheres from lysozyme or PMA_{SH}. The microspheres encapsulated either an air bubble or an oil droplet. Evidence from radical trapping experiments, comparison with an alternative homogenisation protocol and FTIR spectroscopy of microsphere shells suggested that the microspheres were stabilised by disulfide cross links, as expected from reports by Suslick *et al.*[1]. In the case of oil filled microspheres confocal micrographs provided evidence for encapsulation of a tetradecane phase containing the lipophilic dye nile red. Release of the lipophilic dye sudan III from the encapsulated oil phase was characterised *in vitro*. Release of the oil and dye from the microspheres was achieved as a result of either high intensity sonication or cleavage of the disulfide cross links.

Further to production of disulfide cross linked microspheres, ultrasound initiation of the thiol-ene reaction was investigated. It was proposed that sonochemical thiol-ene coupling would provide an alternative means of cross-linking the microspheres providing greater utility and the potential for surface functionalisation. It was shown that in water, under air, reaction rates could be achieved at 24 ^{o}C under ultrasound irradiation that were comparable to those observed for conventional thermal initiation at 45 ^{o}C[252]. This reaction was used in place of disulfide bonding to stabilise microspheres produced sonochemically from PMA_{ene} with DTT as a dithiol cross linker, however further characterisation is required to provide conclusive

evidence for thiol-ene coupling being the main form of crosslinking in the microsphere shells. Although more sophisticated crosslinkers were not explored this demonstration with DTT opens up the potential for sonochemically produced microspheres to be extended to include cross linking molecules which contain a stimulus responsive 'cleavage point', for example a photo-labile bond. The original aim to attempt *in-situ* surface functionalisation of the microspheres using sonochemical thiol-ene coupling was not reached, however the work reported has demonstrated that ultrasound initiated thiol-ene chemistry is a worthwhile avenue for future investigations.

Novel use of the sonochemical method to encapsulate a water-in-oil emulsion within protein and polymer microspheres was reported in chapter 4[253]. Both lipophilic and hydrophilic molecules were encapsulated within the microspheres upon formation, via encapsulation of a pre-formed water in oil emulsion. The optical transmission and confocal micrographs collected clearly demonstrated that the water in oil emulsion had been retained within the microspheres. Release of 5,6-carboxyfluroescein, NaCl and 5-Fluorouracil from w/o emulsion filled microspheres, *in vitro*, as a result of high intensity sonication or disulfide cleavage of the microsphere shells was characterised. These results demonstrate that the sonochemical method can be used to efficiently encapsulate an aqueous phase loaded with a dye, drug or similar hydrophilic species within protein or polymer microspheres. In addition the microspheres can be triggered to release their payload as a result of mechanical or chemical disruption to the shell. Initial indications from the release studies are that PMA_{SH} microspheres in particular are only stable to release over a period of hours, this would need to be addressed in order to facilitate use of w/o emulsion filled microspheres in delivery applications.

Finally microspheres were produced from the diblock copolymer P(MA_{SH}-b-NIPAm) (LCST: 37ºC). The diblock copolymer was synthesised via RAFT polymerisation and used in the sonochemical method discussed in chapters 3 and 4 to produce disulfide crosslinked microspheres. This is the first report of sonochemical production of microspheres from a synthetic block copolymer. PNIPAm was incorporated into the polymer with a view to facilitating temperature responsive release of a drug payload. Confocal micrographs of

P(MA_{SH}-b-NIPAm) microspheres containing a solution of nile red in tetradecane, heated to 43°C *in-situ*, display coalescence consistent with rupture of the microspheres at approximately 37°C. These observations were very promising, although at this stage they are not supported by conclusive drug release studies because insufficient polymer was produced to allow further studies to be carried out. However this work provides a starting point from which to further develop sonochemically produced responsive polymer microspheres and to characterise more fully their temperature responsive release behaviour.

The sonochemical method provides a facile and time effective means by which to produce microspheres containing aqueous and oil phases. The main limitation to the application of the these microspheres as drug delivery devices still lies in narrowing their polydisperse size distribution. It is essential for safe administration of drug carriers *in vivo* that they have a predetermined size and a narrow, if possible monodisperse size distribution. Recent work by Zhou *et al*.[41] has demonstrated that it is possible to form a near monodisperse population of microspheres sonochemically. Application of this technology to the systems reported above would facilitate a more robust proposition for their use in drug delivery applications.

The challenge of controlled drug delivery has attracted a great deal of research effort in recent years and many possible methods have been reported. However, the simplicity of sonochemical microsphere production, together with the variety of species that can potentially be encapsulated for triggered release and the utility of the microspheres produced as imaging agents makes sonochemically produced microspheres an attractive proposition for future research.

Ultrasound is an energy intensive means of producing microspheres[254] which is perhaps not ideal for large scale applications. However the speed and simplicity with which the protocol can be carried out does have practical application in small scale batch production. The ultrasound equipment used requires small financial outlay compared to techniques such as microfluidics and can be carried out more quickly than other wet chemistry methods including emulsion and layer-by-layer techniques. This may facilitate potential for use in hospital laboratories for the preparation of microsphere suspensions

'on demand' from pre-prepared drug and polymer solutions. This method of formulation would support the trends in medical research towards drug design tailored for individuals[255] and would allow simultaneous delivery of multiple drugs in one suspension.

In order to make a meaningful contribution to the field of drug delivery and compete with other methods of drug delivery the following areas should be addressed:

- Robust and extensively characterised control of the size distribution of the populations of microspheres produced should be achieved.

- The shelf life of the microspheres produced, especially with respect to retention of encapsulated hydrophilic species, should be improved. This could be achieved by addressing cross linking and polymer composition, architecture and chain length in the microsphere shells.

- Extensive release studies are needed to characterise the release of drug molecules in response to external triggers, e.g. heating, *in vitro* in order to provide a sound basis of knowledge from which to recommend studies *in vivo*.

- A biocompatible alternative to the tetradecane emulsions reported here, perhaps based on perfluorocarbons, should be developed to facilitate application of w/o emulsion filled microspheres *in vivo*.

With these considerations in mind the following recommendations are made for further work leading from the results reported in this thesis:

Following the successful formation of microspheres from P(MA_{SH}-b-NIPAm) it would be of interest to form microspheres from P(MA_{SH}-b-NIPAm-b-MA_{SH}). Use of a di-functional RAFT agent[256;257] could be explored to access P(MA_{SH}-b-NIPAm-b-MA_{SH}) in higher yields than achieved in the linear synthesis above. Use of the triblock copolymer would facilitate formation of a more highly crosslinked shell structure. This may allow the phase change in the PNIPAm block to cause more abrupt disruption of the microsphere structure, leading to more rapid release of the microspheres' contents. In addition the use of star or graft copolymers of PMA_{SH} and PNIPAm as shell materials should be investigated. Such architectures may provide access to microspheres with better structural integrity for storage or more well defined release characteristics.

Further to the temperature responsive copolymers discussed other block copolymers could be investigated to form analogous microspheres that respond to other triggers, for example photo or enzymatic degradation[193].

The study of w/o emulsion filled microspheres could be extended to explore the effect of shell crosslinking density and polymer chain length on the encapsulation stability of the microspheres. Dual release of hydrophilic and lipophilic species from w/o emulsion filled microspheres should be characterised in order to further demonstrate the utility of sonochemically produced microspheres as delivery agents.

By utilising sonochemical thiol-ene coupling as an alternative means of crosslinking, it is suggested that microspheres could be formed from responsive block copolymers of PMA_{ene} and crosslinked using a thiol crosslinker containing a labile bond to produce dual responsive delivery vehicles. Sonochemical thiol-ene coupling also provides the opportunity to 'label' the microsphere shells with biological markers, e.g. polysaccharides, during microsphere production. This line of research should be addressed with a view to forming microspheres sonochemically that can target a chosen location or cell type *in vivo*.

Producing stimulus responsive microspheres in one synthetic step that are capable of targeted delivery *in vivo* would make a significant contribution to the field of drug delivery.

References

[1] K. S. Suslick, M. W. Grinstaff, Protein microencapsulation of nonaqueous liquids, J. Am. Chem. Soc. 112 (1990) 7807–7809.

[2] U. Shimanovich, D. Eliaz, A. Aizer, I. Vayman, S. Michaeli, Y. Shav-Tal, A. Gedanken, Sonochemical synthesis of DNA nanospheres, Chembiochem 12 (2011) 1678–1681.

[3] U. Shimanovich, V. Volkov, D. Eliaz, A. Aizer, S. Michaeli, A. Gedanken, Stabilizing RNA by the sonochemical formation of RNA nanospheres, Small 7 (2011) 1068–1074.

[4] M. Sametband, U. Shimanovich, A. Gedanken, Graphene oxide microspheres prepared by a simple, one-step ultrasonication method, New Journal of Chemistry 36 (2012) 36–39.

[5] N. Skirtenko, T. Tzanov, A. Gedanken, S. Rahimipour, One-step preparation of multifunctional chitosan microspheres by a simple sonochemical method, Chemistry - A European Journal 16 (2010) 562–567.

[6] E. D. Vassileva, N. S. Koseva, Sonochemically born proteinaceous micro- and nanocapsules, in: R. Donev (Ed.), Advances in Protein Chemistry and Structural Biology, Elsevier Inc, 2010, pp. 205–252.

[7] F. Cavalieri, M. Ashokkumar, F. Grieser, F. Caruso, Ultrasonic synthesis of stable, functional lysozyme microbubbles, Langmuir 24 (2008) 10078–10083.

[8] M. Zhou, T. S. H. Leong, S. Melino, F. Cavalieri, S. Kentish, M. Ashokkumar, Sonochemical synthesis of liquid-encapsulated lysozyme microspheres, Ultrasonics Sonochemistry 17 (2010) 333–337.

[9] O. Grinberg, M. Hayun, B. Sredni, A. Gedanken, Characterization and activity of sonochemically-prepared BSA microspheres

containing taxol - an anticancer drug, Ultrasonics Sonochemistry 14 (2007) 661–666.

[10] S. Avivi, Y. Nitzan, R. Dror, A. Gedanken, An easy sonochemical route for the encapsulation of tetracycline in bovine serum albumin microspheres, Journal of the American Chemical Society 125 (2003) 15712–15713.

[11] R. Silva, H. Ferreira, A. C. Carvalho, A. C. Gomes, A. Cavaco-Paulo, Protein microspheres as suitable devices for piroxicam release, Colloids and Surfaces B: Biointerfaces 92 (2012) 277–285.

[12] O. Grinberg, A. Gedanken, The development and characterization of starch microspheres prepared by a sonochemical method for the potential drug delivery of insulin, Macromolecular Chemistry and Physics 211 (2010) 924–931.

[13] F. Cavalieri, M. Zhou, M. Ashokkumar, The design of multifunctional microbubbles for ultrasound image-guided cancer therapy, Current Topics in Medicinal Chemistry 10 (2010) 1198–1210.

[14] S. Melino, M. Zhou, M. Tortora, M. Paci, F. Cavalieri, M. Ashokkumar, Molecular properties of lysozyme-microbubbles: towards the protein and nucleic acid delivery, Amino Acids 43 (2012) 885–896.

[15] M. Wong, K. S. Suslick, Sonochemically produced hemoglobin microbubbles, in: D. L. Wilcox, M. Berg, T. Bernat, D. Kellerman, J. K. Cochran (Eds.), Hollow and Solid Spheres and Microspheres: Science and Technology Associated with Their Fabrication and Application, Materials Research Society Symposium Proceedings, Materials Research Soc, Pittsburgh, 1995, pp. 89–94.

[16] S. Avivi, A. Gedanken, S-s bonds are not required for the sonochemecial formation proteinaceous microspheres: the case of streptavidin, Biochemical Journal 366 (2002) 705–707.

[17] F. Cavalieri, M. Zhou, F. Caruso, M. Ashokkumar, One-pot ultrasonic synthesis of multifunctional microbubbles and microcapsules using synthetic thiolated macromolecules, Chemical Communications 47 (2011) 4096–4098.

[18] T. J. Mason, Sonochemistry, Oxford University Press, 1999.

[19] G. J. Price, Current trends in sonochemistry, Royal Society of Chemistry, London, 1992.

[20] T. J. Mason, Practical Sonochemistry, Ellis Horwood Books in Organic Chemistry, Ellis Horwood, Chichester, 1991.

[21] W. T. Richards, A. L. Loomis, The chemical effects of high frequency sound waves i. a preliminary survey, Journal of the American Chemical Society 49 (1927) 3086–3100.

[22] D. Ensminger, Ultrasonics; fundamentals, technology,applications, 2nd ed., Marcel Dekker, New York, 1988.

[23] S. Fokong, B. Theek, Z. Wu, P. Koczera, L. Appold, S. Jorge, U. Resch-Genger, M. van Zandvoort, G. Storm, F. Kiessling, T. Lammers, Image-guided, targeted and triggered drug delivery to tumors using polymer-based microbubbles., Journal of controlled release : official journal of the Controlled Release Society 163 (2012).

[24] D. Lensen, E. C. Gelderblom, D. M. Vriezema, P. Marmottant, N. Verdonschot, M. Versluis, N. de Jong, J. C. M. van Hest, Biodegradable polymeric microcapsules for selective ultrasound-triggered drug release, Soft Matter 7 (2011) 5417–5422.

[25] K. Hanajiri, T. Maruyama, Y. Kaneko, H. Mitsui, S. Watanabe, M. Sata, R. Nagai, T. Kashima, J. Shibahara, M. Omata, Y. Matsumoto, Microbubble-induced increase in ablation of liver tumors by high-intensity focused ultrasound, Hepatology Research 36 (2006) 308–314.

[26] S. L. Poliachik, W. L. Chandler, P. D. Mourad, R. J. Ollos, L. A. Crum, Activation, aggregation and adhesion of platelets exposed to high-intensity focused ultrasound, Ultrasound in Medicine & Biology 27 (2001) 1567–1576.

[27] Y.-S. Tung, H.-L. Liu, C.-C. Wu, K.-C. Ju, W.-S. Chen, W.-L. Lin, Contrast-agent-enhanced ultrasound thermal ablation, Ultrasound in Medicine and Biology 32 (2006) 1103–1110.

[28] C.-W. Zhou, F.-Q. Li, Y. Qin, C.-M. Liu, X.-L. Zheng, Z.-B. Wang, Non-thermal ablation of rabbit liver VX2 tumor by pulsed high

intensity focused ultrasound with ultrasound contrast agent: Pathological characteristics, World Journal of Gastroenterology 14 (2008) 6743–6747.

[29] L. Qiu, Y. Jiang, L. Zhang, L. Wang, Y. Luo, Ablation of synovial pannus using microbubble-mediated ultrasonic cavitation in antigen-induced arthritis in rabbits, Rheumatology International 32 (2012) 3813–3821.

[30] K. S. Suslick, Y. Didenko, M. M. Fang, T. Hyeon, K. J. Kolbeck, W. B. McNamara, M. M. Mdleleni, M. Wong, Acoustic cavitation and its chemical consequences, Philosophical Transactions of the Royal Society of London Series A-Mathematical Physical and Engineering Sciences 357 (1999) 335–353.

[31] J.-L. Luche, Synthetic Organic Sonochemistry, Plenum Press, New York, 1998.

[32] M. Siddique, R. Farooq, Z. M. Khan, Z. Khan, S. Shaukat, Enhanced decomposition of reactive blue 19 dye in ultrasound assisted electrochemical reactor, Ultrasonics Sonochemistry 18 (2011) 190–196.

[33] G. J. Price, Applications of high intensity ultrasound in polymer chemistry, in: R. van Eldik, C. D. Hubbard (Eds.), Chemistry Under Extreme or Non-Classical Conditions, volume First, John Wiley and Sons, Inc., New York, 1997, pp. 381–427.

[34] M. T. Taghizadeh, T. Asadpour, Effect of molecular weight on the ultrasonic degradation of poly(vinyl-pyrrolidone), Ultrasonics Sonochemistry 16 (2009) 280–286.

[35] J. P. Canselier, H. Delmas, A. M. Wilhelm, B. Abismail, Ultrasound emulsification-an overview, Journal of Dispersion Science and Technology 23 (2002) 333–349.

[36] N. K. Morya, P. K. Iyer, V. S. Moholkar, A physical insight into sonochemical emulsion polymerization with cavitation bubble dynamics, Polymer 49 (2008) 1910–1925.

[37] T. G. Leighton, The Acoustic Bubble, Academic Press, 1997.

[38] H. N. McMurray, B. P. Wilson, Mechanistic and spatial study of ultrasonically induced luminol chemiluminescence, The Journal of Physical Chemistry A 103 (1999) 3955–3962.

[39] M. Richman, S. Wilk, N. Skirtenko, A. Perelman, S. Rahimipour, Surface-modified protein microspheres capture amyloid-beta and inhibit its aggregation and toxicity, Chemistry - A European Journal 17 (2011) 11171–11177.

[40] N. Skirtenko, M. Richman, Y. Nitzan, A. Gedanken, S. Rahimipour, A facile one-pot sonochemical synthesis of surface-coated mannosyl protein microspheres for detection and killing of bacteria, Chemical Communications 47 (2011) 12277–12279.

[41] M. Zhou, F. Cavalieri, F. Caruso, M. Ashokkumar, Confinement of acoustic cavitation for the synthesis of protein-shelled nanobubbles for diagnostics and nucleic acid delivery, ACS Macro Letters 1 (2012) 853–856.

[42] M. W. Grinstaff, K. S. Suslick, Air-filled proteinaceous microbubbles - synthesis of an echo-contrast agent, Proceedings of the National Academy of Sciences U. S. A. 88 (1991) 7708–7710.

[43] Lysozyme gram positive, http://lysozyme.co.uk/, [Accessed 2012-10-22].

[44] Lysozyme, http://users.rcn.com/jkimball.ma.ultranet, [Accessed 2012-10-22].

[45] M. Zhou, F. Cavalieri, M. Ashokkumar, Modification of the size distribution of lysozyme microbubbles using a post-sonication technique, Instrumentation Science and Technology 40 (2012) 51–60.

[46] Y. S. Han, D. Radziuk, D. Shchukin, H. Moehwald, Stability and size dependence of protein microspheres prepared by ultrasonication, Journal of Materials Chemistry 18 (2008) 5162–5166.

[47] M. Zhou, F. Cavalieri, M. Ashokkumar, Tailoring the properties of ultrasonically synthesised microbubbles, Soft Matter 7 (2011) 623–630.

[48] K. Makino, T. Mizorogi, S. Ando, T. Tsukamoto, H. Ohshima, Sonochemically prepared bovine serum albumin microcapsules: factors affecting the size distribution and the microencapsulation yield, Colloids and Surfaces B: Biointerfaces 22 (2001) 251–255.

[49] A. Gedanken, Preparation and properties of proteinaceous microspheres made sonochemically, Chemistry - A European Journal 14 (2008) 3840–3853.

[50] S. Avivi, A. Gedanken, The preparation of avidin microspheres using the sonochemical method and the interaction of the microspheres with biotin, Ultrasonics Sonochemistry 12 (2005) 405–409.

[51] L. Lins, R. Brasseur, The hydrophobic effect in protein folding, FASEB Journal 9 (1995) 535–540.

[52] E. M. Dibbern, F. J.-J. Toublan, K. S. Suslick, Formation and characterization of polyglutamate core-shell microspheres, Journal of the American Chemical Society 128 (2006) 6540–6541.

[53] R. Silva, H. Ferreira, N. G. Azoia, U. Shimanovich, G. Freddi, A. Gedanken, A. Cavaco-Paulo, Insights on the mechanism of formation of protein microspheres in a biphasic system, Molecular Pharmaceutics 9 (2012) 3079–3088.

[54] U. Scheffel, H. Wagner, B. Rhodes, Nataraja.tk, Albumin microspheres for study of reticuloendothelial system, Journal of Nuclear Medicine 13 (1972) 498–&.

[55] B. Jiang, C. Gao, J. Shen, Polylactide hollow spheres fabricated by interfacial polymerization in an oil-in-water emulsion system, Colloid and Polymer Science 284 (2006) 513–519.

[56] W. Li, K. Matyjaszewski, K. Albrecht, M. Móller, Reactive surfactants for polymeric nanocapsules via interfacially confined miniemulsion ATRP, Macromolecules 42 (2009) 8228–8233.

[57] Y. Luo, H. Gu, Nanoencapsulation via interfacially confined reversible addition fragmentation transfer (RAFT) miniemulsion polymerization, Polymer 48 (2007) 3262–3272.

[58] A. Limer, F. Gayet, N. Jagielski, A. Heming, I. Shirley, D. M. Haddleton, Synthesis of microcapsules via reactive surfactants, Soft Matter 7 (2011) 5408–5416.

[59] S. van der Graaf, C. G. P. H. Schroën, R. M. Boom, Preparation of double emulsions by membrane emulsification-a review, Journal of Membrane Science 251 (2005) 7–15.

[60] E. Stride, M. Edirisinghe, Novel microbubble preparation technologies, Soft Matter 4 (2008) 2350–2359.

[61] K. Akamatsu, D. Kaneko, T. Sugawara, R. Kikuchi, S.-i. Nakao, Three preparation methods for monodispersed chitosan microspheres using the shirasu porous glass membrane emulsification technique and mechanisms of microsphere formation, Industrial and Engineering Chemistry Research 49 (2010) 3236–3241.

[62] B. G. D. Geest, N. N. Sanders, G. B. Sukhorukov, J. Demeester, S. C. D. Smedt, Release mechanisms for polyelectrolyte capsules, Chemical Society Reviews 36 (2007) 636–649.

[63] J. F. Quinn, A. P. R. Johnston, G. K. Such, A. N. Zelikin, F. Caruso, Next generation, sequentially assembled ultrathin films: beyond electrostatics, Chemical Society Reviews 36 (2007) 707–718.

[64] C. J. Ochs, G. K. Such, Y. Yan, M. P. van Koeverden, F. Caruso, Biodegradable click capsules with engineered drug-loaded multilayers, ACS Nano 4 (2010) 1653–1663.

[65] Z. Zhu, S. A. Sukhishvili, Temperature-induced swelling and small molecule release with hydrogen-bonded multilayers of block copolymer micelles, ACS Nano 3 (2009) 3595–3605.

[66] L. A. Connal, C. R. Kinnane, A. N. Zelikin, F. Caruso, Stabilization and functionalization of polymer multilayers and capsules via thiol-ene click chemistry, Chemistry of Materials 21 (2009) 576–578.

[67] G. K. Such, A. P. R. Johnston, F. Caruso, Engineered hydrogen-bonded polymer multilayers: from assembly to biomedical applications, Chemical Society Reviews 40 (2010) 19–29.

[68] J. Zhang, D. M. Lynn, Ultrathin multilayered films assembled from "Charge-Shifting" cationic polymers: Extended, long-term release of plasmid DNA from surfaces, Advanced Materials 19 (2007) 4218–4223.

[69] B.-S. Kim, S. W. Park, P. T. Hammond, Hydrogen-bonding layer-by-layer-assembled biodegradable polymeric micelles as drug delivery vehicles from surfaces, ACS Nano 2 (2008) 386–392.

[70] Y. Zhao, J. Bertrand, X. Tong, Y. Zhao, Photo-cross-linkable polymer micelles in hydrogen-bonding-built layer-by-layer films, Langmuir 25 (2009) 13151–13157.

[71] S. Sivakumar, V. Bansal, C. Cortez, S.-F. Chong, A. N. Zelikin, F. Caruso, Degradable, surfactant-free, monodisperse polymer-encapsulated emulsions as anticancer drug carriers, Advanced Materials 21 (2009) 1820–1824.

[72] A. N. Zelikin, A. L. Becker, A. P. R. Johnston, K. L. Wark, F. Turatti, F. Caruso, A general approach for DNA encapsulation in degradable polymer microcapsules, ACS Nano 1 (2007) 63–69.

[73] B. V. Antohe, D. B. Wallace, Ink-jet as a manufacturing method for drug delivery applications, in: International Manufacturing science and engineering conference, Evanston, Illinois, USA, 2008.

[74] Z. Ahmad, H. B. Zhang, U. Farook, M. Edirisinghe, E. Stride, P. Colombo, Generation of multilayered structures for biomedical applications using a novel tri-needle coaxial device and electrohydrodynamic flow, Journal of The Royal Society Interface 5 (2008) 1255–1261.

[75] U. Farook, M. J. Edirisinghe, E. Stride, P. Colombo, Novel co-axial electrohydrodynamic in-situ preparation of liquid-filled polymer-shell microspheres for biomedical applications, Journal of Microencapsulation 25 (2008) 241–247.

[76] E. Talu, K. Hettiarachchi, R. L. Powell, A. P. Lee, P. A. Dayton, M. L. Longo, Maintaining monodispersity in a microbubble population formed by flow-focusing, Langmuir 24 (2008) 1745–1749.

[77] K. Pancholi, U. Farook, R. Moaleji, E. Stride, M. Edirisinghe, Novel methods for preparing phospholipid coated microbubbles, European Biophysics Journal 37 (2008) 515–520.

[78] D. N. Breslauer, S. J. Muller, L. P. Lee, Generation of monodisperse silk microspheres prepared with microfluidics, Biomacromolecules 11 (2010) 643–647.

[79] O. Grinberg, A. Gedanken, C. R. Patra, S. Patra, P. Mukherjee, D. Mukhopadhyay, Sonochemically prepared BSA microspheres

containing gemcitabine, and their potential application in renal cancer therapeutics, Acta Biomaterialia 5 (2009) 3031–3037.

[80] D. B. Longley, D. P. Harkin, P. G. Johnston, 5-fluorouracil: mechanisms of action and clinical strategies, Nature Reviews Cancer 3 (2003) 330–338.

[81] J. P. Magnusson, A. O. Saeed, F. FernÃ¡ndez-Trillo, C. Alexander, Synthetic polymers for biopharmaceutical delivery, Polymer Chemistry 2 (2010) 48–59.

[82] F. Cavalieri, A. El Hamassi, E. Chiessi, G. Paradossi, R. Villa, N. Zaffaroni, Ligands tethering to biocompatible ultrasound active polymeric microbubbles surface, in: A. Technol, D. S. Univ Roma Tor Vergata, I. R. I. Tecnol Chim, I. R. I. Infm, S. Ist Nazl, I. M. I. Cura Tumori (Eds.), 17th Symposium of the Italian-Macromolecules-Science-and-Technology-Association (AIM), volume 234, Wiley-V C H Verlag Gmbh, Naples, ITALY, 2005, pp. 94–101.

[83] F. J.-J. Toublan, S. Boppart, K. S. Suslick, Tumor targeting by surface-modified protein microspheres, Journal of the American Chemical Society 128 (2006) 3472–3473.

[84] R. Krishnamurthy, J. A. Lumpkin, R. Sridhar, Inactivation of lysozyme by sonication under conditions relevant to microencapsulation, International Journal of Pharmaceutics 205 (2000) 23–34.

[85] S. Avivi, A. Gedanken, Are sonochemically prepared [alpha]-amylase protein microspheres biologically active?, Ultrasonics Sonochemistry 14 (2007) 1–5.

[86] I. Lentacker, B. G. De Geest, R. E. Vandenbroucke, L. Peeters, J. Demeester, S. C. De Smedt, N. N. Sanders, Ultrasound-responsive polymer-coated microbubbles that bind and protect DNA, Langmuir 22 (2006) 7273–7278.

[87] M. M. Fernandes, R. Silva, H. Ferreira, I. Donelli, G. Freddi, A. Cavaco-Paulo, Protein disulphide isomerase-induced refolding of sonochemically prepared ribonuclease a microspheres, Journal of Biotechnology 159 (2012) 78–82.

[88] T. Borodina, D. Grigoriev, E. Markvicheva, H. Moehwald, D. Shchukin, Vitamin e microspheres embedded within a biocompatible film for planar delivery, Advanced Engineering Materials 13 (2011) B123–B130.

[89] K. Makino, T. Mizorogi, S. Ando, T. Tsukamoto, H. Ohshima, Sustained release of hydrophobic materials from sonochemically prepared bovine serum albumin microcapsules, Colloids and Surfaces B-Biointerfaces 23 (2002) 59–64.

[90] S. Muro, C. Garnacho, J. A. Champion, J. Leferovich, C. Gajewski, E. H. Schuchman, S. Mitragotri, V. R. Muzykantov, Control of endothelial targeting and intracellular delivery of therapeutic enzymes by modulating the size and shape of ICAM-1-targeted carriers, Molecular Therapy 16 (2008) 1450–1458.

[91] X. Hua, P. Liu, Y. H. Gao, K. B. Tan, L. N. Zhou, Z. Liu, X. Li, S. W. Zhou, Y. J. Gao, Construction of thrombus-targeted microbubbles carrying tissue plasminogen activator and their in vitro thrombolysis efficacy: a primary research, Journal of Thrombrosis and Thrombolysis 30 (2010) 29–35.

[92] Y. Ozkan, N. Dikmen, A. Isimer, O. Gunhan, H. Y. Aboul-Enein, Clarithromycin targeting to lung: characterization, size distribution and in vivo evaluation of the human serum albumin microspheres, Farmaco 55 (2000) 303–307.

[93] P. Walday, H. Tolleshaug, T. Gjoen, G. Kindberg, T. Berg, T. Skotland, E. Holtz, Biodistributions of air-filled albumin microspheres in rats and pigs, Biochemical Journal 299 (1994) 437–443.

[94] Y.-z. Hu, J.-a. Zhu, Y.-g. Jiang, B. Hu, Ultrasound microbubble contrast agents: Application to therapy for peripheral vascular disease, Advances in Therapy 26 (2009) 425–434.

[95] J. Owen, Q. Pankhurst, E. Stride, Magnetic targeting and ultrasound mediated drug delivery: Benefits, limitations and combination, International Journal of Hyperthermia 28 (2012) 362–373.

[96] Y. S. Han, D. Radziuk, D. Shchukin, H. Moehwald, Sonochemical synthesis of magnetic protien container for targeted

delivery, Macromolmolecular Rapid Communications 29 (2008) 1203–1207.

[97] C.-A. J. Lin, W.-K. Chuang, Z.-Y. Huang, S.-T. Kang, C.-Y. Chang, C.-T. Chen, J.-L. Li, J. K. Li, H.-H. Wang, F.-C. Kung, J.-L. Shen, W.-H. Chan, C.-K. Yeh, H.-I. Yeh, W.-F. T. Lai, W. H. Chang, Rapid transformation of protein-caged nanomaterials into microbubbles as bimodal imaging agents, ACS Nano 6 (2012) 5111–5121.

[98] F. Calliada, R. Campani, O. Bottinelli, A. Bozzini, M. G. Sommaruga, Ultrasound contrast agents: Basic principles, European Journal of Radiology 27 (1998) S157–S160.

[99] S. Ohlerth, R. T. O'Brien, Contrast ultrasound: General principles and veterinary clinical applications, The Veterinary Journal 174 (2007) 501–512.

[100] R. Díaz-López, N. Tsapis, E. Fattal, Liquid perfluorocarbons as contrast agents for ultrasonography and 19F-MRI, Pharmaceutical Research 27 (2009) 1–16.

[101] R. Schwarz, M. Schuurmans, J. Seelig, B. Künnecke, 19F-MRI of perfluorononane as a novel contrast modality for gastrointestinal imaging, Magnetic Resonance in Medicine 41 (1999) 80–86.

[102] A. G. Webb, M. Wong, K. J. Kolbeck, R. L. Magin, K. S. Suslick, Sonochemically produced fluorocarbon microspheres: A new class of magnetic resonance imaging agent, Journal of Magnetic Resonance Imaging 6 (1996) 675–683.

[103] S. Avivi, I. Felner, I. Novik, A. Gedanken, The preparation of magnetic proteinaceous microspheres using the sonochemical method, Biochimica Et Biophysica Acta-General Subjects 1527 (2001) 123–129.

[104] G.-P. Yan, L. Robinson, P. Hogg, Magnetic resonance imaging contrast agents: Overview and perspectives, Radiography 13, Supplement 1 (2007) e5–e19.

[105] A. van Wamel, K. Kooiman, M. Harteveld, M. Emmer, F. J. ten Cate, M. Versluis, N. de Jong, Vibrating microbubbles poking individual cells: Drug transfer into cells via sonoporation, Journal of Controlled Release 112 (2006) 149–155.

[106] M. Azmin, C. Harfield, Z. Ahmad, M. Edirisinghe, E. Stride, How do microbubbles and ultrasound interact? basic physical, dynamic and engineering principles, Current Pharmaceutical Design 18 (2012) 2118–2134.

[107] S. Mehier-Humbert, T. Bettinger, F. Yan, R. H. Guy, Plasma membrane poration induced by ultrasound exposure: Implication for drug delivery, Journal of Controlled Release 104 (2005) 213–222.

[108] L. J. M. Juffermans, A. van Dijk, C. A. M. Jongenelen, B. Drukarch, A. Reijerkerk, H. E. de Vries, O. Kamp, R. J. P. Musters, Ultrasound and microbubble-induced intra- and intercellular bioeffects, Ultrasound in Medicine and Biology 35 (2009) 1917–1927.

[109] Y. Han, D. Shchukin, P. Fernandes, R.-C. Mutihac, H. Moehwald, Mechanism and kinetics of controlled drug release by temperature stimuli responsive protein nanocontainers, Soft Matter 6 (2010) 4942–4947.

[110] U. Shimanovich, A. Cavaco-Paulo, Y. Nitzan, A. Gedanken, Sonochemical coating of cotton and polyester fabrics with "Antibacterial" BSA and casein spheres, Chemistry-A European Journal 18 (2012) 365–369.

[111] I. C. Gouveia, Synthesis and characterization of a microsphere-based coating for textiles with potential as an in situ bioactive delivery system, Polymers for Advanced Technologies 23 (2011) 350–356.

[112] U. Angel, C. M. Silva, A. Cavaco-Paulo, A. Gedanken, Attaching different kinds of proteinaceous nanospheres to a variety of fabrics using ultrasound radiation, Israel Journal of Chemistry 50 (2010) 524–529.

[113] E. Marcuzzo, A. Sensidani, F. Debeaufort, A. Voilley, Encapsulation of aroma compounds in biopolymeric emulsion based edible films to control flavour release, Carbohydrate Polymers 80 (2010) 984–988.

[114] A. Ye, J. Cui, A. Taneja, X. Zhu, H. Singh, Evaluation of processed cheese fortified with fish oil emulsion, Food Research International 42 (2009) 1093–1098.

[115] L. Y. Chen, G. E. Remondetto, M. Subirade, Food protein-based materials as nutraceutical delivery systems, Trends in Food Science and Technology 17 (2006) 272–283.

[116] O. Tzhayik, A. Cavaco-Paulo, A. Gedanken, Fragrance release profile from sonochemically prepared protein microsphere containers, Ultrasonics Sonochemistry 19 (2012) 858–863.

[117] N. Devi, T. K. Maji, A novel microencapsulation of neem (azadirachta indica a. juss.) seed oil (NSO) in polyelectrolyte complex of kappa-carrageenan and chitosan, Journal of Applied Polymer Science 113 (2009) 1576–1583.

[118] T. J. Tiong, Sonochemical and Ultrasonic Output Analyses on Dental Endosonic Instruments, Ph.D. thesis, University of Bath, 2012.

[119] J. Lee, M. Ashokkumar, S. Kentish, F. Grieser, Effect of alcohols on the initial growth of multibubble sonoluminescence, The Journal of Physical Chemistry B 110 (2006) 17282–17285.

[120] W. W. Cleland, Dithiothreitol, a new protective reagent for SH groups, Biochemistry 3 (1964) 480–482.

[121] I. Gültekin, N. H. Ince, Ultrasonic destruction of bisphenol-a: The operating parameters, Ultrasonics Sonochemistry 15 (2008) 524–529.

[122] B. Lippitt, J. M. McCord, I. Fridovich, The sonochemical reduction of cytochrome c and its inhibition by superoxide dismutase, Journal of Biological Chemistry 247 (1972) 4688–4690.

[123] K. Yasui, T. Tuziuti, M. Sivakumar, Y. Iida, Sonoluminescence, Applied Spectroscopy Reviews 39 (2004) 399–436.

[124] L. A. Girifalco, R. J. Good, A theory for the estimation of surface and interfacial energies. i. derivation and application to interfacial tension, The Journal of Physical Chemistry 61 (1957) 904–909.

[125] A. K. Dutta, K. Kamada, K. Ohta, Spectroscopic studies of nile red in organic solvents and polymers, Journal of Photochemistry and Photobiology A-Chemistry 93 (1996) 57–64.

[126] P. Greenspan, S. D. Fowler, Spectrofluorometric studies of the lipid probe, nile red, Journal of Lipid Research 26 (1985) 781–9.

[127] S. Anandhakumar, V. Nagaraja, A. M. Raichur, Reversible polyelectrolyte capsules as carriers for protein delivery, Colloids and Surfaces B-Biointerfaces 78 (2010) 266–274.

[128] A. N. Zelikin, J. F. Quinn, F. Caruso, Disulfide cross-linked polymer capsules: En route to biodeconstructible systems, Biomacromolecules 7 (2005) 27–30.

[129] H. Dong, H. Du, X. Qian, Theoretical prediction of pKa values for methacrylic acid oligomers using combined quantum mechanical and continuum solvation methods, The Journal of Physical Chemistry A 112 (2008) 12687–12694.

[130] M. C. Tobin, Laser raman spectra of polymethacrylic acid, The Journal of Chemical Physics 50 (1969) 4551–4554.

[131] D. Haufe, K. G. Dahmen, O. Tiebel, M. HÃŒbler, T. Koch, Effect of perfluorohexane on the expression of cellular adhesion molecules and surfactant protein a in human mesothelial cells in vitro, Artificial Cells, Blood Substitutes and Biotechnology 39 (2011) 239–246.

[132] R. Alvarez-Román, A. Naik, Y. N. Kalia, R. H. Guy, H. Fessi, Enhancement of topical delivery from biodegradable nanoparticles, Pharmaceutical Research 21 (2004) 1818–1825.

[133] A. Hawe, M. Sutter, W. Jiskoot, Extrinsic fluorescent dyes as tools for protein characterization, Pharmaceutical Research 25 (2008) 1487–1499.

[134] K. Nishida, M. Kobayashi, H. Miyamoto, N. Yoshikawa, S. Fumoto, H. Sasaki, J. Nakamura, Relationship between lipophilicity and absorption from the liver surface of paraben derivatives and antipyrine in rats, Journal of Pharmacy and Pharmacology 63 (2011) 736–740.

[135] C. Walling, W. Helmreich, Reactivity and reversibility in the reaction of thiyl radicals with olefins, Journal of the American Chemical Society 81 (1959) 1144–1148.

[136] K. Griesbaum, Problems and possibilities of the free-radical addition of thiols to unsaturated compounds, Angewandte Chemie International Edition in English 9 (1970) 273–287.

[137] T. Posner, Beiträge zur kenntniss der ungesättigten verbindungen. II. ueber die addition von mercaptanen an ungesättigte kohlenwasserstoffe, Berichte der deutschen chemischen Gesellschaft 38 (1905) 646–657.

[138] C. E. Hoyle, C. N. Bowman, Thiol-ene click chemistry, Angewandte Chemie International Edition 49 (2010) 1540–1573.

[139] H. C. Kolb, M. G. Finn, K. B. Sharpless, Click chemistry: Diverse chemical function from a few good reactions, Angewandte Chemie International Edition 40 (2001) 2004–2021.

[140] A. B. Lowe, Thiol-ene "click" reactions and recent applications in polymer and materials synthesis, Polymer Chemistry 1 (2010) 17–36.

[141] C. E. Hoyle, A. B. Lowe, C. N. Bowman, Thiol-click chemistry: a multifaceted toolbox for small molecule and polymer synthesis, Chemical Society Reviews 39 (2010) 1355–1387.

[142] A. E. Rydholm, S. K. Reddy, K. S. Anseth, C. N. Bowman, Controlling network structure in degradable thiol-acrylate biomaterials to tune mass loss behavior, Biomacromolecules 7 (2006) 2827–2836.

[143] V. S. Khire, A. W. Harant, A. W. Watkins, K. S. Anseth, C. N. Bowman, Ultrathin patterned polymer films on surfaces using thiol-ene polymerizations, Macromolecules 39 (2006) 5081–5086.

[144] C. E. Hoyle, T. Y. Lee, T. Roper, Thiol-enes: Chemistry of the past with promise for the future, Journal of Polymer Science Part A: Polymer Chemistry 42 (2004) 5301–5338.

[145] M. Uygun, M. A. Tasdelen, Y. Yagci, Influence of type of initiation on thiol-ene 'Click' chemistry, Macromolecular Chemistry and Physics 211 (2010) 103–110.

[146] L. M. Campos, K. L. Killops, R. Sakai, J. M. J. Paulusse, D. Damiron, E. Drockenmuller, B. W. Messmore, C. J. Hawker, Development of thermal and photochemical strategies for thiol-ene click polymer functionalization, Macromolecules 41 (2008) 7063–7070.

[147] G. Cravotto, P. Cintas, Forcing and controlling chemical reactions with ultrasound, Angewandte Chemie International Edition 46 (2007) 5476–5478.

[148] P. Cintas, J.-L. Luche, Green chemistry. the sonochemical approach, Green Chemistry 1 (1999) 115–125.

[149] G. J. Price, L. Garland, J. Comina, M. Davis, D. J. Snell, P. J. West, Investigation of radical intermediates in polymer sonochemistry, Research on Chemical Intermediates 30 (2004) 807–827.

[150] P. Riesz, T. Kondo, Free radical formation induced by ultrasound and its biological implications, Free Radical Biology and Medicine 13 (1992) 247–270.

[151] G. J. Price, D. J. Norris, P. J. West, Polymerization of methylmethacrylate initiated by ultrasound, Macromolecules 25 (1992) 6447–6454.

[152] M. S. M. Alger, Polymer Science Dictionary, Springer, 1997.

[153] J. Brandrup, E. H. Immergut, E. A. Grulke, Polymer Handbook, 4th ed., Wiley, New York, Chichester, 2003.

[154] Z. L. Wu, B. Ondruschka, A. Stark, Ultrasonic cleavage of thioethers, J. Phys. Chem. A 109 (2005) 3762–3766.

[155] B. M. Teo, S. W. Prescott, G. J. Price, F. Grieser, M. Ashokkumar, Synthesis of temperature responsive poly(n-isopropylacrylamide) using ultrasound irradiation, The Journal of Physical Chemistry B 114 (2010) 3178–3184.

[156] G. J. Price, E. J. Lenz, The use of dosimeters to measure radical production in aqueous sonochemical systems, Ultrasonics 31 (1993) 451–456.

[157] Z. L. Wu, B. Ondruschka, Aquasonolysis of thioethers, Ultrasonics Sonochemistry 13 (2006) 371–378.

[158] A. W. Adamson, Chapter XIV: emulsions and foams, in: Physical Chemistry of Surfaces, 4th ed., Wiley Interscience, 1982.

[159] B. Abismail, J. Canselier, A. Wilhelm, H. Delmas, C. Gourdon, Emulsification by ultrasound: drop size distribution and stability, Ultrasonics Sonochemistry 6 (1999) 75–83.

[160] P. W. Atkins, J. De Paula, Atkins' physical chemistry, 8th ed., Oxford University Press, Oxford, 2006.

[161] P. C. Hiemenz, R. Rajagopalan, Chapter 6: Surface tension and contact angle, in: Principles of Colloid and Surface Chemistry, 3rd ed., Marcel Dekker, 1997.

[162] G. G. Badolato, F. Aguilar, H. P. Schuchmann, T. Sobisch, D. Lerche, Evaluation of long term stability of model emulsions by multisample analytical centrifugation, in: Surface and Interfacial Forces - From Fundamentals to Applications, volume 134 of *Progress in Colloid and Polymer Science*, Springer-Verlag, 2008.

[163] L. Ratke, P. W. Voorhees, Growth and coarsening: Ostwald ripening in material processing, Springer-Verlag, 2002.

[164] S. S. Davis, H. P. Round, T. S. Purewal, Ostwald ripening and the stability of emulsion systems: an explanation for the effect of an added third component, Journal of Colloid and Interface Science 80 (1981) 508–511.

[165] B. Tal-Figiel, The formation of stable W/O, O/W, W/O/W cosmetic emulsions in an ultrasonic field, Chemical Engineering Research and Design 85 (2007) 730–734.

[166] O. Behrend, K. Ax, H. Schubert, Influence of continuous phase viscosity on emulsification by ultrasound, Ultrasonics Sonochemistry 7 (2000) 77–85.

[167] M. K. Li, H. S. Fogler, Acoustic emulsification. part 1. the instability of the oil-water interface to form the initial droplets, Journal of Fluid Mechanics 88 (1978) 499–511.

[168] M. K. Li, H. S. Fogler, Acoustic emulsification. part 2. breakup of the large primary oil droplets in a water medium, Journal of Fluid Mechanics 88 (1978) 513–528.

[169] A. Márquez, G. Palazolo, J. Wagner, Water in oil (w/o) and double (w/o/w) emulsions prepared with spans: microstructure, stability, and rheology, Colloid $0 Polymer Science 285 (2007) 1119–1128.

[170] M. Capdevila, A. Maestro, M. Porras, J. M. Gutierrez, Preparation of span 80/oil/water highly concentrated emulsions:

Influence of composition and formation variables and scale-up, Journal of Colloid and Interface Science 345 (2010) 27–33.

[171] J. Jiao, D. J. Burgess, Rheology and stability of water-in-oil-in-water multiple emulsions containing span 83 and tween 80, AAPS PharmSci 5 (2003) E7.

[172] J. Jiao, D. J. Burgess, Ostwald ripening of water-in-hydrocarbon emulsions, Journal of Colloid and Interface Science 264 (2003) 509–516.

[173] Y. Y. Zhu, G. Y. Zhang, H. Q. Yang, X. L. Hong, Influence of surfactants on the parameters of polylactide nanocapsules containing insulin, Journal of Surfactants and Detergents 8 (2005) 353–358.

[174] S.-H. Hu, B.-J. Liao, C.-S. Chiang, P.-J. Chen, I.-W. Chen, S.-Y. Chen, Core-shell nanocapsules stabilized by single-component polymer and nanoparticles for magneto-Chemotherapy/Hyperthermia with multiple drugs, Advanced Materials 24 (2012) 3627–3632.

[175] P. van Rijn, H. Wang, A. Boker, Ultra-sound assisted formation of biodegradable double emulsion capsules from hen egg white, Soft Matter 7 (2011) 5274–5280.

[176] J. O' Regan, D. M. Mulvihill, Water soluble inner aqueous phase markers as indicators of the encapsulation properties of water-in-oil-in-water emulsions stabilized with sodium caseinate, Food Hydrocolloids 23 (2009) 2339–2345.

[177] R. K. Owusu Apenten, Q.-H. Zhu, Interfacial parameters for spans and tweens in relation to water-in-oil-in-water multiple emulsion stability, Food Hydrocolloids 10 (1996) 245–250.

[178] A. Benichou, A. Aserin, N. Garti, W/O/W double emulsions stabilized with WPI-polysaccharide complexes, Colloids and Surfaces A: Physicochemical and Engineering Aspects 294 (2007) 20–32.

[179] Y. Sela, S. Magdassi, N. Garti, Release of markers from the inner water phase of w / o / w emulsions stabilized by silicone based polymeric surfactants, Journal of Controlled Release 33 (1995) 1–12.

[180] F. Cournarie, V. Rosilio, M. Cheron, C. Vauthier, B. Lacour, J. L. Grossiord, M. Seiller, Improved formulation of W/O/W multiple emulsion for insulin encapsulation. influence of the chemical structure of insulin, Colloid Polym. Sci. 282 (2004) 562–568.

[181] M. Hai, K. Bernath, D. Tawfik, S. Magdassi, Flow cytometry: A new method to investigate the properties of water-in-oil-in-water emulsions, Langmuir 20 (2004) 2081–2085.

[182] A. M. Pavlov, V. Saez, A. Cobley, J. Graves, G. B. Sukhorukov, T. J. Mason, Controlled protein release from microcapsules with composite shells using high frequency ultrasound-potential for in vivo medical use, Soft Matter 7 (2011) 4341–4347.

[183] M. Djenouhat, O. Hamdaoui, M. Chiha, M. H. Samar, Ultrasonication-assisted preparation of water-in-oil emulsions and application to the removal of cationic dyes from water by emulsion liquid membrane: Part 1: Membrane stability, Separation and Purification Technology 62 (2008) 636–641.

[184] J. C. Berg, An Introduction to Interfaces and Colloids: The Bridge to Nanoscience, World Scientific, Singapore, 2010.

[185] H. L. Rosano, F. G. Gandolfo, J. D. P. Hidrot, Stability of w-1/O/W-2 multiple emulsions - influence of ripening and interfacial interactions, Colloids and Surfaces A: Physicochemical and Engineering Aspects 138 (1998) 109–121.

[186] M. Y. Koroleva, E. V. Yurtov, Effect of ionic strength of dispersed phase on ostwald ripening in water-in-oil emulsions, Colloid Journal 65 (2003) 40–43.

[187] J. W. D. Comeau, S. Costantino, P. W. Wiseman, A guide to accurate fluorescence microscopy colocalization measurements, Biophysical Journal 91 (2006) 4611–4622.

[188] J. N. Weinstein, S. Yoshikami, P. Henkart, R. Blumenthal, W. A. Hagins, Liposome-cell interaction: Transfer and intracellular release of a trapped fluorescent marker, Science 195 (1977) 489–492.

[189] R. F. Chen, J. R. Knutson, Mechanism of fluorescence concentration quenching of carboxyfluorescein in liposomes: Energy

transfer to nonfluorescent dimers, Analytical Biochemistry 172 (1988) 61–77.

[190] J. Zhou, A. L. Loftus, G. Mulley, A. T. A. Jenkins, A thin film Detection/Response system for pathogenic bacteria, Journal of the American Chemical Society 132 (2010) 6566–6570.

[191] M. C. Perry, The Chemotherapy Source Book, 4th ed., Lippincott, Williams and Wilkins, Philadelphia, 2008.

[192] E. Petit, G. Milano, F. Lévi, A. Thyss, F. Bailleul, M. Schneider, Circadian rhythm-varying plasma concentration of 5-fluorouracil during a five-day continuous venous infusion at a constant rate in cancer patients, Cancer Research 48 (1988) 1676–1679.

[193] A. P. Esser-Kahn, S. A. Odom, N. R. Sottos, S. R. White, J. S. Moore, Triggered release from polymer capsules, Macromolecules 44 (2011) 5539–5553.

[194] Y. Xia, X. Yin, N. A. D. Burke, H. D. H. Stöver, Thermal response of narrow-disperse poly(n-isopropylacrylamide) prepared by atom transfer radical polymerization, Macromolecules 38 (2005) 5937–5943.

[195] H. Schild, Poly(n-isopropylacrylamide): experiment, theory and application, Progress in Polymer Science 17 (1992) 163–249.

[196] C.-L. Lo, K.-M. Lin, G.-H. Hsiue, Preparation and characterization of intelligent core-shell nanoparticles based on poly(d,l-lactide)-g-poly(n-isopropyl acrylamide-co-methacrylic acid), Journal of Controlled Release 104 (2005) 477–488.

[197] C. Oerlemans, W. Bult, M. Bos, G. Storm, J. Nijsen, W. Hennink, Polymeric micelles in anticancer therapy: Targeting, imaging and triggered release, Pharmaceutical Research 27 (2010) 2569–2589.

[198] Y. Guan, Y. Zhang, PNIPAM microgels for biomedical applications: from dispersed particles to 3D assemblies, Soft Matter 7 (2011) 6375–6384.

[199] X. Xu, J. D. Flores, C. L. McCormick, Reversible imine shell cross-linked micelles from aqueous RAFT-Synthesized

thermoresponsive triblock copolymers as potential nanocarriers for "pH-Triggered" drug release, Macromolecules 44 (2011) 1327–1334.

[200] X. He, X. Wu, C. Gao, K. Wang, S. Lin, W. Huang, M. Xie, D. Yan, Synthesis and self-assembly of a hydrophilic, thermo-responsive poly(ethylene oxide) monomethyl ether-block-poly(acrylic acid)-block-poly(n-isopropylacrylamide) copolymer to form micelles for drug delivery, Reactive and Functional Polymers 71 (2011) 544–552.

[201] S. R. Sershen, S. L. Westcott, N. J. Halas, J. L. West, Temperature-sensitive polymer-nanoshell composites for photothermally modulated drug delivery, Journal of Biomedical Materials Research 51 (2000) 293–298.

[202] S. Deshmukh, D. A. Mooney, T. McDermott, S. Kulkarni, J. M. D. MacElroy, Molecular modeling of thermo-responsive hydrogels: observation of lower critical solution temperature, Soft Matter 5 (2009) 1514–1521.

[203] H. Feil, Y. H. Bae, J. Feijen, S. W. Kim, Effect of comonomer hydrophilicity and ionization on the lower critical solution temperature of n-isopropylacrylamide copolymers, Macromolecules 26 (1993) 2496–2500.

[204] Y. Xia, N. A. D. Burke, H. D. H. Stöver, End group effect on the thermal response of narrow-disperse poly(n-isopropylacrylamide) prepared by atom transfer radical polymerization, Macromolecules 39 (2006) 2275–2283.

[205] M. T. Savoji, S. Strandman, X. X. Zhu, Block random copolymers of n-alkyl-substituted acrylamides with double thermosensitivity, Macromolecules 45 (2012) 2001–2006.

[206] T. Furuncuoğlu Özaltın, I. Değirmenci, V. Aviyente, C. Atılgan, B. De Sterck, V. Van Speybroeck, M. Waroquier, Controlling the tacticity in the polymerization of n-isopropylacrylamide: A computational study, Polymer 52 (2011) 5503–5512.

[207] T. Hirano, Y. Okumura, H. Kitajima, M. Seno, T. Sato, Dual roles of alkyl alcohols as syndiotactic-specificity inducers and accelerators in the radical polymerization of

n-isopropylacrylamide and some properties of syndiotactic poly(n-isopropylacrylamide), Journal of Polymer Science Part A: Polymer Chemistry 44 (2006) 4450–4460.

[208] M. Ito, T. Ishizone, Living anionic polymerization of n-methoxymethyl-n-isopropylacrylamide: Synthesis of well-defined poly(n-isopropylacrylamide) having various stereoregularity, Journal of Polymer Science Part A: Polymer Chemistry 44 (2006) 4832–4845.

[209] K. F. Morris, C. S. Johnson, Diffusion-ordered two-dimensional nuclear magnetic resonance spectroscopy, Journal of the American Chemical Society 114 (1992) 3139–3141.

[210] A. Jerschow, N. Müller, Diffusion-separated nuclear magnetic resonance spectroscopy of polymer mixtures, Macromolecules 31 (1998) 6573–6578.

[211] J. Viéville, M. Tanty, M.-A. Delsuc, Polydispersity index of polymers revealed by DOSY NMR, Journal of Magnetic Resonance 212 (2011) 169–173.

[212] A. Chen, D. Wu, C. S. Johnson, Determination of molecular weight distributions for polymers by diffusion-ordered NMR, Journal of the American Chemical Society 117 (1995) 7965–7970.

[213] J. M. Zayed, F. Biedermann, U. Rauwald, O. A. Scherman, Probing cucurbit[8]uril-mediated supramolecular block copolymer assembly in water using diffusion NMR, Polymer Chemistry 1 (2010) 1434–1436.

[214] P. N. Zawaneh, A. M. Doody, A. N. Zelikin, D. Putnam, Diblock copolymers based on dihydroxyacetone and ethylene glycol: Synthesis, characterization, and nanoparticle formulation, Biomacromolecules 7 (2006) 3245–3251.

[215] C. Lefay, D. Glé, M. Rollet, J. Mazzolini, D. Bertin, S. Viel, C. Schmid, C. Boisson, F. D'Agosto, D. Gigmes, C. Barner-Kowollik, Block copolymers via macromercaptan initiated ring opening polymerization, Journal of Polymer Science Part A: Polymer Chemistry 49 (2011) 803–813.

[216] S. Viel, M. Mazarin, R. Giordanengo, T. N. Phan, L. Charles, S. Caldarelli, D. Bertin, Improved compositional analysis of

block copolymers using diffusion ordered NMR spectroscopy, Analytica Chimica Acta 654 (2009) 45–48.

[217] Y. Bakkour, V. Darcos, S. Li, J. Coudane, Diffusion ordered spectroscopy (DOSY) as a powerful tool for amphiphilic block copolymer characterization and for critical micelle concentration (CMC) determination, Polymer Chemistry 3 (2012) 2006–2010.

[218] G. Moad, D. H. Solomon, The Chemistry of Radical Polymerization, volume Second fully revised edition, Elsevier, Oxford, 2006.

[219] M. Szwarc, Living polymers. their discovery, characterization, and properties, Journal of Polymer Science Part A: Poymer Chemistry 36 (1998) IX–XV.

[220] N. V. Tsarevsky, K. Matyjaszewski, "Green" atom transfer radical polymerization: From process design to preparation of well-defined environmentally friendly polymeric materials, Chemical Reviews 107 (2007) 2270–2299.

[221] W. A. Braunecker, K. Matyjaszewski, Controlled/living radical polymerization: Features, developments, and perspectives, Progress in Polymer Science 32 (2007) 93–146.

[222] K. Matyjaszewski, Controlled radical polymerization: State of the art in 2008, in: Controlled/Living Radical Polymerization: Progress in ATRP, ACS Symposium Series, American Chemical Society, Washington DC, 2009, pp. 3–13.

[223] G. Moad, J. Chiefari, Y. K. Chong, J. Krstina, R. T. A. Mayadunne, A. Postma, E. Rizzardo, S. H. Thang, Living free radical polymerization with reversible addition - fragmentation chain transfer (the life of RAFT), Polymer International 49 (2000) 993–1001.

[224] H. Fischer, The persistent radical effect in controlled radical polymerizations, Journal of Polymer Science Part A: Poymer Chemistry 37 (1999) 1885–1901.

[225] A. B. Lowe, C. L. McCormick, Reversible addition-fragmentation chain transfer (RAFT) radical polymerization and the synthesis of water-soluble (co)polymers under homoge-

neous conditions in organic and aqueous media, Progress in Polymer Science 32 (2007) 283–351.

[226] A. Gregory, M. H. Stenzel, Complex polymer architectures via RAFT polymerization: From fundamental process to extending the scope using click chemistry and nature's building blocks, Progress in Polymer Science 37 (2012) 38–105.

[227] H. Li, M. Li, X. Yu, A. P. Bapat, B. S. Sumerlin, Block copolymer conjugates prepared by sequentially grafting from proteins via RAFT, Polymer Chemistry 2 (2011) 1531–1535.

[228] L. Tao, C. S. Kaddis, R. R. O. Loo, G. N. Grover, J. A. Loo, H. D. Maynard, Synthesis of maleimide-end-functionalized star polymers and multimeric protein-polymer conjugates, Macromolecules 42 (2009) 8028–8033.

[229] D. Boschmann, R. Edam, P. J. Schoenmakers, P. Vana, Z-RAFT star polymerization of styrene: Comprehensive characterization using size-exclusion chromatography, Polymer 49 (2008) 5199–5208.

[230] J. Zhu, X. Zhu, E. Kang, K. Neoh, Design and synthesis of star polymers with hetero-arms by the combination of controlled radical polymerizations and click chemistry, Polymer 48 (2007) 6992–6999.

[231] D. L. Patton, P. Taranekar, T. Fulghum, R. Advincula, Electrochemically active dendritic-linear block copolymers via RAFT polymerization: Synthesis, characterization, and electrodeposition properties, Macromolecules 41 (2008) 6703–6713.

[232] S. Wang, Z. Cheng, J. Zhu, Z. Zhang, X. Zhu, Synthesis of amphiphilic and thermosensitive graft copolymers with fluorescence p(st-co-(p-CMS))-g-PNIPAAM by combination of NMP and RAFT methods, Journal of Polymer Science Part A: Polymer Chemistry 45 (2007) 5318–5328.

[233] Y.-G. Li, P.-J. Shi, Y. Zhou, C.-Y. Pan, Synthesis and characterization of block comb-like copolymers p(a-MPEO)-block-PSt, Polymer International 53 (2004) 349–354.

[234] A. Favier, M.-T. Charreyre, Experimental requirements for an efficient control of Free-Radical polymerizations via the rever-

sible Addition-Fragmentation chain transfer (RAFT) process, Macromolecular Rapid Communications 27 (2006) 653–692.

[235] D. J. Keddie, G. Moad, E. Rizzardo, S. H. Thang, RAFT agent design and synthesis, Macromolecules 45 (2012) 5321–5342.

[236] . Y. K. Chong, J. Krstina, T. P. T. Le, G. Moad, A. Postma, E. Rizzardo, S. H. Thang, Thiocarbonylthio compounds [SC(Ph)S-R] in free radical polymerization with reversible addition-fragmentation chain transfer (RAFT polymerization). role of the free-radical leaving group (r), Macromolecules 36 (2003) 2256–2272.

[237] F. Ganachaud, M. J. Monteiro, R. G. Gilbert, M.-A. Dourges, S. H. Thang, E. Rizzardo, Molecular weight characterization of poly(n-isopropylacrylamide) prepared by living free-radical polymerization, Macromolecules 33 (2000) 6738–6745.

[238] M. Nuopponen, H. Tenhu, Gold nanoparticles protected with pH and temperature-sensitive diblock copolymers, Langmuir 23 (2007) 5352–5357.

[239] C. Yang, Y.-L. Cheng, RAFT synthesis of poly(n-isopropylacrylamide) and poly(methacrylic acid) homopolymers and block copolymers: Kinetics and characterization, Journal of Applied Polymer Science 102 (2006) 1191–1201.

[240] J. M. Pelet, D. Putnam, High molecular weight poly(methacrylic acid) with narrow polydispersity by RAFT polymerization, Macromolecules 42 (2009) 1494–1499.

[241] E. Hosseini Nejad, P. Castignolles, R. G. Gilbert, Y. Guillaneuf, Synthesis of methacrylate derivatives oligomers by dithiobenzoate-RAFT-mediated polymerization, Journal of Polymer Science Part A: Polymer Chemistry 46 (2008) 2277–2289.

[242] J. Li, L. Yi, H. Lin, R. Hou, Synthesis of poly(tert-butyl methacrylate)-graft-poly(dimethylsiloxane) graft copolymers via reversible addition-fragmentation chain transfer polymerization, Journal of Polymer Science Part A: Polymer Chemistry 49 (2011) 1483–1493.

[243] S. D. Zaitsev, Y. D. Semchikov, E. V. Vasil'eva, L. V. Kurushina, Controlled radical (co)polymerization of (meth)acrylic esters via the reversible addition-fragmentation chain-transfer mechanism, Polymer Science Series B 54 (2012) 205–214.

[244] S. Kessel, N. P. Truong, Z. Jia, M. J. Monteiro, Aqueous reversible addition-fragmentation chain transfer dispersion polymerization of thermoresponsive diblock copolymer assemblies: Temperature directed morphology transformations, Journal of Polymer Science Part A: Polymer Chemistry 50 (2012) 4879–4887.

[245] I. Chaduc, M. Lansalot, F. D'Agosto, B. Charleux, RAFT polymerization of methacrylic acid in water, Macromolecules 45 (2012) 1241–1247.

[246] I. Chaduc, W. Zhang, J. Rieger, M. Lansalot, F. D'Agosto, B. Charleux, Amphiphilic block copolymers from a direct and one-pot RAFT synthesis in water, Macromolecular Rapid Communications 32 (2011) 1270–1276.

[247] Z.-L. Ding, W.-D. He, J. Tao, W.-X. Jiang, L.-Y. Li, T.-T. Pan, Zwitterionic shell-crosslinked micelles from block-comb copolymer of PtBA-b-P(PEGMEMA-co-DMAEMA), Journal of Polymer Science Part A: Polymer Chemistry 49 (2011) 2783–2789.

[248] T. Ta, A. J. Convertine, C. R. Reyes, P. S. Stayton, T. M. Porter, Thermosensitive liposomes modified with poly(n-isopropylacrylamide-co-propylacrylic acid) copolymers for triggered release of doxorubicin, Biomacromolecules 11 (2010) 1915–1920.

[249] A. Graillot, S. Monge, J.-J. Robin, RAFT polymerization of n-n-propylacrylamide: Evaluation of a new trithiocarbonate chain transfer agent, Polymer Preprints 52 (2011) 653–654.

[250] H. Dong, H. Du, X. Qian, Prediction of pKa values for oligo-methacrylic acids using combined classical and quantum approaches, The Journal of Physical Chemistry B 113 (2009) 12857–12859.

[251] R. Yu, S. Zheng, Poly(acrylic acid)-grafted poly(n-isopropyl acrylamide) networks: Preparation, characterization and hydrogel behavior, Journal of Biomaterials Science, Polymer Edition 22 (2011) 2305–2324.

[252] E. K. Skinner, F. M. Whiffin, G. J. Price, Room temperature sonochemical initiation of thiol-ene reactions, Chemical Communications 48 (2012) 6800–6802.

[253] E. K. Skinner, G. J. Price, Encapsulation and release of aqueous components from sonochemically produced protein microspheres, Chemical Communications 48 (2012) 9260–9262.

[254] T. Y. Wu, N. Guo, C. Y. Teh, J. X. W. Hay, Advances in Ultrasound Technology for Environmental Remediation, Springer, Heidlberg, New York, London, 2013.

[255] ACS white paper: Pharmaceutical chemistry: Drug development goes deeper into the genome, 2012.

[256] A. M. Bivigou-Koumba, J. Kristen, A. Laschewsky, P. MÃŒller-Buschbaum, C. M. Papadakis, Synthesis of symmetrical triblock copolymers of styrene and n-isopropylacrylamide using bifunctional bis(trithiocarbonate)s as RAFT agents, Macromolecular Chemistry and Physics 210 (2009) 565–578.

[257] O. I. Strube, L. Nothdurft, M. Drache, G. Schmidt-Naake, A novel bifunctional trithiocarbonate for styrene and methacrylate RAFT polymerization, Macromolecular Chemistry and Physics 212 (2011) 574–582.